Untersuchungen zur Synthese und Reaktivität von Organozinnselenidclustern

Dissertation

Zur Erlangung des akademischen Grades eines
Doktors der Naturwissenschaften
(Dr. rer. Nat.)

dem
Fachbereich Chemie der Philipps-Universität Marburg
vorgelegt von
Niklas Rinn, M.Sc.
aus Heuchelheim

Erstgutachterin: Prof. Dr. Stefanie Dehnen
Zweitgutachter: Prof. Dr. Sangam Chatterjee

Einreichungstermin: 03.08.2017
Prüfungstermin:

Marburg/Lahn 2017
Hochschulkennziffer 1180

„Wenn ein gewisses technisches Können erreicht ist,
verschmelzen Wissenschaft und Kunst gern zu
Ästhetik, Bildhaftigkeit und Form.
Die größten Wissenschaftler sind immer auch Künstler.“
-Albert Einstein

Inhaltsverzeichnis

Abbildungsverzeichnis

Verzeichnis der Schemata

Erklärung

Ich erkläre, dass eine Promotion noch an keiner anderen Hochschule als der Philipps-Universität Marburg, Fachbereich Chemie, versucht wurde. Weiterhin versichere ich, dass ich meine vorgelegte Dissertation:

„Untersuchungen zur Synthese und Reaktivität von Organozinnselenidclustern“

selbst und ohne fremde Hilfe verfasst, nicht andere als die in ihr angegebenen Quellen oder Hilfsmittel benutzt, alle vollständig oder sinngemäß übernommenen Zitate als solche gekennzeichnet sowie die Dissertation in der vorliegenden oder einer ähnlichen Form noch bei keiner anderen in- oder ausländischen Hochschule anlässlich eines Promotionsgesuchs oder zu anderen Prüfungszwecken eingereicht habe.

Marburg, den _____

Niklas Rinn

Vorbemerkung zu kristallographischen Abbildungen

In allen Molekül- und Kristallstrukturausschnitten, die nicht im kumulativen Teil abgebildet sind, wurden die Atomradien beliebig gewählt. Wasserstoffatome und nicht verbrückende organische Reste in Phosphanliganden sind aufgrund der Übersichtlichkeit nicht gezeigt. Einheiten mit den Elementen C, O, N und P werden zudem nur als Bindungsskelett gezeigt. Folgendes Farbschema wurde verwendet:

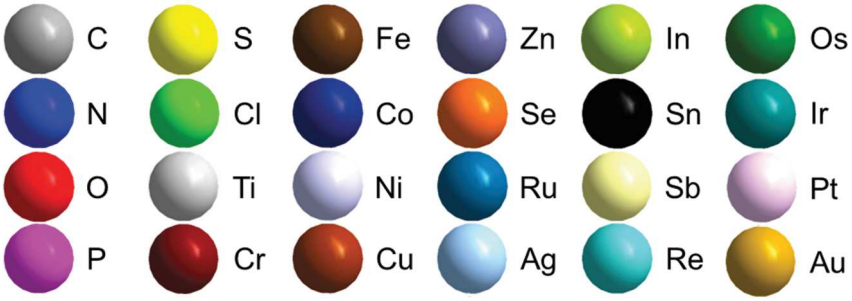

1. Einleitung

1.1. Das Element Selen

Das Element Selen (griechisch: Selene „Mond“; entdeckt 1817 von Jöns Jakob Berzelius) ähnelt in seinem chemischen Verhalten als Nichtmetall der 16. Gruppe stark dem Schwefel. Gründe dafür sind die ähnliche Elektronegativität und Ionisierungsenergie.[1] Allerdings hat Selen bereits in seiner bei Standardbedingungen stabilsten Modifikation, dem hexagonalen grauen Selen, halbmetallische Eigenschaften.[2] Das lässt sich durch seine Struktur erklären: Die Selenatome ordnen sich im Kristallgitter kettenförmig an. Auf den Kanten der Elementarzelle entlang der *c*-Achse befindet sich jeweils ein unendlich ausgedehnter helikaler Strang mit C_3-Symmetrie, in dem nach jeweils drei Selenatomen eine Windung um die Drehachse vollzogen wird. Diese Ketten besitzen untereinander nur leichte Wechselwirkungen mit dispersivem Charakter. Dadurch ergeben sich, wenn auch relativ schlechte, halbleitende Eigenschaften entlang der Se_n-Spiralen. Es existieren weitere metastabile, nicht metallische Modifikationen, wie die drei aus Se_8-Zyklen bestehenden monoklinen Modifikationen von rotem Selen, zudem glasiges schwarzes oder amorphes rotes Selen. Andere oligomere, zumeist ringförmigen Allotrope (Se_2, Se_6, Se_7 und Se_{12}), wurden ebenfalls nachgewiesen. Abbildung 1.1 zeigt einen Ausschnitt aus der Kristallstruktur von grauem Selen und die molekulare Se_8-Einheit in monoklinem rotem Selen.

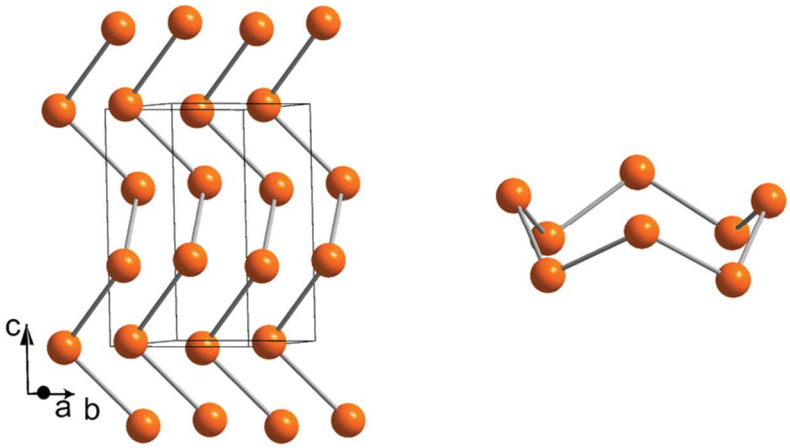

Abbildung 1.1: Beispiele für Elementstrukturen von Selen. Links: Ausschnitt der Kristallstruktur von elementarem grauem Selen.[3] Rechts: Molekulare Einheit von monoklinem rotem Selen.[4]

Selen bildet mit nahezu allen Elementen des Periodensystems Verbindungen. In diesen kommt es in Abhängigkeit von der Natur seiner Nachbaratome in formalen Oxidationsstufen von –II bis +VI vor. Die höheren Oxidationsstufen liegen beispielsweise in binären Halogeniden oder Oxiden wie SeF_6 und SeO_3 vor. Die Oxidationsstufe –II tritt in den meisten Verbindungen mit elektropositiveren Elementen auf. In den folgenden Abschnitten wird an Beispielen auf die Tendenz von Selen hingewiesen, in homo- und heteroatomarer Umgebung Aggregate und Cluster zu bilden.

1.2. (Sub-)Strukturen mit anionischen Polyselenid-Einheiten oder kationischen Polyselen-Einheiten

In kondensierter Phase existieren eine Reihe von Polyselenkationen:Se_4^{2+},[5] Se_8^{2+},[6] Se_{10}^{2+}[7] undSe_{17}^{2+}.[8] Diese werden meist durch Metallatkomplexe wie $[Bi_4Cl_{14}]^{2-}$ stabilisiert. Se_4^{2+} bildet einen quadratisch planaren 6π-Hückel-Aromaten, während Se_8^{2+} durch einen Se_8-Ring mit *exo-endo*-Konformation und drei transannularen Wechselwirkungen beschrieben werden kann. Se_{10}^{2+} bildet einen Bizyklus, bei dem ein Se_8-Ring durch eine Se_2-Brücke intramolekular verbrückt wird. Se_{17}^{2+} liegt als Molekül aus zwei Se_7-Ringen vor, die durch eine Se_3-Einheit verknüpft sind. Die polykationischen Strukturen sind in Abbildung 1.2 gezeigt.

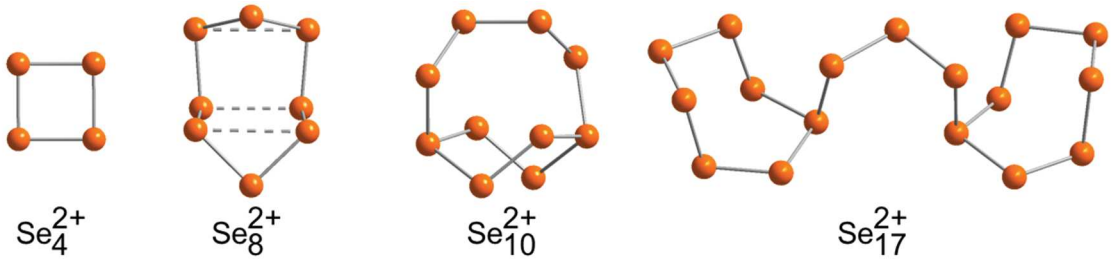

Abbildung 1.2: Molekülstrukturen homoatomarer Polyselenkationen.

Verwandte kationischePolyselen-Einheiten treten in einigen Selenhalogeniden auf.[9] Dimere Einheiten finden sich in den Verbindungen Se_2X_2 (X = Cl, Br), dem entsprechenden Halogenidaddukt $(Se_2X_4)^{2-}$ sowie $(Se_2I_4)^{2+}$. Kettenförmige Se_3- und Se_4-Einheiten sind Bestandteil der Kationen $(BrSe_3Br_2)^+$ und $(I_2Se_4I_2)^+$. $(Se_6I_2)^{2+}$ und $[(Se_6I)^+]_n$ (Se_6-Ringe) sowie $(Se_9Cl)^+$ (Se_7-Ring mit Se_2Cl-Seitenkette) enthalten ringförmige Fragmente.

Hauptsächlich in Verbindungen mit Elementen der ersten beiden Gruppen lassen sich verschiedene homoatomare Polyselenide Se_n^{2-} isolieren. Bis hin zu n = 8 wurden kettenförmige Anordnungen beobachtet.[10] In Se_9^{2-} liegt ein Se_6-Ring mit einer Se_3-Seitenkette vor.[10] In Se_{10}^{2-} liegen zwei kantenverknüpfte Se_6-Ringe vor,[11] in dem *spiro*-Anion Se_{11}^{2-} zwei eckenverknüpfte.[12] Se_{16}^{4-} besteht aus einem Se_6-Ring, bei dem zwei Se_5-Seitenketten schwach an das gleiche Selenatom koordinieren.[13] Die polyanionischen Strukturen zeigt Abbildung 1.3.

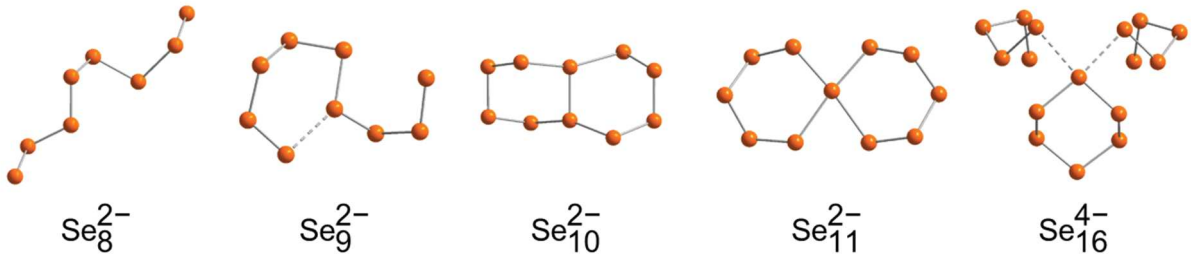

Abbildung 1.3: Molekülstruktur homoatomarer Polyselenide.

Polyselenide können mit Metallkationen Komplexe bilden. Beispielsweise entstehen Verbindungen der Art $[M(Se_5)L_x]$ (M = Metall, hier Ti, Zr, Hf, Cr, Mo, W, Mn, Fe, Cu, Pd und Sb; L = Ligand), indem elementares Selen und einfache Selenide mit Metallkomplexen umgesetzt werden.[14–21] Größere zweikernige Metallpolyselenide sind zudem in Verbindung mit Metallen des d- und p-Blocks bekannt, wie in $[(Cp^*Ir)_2Se_8]$ (Cp^* = Pentamethylcyclopentadienyl),[22] $[In_2Se_{21}]^{4-}$,[23] oder $[(Se_5Sb)_2(\mu\text{-}Se)_2]^{2-}$.[20] Die Molekülstrukturen dieser Verbindungen sind in Abbildung 1.4 gezeigt.

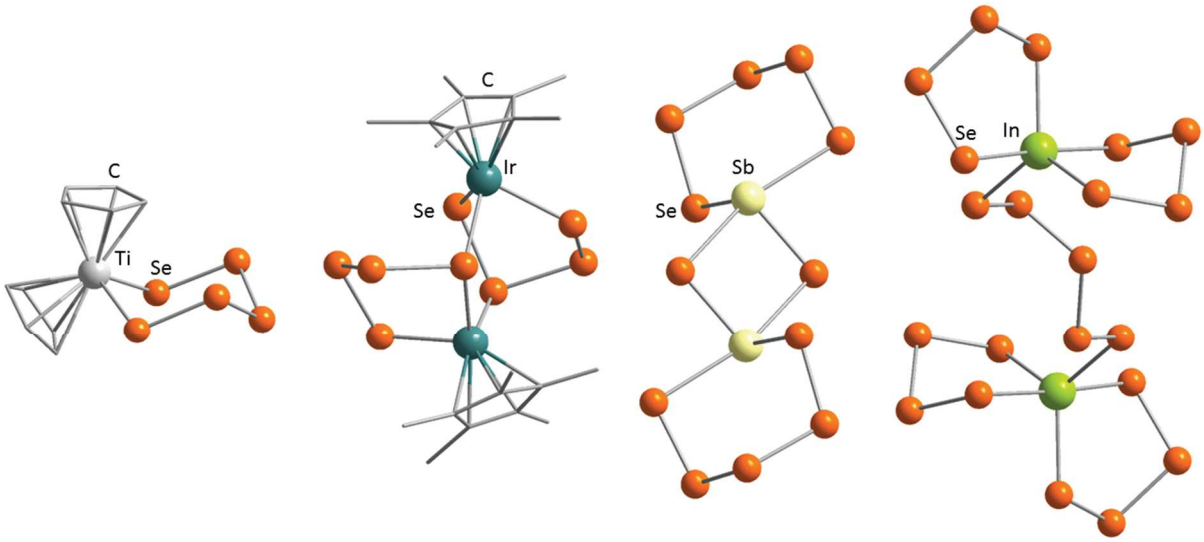

Abbildung 1.4: Molekülstrukturen von Metallpolyselenidkomplexen. Von links nach rechts: $[Ti(Se_5)Cp_2]$, $[(Cp^*Ir)_2Se_8]$, $[(Se_5Sb)_2(\mu\text{-}Se)_2]^{2-}$ und $[In_2Se_{21}]^{4-}$.

1.3. Metallselenidcluster

Von annähernd allen Metallen des d- und p-Blocks sowie einigen Elementen des f-Blocks sind Metallselenidcluster bekannt, weshalb diese Stoffklasse zu umfangreich ist, um sie hier vollständig zu beschreiben. In diesem Abschnitt soll daher nur beispielhaft auf die Strukturchemie dieser Clusterfamilie(n) eingegangen werden. Interchalkogenide sowie Verbindungen mit oxid- und halogenidhaltigen Clusterkernen werden nicht berücksichtigt. Zunächst werden einige archetypische Strukturen vorgestellt und anschließend auf einzelne Verbindungen der f-, d- und p-Block-Metalle eingegangen. Hierbei konzentriert sich die Beschreibung auf Cluster (Komplexe mit mindestens drei Metallatomen) sowie auf Verbindungen mit binärem anorganischem Grundgerüst, wobei einige Verbindungen mit ternärem Grundgerüst die Beschreibung ergänzen.

Selenatome treten in diesen Verbindungen im Clusterkern auf, und zwar meist in Form μ- oder μ_3-verbrückender Liganden. Als zentrales Atom einer Verbindung kann sich die Koordinationszahl jedoch weiter erhöhen. Oft werden organisch funktionalisierte Selensynthone RSe^- (R = organischer Ligand, zumeist Ph), eingesetzt, um das Clusterwachstum zu begrenzen und die Verbindungen durch sterische Abschirmung zu stabilisieren. Diese Einheiten befinden sich in der Regel als μ_2-SePh-Liganden am der Peripherie des Clusters. Die Metallatome an der Oberfläche der anorganischen Clusterkerne tragen in den meisten Fällen Phosphanliganden, Halogenidliganden oder organische Liganden.

Eine Topologie, die bei vielen der besprochenen Metallselenidcluster vertreten ist, ist die Heterokuban-Struktur (HK-Struktur), bei der vier Selenatome und vier Metallatome alternierend die Ecken eines meist leicht verzerrten Kubus bilden. Binäre Verbindungen dieser Topologie gibt es mit Kationen der Metalle Yb,[24] Cr,[25] Mo, W,[26] Mn,[27] Re,[28] Fe,[29] Ru,[30] Co,[31] Rh, Ir,[32] Ni,[33] Al,[34] Ga,[35] In,[36] Tl[37] und Bi.[38] Atome der Elemente Nb, Ta,[39] Pd,[40]

Cu und Ag[41] kommen zudem in ternären HK-Typ-Clustern der Art $[M_{4-x}M'_xSe]$ (M' = Metall ≠ M; x = 1–3) vor. Ein Beispiel für eine solche Verbindung ist in Abbildung 1.5 (links) gezeigt.

In den Gruppen 6 bis 8 und dort vor allem für die Chemie des Rheniums ist ein Strukturmotiv dominant, das sich von den Chevrel-Phasen (CH-Phasen) ableitet. Ein Oktaeder aus Metallatomen ist hierbei von einem Kubus aus Selenatomen umgeben. Für die Elemente V,[42] Cr,[43] Mo,[44] W,[45] Tc,[46] Re,[47] Fe,[48] Ru,[49] Co,[31] und Rh[50] existieren homometallische Varianten; für Osmium und Rhenium sind gemischte Cluster bekannt.[51] Auch für diese Gruppe zeigt Abbildung 1.5 (Mitte) ein Beispiel.

Die Metallselenidcluster der Gruppen 10 bis 14 haben von Tetraedern abgeleitete Clustertopologien. Die Verbindungen lassen sich formal meist durch Kondensation von $[MSe_4]$-Tetraedern verstehen, wobei andere Liganden, beispielsweise Phosphane oder einfache organische Reste, die Selenatome an den Ecken der tetraedrischen Cluster ersetzen können. Ein einfaches Beispiel dieser Art ist die Adamantan-Topologie (AD-Topologie) in $[(LM)_4Se_6]$, bei der vier tetraedrisch angeordnete, jedoch nicht miteinander verbundene Metallatome an allen Kanten des so aufgespannten Tetraeders von einem Selenatom überkappt sind. Je nach Metallsorte kann es sich bei den Selenatomen um μ-Se- oder μ_3-SeR-Einheiten handeln. Homoatomare Beispiele gibt es mit Mn,[52] Cu,[53] Ag,[54] Zn,[55] Cd,[56] Hg,[57] Ga, In,[58] Ge[59] und Sn.[60] Ein Beispiel für diese Topologie ist in Abbildung 1.5 (rechts) gegeben.

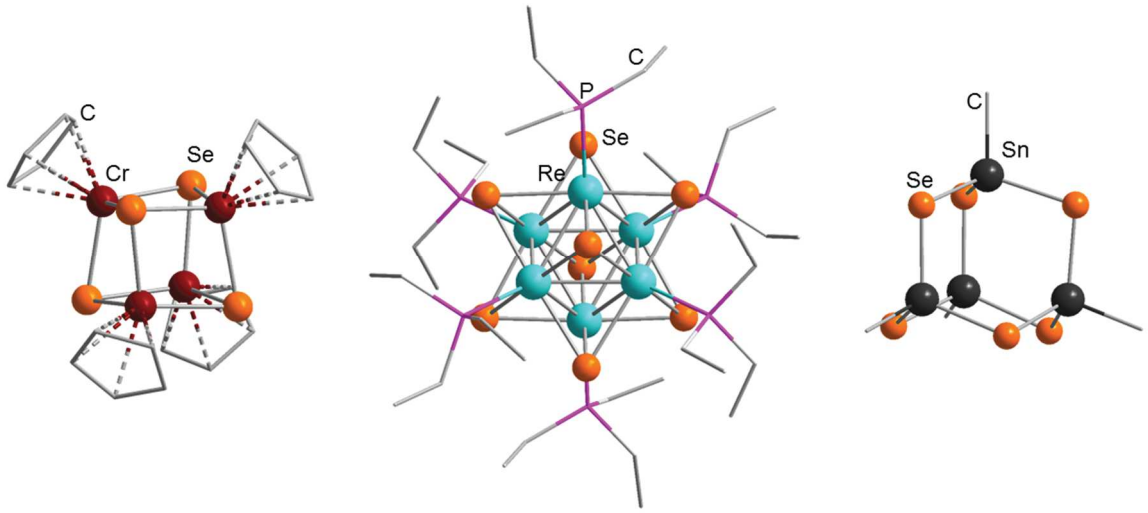

Abbildung 1.5: Beispiele für typische Metallselenidcluster-Topologien. Links: $[(CpCr)_4Se_4]$-Heterokuban (Cp = Cyclopentadienyl).[25] Mitte: $[(PEt_3Re)_6Se_8]^{2-}$-Anion, mit von Chevrel-Phasen abgeleiteter Molekülstruktur.[47] Rechts: $[(MeSn)_4Se_6]$ mit adamantanartiger Topologie.[60]

Das Adamantangerüst kann durch formale Anlagerung von $[MSe_4]$-Tetraedern – unter Abspaltung von Selenidliganden – expandieren, was zur Bildung sogenannter supertetraedrischer Clustergerüste führt.[61–63] Im Sonderfall regelmäßiger Supertetraeder wird die Clustergröße mittels Tn-Nomenklatur benannt, wobei n die Zahl der kondensierten Tetraederschichten angibt. Somit wäre ein T1-Cluster ein einzelnes $[MSe_4]$-Tetraeder und ein T2-Cluster eine Verbindung mit AD-Topologie. Hierbei existieren einige Cluster, bei denen neben der ursprünglichen Sorte an Metallatomen eine zweite Metallatomsorte auf einem Teil der entsprechenden Atompositionen gefunden wird.[64,65] Es ist zudem möglich, Verbindungen alternierend aus $[MSe_4]$- und $[SeM'_4]$-Einheiten aufzubauen. Vier Tn-Einheiten koordiniert hierbei mit den drei Selenatomen einer ihrer Flächen an jede Fläche einer gleichgroßen Tn-Einheit, bei der die Metall- und Selenpositionen invers besetzt sind.[66,67] Analog der Tn-Nomenklatur ergibt sich eine Pn-Nomenklatur, wobei n hier die Größe der einzelnen Tn-Einheiten angibt. Beispiele für einen T3- und einen P1-Cluster zeigt Abbildung 1.6.

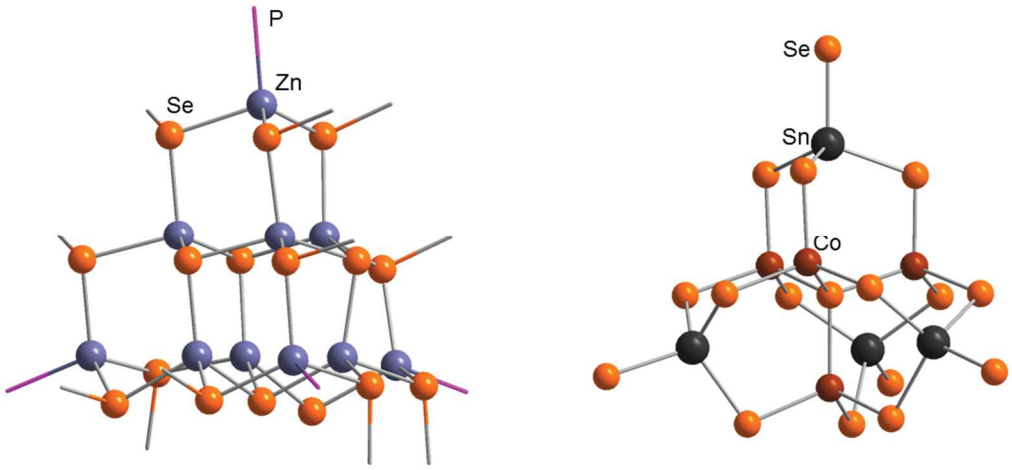

Abbildung 1.6: Beispiele für Selenidcluster mit supertetraederischer Grundstruktur. Links: T3-Cluster $[Zn_6Se_4(PPh_3Zn)_4(SePh)_{12}]$ (Phenylgruppen der PhSe-Liganden wurden auf einen Punkt reduziert).[63] Rechts: Anionischer P1-Cluster $[Co_4Sn_4Se_{17}]^{10-}$.[66]

Auch die Synthese von Metallselenidclustern mit makrozyklischem Aufbau ist möglich. Beispiele hierfür sind $[(CO)_2Ru)(\mu\text{-}SePh)_2]_n$ (n = 6, 8)[68] oder der Trizyklus $[(Fe_4Se_4)_2(\mu\text{-}Fe_4Se_{10})_3]^{18-}$.[69] Oft werden einzelne Metalle durch Polyselenideinheiten verbrückt, wie in $[(\eta^2\text{-}Se_3ReCp^*)\mu\text{-}Se_2]_8$.[70] Die Molekülstrukturen dieser Verbindungen sind in Abbildung 1.7 dargestellt.

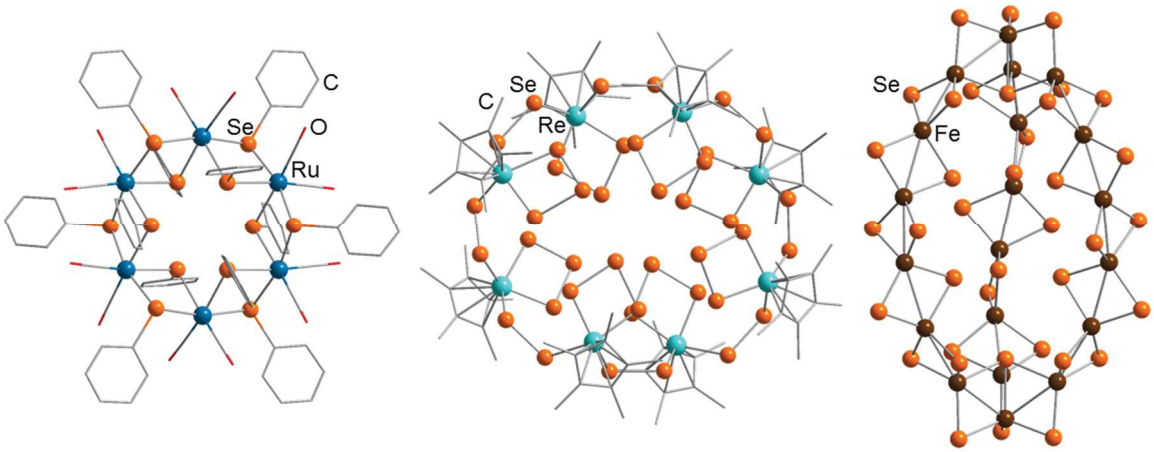

Abbildung 1.7: Molekülstrukturen von makrozyklischen Metallselenidclustern. Links: $[(CO)_2Ru)(\mu\text{-}SePh)_2]_6$.[68] Mitte: $[(\eta^2\text{-}Se_3ReCp^*)\mu\text{-}Se_2]_8$.[70] Rechts: $[(Fe_4Se_4)_2(\mu\text{-}Fe_4Se_{10})_3]^{18-}$.[69]

Eine mögliche Syntheseroute, um Metallselenidcluster zu erhalten, ist die Umsetzung von Metallkomplexen $[ML_xX_y]$ (X = Anion) oder Salzen MX_y mit $(SiMe_3)_2Se$ und/oder $(SiMe_3)SePh$ in einer Kondensationsreaktion. Die Triebkraft dieser Reaktionen ist die Bildung von $SiMe_3X$. Oft werden Metallkomplexe mit Phophanliganden verwendet, da diese eine gegenüber den einfachen, binären Metallsalzen höhere Löslichkeit in organischen Lösungsmitteln zeigen, allerdings weniger reaktiv sind (und damit besser kontrollierbar reagieren) als gelöste Metallsalze. Zudem können sie die Produktcluster zwar an der Oberfläche stabilisieren, sind aber dennoch labil genug gebunden, um den Einbau der Metalle in den inneren Clusterkern zu ermöglichen. Auf diese Art ist es möglich, polynukleare Cluster einer Vielzahl von Metallen zu erhalten. Beispiele hierfür sind die in Abbildung 1.8 dargestellten Cluster(-Kationen) $[Au_{18}Se_8(dppe)_6]^{2+}$[71] (dppe = Bis(diphenylphosphanyl)ethan), $[Ni_{34}Se_{22}(PPh_3)_{10}]$ und $[Co_9Se_{11}(PPh_3)_6]$.[31]

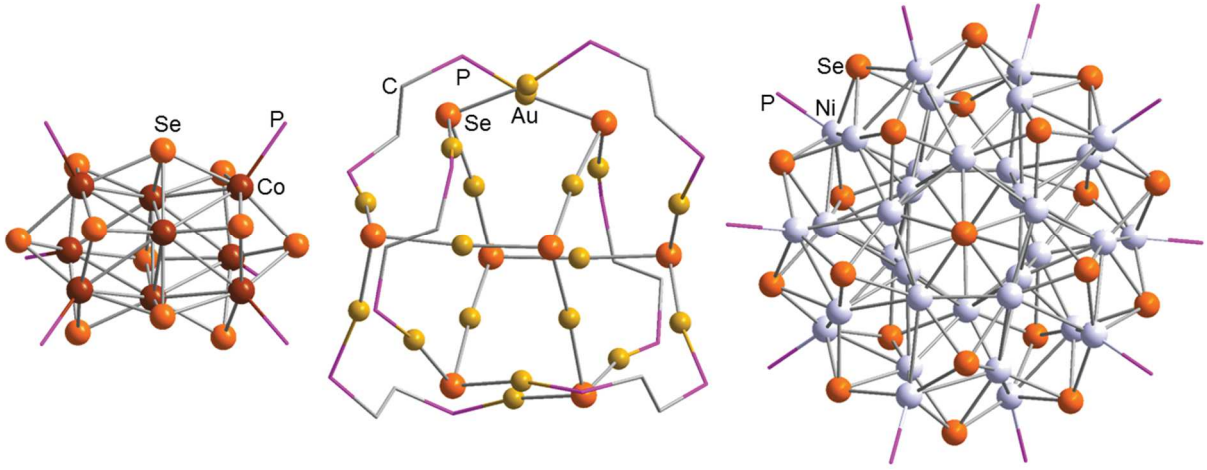

Abbildung 1.8: Molekülstrukturen von phosphanstabilisierten Metallselenidclustern. Links: $[Co_9Se_{11}(PPh_3)_6]$.[31] Mitte: $[Au_{18}Se_8(dppe)_6]^{2+}$ (dppe = Bis(diphenylphosphanyl)ethan).[71] Rechts: $[Ni_{34}Se_{22}(PPh_3)_{10}]$.[31]

Der Arbeitsgruppe um Fenske gelang es, ungewöhnlich große Moleküle wie $[Ag_{154}Se_{77}(dppxy)_{18}]$[72] (dppxy = 1,4-Bis(diphenylphosphanylmethyl)benzol) (Abbildung 1.9), $[Ag_{172}Se_{40}(Se\textit{n}\text{-}Bu)_{92}(dppp)_4]$ (Bu = Butyl; dppp = Bis(diphenylphosphanyl)propan) und $[Cu_{146}Se_{73}(PPh_3)_{30}]$ darzustellen.[73,74]

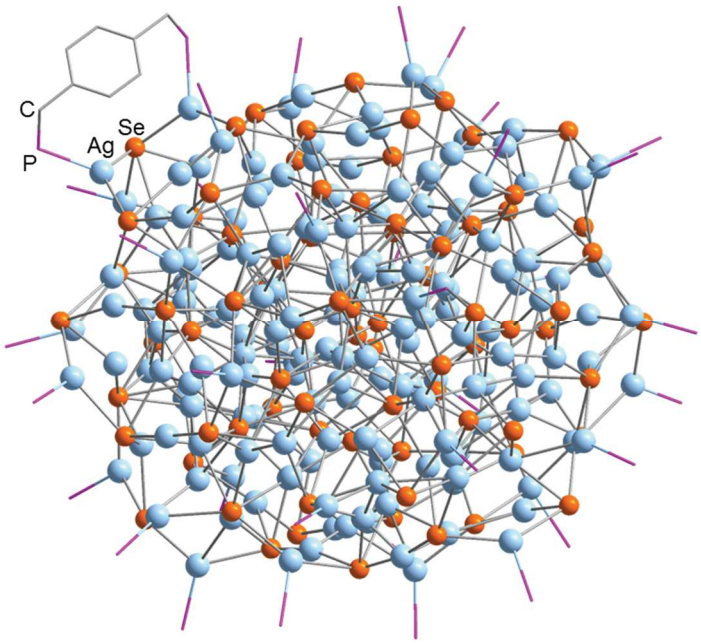

Abbildung 1.9: Molekülstruktur von $[Ag_{154}Se_{77}(dppxy)_{18}]$ (dppxy = 1,4-Bis(diphenylphosphanylmethyl)benzol).[72] Es wird aus Übersichtlichkeitsgründen nur einer der verbrückenden Liganden gezeigt.

1.4. Organozinnchalkogenidcluster

1.4.1. Verbindungen mit binärem anorganischem Grundgerüst

Die ersten organisch substituierten Zinnchalkogenidcluster wurden im Jahr 1972 als Sesquisulfide $[(RSn)_4S_6]$ mit AD-Topologie isoliert, wobei die organischen Liganden R unreaktive Substituenten wie Methyl oder Pentafluorphenyl waren.[75,76] Die Struktur eines Selenanalogons, $[(MeSn)_4Se_6]$, ließ sich im Jahr 1981 aufklären.[60] In allen Fällen entstehen diese Cluster durch die Reaktion eines Organotrichlorostannans Cl_3SnR mit einer Chalkogenidquelle A_2E (A = Na, $SiMe_3$). Es existiert eine zum AD-Typ isomere „Doppeldecker"-Topologie (DD-Topologie). Hier sind zwei Sn_2E_2-Vierringe über ihre

Zinnatome durch zwei μ-E-Atome verbunden. Diese Topologie lässt sich durch Lewis-basische Gruppen wie Amine, Carbonsäuren oder Ketone an den organischen Liganden stabilisieren, da druch eine intramolekulare Koordination der N- oder O-Donoratome an das Zinnatom dessen Koordinationszahl auf 5 erhöht wird.[77,78] Für die Elementkombination Sn/Se war dieses Strukturmotiv bisher allerdings unbekannt. Zudem ist in manchen Verbindungen eine Defektheterokuban-Topologie (DHK-Topologie) der allgemeinen Formel $[(RSn)_3E_4]^+$ zu beobachten, welche formal durch das Entfernen einer $(SnR)^-$-Einheit aus einem $[(SnR)_4E_4]$-Heterokuban entsteht. Auch dieser Strukturtyp tritt zumeist dann auf, wenn koordinierende Liganden vorliegen.[77,79] Es gibt allerdings auch Beispiele für entsprechende Cluster ohne koordinierende Liganden.[80,81] Eine weitere Topologie für Zinnsulfidcluster, in der eine Sn–Sn-Bindung auftritt, ließ sich durch den Zusatz von CS_2 aus einer DD-Typ-Verbindung herstellen: In $[\{(R^1Sn)_2S_4\}_3Sn_2]$ (R^1 = $CMe_2CH_2C(O)Me$) kommen zwei Zinnatome auf einer *pseudo*-C_3-Achse zu liegen und binden an drei $[(R^1Sn)_2S_4]$-Fragmente. Dadurch ergibt sich in der Projektion entlang der idealisierten Drehachse die Form eines Schaufelrads (SR) mit drei Armen.[82,83]

Der organische Rest R^1 lässt sich weiter funktionalisieren, wenn er mit Hydrazin oder dessen Derivaten umgesetzt wird. Bei der Kondensationsreaktion der Ketogruppe mit Hydrazin oder Hydrazinderivaten H_2NNHR (R = H oder organischer Rest) wandelt sich vor allem bei sterisch anspruchsvolleren Hydrazinderivaten das anorganische Grundgerüst zu einem *pseudo*-Dimer der DHK-Struktur um, bei dem zwei DHK. Einheiten durch zwei μ-E-Atome verknüpft sind (Bisdefektheterokuban-Topologie (BDHK-Topologie)).[77,79,84–87] Eine inverse Reaktionsführung, bei der ein Cluster zuerst durch die Umsetzung mit Hydrazinhydrat in sein Hydrazonderivat überführt und anschließend mit einer organischen Carbonylverbindung umgesetzt wird, ist ebenfalls möglich. Durch diese Art der Postfunktionalisierung lassen sich beispielsweise Metallocene an Cluster anbringen.[87–91] Durch bisfunktionelle organische Linker wurden Cluster zudem intra- und intermolekular verbrückt.[88,91–93] Beispiele für die oben genannten Strukturmotive zeigt Abbildung 1.10.

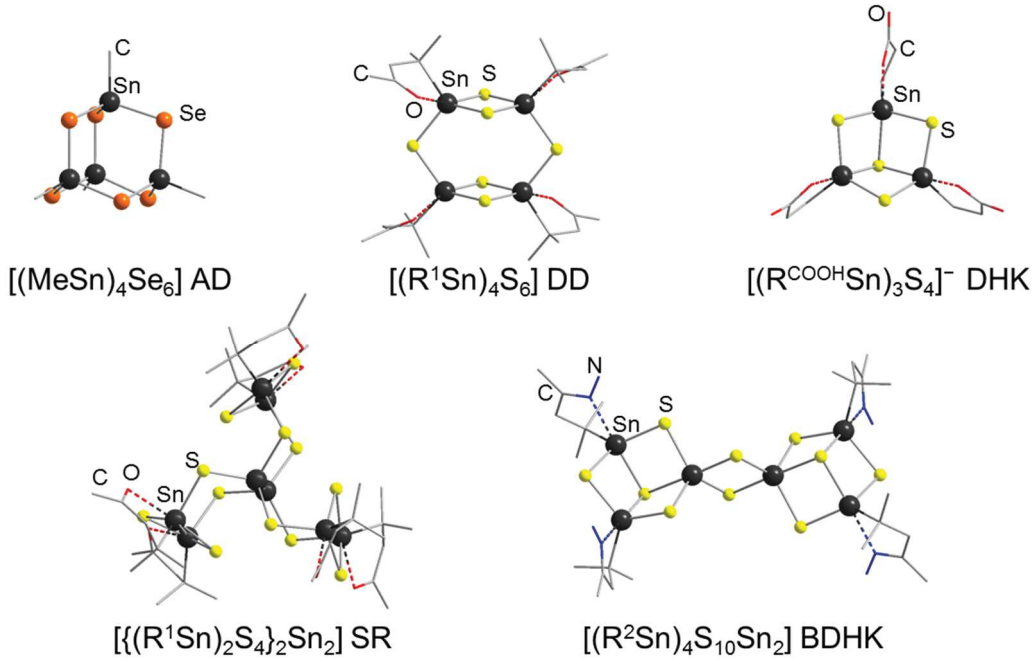

Abbildung 1.10: Beispiele für Topologien der Organozinnchalkogenidcluster. Oben links: Adamantan-Strukturtyp $[(MeSn)_4Se_6]$.[60] Oben Mitte: Doppeldecker-Strukturmotiv: $[(R^1Sn)_4S_6]$.[77] Oben rechts: Anionischer Cluster mit Defektheterokuban-Topologie $[(R^{COOH}Sn)_3S_4]$ (R^{COOH} = CH_2CH_2COOH).[77] Unten links: Schaufelrad(SR)-Topologie $[\{(R^1Sn)_2S_4\}_3Sn_2]$.[83] Unten rechts: Cluster mit Bisdefektheterokuban-Grundgerüst $[(R^2Sn)_4S_{10}Sn_2]$ (R^2 = $CMe_2CH_2C(NNH_2)Me$).[79]

1.4.2. Verbindungen mit ternärem anorganischem Grundgerüst

Durch Merzweiler und Mitarbeiter wurde erstmals das anorganische Grundgerüst von Organozinnchalkogenidclustern durch Übergangsmetallatome erweitert. Dies geschah durch eine Umsetzung des AD-Typ-Clusters $[(PhSn)_4S_6]$ mit $[(PhPMe_2)bipyCuCl]$ (bipy = 2,2´-Bipyridyl) zu $[(PhSnS_3)_2(CuPPhMe_2)_6]$.[94] Hierzu nutzten die Autoren einen Überschuss einer Sulfidquelle vor Zugabe eines Übergangsmetallkomplexes, in diesem Fall Na_2S. Dadurch wurde der ursprüngliche Cluster zu anionischen Organozinnsulfid-Bausteinen fragmentiert,welche unter Bildung eines neuen Clusters an die $[CuPPh_3]$-Einheiten binden. Inspiriert von dieser Methode wurden im Arbeitskreis Dehnen ähnliche Reaktionen mit unterschiedlichen Ausgangsclustern, Sulfidquellen und Übergangsmetallverbindungen durchgeführt.[77,84,86,95–97] Dabei hängt die Topologie des entstehenden Clusters nicht nur von der Elementkombination sondern auch von dem organischen Liganden an den Zinnatomen, von der Natur der Sulfidquelle und der Topologie des Eduktclusters ab. So wurden drei mit Kupfer erweiterte Zinnsulfidcluster mit unterschiedlichen Topologien synthetisiert. Die beiden Cluster $[(CuPPh_3)_6(R^1SnS_3)_2]$, mit anorganischen Grundgerüsten isotyp zu der von der Arbeitsgruppe Merzweiler gefundenen Verbindung, und $[(CuPPh_3)_2(SnCl)_2\{(R^1Sn)_2S_4\}_2]$ wurden mit dem gleichen Kupferkomplex ($[Cu(PPh_3)_3Cl]$) und den gleichen organischen Substituenten R^1 hergestellt, aber einem DD-Typ beziehungsweise DHK-Typ Eduktcluster. Zudem kam im zweiten Fall $(SiMe_3)_2S$ an Stelle von Na_2S als Sulfidquelle zum Einsatz. Der Cluster $[R^{CH}_2\{Sn(\mu\text{-}S)_2Cu(PPh_2Me)\}_4]$ ($R^N = (CMe_2CH_2CMeNNH)_2CO$) ließ sich durch Verbrückung der Liganden durch Carbohydrazid synthetisieren. Die drei Verbindungen zeigt Abbildung 1.11.

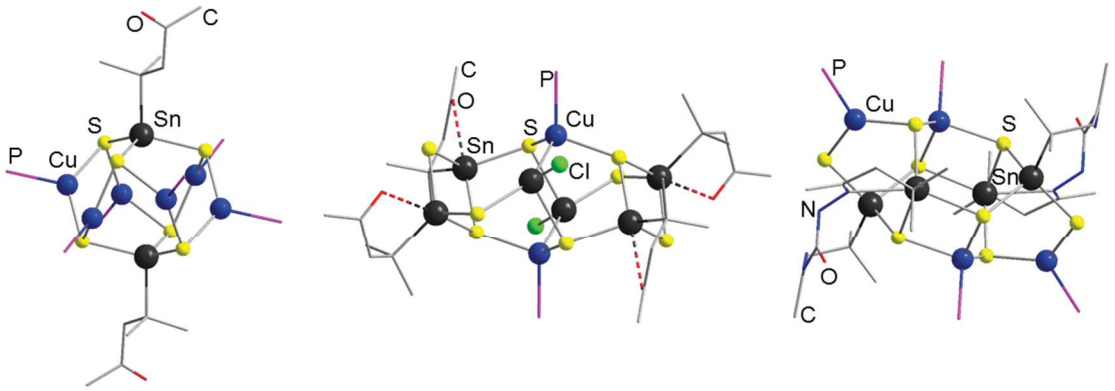

Abbildung 1.11: Drei durch Kupferatome erweiterte Organozinnsulfidcluster mit unterschiedlichen Topologien. Links: $[(R^1SnS_3)_2(CuPPh_3)_6]$.[77] Mitte: $[\{(R^1Sn)_2S_4\}_2(CuPPh_3)_2(SnCl)_2]$.[96] Rechts: $[R^N_2\{Sn(\mu\text{-}S)_2Cu(PPh_2Me)\}_4]$.[97]

Zudem gibt es einen gemischten Sulfid/Selenid-Cluster mit Ferrocenylliganden, $[(FcSnE_3)_2(CuPPh_3)_6]$ (Fc = Ferrocenyl, E = S, Se im Verhältnis 2,75 zu 3,25), mit $[Cu_6Sn_2E_6]$-Grundgerüst isotyp zu dem in Abbildung 1.11 gezeigten Cluster $[(R^1SnS_3)_2(CuPPh_3)_6]$. Der gemischte Cluster lässt sich durch Reaktion eines AD-Typ-Zinnselenidclusters mit Na_2S und $[Cu(PPh_3)_3Cl]$ herstellen.[89]

Es existieren wenige auf andere Art hergestellte Organozinnselenidcluster mit ternärem Grundgerüst. Es handelt sich zum einen um die trigonal-bipyramidal aufgebauten Verbindungen $[(ML_z)_2(\mu_3\text{-}Se)_2(R_XX_ySn)]$ (M = Co, Ru, Os, Pt)[98–100] und zum anderen durch Kombinationen von $[R_2SnSe_x]$- mit $[(ML_z)_2(\mu_3\text{-}Se)_2]$-Einheiten.[100] In diesen Verbindungen sind lediglich unreaktive organische Substituenten an einem einzigen Zinnatom vorhanden.

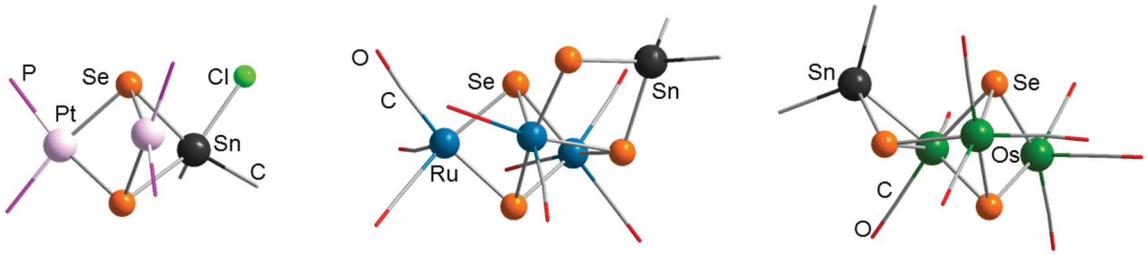

Abbildung 1.12: Bisher bekannte Organozinnselenidcluster mit ternärem Grundgerüst. Links: $[Pt_2(PPh_3)_4Se_2(SnMe_2Cl)]^+$.[99] Mitte: $[Ru_3(CO)_7(H_2O)Se_4(Sn(Tb)Tip)]$ (Tb = 2,4,6,-Tris[bis(trimethylsilyl)methyl; Tip = 2,4,6-Triisopropylphenyl).[100] Rechts: $[Os_3(CO)_8Se_3(Sn(Tb)Tip)]$.[100] Die Tb- und Tip-Gruppen an den Zinnatomen wurden aus Übersichtlichkeitsgründen zu Methylgruppen vereinfacht.

2. Motivation und Zielsetzung

Zinnsulfidcluster mit organischer Funktionalität haben eine große Strukturvielfalt und bieten die Möglichkeit zur weiteren Modifikation am organischen Liganden und im anorganischen Grundgerüst. Die einzigen bekannten Orgnaozinnselenidcluster waren vor Beginn dieser Dissertation Moleküle vom AD-Typ mit inerten Liganden und Verbindungen mit DHK-Strukturmotiv. Es lag daher nahe, die Erkenntnisse der Sulfidchemie auf entsprechende Selenidverbindungen zu übertragen. Während der vorangegangenen Masterarbeit wurde die Synthese des Organozinnselenidclusters $[(R^1Sn)_4Se_6]$ mit DHK-Topologie optimiert, dessen Bildungsmechanismus untersucht und erste Reaktivitäten gegenüber Hydrazin(derivaten) und sowie $[Cu(PPh_3)_3Cl]$ überprüft. Diese Ergebnisse wurden zusammen mit den direkt darauf aufbauenden Untersuchungen zu Beginn der Dissertation in der ersten der im Anschluss vorgestellten Veröffentlichungen besprochen. Diese Arbeiten zeigten vor allen Dingen die Möglichkeit der Clustererweiterung bei Organozinnselenid-Systemen auf und stellten die Unterschiede zu den Produkten aus der entsprechenden Sulfidchemie heraus. Für die im Anschluss an diese ersten Untersuchungen geplante Forschung im Rahmen meiner Promotion ließen sich zwei Forschungsziele formulieren:

1. Synthese weiterer Organozinnselenidcluster mit zu bekannten Organozinnsulfidclustern isotyper oder neuartiger Topologie

   Dieses Ziel sollte durch Clusterbildung aus einem Organotrichlorostannan mit Keto-Funktionalität und $(SiMe_3)_2Se$ oder durch Modifikation der Ligandenhülle bereits bestehender Cluster mit Hydrazinen realisiert werden. Die Strukturmerkmale dieser Verbindungen sowie deren chemisches Verhalten sollte mit bekannten Schwefelverbindungen verglichen werden. Dieser Teil des Arbeitsauftrags der vorliegenden Dissertation ist in Schema 2.1 illustriert.

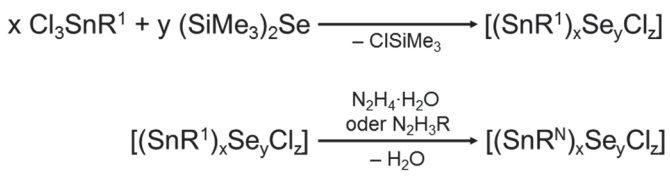

   Schema 2.1: Synthesechemische Vorgehensweise zur Darstellung neuer Organozinnselenidcluster. R^N = Hydrazonderivat als Ligand.

2. Erweiterung binärer Organozinnselenidcluster durch Übergangsmetallatome zu Clustern mit ternärem anorganischem Kern, analog zum Syntheseansatz von Merzweiler und Mitarbeitern.

   Auch hier sollte die Möglichkeit weiterer Derivatisierungen der organischen Liganden überprüft werden. Reaktionen dieser Art werden in Schema 2.2 vereinfacht dargestellt.

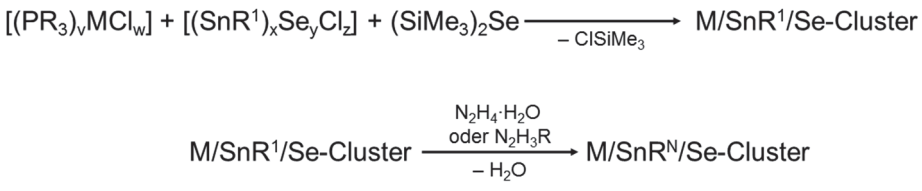

   Schema 2.2: Synthesechemische Vorgehensweise zur Darstellung neuer Organozinn-Metallselenidcluster.

Die Untersuchung aller Verbindungen sollte nach Möglichkeit durch Einkristallstrukturanalysen und NMR-Spektroskopie erfolgen und durch quantenchemische Rechnungen unterstützt werden. Vor allem im Falle von Verbindungen mit ternärem Grundgerüst war darüber hinaus die Untersuchung opto-elektronischer Eigenschaften geplant. Zusätzliche Analysemethoden wie Elementaranalyse, Massenspektrometrie, Schwingungs- und Mößbauerspektroskopie sollten gegebenenfalls die analytischen Daten komplettieren.

3. Kumulativer Teil

Die Forschungsarbeiten im Rahmen dieser Doktorarbeit haben zur Erstellung von vier Veröffentlichungen geführt, die in diesem Kapitel der Dissertation vorgestellt werden sollen.

3.1 „ Formation and Reactivity of Organo-Functionalized Tin Selenide Cluster"

Niklas Rinn, Jens P. Eußner, Willy Kaschuba, Xiulan Xie und Stefanie Dehnen, *Chem. Eur. J.* **2015**, *22*, 3094-3104.

3.2 „Ternary Mixed-Valence Organotin Copper Selenide Clusters"

Niklas Rinn, Lukas Guggolz, Jurek Lange, Sangam Chatterjee, Theresa Block, Rainer Pöttgen und Stefanie Dehnen, *Chem. Sci.* **2017**, eingereichtes Manuskript.

3.3 „Formation and Structural Diversity of Organo-Functionalized Silver-Tin-Selenide Clusters"

Niklas Rinn, Lukas Guggolz, Katharina Gries, Kerstin Volz, Jürgen Senker und Stefanie Dehnen, *Chem. Eur. J.* **2017**, eingereichtes Manuskript.

3.4 „ Trigonal Bipyramidal Metalselenide Clusters with Palladium and Tin Atoms in Various Postions"

Niklas Rinn, Lukas Guggolz, Katharina Hanau, Andre Rinn, Sangam Chatterjee und Stefanie Dehnen Z. Allg. *Anorg. Chem.* **2017**, eingereichtes Manuskript.

Zudem war ich Erstautor einer weiteren Veröffentlichung über peptidfunktionalisierte Zinnsulfidcluster, bei der ich die Forschungsarbeiten maßgeblich angestoßen und im Anschluss über die Betreuung einer Masterarbeit begleitet habe.

3.5 „Peptide – Functionalized Organotin Sulfide Clusters"

Niklas Rinn, Jan-Philipp Berndt, Annikka Kreher, Radim Hrdina, Matthias Reinmuth, Peter R. Schreiner, Stefanie Dehnen, *Organometallics*, **2016**, *35* (18), 3215-3220.

3.1. Formation and Reactivity of Organo-Functionalized Tin Selenide Cluster

Niklas Rinn, Jens P. Eußner, Willy Kaschuba, Xiulan Xie and Stefanie Dehnen, *Chem. Eur. J.* **2015**, *22*, 3094-3104.

Abstract: Reactions of R^1SnCl_3 ($R^1 = CMe_2CH_2C(O)Me$) with $(SiMe_3)_2Se$ yield a series of organo-functionalized tin selenide clusters, $[(SnR^1)2SeCl_4]$ (**1**), $[(SnR^1)_2Se_2Cl_2]$ (**2**), $[(SnR^1)_3Se_4Cl]$ (**3**), and $[(SnR^1)_4Se_6]$ (**4**), depending on the solvent and ratio of the reactants used. NMR experiments clearly suggest a stepwise formation of **1** through **4** by subsequent condensation steps with the concomitant release of Me_3SiCl. Furthermore, addition of hydrazines to the keto-functionalized clusters leads to the formation of hydrazone derivatives, $[(Sn_2(\mu\text{-}R^3)(\mu\text{-}Se)Cl_4]$ (**5**, $R^3 = [CMe_2CH_2CMe(NH)]_2$), $[(SnR^2)_3Se_4Cl]$ (**6**, $R^2 = CMe_2CH_2C(NNH_2)Me$), $[(SnR^4)_3Se_4][SnCl_3]$ (**7**, $R^4 = CMe_2CH_2C(NNHPh)Me$), $[(SnR^2)_4Se_6]$ (**8**), and $[(SnR^4)_4Se_6]$ (**9**). Upon treatment of **4** with $[Cu(PPh_3)_3Cl]$ and excess $(SiMe_3)_2Se$, the cluster fragments to form $[(R^1Sn)_2Se_2(CuPPh_3)_2Se_2]$ (**10**), the first discrete Sn/Se/Cu cluster compound reported in the literature. The derivatization reactions indicate fundamental differences between organotin sulfide and organotin selenide chemistry.

Inhaltsangabe: Die Synthese und Charakterisierung von Organozinnselenidclustern mit funktionellen organischen Liganden wird beschrieben. Die Verbindungen $[(R^1Sn)_xSe_yCl_z]$ können aus einem Reaktionsgemisch von R^1SnCl_3 und $(SiMe_3)_2Se$ isoliert werden, wobei ein höherer $(SiMe_3)_2Se$-Anteil zu Clustern mit größerem anorganischem Grundgerüst führt. So entstehen nacheinander $[(SnR^1)_2SeCl_4]$ (**1**), $[(SnR^1)_2Se_2Cl_2]$ (**2**), $[(SnR^1)_3Se_4Cl]$ (**3**), und $[(SnR^1)_4Se_6]$ (**4**). Diese Reaktionskaskade ließ sich mittels ^{1}H- und ^{119}Sn-NMR-spektroskopischen Studien verfolgen, die durch quantenchemische Rechnungen unterstützt wurden. Durch die Wahl eines geeigneten Lösungsmittels ließen sich einzelne Verbindungen ausfällen. Das auf diese Weise in Toluol gewonnene Pulver von **3** wurde durch ^{119}Sn-magic-angle-spinning-NMR-Spektroskopie (MAS-NMR-Spektroskopie) genauer untersucht. So wurde sichergestellt, dass es sich bei der Verbindung nicht um $[(SnR^1)_3Se_4][SnCl_3]$ handelte. Reaktivitäten der einzelnen Verbindungen gegenüber Hydraziden wurden überprüft. Dadurch konnten mit Hydrazinhydrat die Verbindungen $[(Sn_2(\mu\text{-}R^3)(\mu\text{-}Se)Cl_4]$ (**5**, $R^3 = [CMe_2CH_2CMe(NH)]_2$), $[(SnR^2)_3Se_4Cl]$ (**6**) und $[(SnR^2)_4Se_6]$ (**8**), sowie mit Phenylhydrazin $[(SnR^4)_3Se_4][SnCl_3]$ (**7**, $R^4 = CMe_2CH_2C(NNHPh)Me$) und $[(SnR^4)_4Se_6]$ (**9**) isoliert und charakterisiert werden. Das chemische Verhalten **3** gegenüber $[Cu(PPh_3)_3Cl]$ in Anwesenheit von $(SiMe_3)_2Se$ wurde überprüft. Hierbei konnte ein Cluster mit einem HK-Grundgerüst isoliert werden: $[(R^1Sn)_2Se_2(CuPPh_3)_2Se_2]$ (**10**). Alle Verbindungen wurden durch Einkristallstrukturanalyse strukturell charakterisiert und (mit Ausnahme von **10**) auch mittels NMR-Methoden weiter untersucht. Die Ergebnisse dieser Veröffentlichung sind in Abbildung 3.1 dargestellt.

Eigener Anteil: Alle Reaktionen wurden von mir geplant und alle analytischen Daten wurden von mir ausgewertet. Alle Reaktionen wurden von mir durchgeführt – mit Ausnahme derjenigen, die zur Bildung der Verbindungen **5**, **9** und **10** führten (unter meiner Anleitung durchgeführt von Willy Kaschuba im Rahmen seiner Bachelorarbeit. Die Verbindungen **1**–**3** sowie die NMR-Bildungsstudie bis hin zu **3** wurden von mir bereits in meiner Masterarbeit beschrieben. Auch die Verbindungen **6** und **7** wurden bereits im Rahmen der Masterarbeit charakterisiert. Die röntgenographischen Daten (bis auf die zu **1** und **10**) wurden von mir selbst aufgenommen. Dr. Jens P. Eußner, der meine Masterarbeit betreute, führte die Einkristallstrukturanalyse von Verbindung **1** durch, die zentrale Abteilung für Kristallstrukturanalyse am Fachbereich Chemie der Philipps-Universität Marburg unter der Leitung von Dr. Klaus Harms löste die Struktur von Verbindung **10**. ^{1}H- und ^{13}C-NMR-Experimente wurden von mir, ^{77}Se- und ^{119}Sn-NMR zu **3** von Prof. Dr. Berthold Hoge und Michael Grasse an der Universität Bielefeld durchgeführt. Weitere ^{119}Sn-NMR Experimente, sowohl im Festkörper als auch in Lösung, erfolgten unter Anleitung von Dr. Xiulan Xie in der

zentralen NMR-Abteilung des Fachbereichs Chemie an der Philipps-Universität Marburg. Raman-Spektren wurden von Dr. Istemi Kuzu, Infrarot-Spektren (IR-Spektren) wurden von mir gemessen. Energiedispersive Röntgenspektroskopie (EDX) wurde ebenfalls von mir durchgeführt. Auch alle quantenchemischen Rechnungen habe ich selbst durchgeführt. Das Manuskript habe ich in Kooperation mit Prof. Dr. Stefanie Dehnen verfasst. Die Co-Autoren haben jeweils kurze Abschnitte über ihre Beiträge eingefügt oder die von uns vorgeschlagenen Abschnitte dazu überarbeitet.

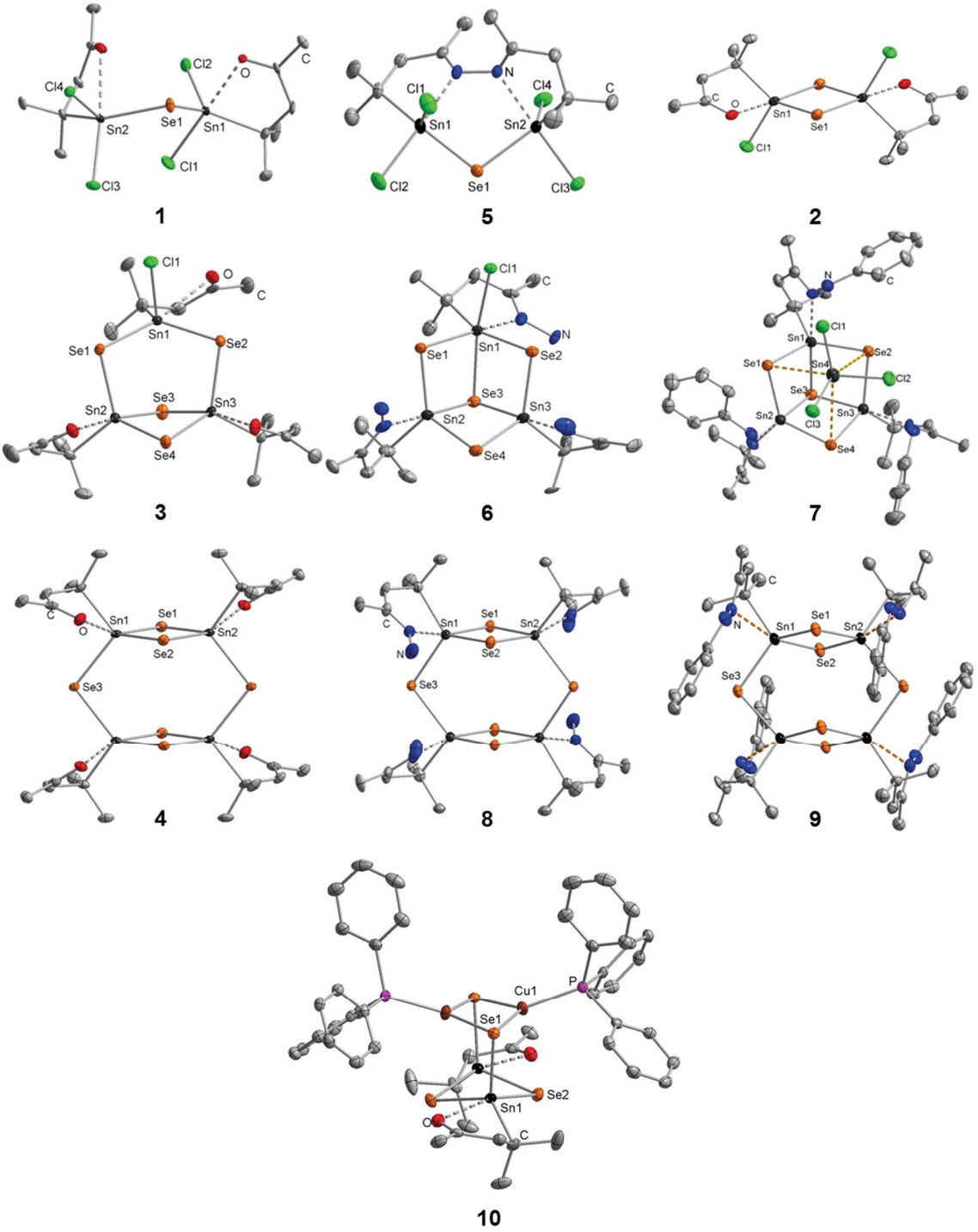

Abbildung 3.1: In „Formation and Reactivity of Organo-Functionalized Tin Selenide Cluster" beschriebene Molekülstrukturen. Wasserstoffatome wurden aus Übersichtlichkeitsgründen nicht angezeigt.

ChemPubSoc Europe

DOI: 10.1002/chem.201503562

CHEMISTRY A European Journal Full Paper

Tin Selenide Clusters

Formation and Reactivity of Organo-Functionalized Tin Selenide Clusters

Niklas Rinn, Jens P. Eußner, Willy Kaschuba, Xiulan Xie, and Stefanie Dehnen*[a]

Abstract: Reactions of R^1SnCl_3 ($R^1 = CMe_2CH_2C(O)Me$) with $(SiMe_3)_2Se$ yield a series of organo-functionalized tin selenide clusters, $[(SnR^1)_2SeCl_4]$ (**1**), $[(SnR^1)_2Se_2Cl_2]$ (**2**), $[(SnR^1)_3Se_4Cl]$ (**3**), and $[(SnR^1)_4Se_6]$ (**4**), depending on the solvent and ratio of the reactants used. NMR experiments clearly suggest a stepwise formation of **1** through **4** by subsequent condensation steps with the concomitant release of Me_3SiCl. Furthermore, addition of hydrazines to the keto-functionalized clusters leads to the formation of hydrazone derivatives, $[(Sn_2(\mu\text{-}R^3)(\mu\text{-}Se)Cl_4]$ (**5**, $R^3 = [CMe_2CH_2CMe(NH)]_2$), $[(SnR^2)_3Se_4Cl]$ (**6**, $R^2 = CMe_2CH_2C(NNH_2)Me$), $[(SnR^4)_3Se_4][SnCl_3]$ (**7**, $R^4 = CMe_2CH_2C(NNHPh)Me$), $[(SnR^2)_4Se_6]$ (**8**), and $[(SnR^4)_4Se_6]$ (**9**). Upon treatment of **4** with $[Cu(PPh_3)_3Cl]$ and excess $(SiMe_3)_2Se$, the cluster fragments to form $[(R^1Sn)_2Se_2(CuPPh_3)_2Se_2]$ (**10**), the first discrete Sn/Se/Cu cluster compound reported in the literature. The derivatization reactions indicate fundamental differences between organotin sulfide and organotin selenide chemistry.

Introduction

The chalcogenidometalate family encompasses a broad spectrum of compounds with a multitude of applications stemming from their tunable optoelectronic and semiconducting properties;[1–6] a large subgroup of this family are the chalcogenidotetrelates.[7,8] A characteristic feature of tin chalcogenide chemistry is the reoccurrence of topologies, such as the $[Sn_3E_4]$ defect—a heterocubane unit (DC, E = S, Se), most often aggregated through further E atoms into frameworks[9–11]—or the adamantane-like $[Sn_4E_6]$ tin sesquichalcogenide unit (AD), which is also known for a few tin telluride clusters (E = Te).[12,13]

By attaching organic ligands to the tin atoms in chalcogenidostannate complexes or clusters, discrete AD-type clusters were obtained, at first with rather unreactive organic ligands such as phenyl or methyl groups.[14,15] The utilization of organic ligands that additionally comprise Lewis basic sites, such as carbonyl or carboxylate functionalities, enabled the stabilization of discrete clusters with DC topology through additional intramolecular O→Sn coordination, shown first for the anionic cluster $Na_2[(SnR^{COO})_3S_4]$ ($R^{COOH} = C_2H_4COO$).[16] However, such ligands are also suitable for the stabilization of an isomeric tin sesquisulfide $[Sn_4S_6]$ architecture, namely the so-called "double-decker" (DD) topology.[17] Different from the AD structure, two parallel four-membered $[(RSn)_2(\mu\text{-}S)_2]$ rings are connected here by two Sn–(μ-S)–Sn bridges. As confirmed by DFT calculations, the DD topology is favored over the isomeric AD scaffold as soon as intramolecular O→Sn coordination is possible.

The first neutral DC tin sulfide cluster, $[(SnR^1)_3S_4Cl]$ ($R^1 = CMe_2CH_2C(O)Me$), was obtained by reaction of R^1SnCl_3 (A) with $(SiMe_3)_2S$.[18] Investigations of this system have shown that different cluster topologies can be selectively and systematically obtained by tuning the Sn/S ratio of the corresponding precursor mixture, thereby initiating a stepwise reaction cascade between R^1SnCl_3 and $S(SiMe_3)_2$ with the concomitant release of Me_3SiCl. It passes through the formation of mononuclear or dinuclear complexes $[(SnR^1)_2SCl_4]$ and $[(SnR^1)_2S_2Cl_2]$, prior to the assembly of clusters with DC and finally DD topology upon addition of further equivalents of $S(SiMe_3)_2$. Further compounds with $[Sn_2S_2]$ four-membered rings, similar to the second intermediate $[(SnR^1)_2S_2Cl_2]$, have been reported to be stabilized either by bulky ligands (e.g., R = *t*-butyl) or by ligands that allow for intramolecular ligand→Sn coordination, such as observed for $[Sn(\{CH_2\}_3NMe_2)_2S]_2$.[19]

Post-derivatization of organo-functionalized tin sulfide clusters is possible either at the organic ligands or through introduction of further metal atoms into the inorganic core. In particular, hydrazine and its derivatives have been used to form hydrazones in condensation reactions with R^1, for example, forming $[(SnR^2)_4S_6]$ ($R^2 = CMe_2CH_2C(NNH_2)Me$) with DD topology from the corresponding R^1-decorated compound by using hydrazine hydrate.[16] More bulky hydrazines, such as 2,2′-bispyridyl ketone hydrazine, can trigger a rearrangement of the DD-type cluster structure to form a DC-like unit, such as observed for $[(SnR^{bispy})_3S_4]^+$ ($R^{bispy} = CMe_2CH_2C(Me)NNC(2\text{-}py)_2$).[20] In all of these cases, intramolecular N–Sn bonding occurs, which is important for the stability of the structures; similar to other polynuclear aggregates with N→Sn stabilized Sn=E units (E = S, Se, Te).[21] An example for the extension of the inorganic core is given by the reaction of $[(SnR^1)_4S_6]$ with Na_2S (as a sul-

[a] N. Rinn, Dr. J. P. Eußner, W. Kaschuba, Dr. X. Xie, Prof. Dr. S. Dehnen
Fachbereich Chemie and Wissenschaftliches Zentrum für Materialwissenschaften (WZMW), Philipps-Universität Marburg
Hans-Meerwein-Straße, 35043 Marburg (Germany)
E-mail: dehnen@chemie.uni-marburg.de

Supporting information for this article is available on the WWW under http://dx.doi.org/10.1002/chem.201503562.

fide source to initially break up the original cluster scaffold) and $[Cu(PPh_3)_3Cl]$. This yielded $[(R^1Sn)_2(CuPPh_3)_6S_6]$, a cluster compound with a ternary inorganic core.[16]

The chemistry of discrete organotin selenide compounds shows a lower diversity thus far, even though several examples based on binuclear Sn/Se units, as mentioned above for the lighter homologs, have been reported.[21–24] The first clusters with DC or AD topologies, respectively, $[(SnCp(CO)_2Fe)_3Se_4Cl]$ and $[(SnCp(CO)_2Fe)_4Se_6]$ (Cp = cyclopentadienyl), were synthesized by using $\{Cp(CO)_2Fe\}SnCl_3$ as a precursor.[24] The first DC-type tin selenide cluster with purely organic ligands to be published was $[Na(MeOH)_2][R^{COO}(R^{COO}H)_2Sn_3Se_4][R^{COO}{}_2(R^{COO}H)Sn_3Se_4]$, obtained by in situ generation of Na_2Se in liquid ammonia and subsequent addition of $R^{COO}HSnCl_3$.[25] Recent work in our group has showcased the chemistry of Sn/Se[18] as well as Sn/Te clusters[26] starting from R^1SnCl_3 (**A**) and $(SiMe_3)_2Se$ (**B**) or $(SiMe_3)_2Te$ as precursors in room-temperature syntheses. The ionic compound $[(SnR^1)_3Se_4][SnCl_3]$ (**C**) was obtained upon redissolving the white precipitate that formed on treatment of **A** with **B** in toluene. The corresponding hydrazone derivative $[(SnR^2)_3Se_4][SnCl_3]$ (**D**) resulted from the reaction of **C** with hydrazine hydrate (Scheme 1).[18]

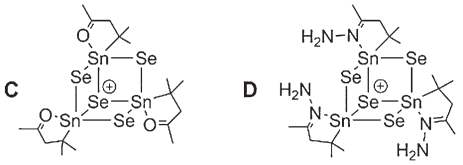

Scheme 1. Structural diagram of the cluster cations in compounds **C** and **D**.

Herein, we present the results of a systematic extension of the preliminary studies into (RSn)/Se chemistry. Upon changing the ratio of **A** and **B** from 2:3 to an excess of **A**, two intermediates from the formation process of **C** were isolated: $[(SnR^1)_2SeCl_4]$ (**1**) at a 4:1 ratio and $[(SnR^1)_2Se_2Cl_2]$ (**2**) at a 2:1 ratio, which can formally be described as condensation products of **A** with one or two equivalents of **B**, respectively. This correlates with the idea of a step-wise formation in analogy with the observations made in (RSn)/S cluster chemistry. A systematic study of the whole reaction also included the investigation of the white precipitate that had been obtained and redissolved prior to the isolation of **C**. It was shown by means of ^{119}Sn magic angle spinning (MAS) NMR spectroscopy that the powder does not contain **C** but another compound, which prompted us to also re-visit the crystalline material. Indeed, the latter turned out to be a mixture of **C** and a second cluster compound, $[(SnR^1)_3Se_4Cl]$ (**3**), which was previously overlooked as both **C** and **3** form colorless blocks. By increasing the amount of **B** to 1.5 equivalents, a cluster with the maximum condensation level was obtained: $[(SnR^1)_4Se_6]$ (**4**). ^1H and ^{119}Sn NMR spectroscopy of the reaction solutions indicated an dynamic equilibrium between **A** and the diverse $[(SnR^1)_xSe_yCl_z]$ compounds.

Derivatization of **1** with hydrazine hydrate yielded $[(Sn_2(\mu\text{-}R^3)(\mu\text{-}Se)Cl_4]$ (**5**, $R^3 = [CMe_2CH_2CMe(N)]_2$), with the two ligand molecules connected by an N_2 unit. Compounds **3** and **4** reacted with hydrazine hydrate or phenylhydrazine, affording terminal hydrazone groups in $[(SnR^2)_3Se_4Cl]$ (**6**; co-crystallizing with **D**), $[(SnR^4)_3Se_4][SnCl_3]$ (**7**, $R^4 = CMe_2CH_2C(NNHPh)Me$), $[(SnR^2)_4Se_6]$ (**8**), or $[(SnR^4)_4Se_6]$ (**9**). The original cluster topologies were retained in all cases.

First experiments towards the incorporation of transition-metal atoms into the previously binary clusters have been carried out by addition of **B** and $[Cu(PPh_3)_3Cl]$ to compound **4**, leading to the formation of $[(R^1Sn)_2Se_2(CuPPh_3)_2Se_2]$ (**10**).

Results and Discussion

Synthesis

An overview of the reactions yielding compounds **1**–**10** is provided in Scheme 2. Compounds **1**–**3** were synthesized by condensation reactions of **A** with **B** in toluene, in a 1:0.25, 1:1, or 1:1.5 ratio, respectively, under elimination of $SiMe_3Cl$. Although **1** remains in solution and can only be isolated by crystallization through layering with *n*-hexane, **2** and **3** precipitate as colorless powders after 3 h of stirring at room temperature. Compound **4** is obtained by a similar reaction, however, with **A**/**B** = 1:1.5 in CH_2Cl_2 and subsequent layering with *n*-hexane. Compounds **5**–**9** were prepared by treating **1**, **3**, or **4** with stoichiometric amounts of either hydrazine hydrate or phenylhydrazine in CH_2Cl_2, with elimination of water. Through reaction of **4** with two equivalents of **B** and four equivalents of $[Cu(PPh_3)Cl]$ in $CHCl_3$, compound **10** was synthesized and obtained in single-crystalline form by layering with *n*-hexane.

Crystal structures

Compounds **B** and **1**–**10** were isolated as single crystals, and their crystal structures were determined by X-ray diffraction. Technical details, crystallographic data, and structural parameters are provided in Table 1 and Table 2 and in the Supporting Information. The molecular structures are shown in Figure 1 (**B**), Figure 2 (**1**–**9**), Figure 3 (details of **4**, **8**, and **9**), and Figure 4 (**10**).

The reactant **B** has been known for more than 50 years, but its crystal structure has not been determined so far.[27] We were able to grow single crystals by slow cooling of the pure liquid down to 233 K. Compound **B** crystallizes in the monoclinic space group *C2/c* (Figure 1) with an Si-Se-Si angle of 104.3(1)°.

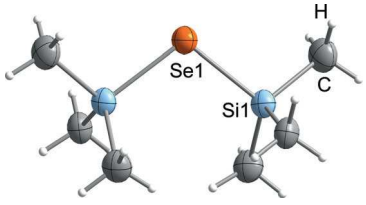

Figure 1. Molecular structure of compound **B**. Ellipsoids are drawn at the 50% probability level. H atoms are shown as white spheres with arbitrary radii.

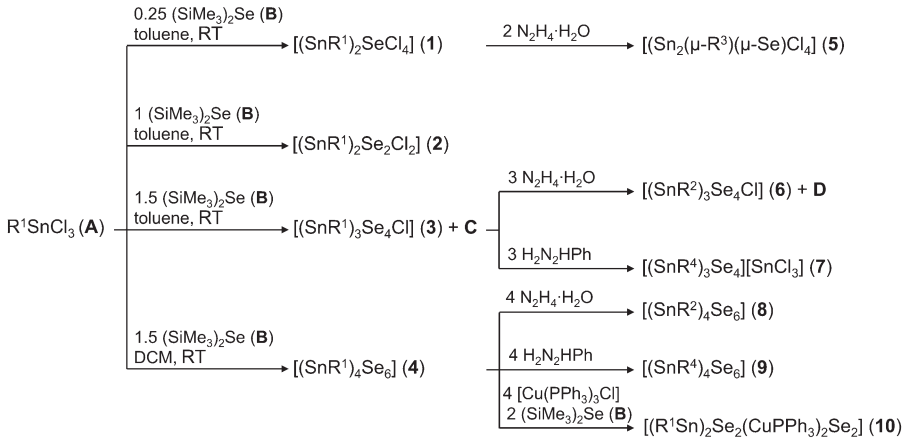

Scheme 2. Synthesis of compounds **1**–**10**.

Table 1. Crystallographic data and refinement results of **B** and **1**–**5**.

Compound	**B**	**1**	**2**	**3**	**4**	**5**
formula	$C_6H_{18}Si_2Se$	$C_{12}H_{22}Cl_4O_2SeSn_2$	$C_{12}H_{22}Cl_2O_2Se_2Sn_2$	$C_{18}H_{33}Cl_1O_3Se_4Sn_3$	$C_{24}H_{44}O_4Se_6Sn_4$	$C_{12}H_{22}Cl_4N_2SeSn_2$
F_w [g mol^{-1}]	224.34	656.50	664.56	1004.88	1345.23	652.51
crystal color and shape	colorless block	colorless plate	colorless needles	colorless block	colorless block	colorless block
crystal size [mm^3]	0.54×0.50×0.44	0.11×0.06×0.03	0.08×0.08×0.17	0.08×0.02×0.02	0.22×0.21×0.26	0.25×0.16×0.13
crystal system	monoclinic	orthorhombic	monoclinic	monoclinic	monoclinic	Monoclinic
space group	*C*2/*c*	*Pca*2$_1$	*P*2$_1$/*c*	*P*2$_1$/*n*	*P*2$_1$/*n*	*P*2$_1$/*n*
a [Å]	9.1640(16)	14.3741(6)	8.1131(5)	10.9022(12)	11.7850(12)	11.8143(6)
b [Å]	11.007(7)	13.4023(8)	11.7426(9)	12.7445(14)	12.8611(10)	12.8753(7)
c [Å]	11.651(2)	10.8570(4)	10.8968(7)	21.762(2)	12.6279(12)	14.7359(8)
α [°]	90	90	90	90	90	90
β [°]	102.588(15)	90	105.290(5)	101.647(4)	90.829(8)	110.553(2)
γ [°]	90	90	90	90	90	90
V [Å^3]	1147.0(3)	2091.6(2)	1001.4(1)	2961.4(5)	1913.8(3)	2098.8(2)
Z	4	4	2	4	2	4
ρ_{calcd} [g cm^{-3}]	1.305	2.085	2.204	2.254	2.334	2.090
μ(Mo$_{K\alpha}$) [mm^{-1}]	3.421	4.639	6.394	7.533	8.312	4.621
absorption correction type	multiscan	numerical	multiscan	multiscan	multiscan	multiscan
min./max. transmission	0.1010/0.1240	0.6775/0.8613	0.2286/0.4952	0.5960/1.0000	0.0856/0.1846	0.6128/0.7457
2θ range [°]	5.86/50.50	3.54/53.46	4.20/54.22	4.98/54.31	4.52/51.37	4.96/56.70
no. of meas. reflns	2616	19669	2873	19854	25137	55776
R(int)	0.1399	0.1081	0.0527	0.0539	0.1387	0.0361
indep. reflns	1036	4375	1559	6527	4025	5241
indep. reflns ($I>2\sigma(I)$)	685	4262	1394	5289	3841	4624
no. of parameters	45	196	94	262	178	230
R_1 ($I>2\sigma(I)$)/wR_2 (all data)	0.0989/0.1276	0.0425/0.1044	0.0521/0.11261	0.0347/0.0739	0.0200/0.0388	0.0319/0.0714
S (all data)	0.873	1.046	1.041	1.031	1.125	1.113
max. peak/hole/e$^-$ [Å^3]	0.945/−0.808	3.017/−1.748	1.607/−1.987	1.298/−1.193	0.506/−0.733	3.284/−1.328

Compound **1** crystallizes in the orthorhombic space group *Pca*2$_1$ and is based on a V-shaped Sn-Se-Sn unit (Sn-Se-Sn 102.39(2)°) with the Sn–Se distances (249.08(8) and 251.37(8) pm) being similar to those in reported Sn–Se-based compounds.[23] The ligands at the tin atoms adopt a trigonal bipyramidal coordination geometry, with the oxygen and one chloride ligand occupying the apical sites.

Compound **2** can be viewed as the next step in the condensation cascade initiated by subsequent addition of **B** to **A**, eventually leading to the formation of **4**. The compound crystallizes in the monoclinic space group *P*2$_1$/*c* with a second selenide atom being present. The inorganic core of the complex resembles a slightly rhombic four-membered ring (Se-Sn-Se 95.48(3)°, Sn-Se-Sn 84.52(3)°). All angles are more acute than those in **1** as expected for the four-membered ring. The coordination geometry at the tin atoms is trigonal bipyramidal as in **1** but the apical positions are occupied by an oxygen and a selenide ligand in this case, which naturally leads to an elongation of the Sn–Se bond (259.23(8) pm) as opposed to that in **1** (250.29(8) pm).

Compound **3** (monoclinic space group *P*2$_1$/*n*) is based on a DC scaffold as in **C**, but as opposed to the latter, the cluster is uncharged overall as it contains an additional chlorine ligand at Sn1, with a concurrent elongation of the Sn1–Se3 distance

Table 2. Crystallographic data and refinement results of (the solvates of) **6**–**10**.

Compound	**6**·2 CH_2Cl	**6**·3 CH_2Cl_2	**7**·C_7H_8	**8**	**9**	**10**·2 $CHCl_3$
formula	$C_{20}H_{43}Cl_5N_6Se_4Sn_3$	$C_{21}H_{45}Cl_7N_6Se_4Sn_3$	$C_{43}H_{59}Cl_3N_6Se_4Sn_4$	$C_{24}H_{52}N_8Se_6Sn_4$	$C_{48}H_{68}N_8Se_6Sn_4$	$C_{50}H_{54}O_2P_2Cl_6Se_4Sn_2Cu_2$
F_w [g mol^{-1}]	1216.85	1301.78	1557.03	1401.25	1705.71	1642.0
crystal color and shape	colorless block	colorless block	colorless block	colorless plate	colorless block	orange plate
crystal size [mm^3]	0.20×0.20×0.20	0.22×0.21×0.09	0.30×0.04×0.04	0.14×013×0.26	0.10×014×0.14	0.07×0.10×0.08
crystal system	triclinic	triclinic	monoclinic	monoclinic	triclinic	monoclinic
space group	$P\bar{1}$	$P\bar{1}$	$P2_1/c$	$P2_1/c$	$P\bar{1}$	$C2/c$
a [Å]	12.4797(16)	12.076(2)	11.1885(5)	10.7309(5)	10.7778(14)	17.9839(10)
b [Å]	13.4919(15)	13.539(2)	22.1742(11)	11.4101(5)	11.6720(15)	11.8962(6)
c [Å]	13.7615(16)	14.776(2)	22.2356(9)	16.7979(8)	12.3742(17)	27.6184(16)
α [°]	66.988(4)	69.844(6)	90	90	106.879(10)	90
β [°]	64.672(4)	71.549(7)	101.527(3)	96.823(4)	101.389(11)	92.208(5)
γ [°]	87.030(4)	69.936(7)	90	90	93.877(11)	90
V [Å^3]	1909.0(4)	2075.9(6)	5405.3(4)	2042.18(16)	1447.3(3)	5874.03(33)
Z	2	2	4	2	1	4
ρ_{calcd} [g cm^{-3}]	2.117	2.082	1.913	2.279	1.957	1.857
$\mu(Mo_{K\alpha})$ [mm^{-1}]	6.132	5.771	4.704	7.792	5.517	4.398
absorption correction type	multiscan	multiscan	numerical	numerical	numerical	numerical
min./max. transmission	0.3460/0.7455	0.6775/0.8613	0.3327/0.8342	0.2088/0.4992	0.4470/0.6570	0.4742/0.5493
2θ range [°]	4.58/54.36	4.12/54.32	3.68/53.44	3.82/54.27	3.53/54.28	2.96/53.48
no. of meas. reflns	26092	18478	30674	22408	24927	23706
R(int)	0.0574	0.1451	0.1044	0.1023	0.1478	0.0640
indep. reflns	8419	8855	11425	4327	6130	6124
indep. Reflns ($I > 2\sigma(I)$)	6264	5036	7429	2885	4918	4934
no. of parameters	423	370	544	196	304	310
R_1 ($I > 2\sigma(I)$)/wR_2 (all data)	0.0378/0.0837	0.0663/0.1751	0.0557/0.1198	0.0482/0.1101	0.0514/0.1334	0.0242/0.0405
S (all data)	1.008	1.015	0.927	0.953	0.967	0.920
max. peak/hole/e$^-$·[Å^3]	1.647/−1.828	3.030/−1.824	1.095/−1.929	1.610/−1.414	1.453/−1.912	0.511/−0.487

from 270.0(7)–274.5(1) pm in **C** to 346.79(7) pm in **3**. Thus, Sn1 retains its original trigonal bipyramidal coordination geometry, with the chloride ligand instead of selenide ligand, and Se3 retains its original μ-bridging function instead of becoming a μ_3-bridge as observed in **C**. The other interatomic distances involving Sn1, including the Sn···O contact, also slightly increased in **3** compared with the other tin atoms in **3** (276.8(4) pm for Sn1···O1 compared with 253.0(4) and 259.6(4) pm for Sn2/3···O2/3) and those in **C** (Sn···O 229.5(8)–236.5(8) pm). Different from **2**, the four-membered Sn2-Se3-Sn3-Se4 ring is inclined (dihedral angle Sn2-Se3-Sn3-Se4 = 20.17(2)°) as a consequence of the Se-SnClR^1-Se "handle" being attached at one side of the four-membered ring, whereas the two terminal Cl ligands coordinate at either side of the Sn_2Se_2 unit in **2**. The Sn-Se-Sn angles in **3** are 81.50(2) and 83.26(2)° and the Se-Sn-Se angles are 93.78(2) and 94.14(2)°.

Compound **4** (monoclinic space group $P2_1/n$) exhibits a DD-type topology, which can be regarded as an extension of **3** by adding a $[(R^1Sn)Se_2]^-$ unit, thereby replacing the Cl^- ligand at Sn1. The four-membered rings are nearly planar (Sn1-Se1-Sn2-Se2 = 0.27(1)°), with inner angles of 85.55(1)–85.73(1)° (Sn-Se-Sn) and 94.03(1)–94.68(1)° (Se-Sn-Se). The angle Sn1-Se3-Sn2′ at the selenium atom, which connects the two four-membered rings, amounts to 104.00(1)°. The Sn–Se distances are 251.56(3)–259.54(3) pm within the four-membered rings and 254.15(3), 254.51(3) pm for Sn–Se3. The Sn···O distances in **4** (270.9(2), 263.0(2) pm) are elongated compared with those previously discussed, with the exception of the Sn1—O bond in **3**.

Upon treatment of **1** with hydrazine hydrate, compound **5** is obtained. It crystallizes in the monoclinic space group $P2_1/n$. The inorganic Cl_2Sn–Se–$SnCl_2$ skeleton of **1** is retained during the reaction, but the organic ligands are linked by a ketazine bridge, thereby also forming a five-membered [Sn···N–N···Sn–S] ring through intermolecular N→Sn coordination (Sn···N = 230.3(3) and 235.2(3) pm). The Sn-Se-Sn angle in **5** is 106.01(2)°, which is similar to the Sn-Se-Sn angle in **1**. The Sn–Se distances are 251.23(5) and 253.61(7) pm. The N–N bond length in **5** (139.8(4) pm) is typical for a ketazine group, but is slightly smaller than the N–N bond in free hydrazine (146.86(1) pm).[28]

The hydrazine-functionalized compound **6** crystallizes in the triclinic space group $P\bar{1}$, as **6**·2 CH_2Cl_2 (**6a**), or in the monoclinic space group $P2_1/c$, as **6**·3 CH_2Cl_2 (**6b**), depending on the amount of solvent included. The cluster in **6** retained the DC-shaped Sn/Se topology of the keto-functionalized analog in **3**. However, in contrast to **3**, the chloride ligand in **6** does not provoke a significant elongation of the Sn1—Se3 bond (276.61(6) pm in **6a**, 277.1(1) pm in **6b**) compared with the corresponding distance found in compound **D** without a chloride ligand (273.65(8) pm); this leads to a (distorted) octahedral coordination sphere at Sn1 in **6**. The Sn···N distances, approximately 237 pm, are shorter and fall within a smaller range than the Sn···O distances in **3**, with 276.8(4) pm for Sn1···O1 and 253.0(4) pm/256.9(4) pm for the other Sn···O contacts.

The formation of the ionic compounds **C** or **D** from the neutral compounds **3** or **6**, and their subsequent co-crystallization, can be attributed to a (partial) decomposition of the neutral species in solution with reductive formation of the $[Sn^{II}Cl_3]^-$ counterion and oxidation of the ligand R^1, as discussed previously.[18, 26, 29]

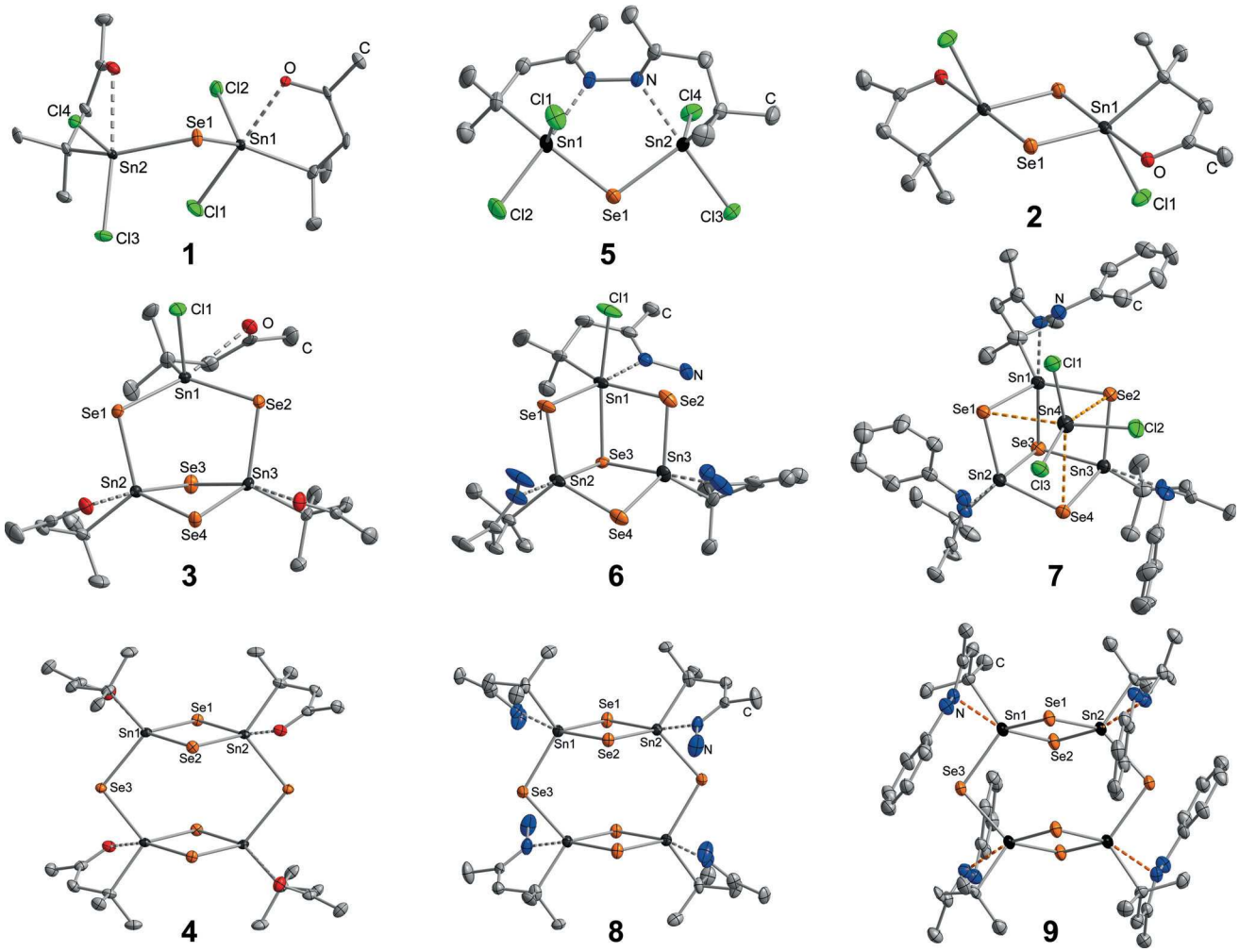

Figure 2. Molecular structures of compounds **1**–**9**; all species except **2** are ordered with regard to the topology of their inorganic core (horizontally) and the type of the organic functionality (vertically). Longer contacts are highlighted by orange dashed lines. Ellipsoids are drawn at the 50% probability level; hydrogen atoms are omitted for clarity.

The phenylhydrazone derivative **7** is obtained in crystalline form as **7**·C_7H_8, which crystallizes in the monoclinic space group $P2_1/c$. Compound **7** comprises a cationic DC-type cluster, whereas a neutral cluster with an additional chloride ligand has so far not been observed. The main difference from the structure of **D** is the location of the $[SnCl_3]^-$ counter anion. The corresponding tin atom, Sn4, is located above the defect site of the DC structure, 435.28(8)–455.70(9) pm from Se1, Se2, and Se4. Overall, the structure can be described as a strongly distorted heterocubane with the Sn–Se3 bonds being 268.7(1)–272.7(1) pm.

The DD-type cluster in **4** was also transformed into its hydrazone and phenyl hydrazone derivatives with retention of the DD topology. The hydrazone-functionalized compound **8** crystallizes in the monoclinic space group $P2_1/c$. The Se–Sn distances in the four-membered ring are 253.07(12) and 250.31(12) pm, or 266.17(11) and 262.34(11) pm, dependent on the position of the Se atom relative to the hydrazone N atom, which provokes a distinct elongation of the Se–Sn distance when located in the *trans* position. The distortion is larger than that observed in **4**. The Sn···N distances in **8** (243.1(8) and 244.3(8) pm) are shorter than the Sn···O distances in **4**, but significantly larger than the corresponding contacts in **6**.

Compound **9** crystallizes in the triclinic space group $P\bar{1}$. It is worth mentioning that for the Sn/S system, a structural reorganization of the inorganic core was observed when going from R^1 to R^4. When treating **E** with phenylhydrazine, the inorganic core undergoes a complete rearrangement of the DD topology to form two doubly μ-S-bridged DC clusters in $[(SnR^4)_4Sn_2S_{10}]$ (**G**).[16] In contrast to all other hydrazone-functionalized compounds presented in this work, the N donor atoms only show a very weak interaction with the Sn atoms, as indicated by rather large Sn···N distances (297.02(47) and 302.23(49) pm). Accordingly, the elongation of the Sn–Se bonds *trans* to the N→Sn interaction is only very small, with Se2–Sn1 = 255.44(8) pm and Se2–Sn2 = 254.98(7) pm, as opposed to 254.17(8) and 254.17(7) pm for the Se1–Sn bonds.

We assume that steric interactions between neighboring substituents inhibit the closer approach of the hydrazine groups to the Sn/S core. As another consequence of their

steric demand, both of the R^4 ligands that belong to the same four-membered ring point toward the same side of the Sn_4 plane of the entire cluster, rather than occupying alternating sides, as found in the other DD-based compounds **4** and **8**. This uneven occupation of space on both sides of the inorganic core comes along with a translational shift of the parallel four-membered rings against each other, with a tilt angle of 82.97(2)° (Figure 3).

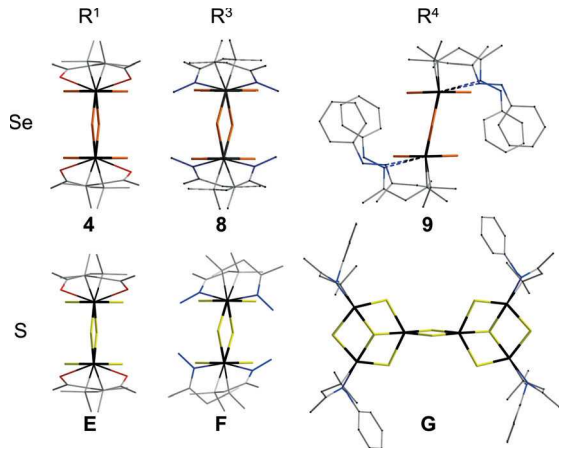

Figure 3. Molecular structures of the related compounds **4**, **8**, **9**, **E**, **F**, and **G**, shown along the Sn1···Sn2 axes for illustration of different structural details of the DD topology. The inorganic core is represented by bold wires; the organic ligand is drawn as thin lines. Hydrogen atoms are omitted for clarity.

The compounds with DD topology (**4**, **8**, and **9**) show slight structural differences regarding their inorganic $[Sn_4Se_6]$ cores compared with each other and the homologous sulfur compounds $[(SnR^1)_4S_6]$ (**E**, equivalent to **4**)[16] and $[(SnR^2)_4S_6]$ (**F**, equivalent to **8**, for details see the Supporting Information).[16,17] Selected structural parameters of these related compounds are given in Table S1 (in the Supporting Information).

None of the quoted compounds with DD topology show a notable twist of the four-membered rings against each other; they show a parallel alignment of their Sn–Sn vectors. The Sn-Sn-Sn angles within the Sn_4 plane are close to 90° in all cases, with a maximum deviation of 3.03(1)° in **9**. The S_4 or Se_4 planes spanned by S1, S2, S1′, and S2′ (**E**, **F**, **G**) or Se1, Se2, Se1′, and Se2′ (**4**, **8**, **9**), respectively, are also very regular with Se-Se-Se or the S-S-S angles close to 90°, except for **9**, where deviations of 12.44(1) or 12.47(1)° are observed, leading to the inclined architecture described above. This steric strain was assumed to be the reason for the rearrangement of the smaller Sn/S cores in **E** upon addition of phenylhydrazine, leading to **G**.[16] Clearly, the larger Sn–Se bonds, and, therefore, the overall larger size of the $[Sn_4Se_6]$ cluster core compared with the size of an $[Sn_4S_6]$ unit, means that the cluster is capable of being decorated by these bulky ligands, albeit with a notable distortion. Addition of hydrazine hydrate to **4** or **E** does not cause such structural perturbations. Only a slightly larger separation of the four-membered rings from each other and a larger deviation of the bridging μ-S or μ-Se atoms from the Sn_4 planes are observed. Interestingly, both effects are nearly negligible in **9**; the distance between the two Sn_2Se_2 rings is smaller in **9** than in **4**.

According to the synthesis protocol (see the Experimental Section), addition of $(SiMe_3)_2Se$ to **4** provoked nucleophilic cleavage of the double-decker Sn–Se–Sn bridges, thereby (intermediately) forming $[(R^1Sn)_2Se_4]^{2-}$ units that capture two $[CuPPh_3]^+$ units from the reacted copper complex in the formation of **10**, $SiMe_3Cl$, and PPh_3 (Scheme 3).

$$[(SnR^1)_4Se_6]\ (\mathbf{4}) + [Cu(PPh_3)_3Cl] + 2\ (SiMe_3)_2Se\ (\mathbf{B}) \xrightarrow{\text{DCM, RT}} 2\ [(R^1Sn)_2Se_2(CuPPh_3)_2Se_2]\ (\mathbf{10}) + 4\ SiMe_3Cl + 8\ PPh_3$$

Scheme 3. Stoichiometric reaction scheme for the synthesis of **10**.

The molecular structure of compound **10** (Figure 4) can be described as being composed of $[(R^1Sn)_2Se_2]$ and $[(PPh_3Cu)_2Se_2]$ subunits that are each connected through Sn–Se and Cu–Se bonds to the other moiety. Both four-membered rings are slightly corrugated, with dihedral angles of 8.81(1)° (Cu1-Se2-Cu1′Se2′) and 22.51(1)° (Sn1-Se1-Sn1′-Se1′). The Se1-Cu1-Se1′ and the Sn1-Se2-Sn1′ angles are tilted away from each other such that Cu1 and Se2 get further apart and do not interact. The Cu–Cu distance of 270.60(4) pm (see also Table S2 in the Supporting Information) is similar to those found in related compounds, such as $\{Cu(PtBu_3)Se(SiMe_3)\}_2$ (273.32(7) pm);[30] thus, $Cu(d^{10})\cdots Cu(d^{10})$ interactions are not expected to be present here.

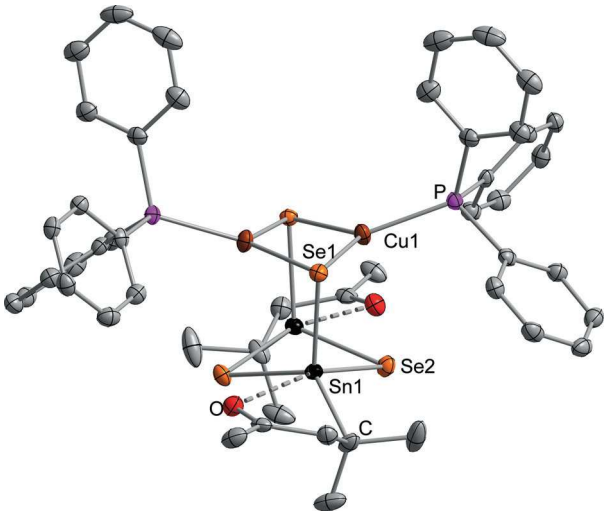

Figure 4. Molecular structure of compound **10**. Ellipsoids are drawn at the 50% probability level and hydrogen atoms are omitted for clarity.

Formation studies

A $CDCl_3$ solution of the colorless powder that forms during the synthesis of **3** produces the ^1H NMR signals expected for the organic ligand. Two signals are found in the ^{119}Sn NMR spectrum, one with higher intensity, at −185 ppm, and one with lower intensity, at −187 ppm. This indicates the presence of **3**

in solution. The three Sn atoms are non-equivalent owing to the additional Cl ligand on Sn1. To check the composition of the white precipitate in the solid state, ^{119}Sn MAS NMR spectra were recorded at spinning speeds of 10.5 and 12.0 kHz, resulting in isotropic chemical shifts at $\delta_1 = -174$ ppm and $\delta_2 = -178$ ppm (Figure 5).

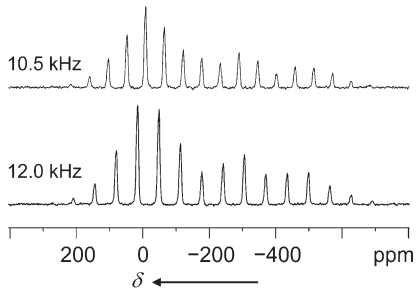

Figure 5. ^{119}Sn MAS NMR spectrum of **3** (187 MHz, 25 °C) at MAS speeds of 10.5 kHz (top) and 12.0 kHz (bottom). The simulated spectra are given in Figure S16 in the Supporting Information.

It was possible to separate the signals and determine the integral intensities by simulation, resulting in a ratio of 1:2 for I_1/I_2 (Figures S16 and S17 in the Supporting Information). Therefore, compound **3** seems to be the first and primary product of the synthesis, whereas **C** (with all-equivalent Sn atoms) is formed later on as a consequence of (partial) decomposition of **3** (see above). When dissolving single crystals of **1** and **2** in $CDCl_3$, signals corresponding to **A**, **3**, and an (intermediate) unidentified species **Z** are observed both in the ^{119}Sn and the ^{1}H NMR spectra (Figure 6). The two experiments produced spectra with identical chemical shifts but differing signal intensities. For the solution of **1**, the ratio **3**/**A**/**Z** was determined to be 1:1.27:0.77, whereas it is 1:1.14:0.82 for the solution of **2**. As the signal for **Z** is slightly larger in the solution of **1**, the observed intermediate should be a species closer to the open-chain compound **1**. We suggest that **Z** is an anionic $[(SnR^1)Se]^-$ fragment, which is also in agreement with the findings from ^{119}Sn spectroscopy; however, **Z** has not been isolated nor otherwise proven so far.

To get a deeper insight in the formation process of the keto-functionalized compounds **1**–**4**, reaction solutions of the syntheses of **1** (**A**/**B** ratio of 1:0.25) or **4** (**A**/**B** ratio of 1:1.5), respectively, and a solution with a 1:1.4 interim ratio of **A**/**B** with regard to the formation of **3** (1:1.33) and **4** (1:1.5) in $CDCl_3$ were investigated by means of time-dependent ^{119}Sn NMR spectroscopy. The recording was started 5 min after addition of **B** to a solution of **A** and repeated at 30 min intervals over a time span of 10 h. The spectra of the reaction solution leading to **1** show only signals for **A** and **Z** (with **Z** being the main product) and no change to be noticed over 10 h of observation (see the Supporting Information). Thus, the reaction seems to be complete within a few minutes. Similarly, the formation of **4** is completed after a reaction time of 5 min, with

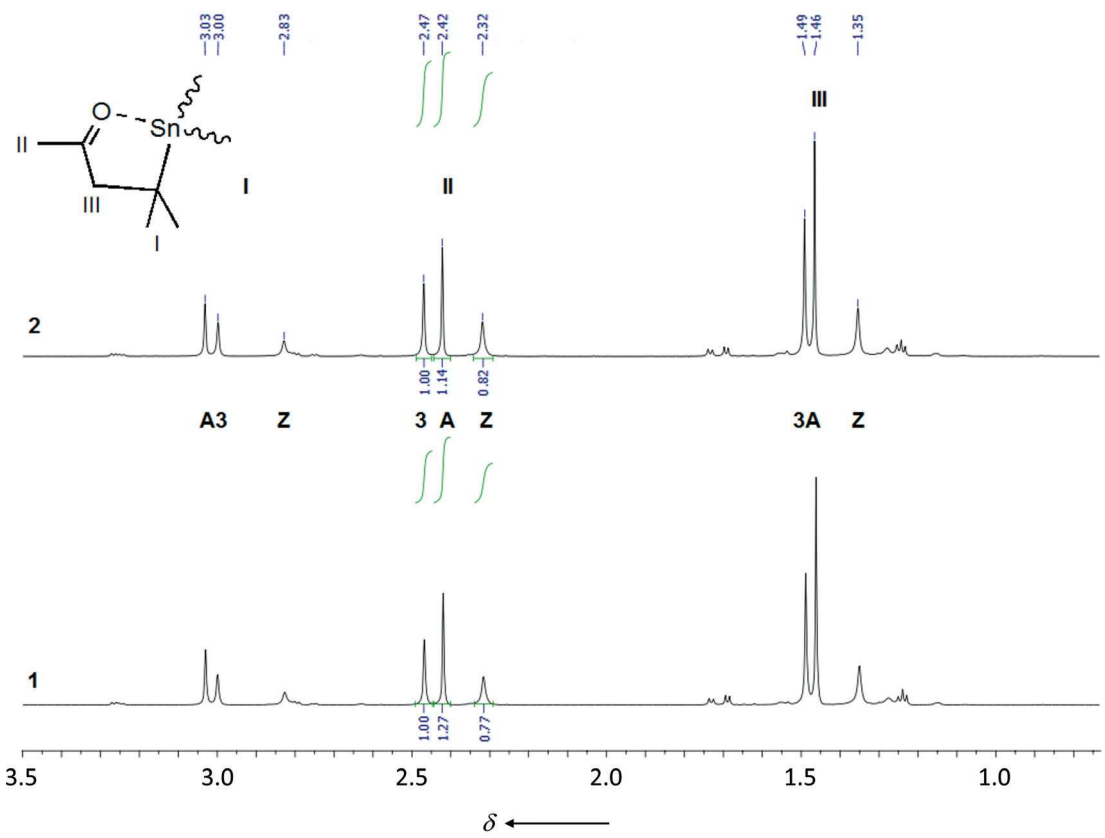

Figure 6. ^{1}H NMR spectrum of solutions of single crystals of **1** (bottom) and **2** (top) in $CDCl_3$.

no further signal changes over the observed period of 10 h (see the Supporting Information). However, the slightly lower excess of **B**, leading to incomplete formation of **4**, allows for the stepwise transformation of **A** to **4** through **Z** and **3** to be monitored (Figure 7). After 5 min, the reactive solution still produces signals of compound **3**, with those of **Z** and **3** at similar intensities, and that of **A** appearing as a minor signal. After 30 min, **3** is the only product observed, with the signal of **4** growing after 60 min and reaching its relative maximum after 3 h, prior to the appearance of a further set of as-yet unidentified products that form at the expense of **4**.

DFT calculations using the program system TURBOMOLE[29] were carried out to analyze the condensation cascade from **A** to **4** more closely. When comparing the energies of the reactants and products at each step, an energy gain can be observed (Table 3), thus indicating a continuous stabilization of the compounds with increasing size.

Table 3. Energy differences of the reactants and products in the condensation cascade leading to the formation of compound **4** according to DFT calculations.[a]

Compound	Reaction	Relative energy [kJ mol^{-1}]
1	$2\,\mathbf{A}+\mathbf{B}\rightarrow\mathbf{1}+2\,Me_3SiCl$	−64.05
2	$\mathbf{1}+\mathbf{B}\rightarrow\mathbf{2}+2\,Me_3SiCl$	−83.73
3	$\mathbf{2}+\mathbf{A}+2\,\mathbf{B}\rightarrow\mathbf{3}+4\,Me_3SiCl$	−106.41
4	$\mathbf{3}+2\,\mathbf{A}+2\,\mathbf{B}\rightarrow\mathbf{4}+4\,Me_3SiCl$	−124.92

[a] **A** = Cl_3SnR^1, **B** = $(SiMe_3)_2Se$.

Conclusions

A cascade of condensation reactions of R^1SnCl_3 (**A**) with $(SiMe_3)_2Se$ (**B**; characterized crystallographically for the first time here) yields four different clusters, **1**–**4**, in a stepwise manner. Time-dependent ^{119}Sn NMR spectroscopy and DFT calculations support the reaction sequence. As neither **1** nor **2** were detected, we propose that a dynamic equilibrium exists between **A**, an organotin selenide fragment **Z**, and **3** in solution, whereas **1** and **2** appear to be stable only in the crystalline form. The nature of **Z** has yet to be explored. Furthermore, we have shed light on reactions that were previously assumed to yield only cationic cluster species (**C** and **D**), but have actually been shown here, by crystallographic and ^{119}Sn MAS NMR experiments, to form neutral clusters **3** and **6** that (partially) decompose with the formation of the afore-known species.

The new compounds were further functionalized by hydrazine or phenylhydrazine with retention of their inorganic cores (compounds **5**–**9**), thus illustrating the fundamental difference between organotin sulfide and organotin selenide cluster chemistry.

Finally, the transformation of an organotin selenide cluster into a derivative with a ternary cluster core was realized by reaction of **4** with excess **B** and $[Cu(PPh_3)_3Cl]$. The resulting cluster (compound **10**) represents the first discrete RSn/Se/Cu compound to be reported.

Experimental Section

General

All synthesis steps were carried out under an argon atmosphere and with the exclusion of moisture. $(SiMe_3)_2Se$ and $Cl_3SnCMe_2CH_2C(O)Me$ were obtained according to procedures reported in the literature.[31,32] Mesityl oxide and $N_2H_4{\cdot}H_2O$ were purchased from Aldrich.

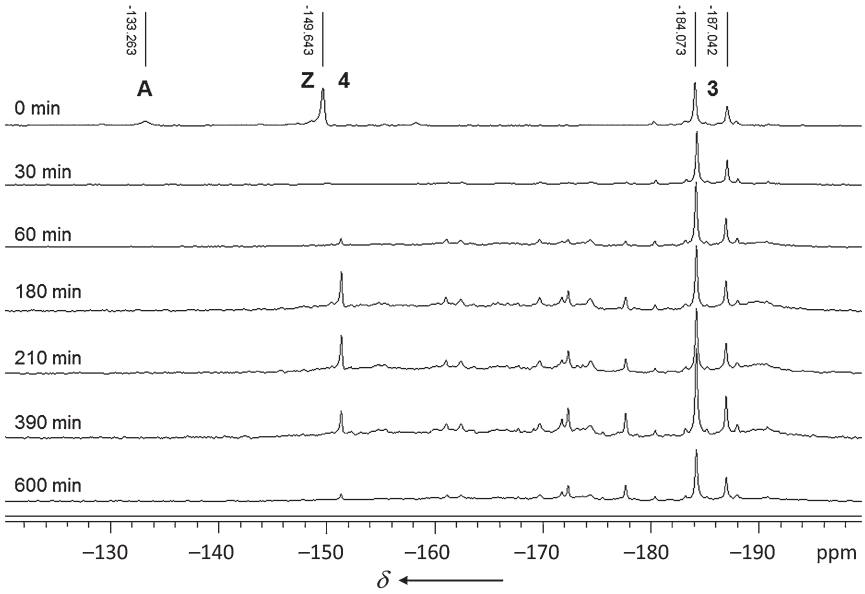

Figure 7. ^{119}Sn NMR spectra of the reaction solution for the formation of **4** in $CDCl_3$, recorded in intervals of 30 min after the start of the reaction.

Synthesis of $[(SnR^1)_2SeCl_4]$ (1)

$(SiMe_3)_2Se$ (0.059 g, 0.26 mmol) was added to a solution of $Cl_3SnCMe_2CH_2C(O)Me$ (0.339 g, 1.05 mmol) in toluene (10 mL) at room temperature (20°C). The mixture was stirred for 12 h. Colorless crystals of **1** were obtained within 2 days upon layering the solution with *n*-hexane (1:1). Yield: 0.16 g (47%, 0.249 mmol; calculated on the basis of $Cl_3SnCMe_2CH_2C(O)Me$); IR: $\tilde{\nu}$ = 2982.8 (w), 2959.7 (w), 2948.6 (w), 2915.2 (w), 2860.9 (w), 2729.8 (w), 2360.5 (w), 2341.8 (w), 1681.2 (s), 1643.9 (vs), 1457.6 (m), 1406.2 (m), 1389.5 (m), 1366.9 (s), 1332.3 (s), 1264.0 (w), 1236.5 (w), 1203.2 (w), 1182.0 (s), 1136.1 (m), 1115.7 (s), 1014.4 (m), 998.27 (w), 968.0 (w), 949.4 (w), 802.3 (w), 668.2 (w), 617.7 (vs), 508.1 (w), 489.0 (w), 464.8 (w), 445.7 (w), 416.9 cm^{-1} (w); Raman: $\tilde{\nu}$ = 1644.0 (w), 1459.9 (w), 1432.0 (w), 1331.5 (w), 1184.6 (w), 1138.1 (w), 1125.5 (m), 846.0 (w), 620.5 (w), 520.4 (m), 510.3 (m), 468.5 (w), 448.1 (w), 341.3 (m), 332.5 (s), 319.2 (m), 299.3 (w), 277.3 (w), 262.2 (w), 225.5 (w), 207.2 (vs), 176.8 (w), 139.7 (m), 130.2 (m), 118.4 (m), 106.5 (m), 95.6 cm^{-1} (m); EDX: Cl/Se/Sn calcd: 4:1:2; found: 3.92:1.00:2.03.

Synthesis of $[(SnR^1)_2Se_2Cl_2]$ (2)

$(SiMe_3)_2Se$ (0.163 g, 0.72 mmol) was added to a solution of $Cl_3SnCMe_2CH_2C(O)Me$ (0.234 g, 0.72 mmol) in toluene (10 mL) at room temperature. The mixture was stirred for 12 h. The white precipitate was collected by filtration, washed with toluene, and dried under vacuum. Colorless crystals of **2** were obtained within 2 days upon layering of a solution of the product in dichloromethane with *n*-hexane (1:1). Yield: 0.166 g (71%, 0.226 mmol; calculated on the basis of $Cl_3SnCMe_2CH_2C(O)Me$); IR: $\tilde{\nu}$ = 2960.9 (w), 2948.4 (w), 2915.3 (w), 2860.2 (w), 2729.1 (w), 2360.5 (m), 2341.8 (m), 1681.4 (s), 1640.5 (vs), 1458.5 (m), 1444.6 (w), 1406.3 (m), 1389.7 (w), 1367.9 (m), 1329.1 (s), 1262.2 (w), 1236.4 (w), 1203.6 (w), 1183.1 (s), 1114.74 (s), 1015.4 (m), 968.1 (w), 950.0 (w), 801.4 (m), 692.1 (w), 668.3 (w), 619.3 (s), 507.1 (w), 488.3 (w), 465.8 (w), 446.1 cm^{-1} (w); Raman: $\tilde{\nu}$ = 1687.7 (w), 1644.7 (w), 1462.3 (w), 1393.4 (w), 1372.6 (w), 1204.1 (w), 1185.4 (m), 1140.4 (w), 1126.5 (s), 859.9 (w), 847.8 (m), 627.4 (w), 522.8 (vs), 512.3 (m), 470.1 (w), 450.3 (m), 342.8 (m), 334.3 (vs), 302.0 (w), 276.6 (w), 264.6 (w), 227.2 (m), 209.3 (vs), 143.5 (m), 131.7 (w), 120.1 (m), 97.7 cm^{-1} (m); EDX: Cl/Se/Sn calcd: 1:1:1; found: 0.95:1.00:1.05.

Synthesis of $[(SnR^1)_3Se_4Cl]$ (3)

$(SiMe_3)_2Se$ (0.529 g, 2.35 mmol) was added to a solution of $Cl_3SnCMe_2CH_2C(O)Me$ (0.507 g, 1.56 mmol) in toluene (10 mL) at room temperature. The mixture was stirred for 12 h. The white precipitate was collected by filtration, washed with toluene, and dried under vacuum. Colorless crystals of **3** were obtained within 2 days upon layering of a solution of the product in dichloromethane with *n*-hexane (1:1). Yield: 0.32 g (62%, 0.322 mmol; calculated on the basis of $Cl_3SnCMe_2CH_2C(O)Me$); HRMS (ESI): *m/z* calc.: 970.6183 $[M-Cl]^+$; found: 970.6196; ^1H NMR (500 MHz, $CDCl_3$, 25°C): δ = 1.35 (s, 18H; CH_3, Me_2, $^3J_{119Sn}$ = 160 Hz), 2.32 (s, 9H; CH_3, Me), 2.83 ppm (s, 6H; CH_2, $^3J_{119Sn}$ = 155 Hz); ^{13}C NMR (101 MHz, $CDCl_3$, 25°C): δ = 26.06 (Me), 30.51 (Me_2), 40.23 (SnC), 55.74 (CH_2), 213.36 ppm; ^{77}Se NMR (95 MHz, $CDCl_3$, 25°C): δ = 174 (3Se; Se1,2,4, $^1J_{119Sn}$ = 1134 Hz, $^1J_{117Sn}$ = 1084 Hz), 166 ppm (1Se; Se3); ^{119}Sn NMR (187 MHz, $CDCl_3$, 25°C): δ = −185 (Sn, $^1J_{77Se}$ = 1135 Hz, $^2J_{119Sn}$ = 295 Hz), −187 ppm (SnCl, $^1J_{77Se}$ = 1134 Hz, $^2J_{Sn}$ = 295 Hz); ^{119}Sn CP-MAS NMR (187 MHz, 25°C): δ_{iso} [$\Delta\delta$ & η] = −178 ppm [−334 & 0.309 ppm], −174 ppm [−490 & 0.411 ppm]; IR: $\tilde{\nu}$ = 2945.7 (m), 2903.8 (m), 2850.8, 2719.7 (w), 2323.9 (w), 1700.6 (m), 1669.54 (vs), 1456.1 (m), 1406.0 (m), 1383.3 (m), 1363.4 (s), 1332.51 (s), 1260.9 (w), 1237.1 (m), 1205.7 (w), 1183.0 (s), 1134.8 (w), 1112.5 (s), 1016.4 (m), 997.3 (w), 964.3 (m), 836.3 (w), 796.4 (w), 731.4 (m), 695.0 (vs), 492.4 (m), 448.6 cm^{-1} (w); Raman: $\tilde{\nu}$ = 1683.3 (w), 1462.7 (w), 1368.4 (w), 1334.6 (w), 1243.4 (w), 1185.9 (w), 1142.1 (w), 1119.6 (m), 868.6 (w), 840.4 (m), 800.9 (w), 619.3 (w), 510.6 (s), 448.1 (w), 320.8 (m), 277.0 (w), 233.4 (w), 214.3 (vs), 206.2 (vs), 196.5 (vs), 114.7 (m), 97.6 (s), 87.2 cm^{-1} (s); EDX: Cl/Se/Sn calcd: 1:4:3; found: 0.85:4.00:3.09.

Synthesis of $[(SnR^1)_4Se_6]$ (4)

$(SiMe_3)_2Se$ (0.365 g, 1.62 mmol) was added to a solution of $Cl_3SnCMe_2CH_2C(O)Me$ (0.175 g, 0.54 mmol) in dichloromethane (15 mL) at room temperature. The mixture was stirred for 12 h. Colorless crystals of **4** were obtained within 2 days upon layering the solution with *n*-hexane (1:1). Yield: 0.38 g (53%, 0.286 mmol; calculated on the basis of $Cl_3SnCMe_2CH_2C(O)Me$); ^1H NMR (500 MHz, $CDCl_3$, 25°C): δ = 1.30 (s, 6H; CH_3, Me_2), 2.20 (s, 3H; CH_3, Me), 2.70 ppm (s, 2H; CH_2); ^{13}C NMR (101 MHz, $CDCl_3$, 25°C): δ = 26.35 (Me), 30.34 (Me_2), 36.96 (SnC), 55.89 (CH_2), 210.87 ppm (CO); ^{119}Sn NMR (187 MHz, $CDCl_3$, 25°C): δ = −151 ppm; EDX: Se/Sn calcd: 1.5:1; found: 1.50:1.07.

Synthesis of $[(Sn_2(\mu\text{-}R^3)(\mu\text{-}Se)Cl_4]$ (5)

$N_2H_4{\cdot}H_2O$ (0.011 g, 0.28 mmol) was added to a solution of compound **3** (0.186 g, 0.28 mmol) in dichloromethane (10 mL) at room temperature. The solution was stirred for 12 h. Colorless crystals of **5** were obtained within 3 days upon layering the solution with *n*-hexane (1:1). The crystalline yield is very low and the crystals do not dissolve well in common solvents, which inhibited the characterization of **5** by standard spectroscopic methods. EDX: Cl/Se/Sn calcd: 4:1:2; found: 4.02:1.00:1.90.

Synthesis of $[(SnR^2)_3Se_4Cl]$ (6)

$N_2H_4{\cdot}H_2O$ (0.017 g, 0.345 mmol) was added to a solution of compound **3** (0.114 g, 0.12 mmol) in dichloromethane (10 mL) at room temperature. The solution was stirred for 12 h. The product was isolated in quantitative yield upon evaporation of the solvent and drying. Colorless crystals of **6**·2 CH_2Cl_2 (**6a**) and **6**·3 CH_2Cl_2 (**6b**) co-crystallized over a period of 1 week upon layering of the solution with *n*-hexane. HRMS (ESI): *m/z* calc.: 1012.6986 $[M-Cl]^+$; found: 1012.7033; ^1H NMR (400 MHz, $CDCl_3$, 25°C): δ = 1.25 (s, 18H; CH_3, Me_2), 1.89 (s, 9H; CH_3, Me), 2.52 (s, 6H; CH_2), 5.60 ppm (br s, 6H; NH_2); ^{13}C NMR (101 MHz, $CDCl_3$, 25°C): δ = 17.17 (Me), 26.87 (Me_2), 50.67 (SnC), 53.40 (CH_2, $^2J_{Sn}$ = 22.6 Hz), 153.05 ppm ($CNNH_2$); ^{119}Sn NMR (187 MHz, $CDCl_3$, 25°C): δ = −281 ppm; IR: $\tilde{\nu}$ = 2961.6 (m), 2930.5 (w), 2903.8 (w), 2864.9 (w), 2844.3 (w), 2811.8 (w), 2360.52 (w), 2341.0 (w), 1662.8 (w), 1604.1 (w), 1454.8 (w), 1437.9 (w), 1418.5 (w), 1383.3 (w), 1366.4 (w), 1259.6 (s), 1201.9 (w), 1148.5 (m), 1091.4 (s), 1015.4 (s), 970.8 (w), 860.15 (m), 795.1 (vs), 724.5 (m), 703.7 (w), 689.3 (m), 657.9 (m), 512.5 cm^{-1} (m); Raman: $\tilde{\nu}$ = 2930.5 (w), 2902.1 (w), 2867.3 (w), 2846.2 (w), 2722.7 (w), 1657.7 (w), 1457.8 (w), 1432.4 (w), 1386.2 (w), 1368.8 (w), 1342.3 (w), 1250.8 (w), 1209.8 (w), 1152.9 (w), 1120.4 (w), 1107.0 (w), 893.6 (w), 842.7 (w), 824.6 (w), 514.3 (m), 479.1 (w), 296.8 (w), 277.8 (w), 224.0 (m), 201.6 (vs), 140.8 (w), 112.0 (m), 98.1 (m), 83.6 cm^{-1} (m); EDX: Cl/Se/Sn calcd: 1:4:3; found: 1.20:4.00:3.09.

Synthesis of $[(SnR^4)_3Se_4][SnCl_3]$ (7)

Phenylhydrazine (0.051 g, 0.47 mmol) was added to a solution of compound **3** (0.159 g, 0.16 mmol) in dichloromethane (5 mL) at

room temperature. The solution was stirred for 12 h. Colorless crystals of $7{\cdot}C_7H_8$ crystallize over a period of 1 week upon layering of the solution with toluene. The crystalline yield was very low. HRMS (ESI): *m/z* calc.: 1240.7936 $[M-SnCl_3]^+$; found: 1240.7950; ^{1}H NMR (400 MHz, $CDCl_3$, 25 °C): $\delta = 1.24$ (s, 18H; CH_3, Me_2, $^3J_{Sn} = 165$ Hz), 2.91 (s, 9H; CH_3, Me), 2.67 (s, 6H; CH_2, $^3J_{Sn} = 145$ Hz), 6.59 (d, 6H; Ph, $^3J_H = 7.90$ Hz), 7.16 ppm (m, 9H; Ph); ^{13}C NMR (101 MHz, $CDCl_3$, 25 °C): $\delta = 20.55$ (Me), 26.04 (Me_2), 26.94 (SnC), 50.95 (CH_2), 115.64 (Ph-*ortho*), 121.44 (Ph-*para*), 129.02 (Ph-*meta*), 144.88 (Ph-α), 171.05 ppm (CN); ^{119}Sn NMR (187 MHz, $CDCl_3$, 25 °C): $\delta = -275$ ppm; EDX: Cl/Se/Sn calcd: 3:4:4; found: 2.88:4.00:3.94.

Synthesis of $[(SnR^2)_4Se_6]$ (8)

$N_2H_4{\cdot}H_2O$ (0.017 g, 0.345 mmol) was added to a solution of compound **4** (0.114 g, 0.12 mmol) in dichloromethane (10 mL) at room temperature. The solution was stirred for 12 h. The product was isolated in quantitative yield upon evaporation of the solvent and drying. Colorless crystals of **8** crystallized over a period of 1 week upon layering of the solution with *n*-hexane. ^{1}H NMR (500 MHz, $CDCl_3$, 25 °C): $\delta = 1.31$ (s, 18H; CH_3, Me_2), 1.79 (s, 9H; CH_3, Me), 2.49 (s, 6H; CH_2), 5.18 ppm (s, 3H; NH); ^{13}C NMR (101 MHz, $CDCl_3$, 25 °C): $\delta = 26.32$ (Me), 30.35 (Me_2), 50.73 (SnC), 55.86 (CH_2, $^2J_{Sn} = 22.6$ Hz), 210.99 ppm (CN); EDX: Se/Sn calcd: 1.5:1; found: 1.50:1.15.

Synthesis of $[(SnR^4)_4Se_6]$ (9)

Phenylhydrazine (0.017 g, 0.345 mmol) was added to a solution of compound **4** (0.114 g, 0.12 mmol) in dichloromethane (10 mL) at room temperature. The solution was stirred for 12 h. The product was isolated in quantitative yield upon evaporation of the solvent and drying. Colorless crystals of **9** crystallized over a period of 1 week upon layering of the solution with *n*-hexane. ^{1}H NMR (500 MHz, $CDCl_3$, 25 °C): $\delta = 1.31$ (s, 18H; CH_3, Me_2), 1.89 (s, 9H; CH_3, Me), 2.57 (s, 6H; CH_2), 3.58 (s, 3H; NH), 6.78 (m, 6H; Ph-*ortho*), 6.86 (m, 3H; Ph-*para*), 7.12 ppm (m, 6H; Ph-*meta*); ^{13}C NMR (101 MHz, $CDCl_3$, 25 °C): $\delta = 20.34$ (Me), 27.10 (Me_2), 51.05 (CH_2), 112.30 (Ph-*ortho*), 115.56 (Ph-*para*), 119.60 (Ph-*meta*), 128.97 (Ph-α), 129.38 ppm (CN); ^{119}Sn NMR (187 MHz, $CDCl_3$, 25 °C): $\delta = -195$ ppm; EDX: Se/Sn calcd: 1.5:1; found: 1.50:0.98.

Synthesis of $[(R^1Sn)_2Se_2(CuPPh_3)_2Se_2]$ (10)

Compound **4** (0.248 g, 0.18 mmo l) and $[Cu(PPh_3)_3Cl]$ (0.468 g, 0.52 mmol) were dissolved in chloroform (20 mL) and treated with $(SiMe_3)_2Se$ (0.324 g, 0.36 mmol) at room temperature. The orange solution was stirred for 18 h and subsequently layered 1:1 with *n*-hexane. After 3 days, orange crystalline plates were obtained, which are insoluble in all common solvents. This and very low yields inhibited the characterization of **10** by standard spectroscopic methods. EDX: Se/Sn/Cu/P calcd: 2:1:1:1; found: 2:1.05:0.97:0.94.

Spectroscopy and spectrometry

^{1}H NMR, ^{13}C NMR, and ^{119}Sn NMR measurements were carried out by using a Bruker DRX 300 MHz, DRX 400 MHz, or DRX 500 MHz spectrometer at 25 °C. The ^{77}Se NMR spectra of compound **3** were recorded on a Bruker AVIII 500 spectrometer. The chemical shifts are quoted in ppm relative to the residual protons of the deuterated solvents in the ^{1}H NMR and ^{13}C NMR spectra. Me_4Sn was used as an internal standard for the ^{119}Sn NMR measurements whereas $SeMe_4$ was used for the ^{77}Se NMR measurements. For the ^{119}Sn CP-MAS NMR measurements at 25 °C, a Bruker DRX 500 MHz spectrometer was employed, by using 4 mm Bruker probe tubes. Tetracyclohexyltin ($\delta = -97$ ppm) was used as a reference. The MAS speed was changed (10.5 and 12 kHz) to locate the isotropic chemical shifts. The ^{119}Sn CP-MAS NMR spectra were analyzed with a Bruker Biospin 3.0, and the ^{119}Sn shielding tensors were extracted by using the Haeberlen approach.[33] ESI-MS measurements were performed on a Thermo Fischer Scientifics Finnigan LTQ-FT. Infrared (IR) spectra were recorded on a Bruker Tensor 37, and Raman spectra on a Jobin Yvon Labram HR 800 in a glass capillary. Energy-dispersive X-ray (EDX) spectroscopic analysis was performed by using the EDX device Voyager 4.0 of Noran Instruments coupled with the electron microscope CamScan CS 4DV. Data acquisition was performed with an acceleration voltage of 20 kV and 100 s accumulation time.

X-ray crystallography

Data collection was performed on STOE IPDS2 and Bruker D8 Quest diffractometers using graphite-monochromatized $Mo_{K\alpha}$ radiation ($\lambda = 71.073$ pm) at 100 K. Structure solution and refinement was done by direct methods and full-matrix least-squares on F^2, respectively, by using the SHELXTL software.[34] Details of the measurements, structure solutions, and refinements as well as additional figures are provided in the Supporting Information. CCDC 1422344–1422354 contain the supplementary crystallographic data for this paper. These data are provided free of charge by The Cambridge Crystallographic Data Centre.

Quantum chemical methods

For the DFT calculations, the program system TURBOMOLE Version 6.2[34] using the RIDFT[36,37] program with the B3-LYP functional[38] and gridsize m3 was applied. Basis sets were of def2-TZVP quality.[39,40] For Sn atoms, effective core potentials (ECP-28)[41] were employed. The simultaneous optimizations of the geometric and electronic structures were done without symmetry restrictions (C_1 symmetry). The accuracy of the structures was found to be within the typical error of the method. The energies in Table 3 were calculated by subtraction of the sum of the total energies of the starting materials **A** and **B** from the sum of the total energies of the respective species plus Me_3SiCl as side product (see equations in Table 3).

Acknowledgments

This work was supported by the Deutsche Forschungsgemeinschaft within the frameworks of GRK 1782 and SFB 1083, and the State of Hessia within the framework of LOEWE SynChemBio. We are indebted to Prof. Dr. Berthold Hoge and Michael Grasse (University of Bielefeld, Germany) for recording additional NMR spectra, in particular ^{77}Se NMR spectra, of compound **3**.

Keywords: clusters · copper · inorganic–organic hybrid materials · selenium · tin

[1] M. Draganjac, T. B. Rauchfuss, *Angew. Chem. Int. Ed. Engl.* **1985**, *24*, 742–757; *Angew. Chem.* **1985**, *97*, 745–760.
[2] M. G. Kanatzidis, S. Huang, *Coord. Chem. Rev.* **1994**, *130*, 509–621.
[3] B. Krebs, *Angew. Chem. Int. Ed. Engl.* **1983**, *22*, 113–134; *Angew. Chem.* **1983**, *95*, 113–134.
[4] P. Feng, X. Bu, N. Zheng, *Acc. Chem. Res.* **2005**, *38*, 293–303.

[5] S. Bag, P. N. Trikalitis, P. J. Chupas, G. S. Armatas, M. G. Kanatzidis, *Science* **2007**, *317*, 490 – 493.
[6] C. Anderer, N. Delwa deAlarcón, C. Näther, W. Bensch, *Chem. Eur. J.* **2014**, *20*, 16953 – 16959.
[7] M. G. Kanatzidis, *Adv. Mater.* **2007**, *19*, 1165 – 1181.
[8] W. Schiwy, B. Krebs, *Angew. Chem. Int. Ed. Engl.* **1975**, *14*, 436 – 436; *Angew. Chem.* **1975**, *87*, 451 – 452.
[9] K. Tan, Y. Ko, J. B. Parise, *Acta Crystallogr. Sect. A* **1995**, *51*, 398 – 401.
[10] T. Jiang, G. A. Ozin, R. L. Bedard, *Adv. Mater.* **1994**, *6*, 860 – 865.
[11] G.-H. Xu, C. Wang, P. Guo, *Acta Crystallogr. Sect. A* **2009**, *65*, m171 – m173.
[12] K. Tsamourtzi, J.-H. Song, T. Bakas, A. J. Freeman, P. N. Trikalitis, M. G. Kanatzidis, *Inorg. Chem.* **2008**, *47*, 11920 – 11929.
[13] P. A. Mercier, D. A. Dixon, H. Borrmann, G. J. Schrobilgen, *Inorg. Chem.* **2001**, *40*, 4823 – 4829.
[14] H. Berwe, A. Haas, *Chem. Ber.* **1987**, *120*, 1175 – 1182.
[15] D. Kobelt, E. F. Paulus, H. Scherer, *Acta Crystallogr. Sect. A* **1972**, *28*, 2323 – 2326.
[16] a) Z. Hassanzadeh Fard, L. Xiong, C. Müller, M. Hołyńska, S. Dehnen, *Chem. Eur. J.* **2009**, *15*, 6595 – 6604; b) Z. Hassanzadeh Fard, M. R. Halvagar, S. Dehnen, *J. Am. Chem. Soc.* **2010**, *132*, 2848 – 2849.
[17] S. Heimann, M. Hołyńska, S. Dehnen, *Chem. Commun.* **2011**, *47*, 1881 – 1883.
[18] J. P. Eußner, B. E. K. Barth, E. Leusmann, Z. You, N. Rinn, S. Dehnen, *Chem. Eur. J.* **2013**, *19*, 13792 – 13802.
[19] a) T. P. Lockhart, H. Puff, T. N. Mitchell, *J. Organomet. Chem.* **1989**, *366*, 61 – 72; b) M. Mehring, C. Lçw, M. Schürmann, F. Uhlig, K. Jurkschat, *Organometallics* **2000**, *19*, 4613 – 4623; c) J. Beckmann, D. Dakternieks, A. Duthie, C. Jones, K. Jurkschat, E. R. T. Tiekink, *J. Organomet. Chem.* **2001**, *636*, 138 – 143; d) J. Turek, Z. Padělková, M. S. Nechaev, A. Růžička, *Organomet. Chem.* **2010**, *695*, 1843 – 4847; e) W.-P. Leung, C.-L. Wan, K.-W. Kann, T. C. W. Mak, *Organometallics* **2010**, *29*, 814 – 820; f) L. Iovkova-Berends, T. Berends, T. Zöller, D. Schollmeyer, G. Bradtmöller, K. Jurkschat, *Eur. J. Inorg. Chem.* **2012**, 3463 – 3473.
[20] B. E. K. Barth, E. Leusmann, K. Harms, S. Dehnen, *Chem. Commun.* **2013**, *49*, 6590 – 6592.
[21] a) T. Chivers, D. J. Eisler, *Angew. Chem. Int. Ed.* **2004**, *43*, 6686 – 6689; *Angew. Chem.* **2004**, *116*, 6854 – 6857; b) M. Bouška, L. Střížik, L. Dostál, A. Růžička, A. Lyčka, L. Beneš, M. Vlček, J. Přikryl, P. Knotek, T. Wágner, R. Jambor, *Chem. Eur. J.* **2013**, *19*, 1877 – 1881; c) M. Bouška, L. Dostál, F. de Proft, A. Růžička, A. Lyčka, R. Jambor, *Chem. Eur. J.* **2011**, *17*, 455 – 459; d) T. Chivers, D. J. Eisler, J. S. Ritch, *Z. Anorg. Allg. Chem.* **2004**, *630*, 1941 – 1946; e) D. J. Eisler, T. Chivers, *Chem. Eur. J.* **2006**, *12*, 233 – 243; f) T. Chivers, T. J. Clark, M. Krahn, M. Parvez, G. Schatte, *Eur. J. Inorg. Chem.* **2003**, 1857 – 1860.
[22] a) H. Puff, R. Gattermayer, R. Hundt, R. Zimmer, *Angew. Chem. Int. Ed. Engl.* **1977**, *16*, 547 – 548; *Angew. Chem.* **1977**, *89*, 556 – 557; b) H. Puff, G. Bertram, B. Ebeling, M. Franken, R. Gattermayer, R. Hundt, W. Schuh, R. Zimmer, *J. Organomet. Chem.* **1989**, *379*, 235 – 245; c) N. Tokitoh, Y. Matsuhashi, M. Goto, R. Okazaki, *Chem. Lett.* **1992**, 1595 – 1598; d) N. Tokitoh, Y. Matsuhashi, R. Okazaki, *Organometallics* **1993**, *12*, 2894 – 2896; e) S. Sportouch, M. Tillard-Charbonnel, C. Belin, *J. Chem. Soc. Dalton Trans.* **1995**, 3113 – 3116; f) J. J. Schneider, J. Hagen, O. Heinemann, J. Bruckmann, C. Krüger, *Thin Solid Films* **1997**, *304*, 144 – 148; g) M. Saito, H. Hashimoto, T. Tajima, M. Ikeda, *J. Organomet. Chem.* **2007**, *692*, 2729 – 2735; h) Z. You, R. Möckel, J. Bergunde, S. Dehnen, *Chem. Eur. J.* **2014**, *20*, 13491 – 13496.
[23] a) B. Krebs, H.-J. Jacobsen, *J. Organomet. Chem.* **1979**, *178*, 301 – 308; b) R. J. Batchelor, F. W. B. Einstein, C. H. W. Jones, R. D. Sharma, *Inorg. Chem.* **1988**, *27*, 4636 – 4640; c) M. Herberhold, M. Steffl, W. Milius, B. Wrackmeyer, *J. Organomet. Chem.* **1997**, *533*, 109 – 115; d) H. Bera, H. Braunschweig, R. Dörfler, K. Hammond, A. Oechsner, K. Radacki, K. Uttinger, *Chem. Eur. J.* **2009**, *15*, 12092 – 12098; e) H. Braunschweig, R. Dörfler, K. Gruss, J. Köhler, K. Radacki, *Organometallics* **2011**, *30*, 305 – 312; f) M. Bouška, L. Dostál, F. de Proft, A. Růžička, A. Lyčka, R. Jambor, *Chem. Eur. J.* **2011**, *17*, 455 – 459; g) H. Braunschweig, R. Dörfler, J. Mies, K. Radacki, M. Schmitt, *J. Organomet. Chem.* **2012**, *699*, 26 – 30.
[24] a) H. Kraus, K. Merzweiler, *Z. Naturforsch. Sect. B* **1993**, *48*, 1009 – 1012; b) K. Merzweiler, L. Weisse, *Z. Naturforsch. Sect. B* **1990**, *45*, 971 – 978.
[25] Z. Hassanzadeh Fard, M. Hołyńska, S. Dehnen, *Inorg. Chem.* **2010**, *49*, 5748 – 5752.
[26] J. P. Eußner, R. O. Kusche, S. Dehnen, *Chem. Eur. J.* **2015**, *21*, 12376 – 12388.
[27] M. Schmidt, H. Ruf, *Angew. Chem.* **1961**, *73*, 64.
[28] R. Liminga, M. Sorensen, *Acta. Chem. Scand.* **1967**, *21*, 2669 – 2678.
[29] a) M. R. Halvagar, Z. Hassanzadeh Fard, S. Dehnen, *Chem. Eur. J.* **2011**, *17*, 4371 – 4374; b) S. Heimann, M. Hołyńska, S. Dehnen, *Z. Anorg. Allg. Chem.* **2012**, *638*, 1663 – 1666.
[30] O. Kluge, K. Grummt, R. Biedermann, H. Krautscheid, *Inorg. Chem.* **2011**, *50*, 4742 – 4752.
[31] M. R. Detty, M. D. Seidler, *J. Org. Chem.* **1982**, *47*, 1354 – 1356.
[32] R. E. Hutton, J. W. Burley, *J. Organomet. Chem.* **1978**, *156*, 369 – 382.
[33] J. S. Waugh, L. M. Huber, U. Haeberlen, *Phys. Rev. Lett.* **1968**, *20*, 180 – 183.
[34] G. M. Sheldrick, *Acta Crystallogr. Sect. A* **2008**, *64*, 112 – 122.
[35] TURBOMOLE Version 6.6, © TURBOMOLE GmbH 2014, TURBOMOLE is a development of University of Karlsruhe and Forschungszentrum Karlsruhe 1989 – 2007, TURBOMOLE GmbH since **2007**.
[36] K. Eichkorn, M. Htiser, R. Ahlrichs, K. Eichkorn, O. Treutler, H. Marco, R. Ahlrichs, *Chem. Phys. Lett.* **1995**, *242*, 652 – 659.
[37] K. Eichkorn, F. Weigend, O. Treutler, R. Ahlrichs, *Theor. Chem. Acc.* **1997**, *97*, 119 – 124.
[38] C. Lee, W. Yang, R. G. Parr, *Phys. Rev. B* **1988**, *37*, 785 – 789.
[39] F. Weigend, R. Ahlrichs, *Phys. Chem. Chem. Phys.* **2005**, *7*, 3297 – 3305.
[40] F. Weigend, *Phys. Chem. Chem. Phys.* **2006**, *8*, 1057 – 1065.
[41] B. Metz, H. Stoll, M. Dolg, *J. Chem. Phys.* **2000**, *113*, 2563 – 2569.

Received: September 6, 2015
Revised: December 15, 2015
Published online on January 25, 2016

CHEMISTRY
A European Journal

Supporting Information

Formation and Reactivity of Organo-Functionalized Tin Selenide Clusters

Niklas Rinn, Jens P. Eußner, Willy Kaschuba, Xiulan Xie, and Stefanie Dehnen*[a]

chem_201503562_sm_miscellaneous_information.pdf

Details of the X-ray diffraction measurements and refinements.

General: All x-ray crystal structures except those of **3**, **5** and **6a**, where measured using *Stoe IPDS2/2T* diffractometers. **3**, **5** and **6a** were measured on a *Bruker D8 Quest* diffractometer. All measurements were carried out at 100 K using a Mo-K_α X-ray source. The structures were solved by direct methods in *SHELXS97* and refined by full-matrix-least-squares refinement against F^2 in SHELXL97 and SHELX2013.[1] Methyl and methylene hydrogen atoms were added assuming ideal geometry on their carbon parent atom, with $U_{eq} = nU_{eq}$ (parent atom), n = 1.2 for methylene and 1.5 for methyl groups. Hydrogen atoms at hydrazone moieties were likewise added with n = 1.2, if not found in the density difference map, which was only the case in **6a**. All given structures are shown with thermal ellipsoids at 50% probability. Hydrogen atoms are omitted for clarity in the structure figures.

Crystal structure of B

To obtain single crystals of **B**, the purified liquid was slowly cooled to 233 K. To prepare the crystals under a light microscope, they were handled in a bath of liquid nitrogen at 77 K and thereafter quickly transferred onto the goniometer head for measurement. The highest peak of residual electron density on the difference Fourier map (0.9 e/Å^3) is found 118.3 pm away from the Se atom. The crystal structure of **B** is shown in Figure S1.

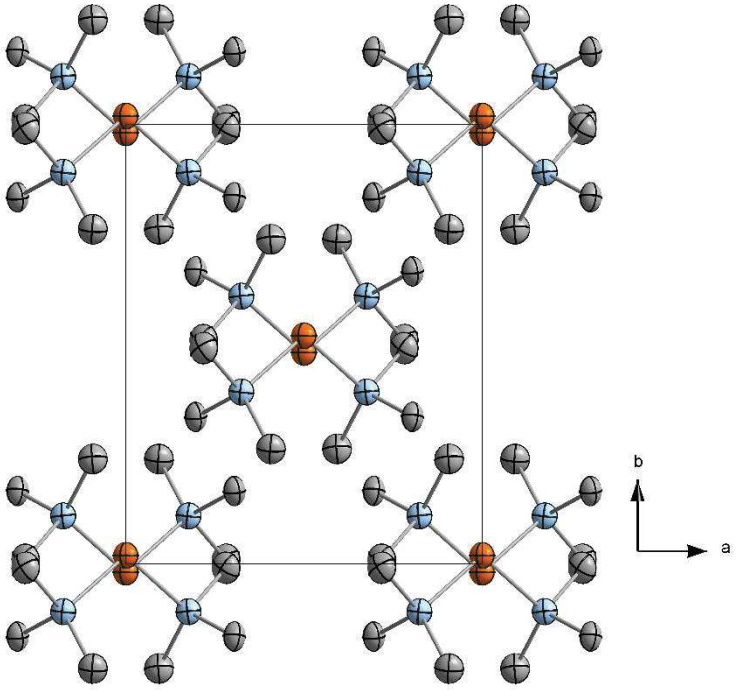

Figure S1: Crystal structure of **B** viewed along the crystallographic *c* axis. **B** crystallizes in the monoclinic space group *C2/c*.

Crystal structure of F

The compound $[(SnR^2)_4S_6]\cdot CHCl_3$ (**E**) has been reported in literature with a distorted **DD** topology due to the hydrazone moiety.[2,3] However, when recrystallizing the compound from DCM, $[(SnR^2)_4S_6] \cdot 2DCM$ (**F**) can be obtained. As discussed in the main document, the **DD** topology in **F** is not notably distorted, which leads to the conclusion that the distortion in **E** is due to packing effects that were obviously caused by the chloroform molecules.

Crystal structure of 1

The highest peak of residual electron density on the difference Fourier map (3.0 $e^{-}/Å^3$) is found 83.1 pm away from Sn2. The crystal structure of **1** is shown in Figure S2.

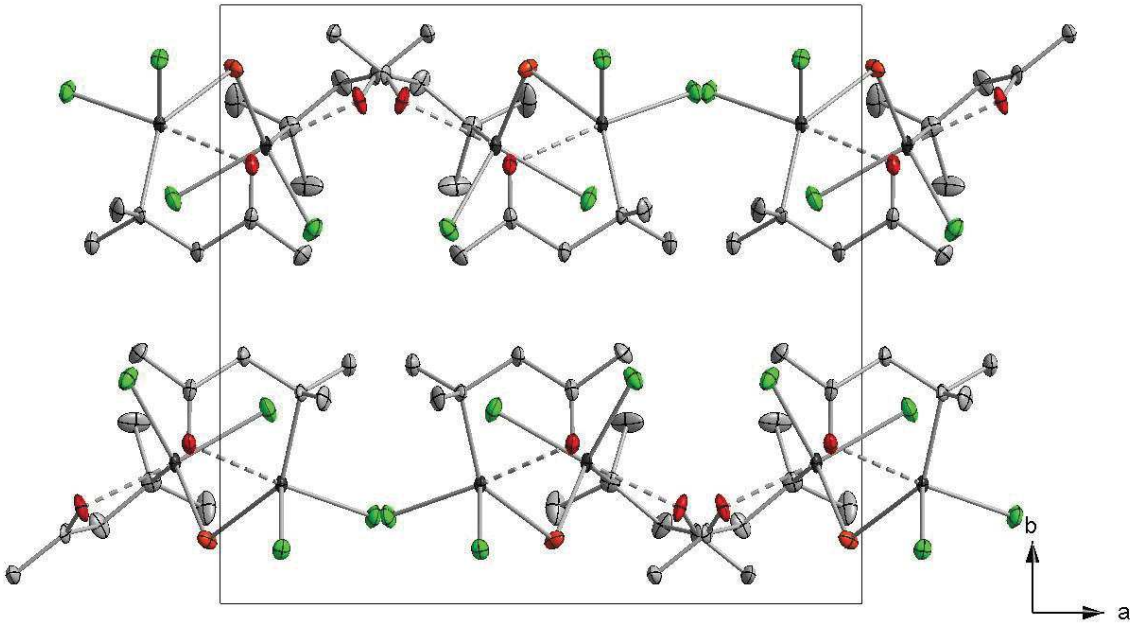

Figure S2: Crystal structure of **1** viewed along the crystallographic *c* axis. **1** crystallizes in the orthorhombic space group $Pca2_1$.

Crystal structure of 2

The highest peak of residual electron density on the difference Fourier map (1.6 $e^{-}/Å^3$) is found 97.4 pm away from Sn1. The crystal structure of **2** is shown in Figure S3.

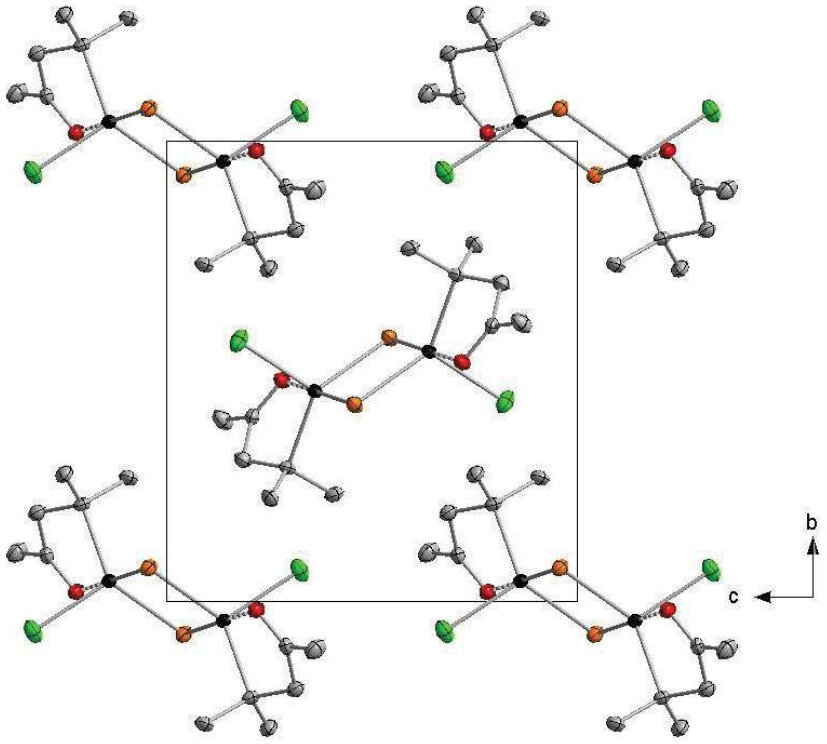

Figure S3: Crystal structure of **2** viewed along the crystallographic *a* axis. **2** crystallizes in the monoclinic space group $P2_1/c$.

Crystal structure of 3

The highest peak of residual electron density on the difference Fourier map (1.3 $e^-/Å^3$) is found 124.0 pm away from Sn1. The crystal structure of **3** is shown in Figure S4.

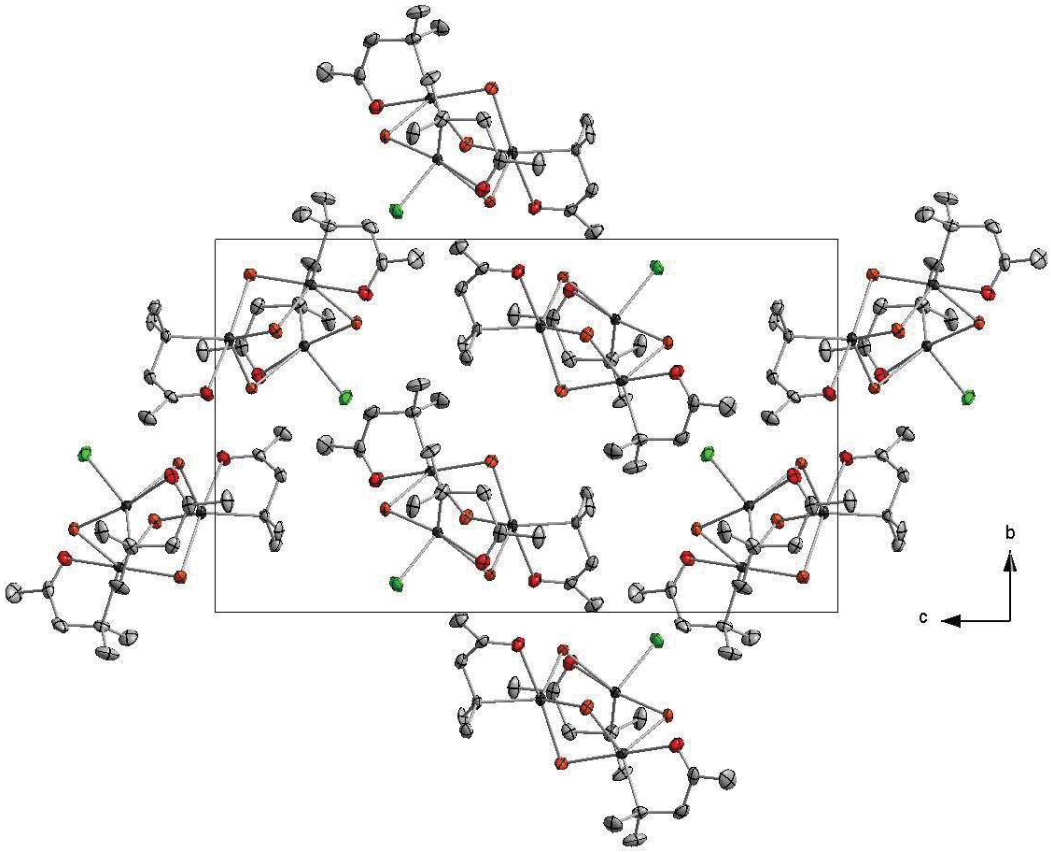

Figure S4: Crystal structure of **3** viewed along the crystallographic *a* axis. **3** crystallizes in the monoclinic space group $P2_1/n$.

Crystal structure of 4

The highest peak of residual electron density on the difference Fourier map (0.5 $e^-/Å^3$) is found 91 pm away from Sn2. The crystal structure of **4** is shown in Figure S5.

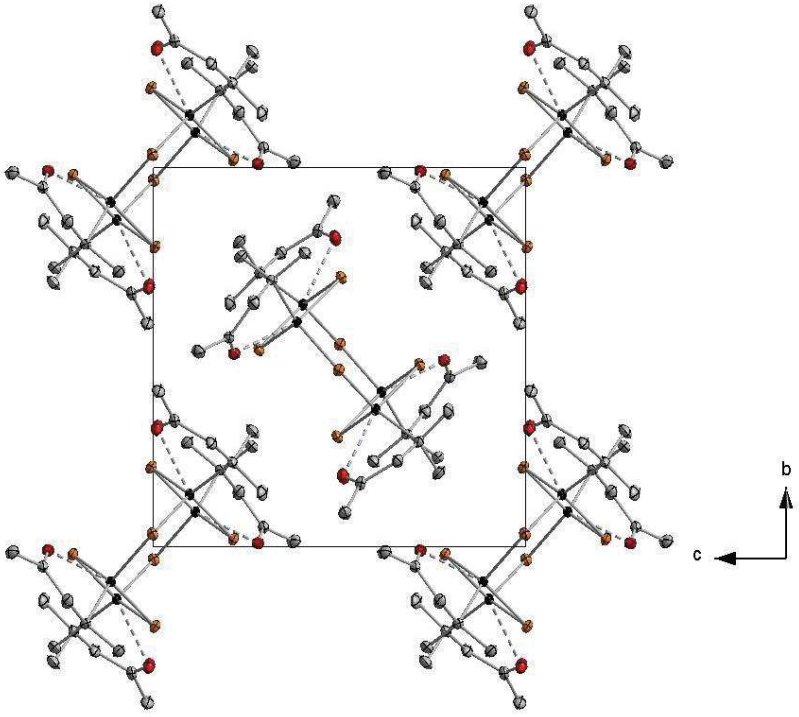

Figure S5: Crystal structure of **6** viewed along the crystallographic *a* axis. **6** crystallizes in the monoclinic space group $P2_1/n$.

Crystal structure of 5

The highest peak of residual electron density on the difference Fourier map (3.3 $e^{-}/Å^3$) is found 75 pm away from C3B. The crystal structure of **5** is shown in Figure S6. One part of the molecule is disordered. The disorder was modelled in two positions with an occupancy of 0.943(2)/0.0378(3). SADI, SIMU and DELU restraints were imposed to the disordered parts.

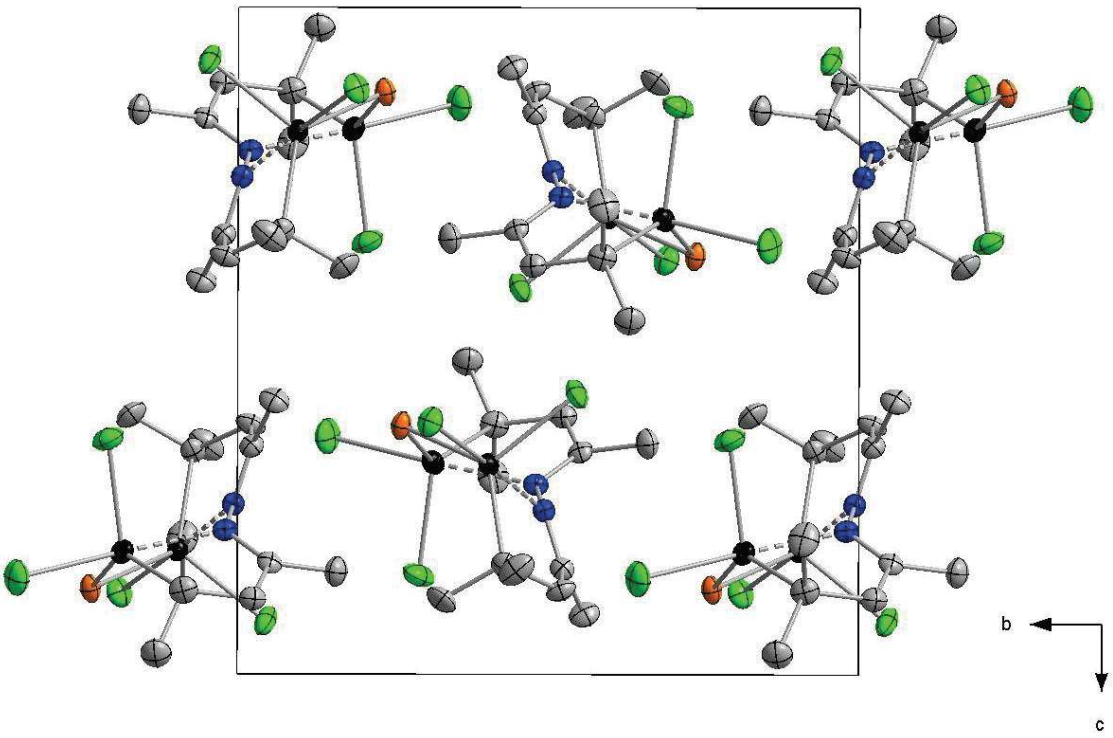

Figure S6: Crystal structure of **5** viewed along the crystallographic *a* axis. **5** crystallizes in the monoclinic space group $P2_1/n$.

Crystal structure of 6a

The highest peak of residual electron density on the difference Fourier map (1.6 $e^{-}/Å^3$) is found 71 pm away from Se1. One part of the organic ligand at Sn2 is disordered (C10-C12, N3 and N4) and is modelled with an occupancy of 0.625(15)/0.375(15) (Figure S7). The resulting pairs of vicinal C and N atoms C12A and C12B and N4A and N4B respectively were imposed with an EADP constraint. Additionally, one DCM solvent molecule is likewise disordered. Within the two disordered corresponding molecules, the geometry was restrained with SADI and SIMU restraints were applied. The crystal structure of **6a** is shown in Figure S8.

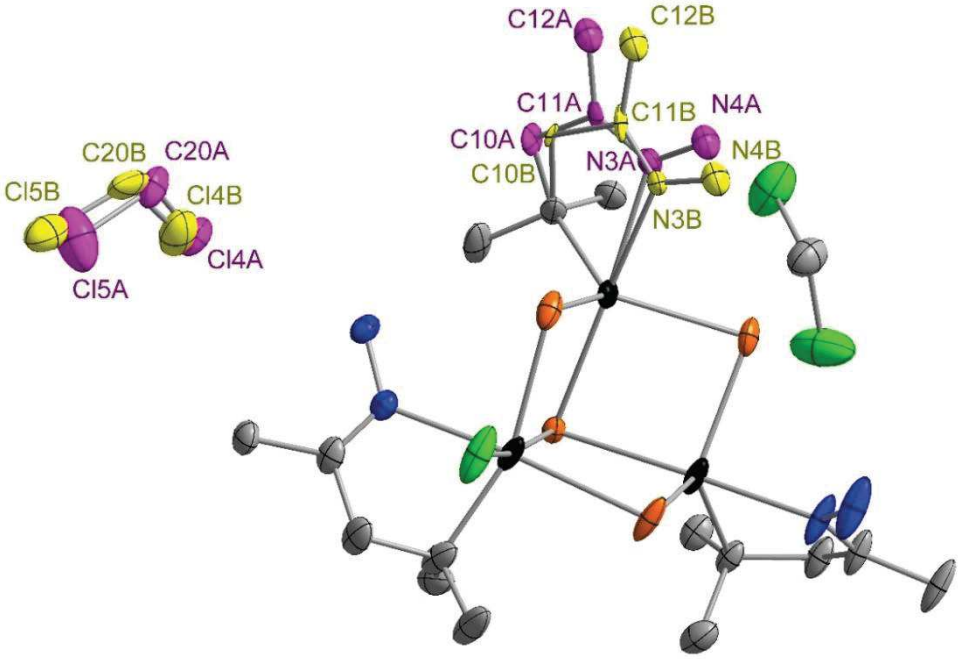

Figure S7: Disorder in the molecular structure of **6a**. The majority components are drawn in pink color, while the minority components are drawn in yellow color.

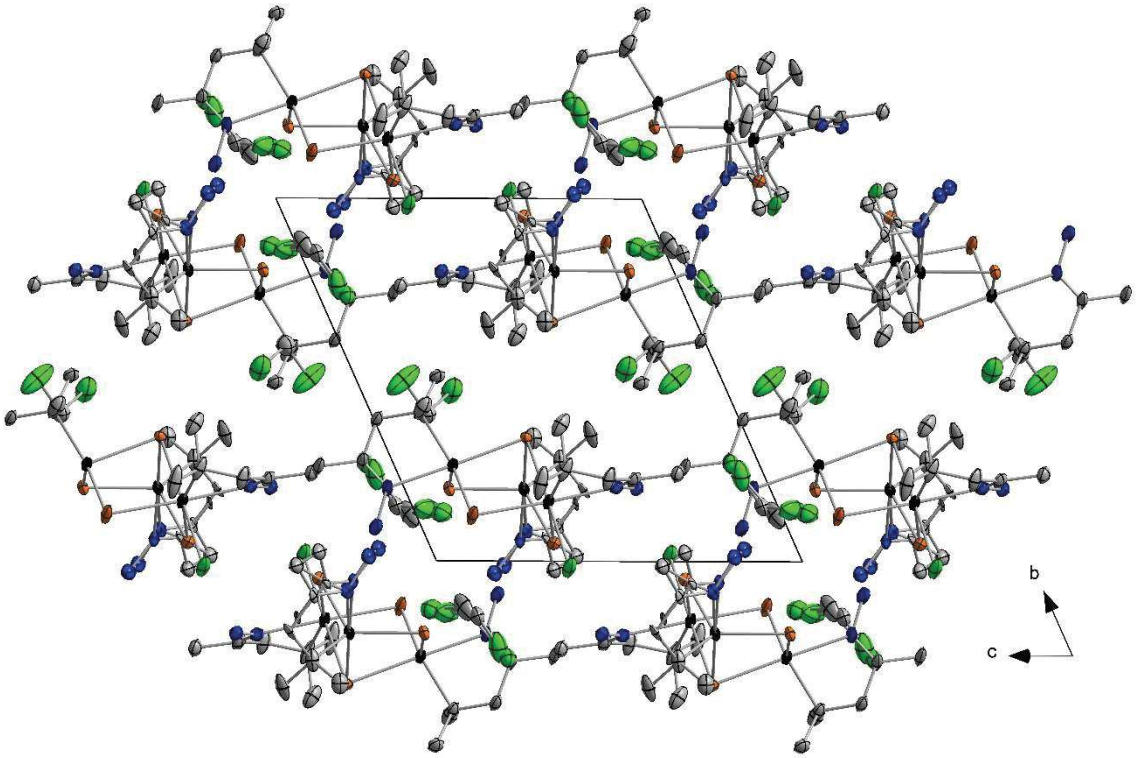

Figure S8: Crystal structure of **6a** viewed along the crystallographic *a* axis. **6a** crystallizes in the triclinic space group $P\bar{1}$.

Crystal structure of 6b

The highest peak of residual electron density on the difference Fourier map (3.0 $e^{-}/Å^3$) is found 117 pm away from Sn1. The crystal structure of **6b** is shown in Figure S9.

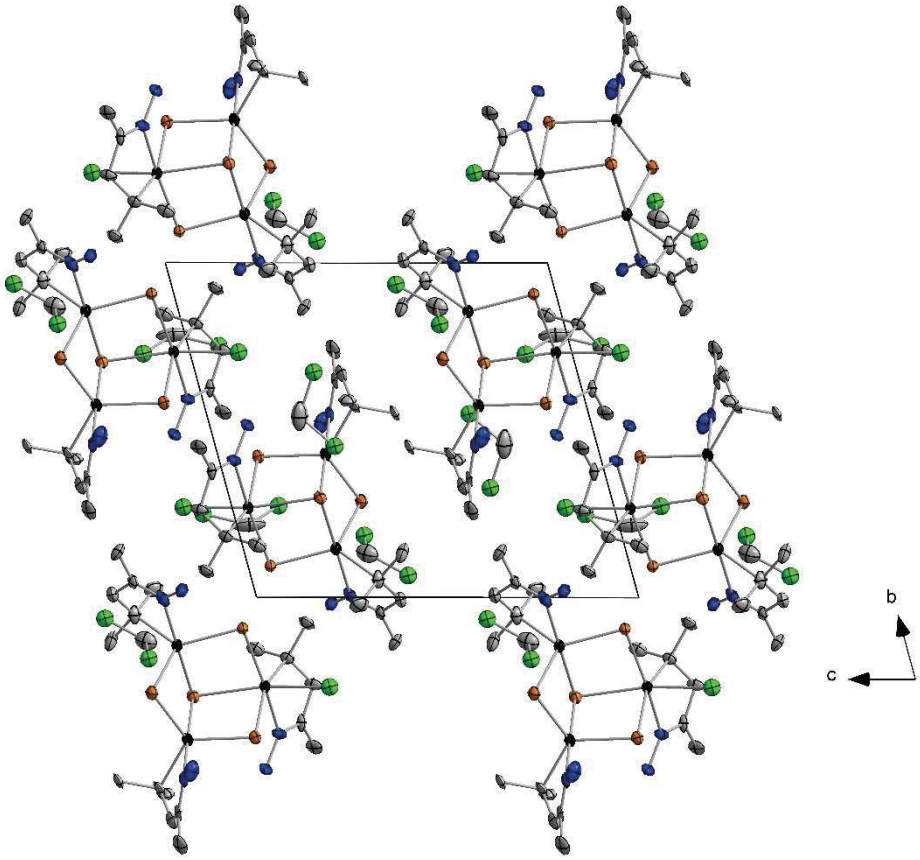

Figure S9: Crystal structure of **6b** viewed along the crystallographic *a* axis. **6b** crystallizes in the triclinic space group $P\bar{1}$.

Crystal structure of 7

The highest peak of residual electron density on the difference Fourier map (1.1 $e^{-}/Å^3$) is found 66.2 pm away from the center of the Sn2−Se3 bond. The crystal structure of **7** is shown in Figure S10.

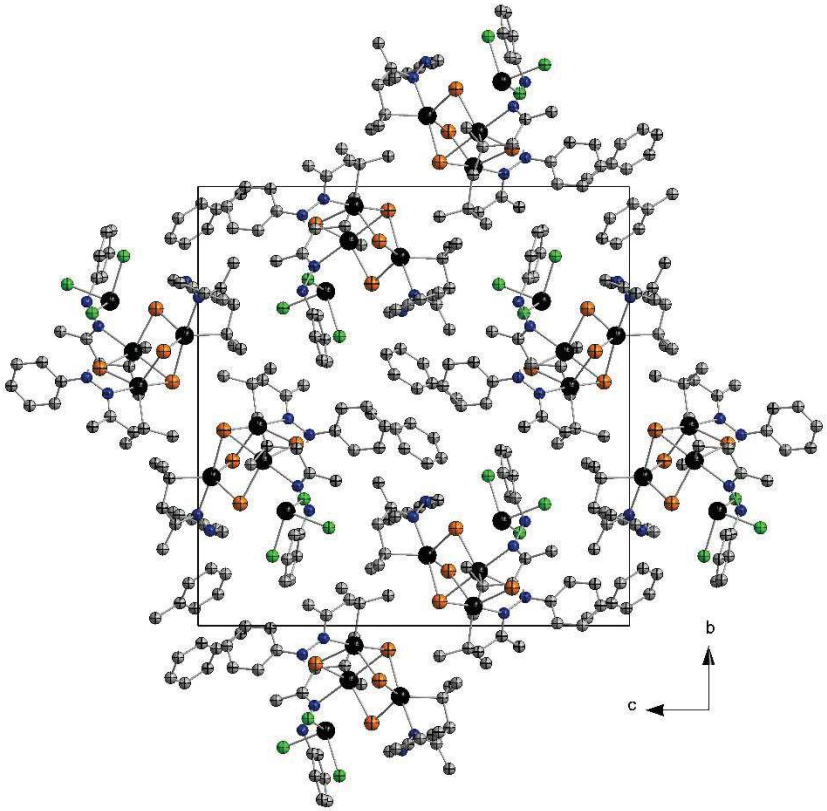

Figure S10: Crystal structure of **7** viewed along the crystallographic *a* axis. **7** crystallizes in the monoclinic space group $P2_1/c$.

Crystal structure of 8

The highest peak of residual electron density on the difference Fourier map (1.6 $e/Å^3$) is found 100 pm away from Sn1. The crystal structure of **8** is shown in Figure S11.

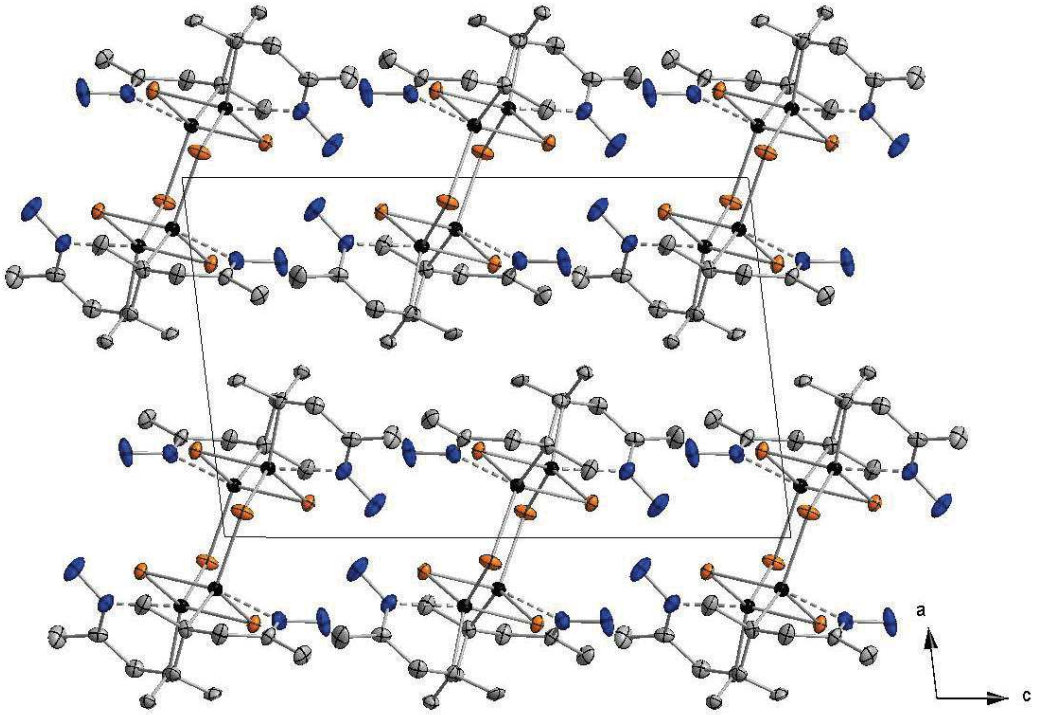

Figure S11: Crystal structure of **8** viewed along the *b* axis. **8** crystallizes in the monoclinic space group $P2_1/c$.

Crystal structure of 9

The highest peak of residual electron density on the difference Fourier map (1.4 $e^{-}/Å^3$) is found 61.5 pm away from the center of the Sn1−C1 bond. The crystal structure of **9** is shown in Figure S12.

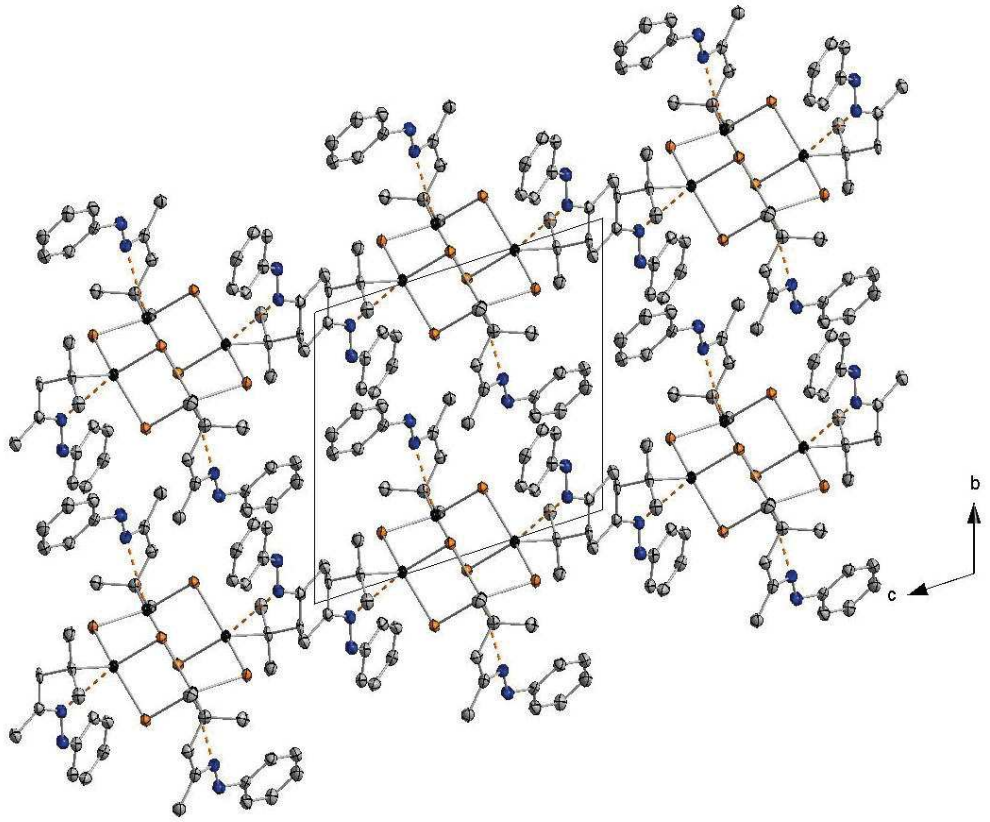

Figure S12: Crystal structure of **9** viewed along the crystallographic *a* axis. **9** crystallizes in the triclinic space group $P\bar{1}$.

Crystal structure of 10

The highest peak of residual electron density on the difference Fourier map (0.5 $e^{-}/Å^3$) is found 39.5 pm away from the center of the Sn1−Se2 bond. The crystal structure of **10** is shown in Figure S13.

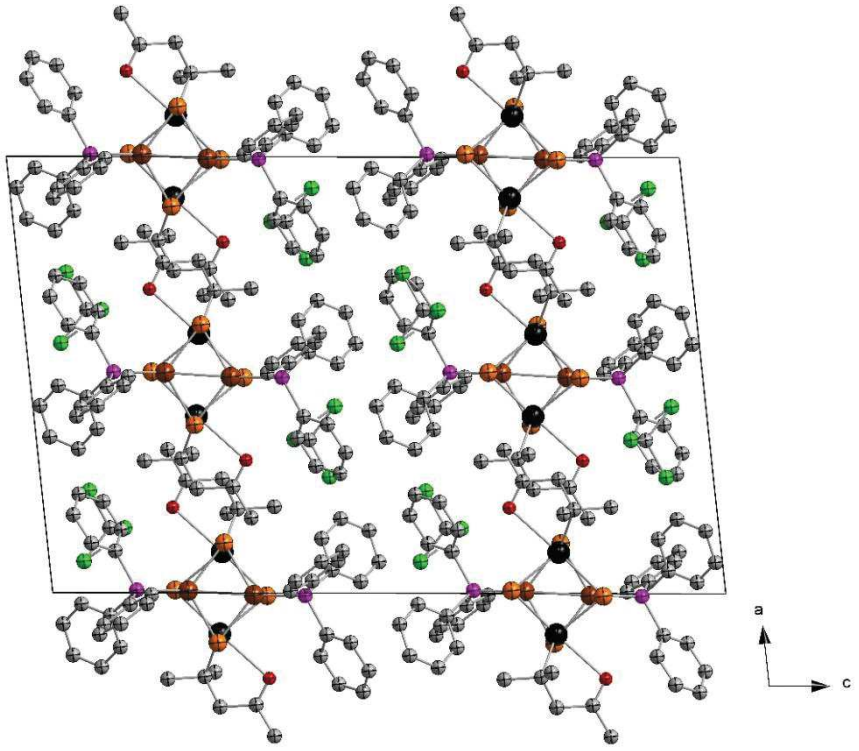

Figure S13: Crystal structure of **10** viewed along the crystallographic *a* axis. **10** crystallizes in the monoclinic space group *C2/c*.

Table S1: Selected structural parameters within compounds **1** – **9**.

Compound	1	2	3	4	5	6·2CH_2Cl_2 (6a)	6·3CH_2Cl_2 (6b)	7·C_7H_8	8	9
Sn1−Se1	249.08(8)	250.29(8)	253.65(6)	251.55(4)	253.05(7)	267.22(8)	267.5(1)	254.7(1)	250.5(1)	254.19(7)
Sn1−Se2/1’		259.24(8)	257.34(6)	257.80(4)		259.45(8)	259.3(2)	254.3(1)	266.4(1)	255.45(8)
Sn1−Se3			346.79(7)	254.50(4)		276.61(7)	277.1(1)	272.8(1)	253.6(1)	253.07(7)
Sn2−Se1	251.37(8)			259.53(4)	251.26(6)				262.3(1)	254.18(8)
Sn2−Se2			252.38(6)	252.47(4)		250.70(8)	250.6(1)	255.1(1)	252.9(1)	254.98(7)
Sn2−Se3/3’			260.11(6)	254.21(4)		265.57(7)	265.9(2)	271.2(1)	255.8(1)	254.04(7)
Sn2−Se4			254.43(6)			254.80(7)	255.3(2)	255.1(1)		
Sn3−Se1			252.47(6)			250.30(7)	250.4(1)	253.5(1)		
Sn3−Se3			258.19(6)			269.69(7)	270.0(2)	268.7(1)		
Sn3−−Se4			254.85(6)			256.38(8)	254.8(2)	254.6(1)		
Sn4−−Se1								376.4(1)		
Sn4−−Se2								379.3(1)		
Sn4−Se4								390.3(1)		
Sn1−N/O	234.5(7)	253.7(5)	276.8(4)	271.0(3)	230.6(5)	237.73(45)	239(1)	236.1(7)	243.1(8)	302.0(5)
Sn2−N/O	253.7(8)		253.0(4)	263.1(2)	235.2(4)	233(2) / 245(1)	239(1)	235.6(7)	244.3(8)	297.1(5)
Sn3−N/O			256.9(4)			236.8(5)	234(1)	237.5(7)		
Sn1−C1	217.4(7)	218.1(6)	220.7(5)	219.1(3)	218.8(6)	219.5(7)	220(1)	217.6(8)	221(1)	219.2(5)
Sn2−C7/13	218.5(6)		219.1(5)	218.9(3)	217.1(5)	218.2(6)	220(1)	219.2(9)	220(1)	219.4(5)
Sn3−C13/25			217.8(5)			218.8(6)	219(1)	219.4(9)		
Sn1−Cl	236.7(2) / 241.4(2)	238.4(2)	239.6(1)		235.8(2) / 243.1(2)	259.1(2)	258.3(3)			
N1−N2					140.0(6)	139.8(6)	139(1)	142(1)	140(19	137.7(7)
Se1−Sn1−Se2/1’		95.48(3)°	113.61(2)°	94.68(1)°		98.06(3)°	100.22(5)°	117.78(3)	92.36(4)°	94.91(2)°
Se3−Sn2−Se4			93.78(2)°			92.94(2)°	93.62(5)°	92.18(3)		
Se3−Sn3−Se4			94.14(2)°			91.62(2)°	92.75(5)°	92.89(3)		
Sn1−Se1−Sn2/1’	102.39(2)°	84.52(3)°		85.56(1)°	106.13(2)°				88.12(4)°	85.23(2)°
Se1−Sn2−Se2				94.03(1)°					92.77(4)°	95.03(2)°
Sn1−Se1−Sn3			96.79(2)°			90.68(2)°	91.53(4)°	88.05(3)		
Sn1−Se2−Sn2			96.39(2)°	85.73(1)°		91.89(2)°	92.91(5)°	88.82(3)	86.75(3)°	84.80(2)°
Sn2−Se3−Sn3			81.50(2)°			80.95(2)°	81.01(4)°	82.45(3)		
Sn2−Se4−Sn3			83.26(2)°			85.64(2)°	86.06(5)°	88.54(3)°		
Sn1−Se3−Sn2’				104.00(1)°					104.06(4)°	102.61(9)°
Se3−Sn1−Cl1			170.77(4)			171.45(5)°	169.62(8)°			
Se1−Sn1−Cl	99.72(7)° / 114.06(7)°	113.65(6)°	97.61(4)		109.22(5)° / 92.35(5)°	91.98.(4)°	94.69(8)°			
Se1−Sn1−O/N	83.5(2)°	82.2(1)°	72.93(8)°	76.58(5)°	89.9(1)°	175.6(1)°	170.4(8)°		83.5(2)°	76.38(9)°
Se1−Sn1−C1	123.87(3)°	128.8(2)°	129.4(1)°	126.4(1)°	135.5(2)°	100.4(2)°	98.9(7)°		122.6(3)°	114.2(2)°

Table S2: Selected structural parameters within compounds **10** and **B**.

Compound 10		Compound **B**	
Sn1−Se1	250.19(3)	Se1−Si1	229.5(2)
Sn1−Se2	262.03(4)	Si1−C1	185.9(7)
Sn1−Se2’	253.90(3)	Si1−C2	185.9(7)
Sn1−O1	273.3(2)	Si1−C3	187.0(6)
Sn1−C1	218.4(3)	Si1−Se1−Si1’	104.3(1)°
Cu1−Se1	246.43(5)		
Cu1−Se1’	245.75(4)		
Cu1−P1	222.45(6)		
Cu1—Se2	321.21(5)		
Cu1−Cu1’	270.60(6)		
Se1−Sn1−Se2	105.88(1)°		
Se2−Sn1−Se2’	93.87(1)°		
Sn1−Se2−Sn1’	81.46(1)°		
Se1−Cu−Se1’	112.67(1)°		
Cu−Se1−Cu1’	66.71(1)°		
Se1−Cu1−P1	120.31(2)°		
Se1−Sn1−C1	113.31(8)°		
Se1−Sn1−O1	88.94(4)°		

NMR spectroscopy

The time dependent ^{119}Sn NMR spectra measured on reaction mixtures of **A** to **B** in 1:1 ratio (Figure S14) or 2:3 ratio (Figure S15) do not change over the monitored time span of 10 hours.

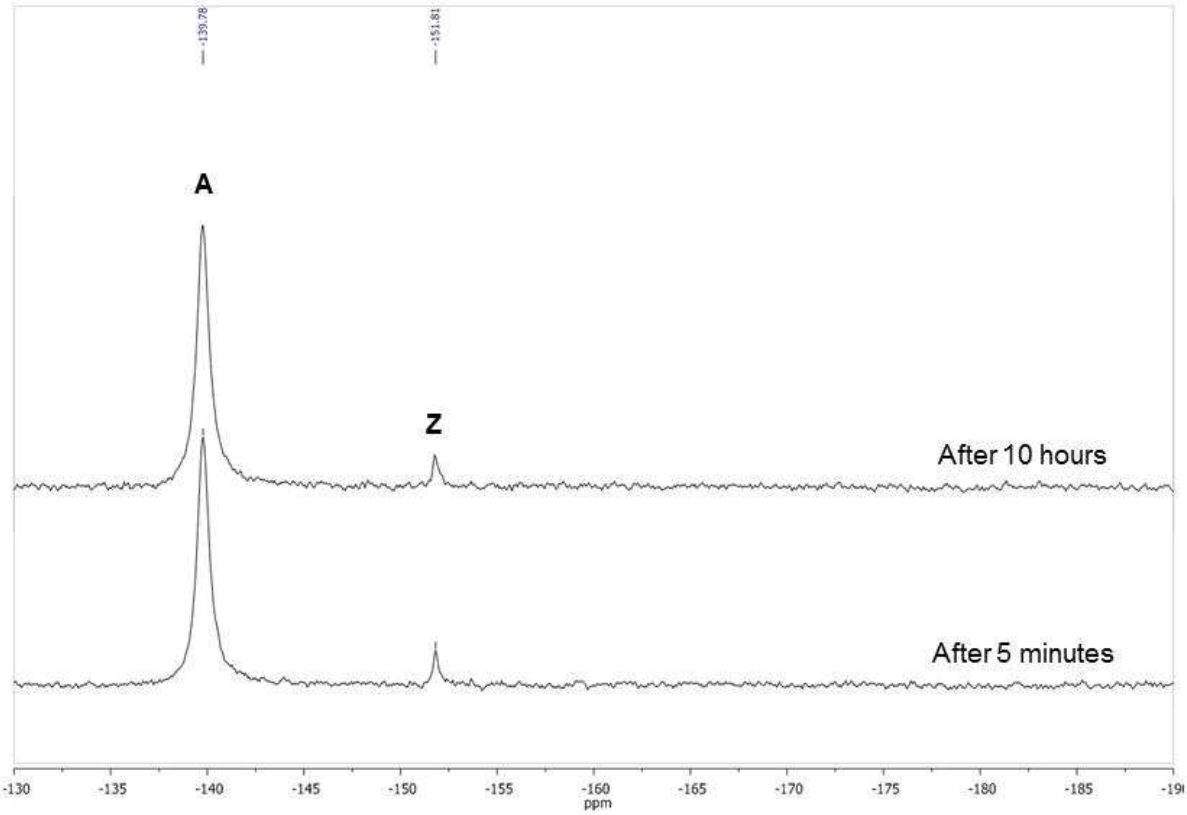

Figure S14: NMR spectrum of a solution of **A** with one equivalent of **B** after 5 minutes and 10 hours of reaction time.

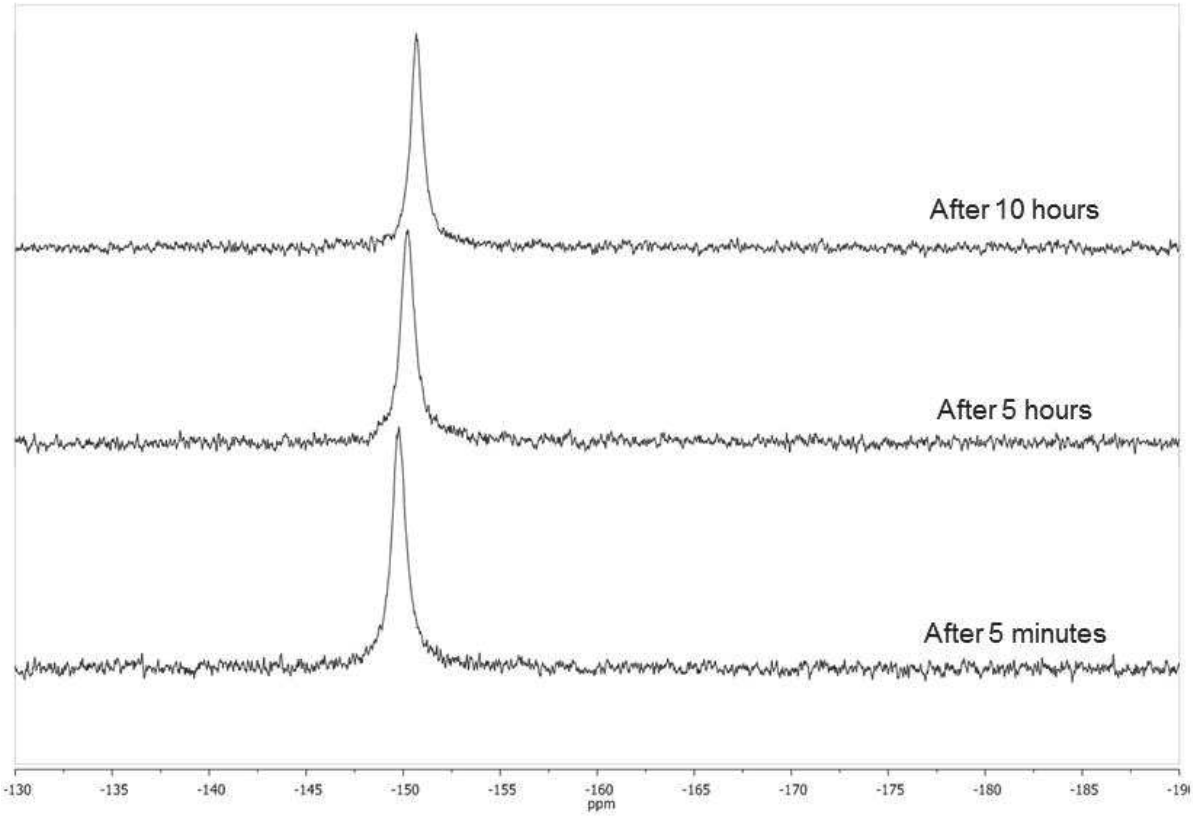

Figure S15: NMR of a solution of **A** with 1.5 equivalents of **B** after 5 minutes, 5 hours and 10 hours of reaction time.

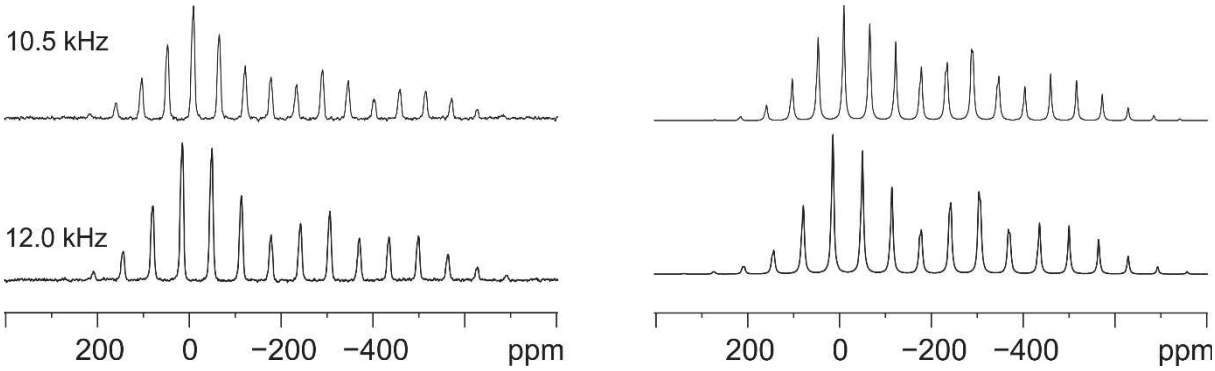

Figure S16: ^{119}Sn-MAS NMR spectra of **3** measured (left) and simulated (right) at 10.5 kHz (top) and 12.0 kHz (bottom).

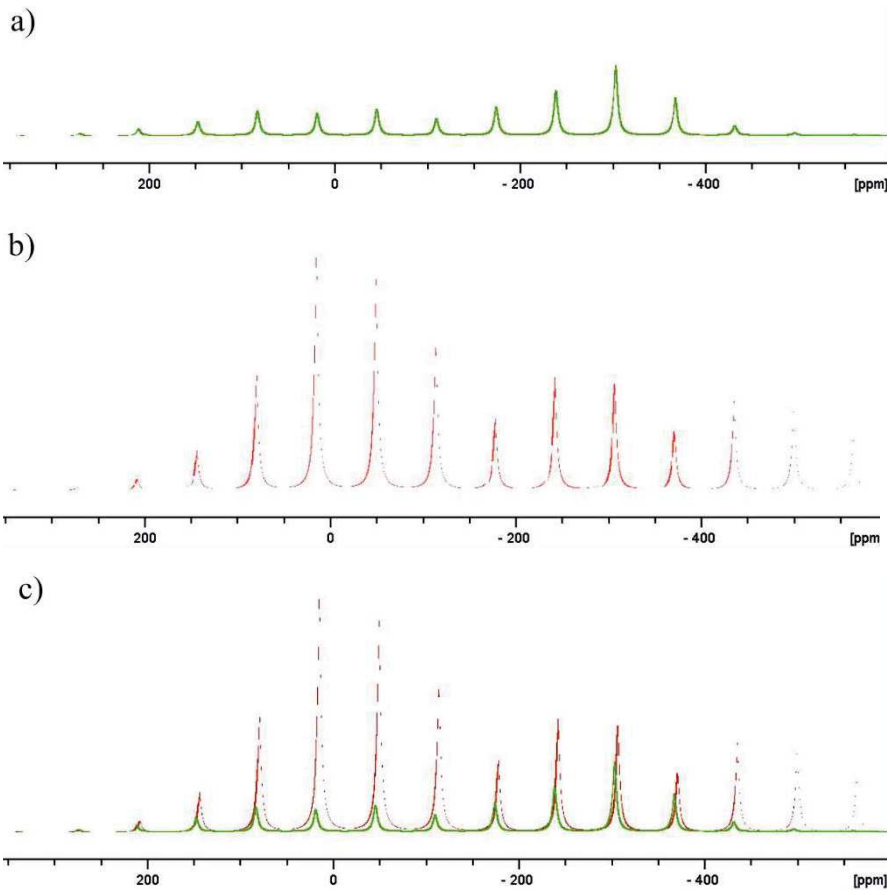

Figure S17: Deconvolution sites to the simulated ^{119}Sn-MAS NMR spectrum of **3** at 12.0 kHz: site-1 (a), site-2 (b) and overlay of them (c).

References for the Electronic Supplementary Information

[1] G. M. Sheldrick, *Acta Crystallogr.* **2008**, *A64*, 112-122.

[2] Z. Hassanzadeh Fard, L. Xiong, C. Müller, M. Hołyńska, S. Dehnen, *Chem. Eur. J.* **2009**, *15*, 6595-6604.

[3] M. R. Halvagar, Z. Hassanzadeh Fard, S. Dehnen, *Chem. Eur. J* **2011**, *17*, 4371-4.

3.2. Ternary Mixed-Valence Organotin Copper Selenide Clusters

Niklas Rinn, Lukas Guggolz, Jurek Lange, Sangam Chatterjee, Theresa Block, Rainer Pöttgen und Stefanie Dehnen, *Chem. Sci.* **2017**, eingereichtes Manuskript.

Abstract: Expansion of the organic functionalized tin selenide clusters $[(R^1Sn)_3Se_4Cl]$ (**A**, $R^1 = CMe_2CH_2C(O)Me$) or $[(R^1Sn)_4Se_6]$ (**B**) with $[Cu(PPh_3)_{3-x}Cl_x]$ yields cluster compounds with different inorganic, mixed-valence core structures: $[Cu_4Sn^{II}Sn^{IV}_6Se_{12}]$, $[Cu_2Sn^{II}_2Sn^{IV}_4Se_8Cl_2]$, $[Cu_2Sn^{II}Sn^{IV}_4Se_8]$, $[Cu_2Sn^{II}_2Sn^{IV}_2Se_4Cl_4]$, and $[Cu_2Sn^{IV}_2Se_4]$. Five of the compounds, namely $[(CuPPh_3)_2\{(R^1Sn)_2Se_4\}]$ (**1**), $[(CuPPh_3)_2Sn\{(R^2Sn)_2Se_4\}_2]$ (**2**), $[(CuPPh_3)_2(SnCl)_2(RSn)_2Se_4\}_2]$ (**3**) $[(CuPPh_3)_2(SnCu_2)\{(R^1Sn)_2Se_4\}_3]$ (**4**), and $[Cu(CuPPh_3)(SnCu_2)\{(R^1Sn)_2Se_4\}_3]$ (**5**) are structurally closely related. They are based on $[(CuPPh_3)_2\{(RSn)_2Se_4\}_n]$ aggregates comprising $[(RSn)_2Se_4]$ and $[CuPPh_3]$ building units, which are linked by further metal atoms. A sixth compound, $[(CuPPh_3)_2(SnCl)_2\{(R^1SnCl)Se_2\}_2]$ (**6**), differs from the others by containing $[(RSnCl)Se_2]$ units instead, which affects the absorption properties. The compounds were analyzed by single-crystal X-ray diffraction, NMR and ^{119}Sn Mößbauer spectroscopy, DFT calculations as well as optical absorption experiments.

Inhaltsangabe: Eine Reihe strukturell verwandter Kupfer-Organozinnselenidcluster wurde durch Umsetzung von Organozinnselenidcluster vom DHK- beziehungsweise DD-Typ, $[(SnR^1)_3Se_4Cl]$ (**A**) beziehungsweise $[(SnR^1)_4Se_6]$ (**B**),[101] mit $[Cu(PPh_3)_{4-x}Cl_x]$ (x = 1-2) und $(SiMe_3)_2Se$ dargestellt und über NMR-Spektroskopie, Absorptions-Spektroskopie Mößbauer-Spektroskopie, Einkristallstrukturanalyse und quantenchemische Rechnungen charakterisiert. Hierbei wurden in Abhängigkeit von der Natur der eingesetzten Ausgangscluster und des Kupferkomplexes Verbindungen mit verschiedenen Clustertopologien erhalten: $[(CuPPh_3)_2\{(R^1Sn)_2Se_4\}]$ (**1**), $[(CuPPh_3)_2(SnCl)_2(R^1Sn)_2Se_4\}_2]$ (**3a**) und $[(CuPPh_3)_2(SnCu_2)\{(R^1Sn)_2Se_4\}_3]$ (**4**). Durch Erhöhung der Eduktkonzentration in der Reaktionslösung ließ sich bei der Synthese zu **4** zudem ein weiterer Cluster isolieren, $[Cu(CuPPh_3)(SnCu_2)\{(R^1Sn)_2Se_4\}_3]$ (**5**), welcher durch das Entfernen eines PPh_3 Liganden aus **4** gebildet werden könnte. **5** liegt in Lösung offenbar in einem dynamischen Gleichgewicht mit der thermodynamisch stabileren Verbindung **4** vor und konnte nur aufgrund seiner geringen Löslichkeit isoliert werden. Reaktionen von **3a** mit Hydrazinen führten zur Bildung der Verbindungen $[(CuPPh_3)_2(SnCl)_2(R^2Sn)_2Se_4\}_2]$ (**3b**) und $[(CuPPh_3)_2(SnCl)_2(R^4Sn)_2Se_4\}_2]$ (**3c**) mit isostrukturellem anorganischem Grundgerüst. Setzt man jedoch **4** mit $N_2H_4{\cdot}H_2O$ um, so führt dies zu einer Umlagerung des anorganischen Grundgerüstes und zur Bildung von $[(CuPPh_3)_2Sn\{(R^2Sn)_2Se_4\}_2]$ (**2**). Die Verbindungen sind insofern strukturell verwandt, als sie aus zwei durch eine (**1**), zwei (**2**, **3**) oder drei (**4**, **5**) $[(SnR)_2Se_4]$-Brücke(n) verknüpften $[CuPPh_3]$-Einheiten bestehen. In den Clustern mit zwei oder drei dieser Verbrückungen finden sich im Clusterinneren entweder ein Sn^{II}-Atom (**2**), zwei $[Sn^{II}Cl]$-Fragmente (**3**) oder ein $[Cu_2Sn^{II}]$-Fragment (**4**, **5**). Eine Reaktion zwischen **A** und $[Cu(PPh_3)_2Cl_2]$ ergibt ohne die Zugabe von $(SiMe_3)_2Se$ eine weitere Verbindung, $[(CuPPh_3)_2(SnCl)_2\{(R^1SnCl)Se_2\}_2]$ (**6**), welche sich formal aus **3a** ableiten lässt, indem die $[(SnR^1)_2Se_2]$-Einheiten durch $[ClSnR^1]$ ersetzt werden. Im Gegensatz zu den anderen, orangeroten Verbindungen liegt **6** farblos vor. Dies lässt sich mit einem Blick auf die Elektronendichteverteilung in den Grenzorbitalen der verwandten Verbindungen **3a** und **6** verstehen. Während das höchte besetzte Molekülorbital (highest occupied molecular orbital, HOMO) in beiden Fällen von Beiträgen der Atome des anorganischen Clusterkerns herrührt, wird das niedrigste unbesetzte Molekülorbital (lowest unoccupied molecular orbital, LUMO) hauptsächlich von Atomen der $[(SnR^1)_2Se_4]$-Einheiten (**3a**) oder eben der $[(ClSnR^1)Se_2]$-Einheiten gespeist. Hieraus resultiert eine deutlich unterschiedliche HOMO-LUMO-Energiedifferenz. Abbildung 3.2 zeigt die in dieser Veröffentlichung bestimmten Molekülstrukturen.

Eigener Anteil: Alle Reaktionen wurden von mir geplant und alle analytischen Daten wurden von mir ausgewertet. **4** wurde bereits während meiner Masterarbeit von mir synthetisiert und

NMR-spektroskopisch sowie röntgenographisch charakterisiert. Alle Reaktionen wurden von mir durchgeführt – mit Ausnahme derjenigen, die zur Bildung der Verbindungen **1** und **6** führten (unter meiner Anleitung durchgeführt von Nils Spang im Rahmen eines Forschungspraktikums), sowie derjenigen, aus denen die Verbingungen **3a**·2CH_2Cl_2, **3b** und **3c** hervorgingen (unter meiner Anleitung durchgeführt von Mario Argentari während seiner Arbeiten als wissenschaftliche Hilfskraft für mich). Alle quantenchemische Rechnungen wurden von Lukas Guggolz durchgeführt. Die Absorptionsspektroskopie an Einkristallen wurde von Jurek Lange in der Arbeitsgruppe von Prof. Dr. Sangam Chatterjee durchgeführt. Mößbauer-Spektren wurden von Theresa Block in der Arbeitsgruppe von Prof. Dr. Rainer Pöttgen gemessen. Sämtliche ^{1}H-NMR-Messungen wurden von mir durchgeführt. ^{119}Sn-NMR- und ^{31}P-NMR-Experimente erfolgten unter Anleitung von Dr. Xiulan Xie in der zentralen NMR-Abteilung des Fachbereichs Chemie an der Philipps-Universität Marburg. Alle Röntgenbeugungsexperimente – mit Ausnahme des Experiments zur Strukturbestmimung des lösungsmittelfreien Kristalls von **5** – wurden von mir betrieben. Die Kristallstrukturanalyse jener Verbindung wurde von der zentralen Abteilung für Kristallstrukturanalyse am Fachbereich Chemie der Philipps-Universität Marburg unter der Leitung von Dr. Klaus Harms durchgeführt. Das Manuskript habe ich in Kooperation mit Stefanie Dehnen geschrieben. Die Co-Autoren haben jeweils kurze Abschnitte über ihre Beiträge eingefügt oder die von uns vorgeschlagenen Abschnitte dazu überarbeitet.

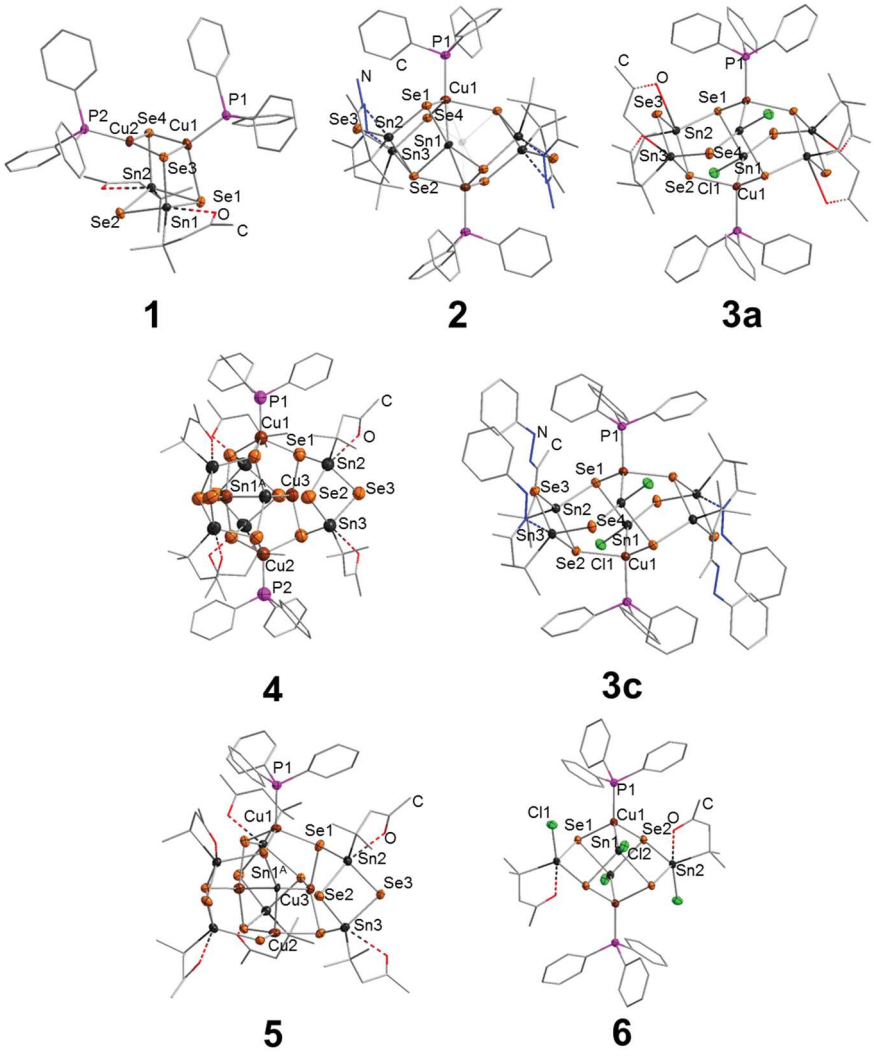

Abbildung 3.2: In „Ternary Mixed-Valence Organotin Copper Selenide Clusters" beschriebene Molekülstrukturen. Wasserstoffatome wurden aus Übersichtlichkeitsgründen nicht angezeigt.

Journal Name

ARTICLE

Ternary Mixed-Valence Organotin Copper Selenide Clusters

Niklas Rinn,[a] Lukas Guggolz,[a] Jurek Lange,[b] Sangam Chatterjee,[b] Theresa Block,[c] Rainer Pöttgen,[c] and Stefanie Dehnen*[a]

Received 00th January 20xx,
Accepted 00th January 20xx

DOI: 10.1039/x0xx00000x

www.rsc.org/

Expansion of the organic functionalized tin selenide clusters $[(R^1Sn)_3Se_4Cl]$ (**A**, $R^1 = CMe_2CH_2C(O)Me$) or $[(R^1Sn)_4Se_6]$ (**B**) with $[Cu(PPh_3)_{3-x}Cl_x]$ yields cluster compounds with different inorganic, mixed-valence core structures: $[Cu_4Sn^{II}Sn^{IV}{}_6Se_{12}]$, $[Cu_2Sn^{II}{}_2Sn^{IV}{}_4Se_8Cl_2]$, $[Cu_2Sn^{II}Sn^{IV}{}_4Se_8]$, $[Cu_2Sn^{II}{}_2Sn^{IV}{}_2Se_4Cl_4]$, and $[Cu_2Sn^{IV}{}_2Se_4]$. Five of the compounds, namely $[(CuPPh_3)_2\{(R^1Sn)_2Se_4\}]$ (**1**), $[(CuPPh_3)_2Sn\{(R^2Sn)_2Se_4\}_2]$ (**2**), $[(CuPPh_3)_2(SnCl)_2\{(RSn)_2Se_4\}_2]$ (**3**) $[(CuPPh_3)_2(SnCu_2)\{(R^1Sn)_2Se_4\}_3]$ (**4**), and $[Cu(CuPPh_3)(SnCu_2)\{(R^1Sn)_2Se_4\}_3]$ (**5**) are structurally closely related. They are based on $[(CuPPh_3)_2\{(RSn)_2Se_4\}_n]$ aggregates comprising $[(RSn)_2Se_4]$ and $[CuPPh_3]$ building units, which are linked by further metal atoms. A sixth compound, $[(CuPPh_3)_2(SnCl)_2\{(R^1SnCl)Se_2\}_2]$ (**6**), differs from the others by containing $[(RSnCl)Se_2]$ units instead, which affects the absorption properties. The compounds were analyzed by single-crystal X-ray diffraction, NMR and ^{119}Sn Mössbauer spectroscopy, DFT calculations as well as optical absorption experiments.

Introduction

The family of discrete metal chalcogenide clusters with a ternary inorganic core comprises a diversity of structural motifs and compositions, ranging from ligand-stabilized neutral heterocubanes,[1–4] to huge anionic supertetrahedra,[5–7] from clusters of moderate size[8] to compounds on a nanometer scale.[9,10] These feature combinations of different transition metal atoms[11–14] or different main group metal atoms,[15] or both,[16–19] or transition metal with lanthanide atoms.[20–22]

Our work aims at the elemental combination of group 14 atoms (T = Ge, Sn, Pb) with transition metal atoms M in ternary chalcogenide-bridged clusters (E = S, Se, Te) for fine-tuning of their structural and optoelectronic properties.[23–27] The elemental combination Cu/Sn/E is currently actively studied regarding molecular multi-component precursors for highly efficient copper-zinc-tin-sulfide/selenide (CZTS/Se) solar cells.[28,29] Our general approach to obtaining ternary M/Sn/E clusters is the expansion of organo-functionalized RSn/E clusters by addition of A_2E (A = Na, $SiMe_3$) and a transition metal salt to form the target compounds,[30–36] a strategy, which was first showcased by Merzweiler and co-workers.[37]

Several Sn/Cu/S clusters were reported by other groups[37–43] as well as by ourselves,[30–32,44] yet only two discrete Sn/Cu/Se compounds have been known so far.[35,36] However, only one of them, $[(CuPPh_3)_2\{(R^1Sn)_2Se_4\}]$ ($R^1 = CMe_2CH_2C(O)Me$), was decorated by a functional organic ligand, which represents the inspiration for this work. Herein, we report reactions of $[(R^1Sn)_3Se_4Cl]$ (**A**) and $[(R^1Sn)_4Se_6]$ (**B**) with $(SiMe_3)_2Se$ (**C**) and $[Cu(PPh_3)_{4-x}Cl_x]$ (**D**, x = 1; **E**, x = 2), yielding a series of ternary organo-functionalized and mixed-valence RSn/Cu/Se clusters.

Results and Discussion

Synthesis

To access the target compounds (Scheme 1), clusters **A** and **B** were treated with $(SiMe_3)_2Se$ (**C**) and $[Cu(PPh_3)_3Cl]$ (**D**) in dichloromethane (DCM), resulting in a color change from colorless to deep orange. **A** was also reacted with $[Cu(PPh_3)_2Cl_2]$ (**E**) both in the presence and absence of additional $(SiMe_3)_2Se$ at low temperatures, which resulted in the formation of a red solution and a small amount of precipitate that was removed by filtration. After layering of the diverse reaction solutions with *n*-hexane, a series of compounds were obtained as single crystals that comprised structurally related clusters.

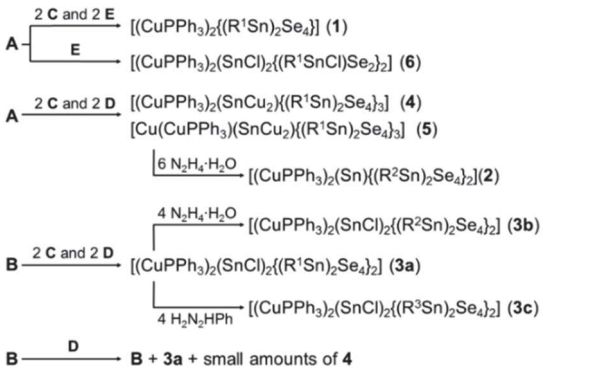

Scheme 1. Reactions (in DCM) to yield the ternary RSn/Cu/Se clusters of this study. **A** = $[(SnR^1)_3Se_4Cl]$, **B** = $[(SnR^1)_4Se_6]$ **C** = $(SiMes_3)_2Se$, **D** = $[Cu(PPh_3)_3Cl]$, **E** = $[Cu(PPh_3)_2Cl_2]$.

[a] Fachbereich Chemie und Wissenschaftliches Zentrum für Materialwissenschaften, Philipps-Universität Marburg, Hans-Meerwein-Straße 4, 35043 Marburg, Germany, E-mail: dehnen@chemie.uni-mabrug.de
[b] Department of Physics, Justus-Liebig University Gießen, Heinrich-Buff-Ring 16, 35392 Gießen, Germany
[c] Institut für Anorganische und Analytische Chemie, Westfälische Wilhelms-Universität Münster, Corrensstraße 30, 48149 Münster, Germany

Electronic Supplementary Information (ESI) available: [details of any supplementary information available should be included here]. See DOI: 10.1039/x0xx00000x

A common feature all of the clusters – except compound **6** – is the presence of ligand-protected ternary units of the general formula $[(CuPPh_3)_2\{(RSn^{IV})_2Se_4\}_n]$ (n = 1–3), which additionally enclose Sn^{II}-containing subunits for n = 2 and 3. In some cases, a mixture of products was isolated, most likely due to an equilibrium in solution and during crystal formation.

Being the compound with the smallest and most simple cluster, $[(CuPPh_3)_2\{(R^1Sn)_2Se_4\}]$ (**1**) was obtained as orange blocks. **1** represents an isomer of the recently reported compound,[35] which was obtained upon reaction of **B** with **C** and the **D**, yet as a minor product.

Two different cluster types based on two $[(SnR)_2Se_4]$ units are present in $[(CuPPh_3)_2Sn\{(R^2Sn)_2Se_4\}_2]$ (**2**), $R^2 = CMe_2CH_2C(NNH_2)Me$), containing a central Sn^{II} atom, and $[(CuPPh_3)_2(SnCl)_2(R^1Sn)_2Se_4\}_2]$ (**3a**), encompassing two $Sn^{II}Cl$ units instead. Addition of hydrazine hydrate or phenylhydrazine to reactive solutions of **B** and $[Cu(PPh_3)_3Cl]$, or to a fresh solution of **3a**, respectively, leads to the formation of derivatives, $[(CuPPh_3)_2(SnCl)_2(R^2Sn)_2Se_4\}_2]$ (**3b**) or $[(CuPPh_3)_2(SnCl)_2(R^3Sn)_2Se_4\}_2]$ (**3c**, $R^3 = CMe_2CH_2C(NNHPh)Me$). It should be mentioned that the identity of **3b** was derived from NMR data only, as no single crystal of **3b** of sufficient quality could be grown so far to verify our structural model. However, from analyzing the NMR data, the molecular structure of **3b** is likely isotype to that of **3a** and **3c**.

C_3 symmetry is observed in $[(CuPPh_3)_2(SnCu_2)\{(R^1Sn)_2Se_4\}_3]$ (**4**) and $[Cu(CuPPh_3)(SnCu_2)\{(R^1Sn)_2Se_4\}_3]$ (**5**), two topologically identical clusters that differ in the presence (**4**) or absence (**5**) of a second PPh_3 ligand, which affects the coordination geometry at one of the Cu atoms and the clusters solubility.

The only compound that does not comprise $[(RSn)_2Se_4]$ units is $[(CuPPh_3)_2(SnCl)_2\{(R^1SnCl)Se_2\}_2]$ (**6**). Yet, it is structurally related to **3c** by formally replacing these units with $[(R^1SnCl)Se_2]$.

We note that the compounds are not always obtained as single products. **1**, **3a** and **4** crystallize alongside each other when using **B** as a starting material; yet, the relative amounts of these three products depend on the reaction pathway chosen. Starting from **A** and **D** however, only crystals of **4** are formed. On the other hand, both the addition of $N_2H_4{\cdot}H_2O$ to **4** or using the hydrazone derivative of **A**, $[(R^2Sn)_3Se_4Cl]$, instead of **A** yields exclusively **2**. As both **4** and **2** exhibit a $[Cu_2Sn]$ unit, it seems obvious that the inorganic cores can be converted into each other in solution, but it is not obvious why the two structural motifs are found exclusively with either hydrazone (**2**) or keto groups (**4**), respectively. **5** is obtained beside **4** when working in high concentration. A dynamic equilibrium seems to exist in the reaction mixture between both compounds, with compound **5** being thermodynamically disfavoured. The isolation of **5** as a solid, hence its withdrawal from the said equilibrium, can be achieved by increasing the concentration, as the smaller number of Ph groups at the cluster periphery causes a lower solubility of **5**. When **A** is reacted with **E** in the absence of **C**, the only crystalline product (besides a small amount of **B**) is **6**. Addition of **C** to the same reactive solution yields **1** upon filtration and layering. By cooling of this reaction solution prior to layering, however, one obtains an orange precipitate that can be partially re-dissolved. Layering of this solution yields crystals of $\mathbf{5}{\cdot}C_6H_{14}$, which at the same time hints at the presence of **4** in the reactive solution. These observations indicate the presence of subtle equilibria between the cluster species in solution, which remain to be understood in detail. While **A** does not react with **D** without addition of **C**, **B** can be partially converted into compounds **3a** (and traces of **4**) upon addition of **D** only. Excess of **D** does not seem to have any influence on the product ratio, as was shown in NMR experiments (see below).

Crystal Structures

All single crystals were obtained within two days upon layering reactive solutions in DCM with *n*-hexane. The molecular structures are shown in Figure 1, while crystallographic details are listed in Tables 1 and 2. In the case of **2**, **3a** and **5**, which crystallize with different amounts of solvent molecules, only the single-crystal structures with best data sets are discussed in the main article. For a summary of all crystal structures and more details of crystallographic data see the Supporting Information.

A cluster that is isomeric to **1**, but crystallizes with two molecules of $CHCl_3$ was reported in our previous publication.[35] **1** possesses the same general connectivity as the reported cluster, with two $[CuPPh_3]$ fragments being connected by two Se atoms of an $[(R^1Sn)Se_4]$ unit. However, unlike the known cluster, the $[Sn_2Se_2]$ and $[Cu_2Se_2]$ subunits are distorted, leading to a smaller and a larger Se–Cu distance between the two rings (Se1–Cu1 2.8222(8) Å, Se2–Cu2 3.4004(8) Å). The short, yet non-bonding, Cu1–Cu2 distance of 2.678(1) Å was found to be notably shorter than in the reported isomer (2.7332(7) Å).

The unit cell of **2**·1.5 DCM contains two crystallographically independent molecules of **2**, both of which are constructed by inversion of a $[PPh_3CuSn^{II}_{0.5}(Sn^{IV}R^2)_2Se_4]$ cluster half (**2A** and **2B**). Two $\{(R^1Sn)Se_4\}$ units connect the two Cu atoms by coordinating one of them with both of their "terminal" Se atoms (Se1, Se4) and the second one with a Se atom of the four-membered ring (Se2). A central Sn^{II} atom, Sn1, is disordered over two equivalent positions close to the inversion center, with a site occupation factor of 0.5. Sn1 is further coordinated by three Se atoms (Se1, $Se2^{i/ii}$, Se3; I = 1–*x*, 1–*y*, 1–*z*; ii = 1–*x*, 2–*y*, 2–*z*), leading to a very asymmetrical distortion of the Cu–Sn–Cu unit (Sn–Cu 2.552(1) and 2.757(1) in **2A**, 2.668(2) and 2.764(2) in **2B**). The two independent molecules differ significantly in their $Sn1\cdots Se3^{i}$ distances (3.448(1) Å in **2A**, 2.997(1) Å in **2B**). The origin of this structural detail is not clear so far, and it was not observed in the crystal structure of **2**·6DCM (see Supporting Information).

3a features a structural motive, which has been described for the homologous sulfur compound.[31] Two $[(SnR^1)_2Se_4]$ units encase an inner unit comprising two $(CuPPh_3)$ and two $(Sn^{II}Cl)$ fragments that are located close to the inversion center of the molecule. The Cu–Sn bonds that link both fragments (2.5831(8) Å) is slightly shorter than reported for the sulfur analogue (2.6054(4) Å). Unlike in **2**, only one of the terminal Se atoms (Se1) in the $[(SnR^1)_2Se_4]$ fragment coordinates a Cu moiety, while the other one (Se4) binds to Sn1. Again, a Se atom of the four-membered ring (Se2) is connected to the second Cu atom.

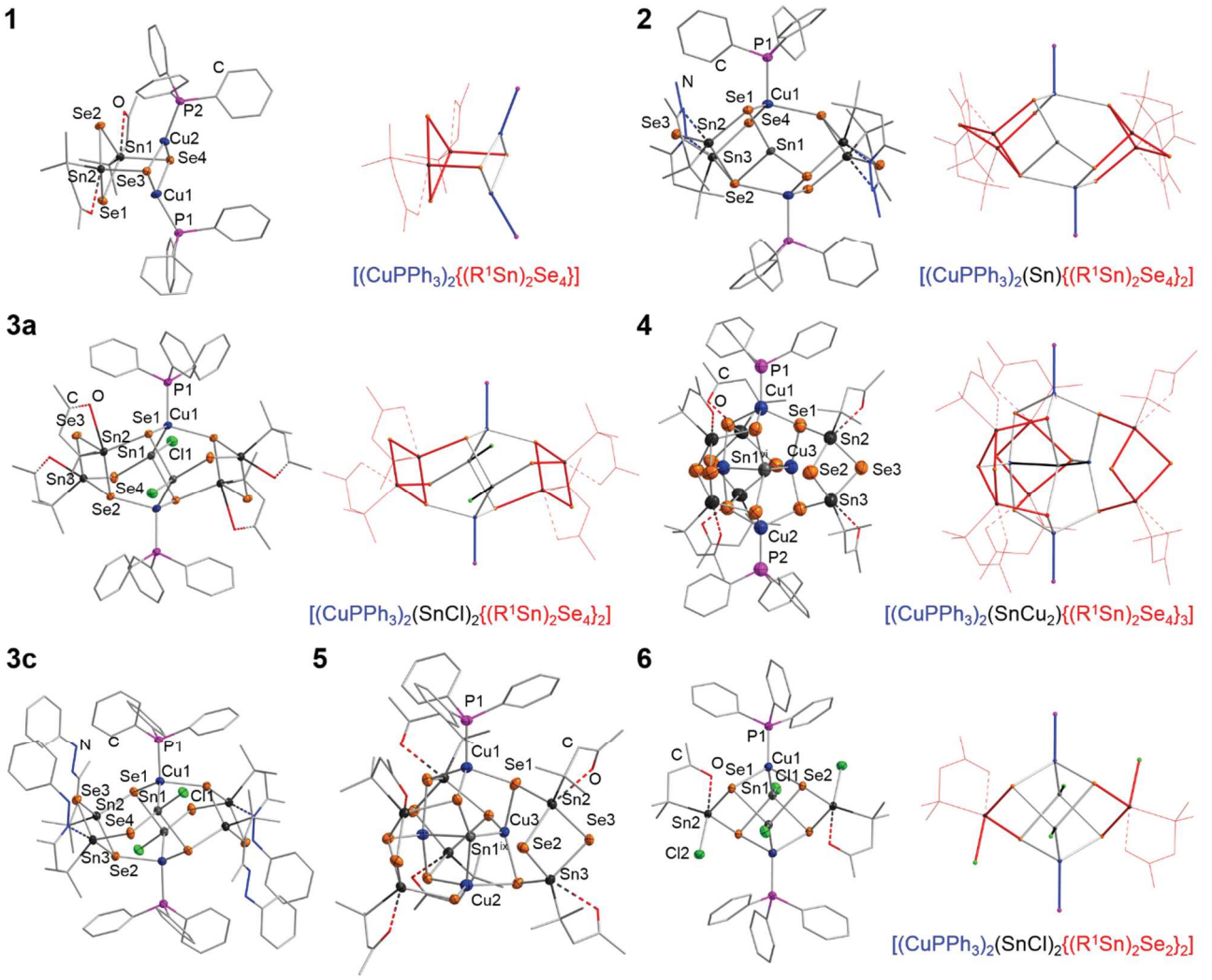

Figure 1 Molecular structures of compounds **1**–**6**. Displacement ellipsoids are shown at 50% probability. Hydrogen atoms are omitted and organic ligands are shown in wire representation for clarity. Additionally, wire model is shown for different structural archetypes, showing the $(SnR)_2Se_4$ (or RSnCl in **6**) unit in red, $CuPPh_3$ in blue and the central atoms in black.

While the organic ligand was modified by expansion, the inorganic core of **3c** remains isostructural to **3a**. Unlike all previously observed molecular structures of organotinselenide clusters obtained with our typical Lewis-basic ligands, one of the two crystallographically independent R^3Sn moieties does not exhibit intramolecular N→Sn coordination (Sn2···N1 2.929(7) Å, as opposed to Sn3–N3 2.358(5) Å). This leads to a clear tetragonal coordination geometry at Sn2 and consequently to a shorter Sn2–Se2 contact.

4 features three $[(R^1Sn)_2Se_4]$ units that connect two $CuPPh_3$ moieties by their "terminal" Se atoms, similar to the structure of **1**. Within this cage-like arrangement, one observes an $Sn^{II}Cu_2$ unit (Sn–Cu 2.699(3), 2.748(3) Å), which is disordered around the crystallographic C_3 axis (depicted in Figure S16). This cluster topology is reminiscent of an organotinsulfide cluster previously reported by us $[\{(R^1Sn)_2S_4\}_3Sn_2]$, in which the $CuPPh_3$ units are formally substituted by an $(Sn^{III})_2$ dumbbell.[45]

The topologically identical cluster core of **5** can be derived from that of **4** by simply removing one of the PPh_3 ligands from one of the Cu atoms. This leads to a retraction of the corresponding Cu2 atom into the cluster core, thereby adopting a trigonal planar coordination sphere. Additionally, a short Cu2–Sn1 bond (2.674(2) Å) goes hand in hand with the elongation of all other interatomic distances involving Sn1. By means of quantum chemical calculations using density functional theory (DFT) methods within the program system TURBOMOLE,[46] the Cu–P bond dissociation energy was estimated as 208 kJ/mol based on the fragmentation of the optimized structure of **4** (all optimized structures are given in the Supporting Information). This supports the assumption of a dynamic equilibrium to be present in solution mentioned above, from which the cluster with lower solubility crystallized under the given conditions. The short $Sn1^{ix}$–Cu2 distance in **5** (2.674(2) Å), which is not found in **4** and thus results from the removal of the PPh_3 group, has a similar shared electron number (SEN; calculated by population analyses based on occupation numbers, Paboon),[47] as all other Sn–Cu bonds in compound **5**.

Table 1 Crystallographic data and refinement results of **1** – **6**.

Compound	**1**·2 CH_2Cl_2	**2**·1.5 CH_2Cl_2	**3a**·2 CH_2Cl_2
Empirical formula	$C_{50}H_{56}Cu_2Cl_4O_2P_2Se_4Sn_2$	$C_{123}H_{170}Cl_6Cu_4N_{16}P_4Se_{16}Sn_{10}$	$C_{62}H_{78}Cl_6Cu_2O_4P_2Se_8Sn_6$
Formula weight / g·mol^{-1}	3152.15	2456.87	2632.78
Crystal color and shape	orange blocks	orange block	Dark orange block
Crystal size / mm^3	0.36×0.27×0.24	0.39x0.29x0.27	0.32×0.07×0.06
Crystal system	Monoclinic	triclinic	triclinic
Space group [Flack parameter]	$P2_1$ [–0.004(5)]	$P\bar{1}$	$P\bar{1}$
a / Å	10.8270(4)	13.8331(6)	12.0962(6)
b / Å	25.7693(8)	16.1979(7)	13.2517(6)
c / Å	1.8579(4)	20.4336(9)	14.9886(7)
α / °	90	80.961(4)	91.547(4)
β / °	112.020(3)	71.486(3)	111.611(4)
γ / °	90	66.517(3)	107.954(4)
V / Å^3	2808.4(2)	3979.5(3)	2097.9(2)
Z	2	2	1
ρcalcd / g·cm^{-3}	1.86	2.05	2.08
μ(Mo Kα) / mm^{-1}	4.5	5.9	5.0
Absorption correction type	numerical	numerical	numerical
Min. / max. transmission	0.450 / 0.663	0.177 / 0.288	0.602 / 0.702
2 θ range / deg	3.16 / 53.42	2.74 / 53.60	3.27 / 53.57
No. of measured Reflections	26065	64641	18119
R(int)	0.0391	0.1302	0.0681
Independent Reflections	11795	16777	8815
Indepemdent Reflections (I > 2σ(I))	10835	9243	6645
No. of parameters	620	836	422
R1 (I > 2σ(I)) / wR2 (all data)	0.0238 / 0.0501	0.0411 / 0.0867	0.0367 / 0.0903
S (all data)	0.937	0.744	0.924
Max. peak / hole / e$^-$· Å^3	0.83 / –0.37	1.75 / –1.00	2.34 / –1.44

The molecular structure of **6** can be described as consisting of two [Cu(PPh_3)–Se–Sn(Cl)–Se] four-membered rings that are connected by two Cu–Sn bonds (2.6178(5) Å) and additionally linked by two [R^1SnCl] units coordinated by two Se atoms (one of each of the four-membered rings, Sn–Se 2.5326(4)-2.5364(5) Å). This topology can be derived from **3a** by replacing the two [($R^1Sn)_2Se_4$] units with two [(R^1SnCl)Se_2] units (or even simpler, by replacing the [($R^1Sn)_2Se_2$] four-membered rings with an [R^1SnCl] unit). This difference might be put down to different reactive conditions leading to **6**. In all other reactions, we added **C** to the reactive solutions to initiate a fragmentation of the educt cluster compounds, which seems to be unnecessary when using **E**.

3c·3 CH_2Cl_2	**4**·3 CH_2Cl_2	**5**·0.5 C_6H_{14}	**6**
$C_{87}H_{104}Cl_8Cu_2N_8P_2Se_8Sn_6$	$C_{75}H_{102}Cu_4Cl_6O_6P_2Se_{12}Sn_7$	$C_{57}H_{89}Cu_4O_6PSe_{12}Sn_7$	$C_{48}H_{52}Cl_4Cu_2O_2P_2Se_4Sn_4$
3078.22	3152.15	2932.74	1782.31
orange blocks	orange pyramids	Red cube	colourless needle
0.28x0.19x0.17	0.36×0.27×0.24	0.12x0.12x0.12	0.12x0.02x0.02
Triclinic	cubic	cubic	monoclinic
$P\bar{1}$	$P2_13$ [(0.014(8)]	$Pa\bar{3}$	$P2_1/c$
13.542(3)	23.6313(2)	25.1063(5)	14.9021(6)
14.952(3)	*a*	*a*	11.4905(3)
15.235(3)	*a*	*a*	18.1166(6)
65.93(3)	90	90	90
76.29(3)	90	90	113.056(3)
77.23(3)	90	90	90
2709(1)	13196.6(2)	15825.2(9)	2854.4(2)
1	4	8	2
1.89	1.79	2.43	2.07
4.7	5.5	8.9	5.3
numerical	numerical	numerical	numerical
0.354 / 0.573	0.246 / 0.357	0.256 / 0.312	0.698 / 0.954
3.01 / 58.38	2.44 / 53.70	3.63 / 53.58	4.63 / 53.49
40757	92192	18768	21519
0.0834	0.1270	0.0978	0.0525
14435	9357	5556	5979
10897	7645	3294	4616
583	380	268	332
0.491 / 0.1347	0.0495 / 0.0968	0.0440 / 0.0462	0.0227 / 0.0389
0.954	0.988	0.833	0.847
5.04 / –2.05	0.57 / –0.50	1.24 / -0.74	0.65 / –0.49

We anticipate, that a redox process between Cu^{2+} and Se^{2-} atoms from **A** led to an initial fragmentation of the precursor cluster, which then captured the in-situ formed $[Cu^{I}PPh_3]$ units. The formation of selenium during the reaction is in line with this assumption. The formation of **6** can thus be attributed to an overall deficiency of selenium in the reactive mixture as compared to the situation at the synthesis of **1**.

Spectroscopy

The solubility of the compounds in common solvents is generally low, hence complicating NMR investigations (except ^{1}H-NMR measurements). The extremely low solubility of **4** and **5** inhibits any reasonable NMR experiments. However, the presence of a broad signal of free PPh_3 in the ^{31}P NMR spectrum of **4** suggests a rapid exchange between bound and free PPh_3

groups in solution, in agreement with the observations at the syntheses and the structural features. All other compounds exhibited the expected signals. ^{119}Sn NMR data of **3a** and **3b** were recorded, albeit in relatively low quality due to the low concentration in solution. NMR data are provided in the Experimental Section.

As indicated in Scheme 1, **B** (partially) reacts with two equivalents of **D** even in the absence of **C**. By means of NMR spectroscopy, we identified an integral ratio of **B**:**3a** ≈ 10:7 (Figure 2, top). Layering of this solution with *n*-hexane leads to the formation of a mixture of single crystals of **B**, **3a**, **3a**·DCM, **3a**·**B** (and a very small amount of **4**). Surprisingly, the relative amount of **3a** cannot be increased by further addition of $[Cu(PPh_3)_3Cl]$. The pale yellow solutions turns a deep red over the course of a week while a plethora of unknown signal sets occur in the ^{1}H NMR spectrum (Figure 2, bottom). Layering of this resulting solution with *n*-hexane does not yield any single crystals, most probably due to a decomposition of the clusters; the red color is a typical indication for polyselenide formation in this chemistry.

To confirm the mixed-valence observed in the clusters, we exemplarily studied compound 4 by means of ^{119}Sn Mössbauer spectroscopy. The 78 K spectrum (Figure 3) could be well reproduced by a superposition of two signals in 6 : 1 ratio, in good agreement with the crystal structure. The tetravalent tin atoms show an isomer shift of 1.61(1) mm·s^{-1} (blue sub-signal in Figure 3), similar to $Sn^{IV}Se_2$ (1.4 mm·s^{-1}) and $Tl_2Sn^{IV}Se_3$ (1.65 mm s^{-1}).[48] The signal is subjected to substantial electric quadrupole splitting of ΔE_Q = 1.69(2) mm·s^{-1}, a consequence of the largely asymmetric coordination shell of the Sn(IV) atoms. The green sub-signal (Figure 3) at δ = 3.44(4) mm·s^{-1} (and weaker quadrupole splitting of 0.47(9) mm·s^{-1}) originates from the divalent tin atoms. Again, we find good comparability with $Sn^{II}Se$ (3.4 mm·s^{-1}).[48] The experimental line widths of 0.89(3) for Sn(IV) mm·s^{-1} and 0.7(1) mm·s^{-1} for Sn(II) are in the usual range. The two isomer shifts determined for 4 nicely correlate with the trend in Sn 5s occupancy studied for a larger series of complex Sn(II) and Sn(IV) chalcogenides.[48]

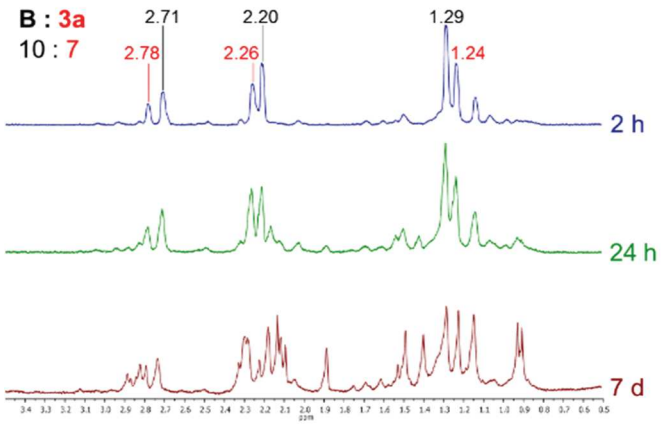

Figure 2 1H NMR spectra of a reactive mixture of B with [Cu(PPh3)3Cl] in CD2Cl2 after 2 hours, 24 hours and 7 days.

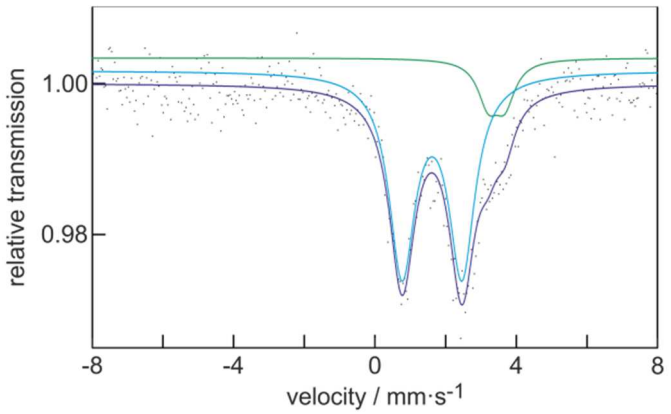

Figure 3 Experimental and simulated ^{119}Sn Mössbauer spectrum of 4.

In order to estimate the optical absorption energies of the new compounds with close topological relationships, we recorded absorption spectra on single crystal of the organotin copper selenide compounds **2–6**, as well as and the organotinselenide compound **B** for comparison. The results are shown in Figure 4. The values of maximum absorption wavelengths and energies are given in Table 2.

The binary starting material **B** possesses an absorption energy of 427 nm (2.9 eV), in agreement with its colorless nature. The respective values determined for the orange-red to red compounds based on ternary Cu/Sn/Se clusters are all within a narrow range, between 476 nm (2.6 eV) and 501 nm (2.5 eV). The only, notable, exception is **6**, the absorption energy of which (3.0 eV, 410 nm) is even larger than the one determined for the copper-free compound **B**, in spite of its structural similarity to **3a**. This indicates, that the $[(RSn)_2Se_4]$ unit seems to play an important role in the absorption properties of the compounds, while the organic ligand and the overall cluster topology seems to have only a small impact.

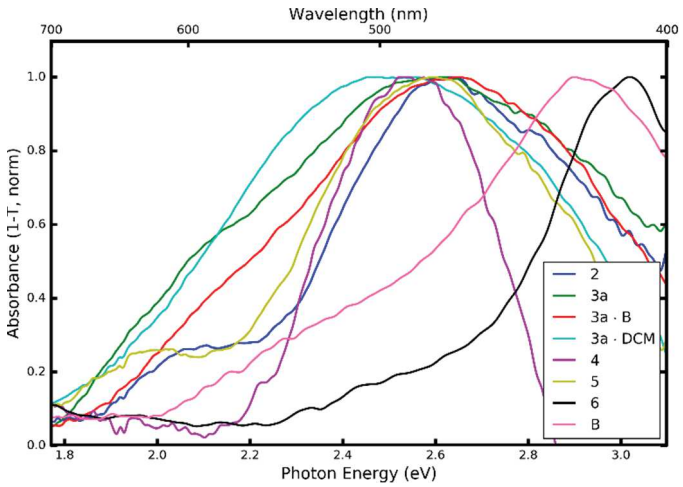

Figure 4 Single-crystal absorption spectra of compounds 2–6 and B. Normalized spectra are shown, as the crystal shapes and sizes did not allow a quantitative comparison of the absorbance.

Table 2. Absorption maxima λmax and maximum absorption energies Emax as determined by single-crystal absorption spectra of compounds **2–6** and **B**

Compound	λ_{max} [nm]	E_{max} [eV]
4	493	2.51
5	478	2.59
3a	476	2.61
3a·2 CH_2Cl_2	501	2.48
3a·B	478	2.59
2	484	2.56
6	410	3.02
B	427	2.90

Quantum chemical studies

Quantum chemical investigations again served to rationalize this assumption. Figure 5 shows the highest occupied molecular orbital (HOMO) and the lowest occupied molecular orbital (LUMO) of **3a** and **6**, respectively.

For both clusters, the HOMO is predominantly located at the inner part of the inorganic cluster core, mainly involving Sn and Se atoms. The extension of the LUMO, however, differs for both clusters. In **3a**, it is mainly located at the [$(R^1Sn)_2Se_4$] units, a feature that is common for all other computationally optimized structures that comprise this structural motif (see Figures S24-S31 in the Supporting Information). As the colorless compound **6** lacks such an [$(RSn)_2Se_4$] moiety, this strongly backs the assumption that they are essential for the observed colors. Indeed, the LUMO involves the two more compact [$(R^1SnCl)Se_2$] units, leading to a larger energetic separation from the HOMO than for the other clusters. Since most heavy metals tend to form metallophilic interactions,[49] we also performed Paboon analyses of the metal-metal contacts for the copper compounds presented herein. The calculated shared electron numbers (SEN), however, showed no significant cuprophilic interactions, whatsoever. The largest, yet insignificant, SEN found was 0.05 and observed in compound **1** (all other SENs are given in the Supporting Information).

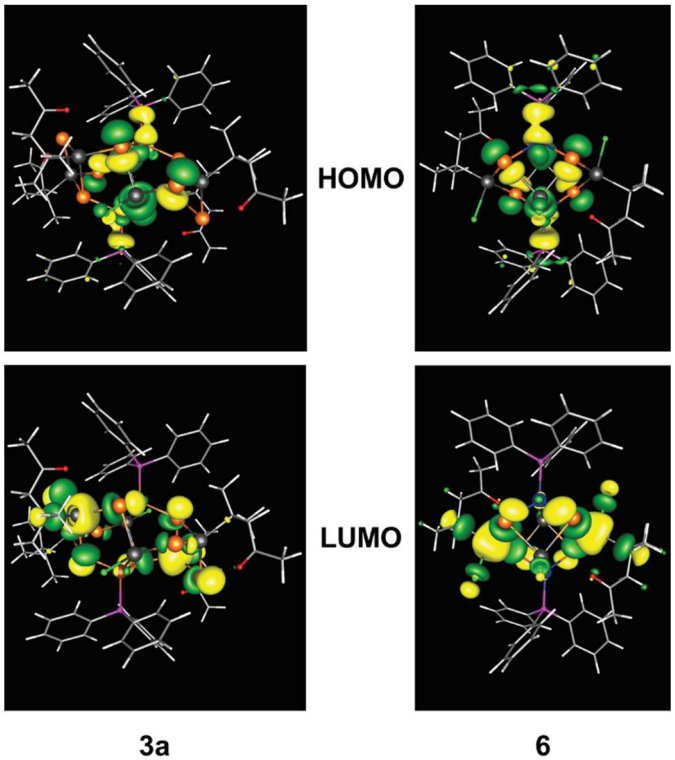

Figure 5 Highest occupied molecular orbitals (HOMOs, top) and lowest unoccupied molecular orbitals (LUMOs, bottom) of clusters 3a (left) and 6 (right), as calculated by means of DFT methods.

Experimental Section

General. All synthesis steps were carried out under argon atmosphere and exclusion of external moisture. $(SiMe_3)_2Se$, $[Cu(PPh_3)_2Cl_2]$ and the cluster compounds **A** and **B** were obtained according to procedures reported in the literature.[35,50,51] $[Cu(PPh_3)_3Cl]$, phenylhydrazine and $N_2H_4{\cdot}H_2O$ were purchased from Aldrich.

Synthesis of [(R1Sn)2Se2(CuPPh3)2Se2] (1). Compound **A** (88 mg, 0.087 mmol) and $[CuPPh_3)_2Cl_2]$ (109 mg, 0.175 mmol) were dissolved in 8 mL DCM each and mixed at −78° C. $Se(SiMe_3)_2$ (79 mg, 0.350 mmol) was added and the mixture was slowly brought to room temperature over 18 hours, leading to the formation of a small amount of brown precipitate in a deeply red solution. This solution was filtered and layered with *n*-hexane (1:1) to obtain orange rhombic crystals of **1** after 2 days. ^{1}H NMR (300 MHz, CD_2Cl_2, 25 °C): δ=1.15 (s, 24 H, C*H*$_3$, Me_2, $^3J_{Sn}$= 64 Hz), 2.24 (s, 12 H, C*H*$_3$, Me), 2.69 (s, 8 H, C*H*$_2$, $^3J_{Sn}$= 64 Hz) ppm.

Synthesis of [(PPh3Cu)2{(SnIVR2)2Se4}2SnII] (2). Compound **A** (0.133 g, 0.132 mmol) was dissolved in 10 mL DCM and treated with $N_2H_4{\cdot}H_2O$ (0.020 g, 0.397 mmol). DCM and water were removed in vacuo to leave dried $[(SnR^2)_3Se_4Cl]$. This was redissolved in 10 mL DCM and treated with $[Cu(PPh_3)_3Cl]$ (0.235 g, 0.265 mmol) and $Se(SiMe_3)_2$ (0.119 g, ,.529 mmol). A color change to orange could be observed after 30 minutes. The mixture was stirred for 18 hours. Layering of the solution with *n*-hexane (1:1) yields orangish yellow blocks of **2**. ^{1}H NMR (300 MHz, CD_2Cl_2, 25 °C): δ= 1.19 (s, 24 H, C*H*$_3$, Me_2, $^3J_{119Sn}$ = 69 Hz, $^3J_{117Sn}$ = 66 Hz), 2.77 (s, 12 H, C*H*$_3$, Me), 2.45 (s, 8 H, C*H*$_2$, $^3J_{Sn}$= 66 Hz), 4.90 (br s, 8 H, N*H*$_2$) ppm.

Synthesis of [{(R1SnIV)2Se2}2(CuPPh3)2(SnIICl)2(μ3-Se)2] (3a). Compound **B** (0.107 g, 0.080 mmol) and $[Cu(PPh_3)_3Cl]$ (0.141 g, 0.159 mmol) were dissolved in 20 mL DCM and $Se(SiMe_3)_2$ (0.072 g, 0.321 mmol) was added to the solution. A color change to orange could be observed after 30 minutes. The mixture was stirred for 18 hours. Layering of the solution with *n*-hexane (1:1) yields orange blocks of **3a** as the main product with impurities of **1** and **4**. ^{1}H NMR (300 MHz, CD_2Cl_2, 25 °C): δ= 1.24 (s, 24 H, C*H*$_3$, Me_2, $^3J_{Sn}$= 78 Hz), 2.26 (s, 12 H, C*H*$_3$, Me), 2.78 (s, 8 H, C*H*$_2$, $^3J_{Sn}$= 76 Hz) ppm.

Synthesis of [{(R2SnIV)2Se2}2(CuPPh3)2(SnIICl)2(μ3-Se)2] (3b). Compound **B** (0.120 g, 0.090 mmol) and $[Cu(PPh_3)_3Cl]$

(0.158 g, 0.178 mmol) were dissolved in 20 mL DCM and $Se(SiMe_3)_2$ (0.081 g, 0.358mmol) and $N_2H_4{\cdot}H_2O$ (0.018 g, 0.358 mmol) was added to the solution. A color change to orange could be observed after 30 minutes. The mixture was stirred for 18 hours. Layering of the solution with *n*-hexane (1:1) led to very fine orange needles of **3b**. ^{1}H NMR (500 MHz, CD_2Cl_2, 25 °C): δ= 1.25 (s, 24 H, C*H*$_3$, Me_2, $^3J_{Sn}$= 78 Hz), 1.88 (s, 12 H, C*H*$_3$, Me), 2.52(s, 8 H, C*H*$_2$, $^3J_{Sn}$= 75 Hz), 5.56 (br s, 8 H, N*H*$_2$) ppm. ^{119}Sn NMR (187 MHz, CD_2Cl_2, 25 °C): δ= −280, −332 ppm.

Synthesis of [{(R3SnIV)2Se2}2(CuPPh3)2(SnIICl)2(μ3-Se)2] (3c). Compound **B** (0.156 g, 0.117 mmol) and $[Cu(PPh_3)_3Cl]$ (0.205 g, 0.231 mmol) were dissolved in 20 mL DCM and $Se(SiMe_3)_2$ (0.105 g, 0.468 mmol) and phenylhydrazine (0.051 g, 0.397 mmol) was added to the solution. A color change to orange could be observed after 30 minutes. The mixture was stirred for 18 hours. Layering of the solution with *n*-hexane (1:1) resulted in orange blocks of **3c**. ^{1}H NMR (300 MHz, CD_2Cl_2, 25 °C): δ=1.26, 1.88, 2.65 ppm.

Synthesis of [(PPh3Cu)2{(SnIVR1)2Se4}3Cu2SnII] (4) and [(PPh3Cu)Cu{(SnIVR1)2Se4}3Cu2SnII] (5). Compound **A** (0.418 g, 0.416 mmol) and $[Cu(PPh_3)_3Cl]$ (0.645 g, 0.728 mmol) were dissolved in 20 mL DCM and $Se(SiMe_3)_2$ (0.375 g, 1.663 mmol) was added to the solution. A color change to orange could be observed after 30 minutes. The mixture was stirred for 18 hours, resulting in a reddish orange precipitate and an orange solution. The solution and the precipitate were separated. Layering of the solution with *n*-hexane (1:1) yields orange tetrahedrons of **4**, while re-dissolving the very badly soluble precipitate in DCM and layering the resulting solution in the same way results in very small dark red hexagons of **5**. Using 40 mL of DCM instead suppresses the formation of **5** and leads to a yield of 168 mg (19% related to the Sn ratio in solution) for **4**.

Synthesis of [{(R1SnIVCl)Se2}2(CuPPh3)2(SnIICl)2] (6). Compound **A** (109 mg, 0.108 mmol) and $[CuPPh_3)_2Cl_2]$ (135 mg, 0.216 mmol) were dissolved in 8 mL DCM each and mixed at −78° C. The mixture was slowly brought to room temperature over 18 hours, leading to the formation of a small amount of a brown precipitate in a deeply red solution. This solution was filtered and layered with *n*-hexane (1:1) to obtain colorless rhombic crystals of **6** after 2 days. ^{1}H NMR (300 MHz, CD_2Cl_2, 25 °C): δ= 1.43 (s, 24 H, C*H*$_3$, Me_2), 2.44 (s, 12 H, C*H*$_3$, Me), 2.99 (s, 8 H, C*H*$_2$, $^3J_{Sn}$= 76 Hz) ppm.

Mössbauer spectroscopy. A $Ca^{119m}SnO_3$ source was used for the ^{119}Sn Mössbauer spectroscopic investigation of **4**. The sample was placed within a thin-walled PMMA container at a thickness of about 10 mg Sn/cm^2. A palladium foil of 0.05 mm thickness was used to reduce the tin K X-rays concurrently emitted by this source. The measurement was conducted in the usual transmission geometry at 78 K with a total counting time of two days. The spectrum was fitted with the Normos-90 software package.[52]

Single-crystal absorption spectroscopy. For the absorption measurements a transmission microscope was used at ambient conditions and room temperature. The objective used has a numerical aperture of 0.5 and 32× magnification. For illumination we used a standard tungsten-halogen bulb. A 50μm pinhole was positioned in the image plane of the microscope. For optical control, a beam splitter was placed between the objective and pinhole to display the real image on a complementary metaloxide-semiconductor color camera chip with a size of 5.632mm × 4.224mm and 2560px × 1920px. For light analysis we used a combination of a Czerny-Turner-spectrometer and a Roper Scientific liquid nitrogen cooled silicon charge-coupled device camera. This setup had a field of view of 220μm × 160μm and a region of interest of less than 2μm × 2μm.

Methods of the quantum chemical investigations. The DFT investigations were performed within the program system Turbomole V7.0.1 by applying the B97-D functional[53] with dispersion correction[54] and BJ-damping,[55] and the def2-TZVP basis set[56] with auxiliary bases[57] and effective core potentials[58] at the Sn atoms. SEN were calculated *via* Paboon[47] as implemented in Turbomole. Pictures of the MOs were made with gOpenMol.[59]

Single-crystal X-ray diffraction. Crystals suitable for X-ray diffraction analyses were investigated with a STOE IPDS-2T or IPDS-II diffractometer at 100 K using Mo-K_α radiation and a graphite monochromator (λ = 0.71073 Å). Upon numerical absorption correction (STOE X-AREA), the structure solution was performed by direct methods, followed by full-matrix-least-squares refinement against F^2, using SHELXT15, SHELXL15, and OLEX2 software.[60]

Crystallographic data (excluding structure factors) for the structures reported in this paper have been deposited with the Cambridge Crystallographic Data Centre as supplementary publication no. CCDC 1565014-1565023. Copies of the data can be obtained free of charge on application to CCDC, 12 Union Road, Cambridge CB2 1EZ, UK [fax.: (internat.) + 44 1223/336-033; e-mail: deposit@ccdc.cam.ac.uk].

Conclusions

The binary inorganic core of organo-functionalized tinselenide clusters can be expanded by reaction with copper complexes to form clusters based on ternary Cu/Sn/Se cluster cores of varying size. The products of according reactions presented in this article seem to form complex equilibria in solution, which correlates with the fact that all of them possess a close structurally relationship. Most of the clusters are based on a $[(CuPPh_3)_2\{(RSn)_2Se_4\}_n]$ arrangement which embeds further endohedral atoms or polyatomic units. Derivatization of the organic ligands of these clusters is possible, in some cases leading to a rearrangement of the inorganic cluster core. Most of the compounds exhibit a Sn^{IV}/Sn^{II} mixed valence situation, which was verified on the example of compound **4** by means of ^{119}Sn Mössbauer spectroscopy. Absorption spectra of single crystals of these compounds indicate the key role of the $[(RSn)_2Se_4]$ units for the absorption properties, which was confirmed and explained by means of quantum chemical calculations.

Conflicts of interest

There are no conflicts to declare.

Acknowledgements

This work was supported by the Deutsche Forschungsgemeinschaft within the framework of SFB 1083.

Notes and references

1 N. Sakai and T. Saito, *Polyhedron*, 2004, **23**, 2611.
2 B. Bechlars, I. Issac, R. Feuerhake, R. Clérac, O. Fuhr and D. Fenske, *Eur. J. Inorg. Chem.*, 2008, **2008**, 1632.
3 M. Koutmos, I. P. Georgakaki, P. Tsiolis and D. Coucouvanis, *Z. Anorg. Allg. Chem.*, 2008, **634**, 255.
4 S. Banerjee, J. Sheckelton, T. J. Emge and J. G. Brennan, *Inorg. Chem.*, 2010, **49**, 1728.
5 T. Wu, X. Bu, X. Zhao, R. Khazhakyan and P. Feng, *J. Am. Chem. Soc.*, 2011, **133**, 9616.
6 A. Eichhöfer, O. Hampe, S. Lebedkin and F. Weigend, *Inorg. Chem.*, 2010, **49**, 7331.
7 S. Dehnen and M. K. Brandmayer, *J. Am. Chem. Soc.*, 2003, **125**, 6618.
8 R. Chen, F. Wang, C. Tang, Y. Zhang and D. Jia, *Chem. Eur. J*, 2013, **19**, 8199.
9 R. Ahlrichs, A. Eichhöfer, D. Fenske, O. Hampe, M. M. Kappes, P. Nava and J. Olkowska-Oetzel, *Angew. Chem. Int. Ed.*, 2004, **43**, 3823.
10 D. T. T. Tran, L. M. C. Beltran, C. M. Kowalchuk, N. R. Trefiak, N. J. Taylor and J. F. Corrigan, *Inorg. Chem.*, 2002, **41**, 2639.
11 D. Fuhrmann, S. Dietrich and H. Krautscheid, *Chem. Eur. J.*, 2017, **23**, 3338.
12 A. Lorenz and D. Fenske, *Angew. Chem. Int. Ed.*, 2001, **40**, 4402.
13 Q. Zhang, J. Ding, Z. Yu, Y. Song, A. Rothenberger, D. Fenske, W. Leung, C. W. Bay, H. Kong and A. Chemie, *Inorg. Chem.*, 2006, **45**, 8638.
14 M. W. Degroot, J. Taylor and J. F. Corrigan, *J. Mater. Chem.*, 2004, **14**, 654.
15 Y. Lin, W. Massa and S. Dehnen, *J. Am. Chem. Soc.*, 2012, **134**, 4497.
16 O. Kluge, K. Grummt, R. Biedermann and H. Krautscheid, *Inorg. Chem.*, 2011, **50**, 4742.
17 O. Kluge, D. Friedrich and H. Krautscheid, *Dalt. Trans.*, 2012, **41**, 8635.
18 O. Kluge, R. Biedermann, J. Holldorf and H. Krautscheid, *Chem. Eur. J.*, 2014, **20**, 1318.
19 J. Olkowska-Oetzel, P. Sevillano, A. Eichhöfer and D. Fenske, *Eur. J. Inorg. Chem.*, 2004, 1100.
20 A. Kornienko, S. Banerjee, G. A. Kumar, R. E. Riman, T. J. Emge and J. G. Brennan, *J. Am. Chem. Soc.*, 2005, **127**, 14008.
21 M. Berardini, T. Emge and J. G. Brennan, *J. Am. Chem. Soc.*, 1994, **116**, 6941.
22 M. Berardini, T. J. Emge and J. G. Brennan, *J. Am. Chem. Soc.*, 1995, **34**, 5327.
23 S. Dehnen and M. Melullis, *Coord. Chem. Rev.*, 2007, **251**, 1259.
24 S. Santner, J. Heine and S. Dehnen, *Angew. Chem. Int. Ed.*, 2016, **55**, 876.
25 N. W. Rosemann, J. P. Eußner, A. Beyer, S. W. Koch, K. Volz, S. Dehnen and S. Chatterjee, *Science*, 2016, **352**, 1301.
26 N. W. Rosemann, J. P. Eußner, E. Dornsiepen, S. Chatterjee and S. Dehnen, *J. Am. Chem. Soc.*, 2016, **138**, 16224.
27 G. Thiele, Y. Franzke, F. Weigend and S. Dehnen, *Angew. Chem. Int. Ed.*, 2015, **54**, 11283; G. Thiele, T. Krüger and S. Dehnen, *Angew. Chem. Int. Ed.*, 2014, **53**, 4699.
28 K. Ito (Ed.), *Copper Zinc Tin Sulfide-Based Thin Film Solar Cells*, John Wiley & Sons, New York, 2014.
29 J.-O. Jeon, K. D. Lee, L. S. Oh, S.-W. Seo, D.-K. Lee, H. Kim, J.-H. Jeong, M. J. Ko, B. S. Kim, H. J. Son and J. Y. Kim, *ChemSusChem*, 2014, **7**, 1073.
30 M. R. Halvagar, Z. Hassanzadeh Fard and S. Dehnen, *Chem. Commun.*, 2010, **46**, 4716.
31 J. P. Eußner and S. Dehnen, *Chem. Commun.*, 2014, **50**, 11385.
32 Z. Hassanzadeh Fard, L. Xiong, C. Müller, M. Hołyńska and S. Dehnen, *Chem. Eur. J.*, 2009, **15**, 6595.
33 E. Leusmann, E. Geringer, B. Weinert and S. Dehnen, *Dalt. Trans.*, 2016, **45**, 15298.
34 B. E. K. Barth, E. Leusmann, K. Harms and S. Dehnen, *Chem. Commun.*, 2013, **49**, 6590.
35 N. Rinn, J. P. Eußner, W. Kaschuba, X. Xie and S. Dehnen, *Chem. Eur. J.*, 2016, **22**, 3094.
36 Z. You, J. Bergunde, B. Gerke, R. Pöttgen and S. Dehnen, *Inorg. Chem.*, 2014, **53**, 12512.
37 K. Merzweiler and R. Hauser, *Z. Anorg. Allg. Chem.*, 2002, **628**, 905.
38 X. Tan, X. Liu, J. Zhou, L. Zhu, R. Zhao and Q. Huang, *J. Clust. Sci.*, 2016, **27**, 257.
39 W. Zhang, X. Wu, M. Ebel, D. Wang and D. Rehder, *Inorg. Chem. Commun.*, 2002, **5**, 768.
40 A. Decken, J. Passmore and X. Wang, *Angew. Chem.*, 2006, **118**, 2839.
41 L. Wang, T. Sheng, X. Wang, D. Chen, S. Hu, R. Fu, S. Xiang and X. Wu, *Inorg. Chem.*, 2008, **47**, 4054.
42 Y.-G. Han, C. Xu, T. Duan, F.-H. Wu, Q.-F. Zhang and W.-H. Leung, *Inorg. Chem.*, 2009, **48**, 8796.
43 A. Eichhöfer, J. Jiang, S. Lebedkin, D. Fenske, D. G. Mcdonald, J. F. Corrigan and C. Su, *Dalt. Trans.*, 2012, **41**, 3321.
44 H. P. Nayek, W. Massa and S. Dehnen, *Inorg. Chem.*, 2008, **47**, 9146.
45 Z. Hassanzadeh Fard, C. Müller, T. Harmening, R. Pöttgen and S. Dehnen, *Angew. Chem. Int. Ed.*, 2009, **48**, 4441.
46 TURBOMOLE V7.0.1 2015, a Development of University of Karlsruhe and Forschungszentrum Karlsruhe GmbH, 1989-2007, TURBOMOLE GmbH, since 2007, Available from Http://www.turbomole.com.
47 S. Grimme, J. Comp. Chem. 2006, ***27***, 1787.
48 P. E. Lippens, *Phys. Rev. B*, 1999, **60**, 4576.
49 H. Schmidbaur and A. Schier, *Angew. Chem. Int. Ed.* 2015, **54**, 746.
50 M. R. Detty and M. D. Seidler, *J. Org. Chem.* 1982, 1354.
51 D. Ramakrishna and B. R. Bhat, *Inorg. Chem. Commun.* 2011, **14**, 690.
52 R. A. Brand, *Normos Mössbauer Fitting Program, University of Duisburg, Duisburg (Germany)* **2002**.
53 S. Grimme, *J. Comput. Chem.* 2006, **27**, 1787.
54 S. Grimme, J. Antony, S. Ehrlich and H. Krieg, *J. Chem. Phys* 2010, **132**, 154104.
55 S. Grimme, S. Ehrlich and L. Goerigk, *J. Comput. Chem.* 2011, **32**, 1456.
56 F. Weigend and R. Ahlrichs, *Phys. Chem. Chem. Phys.* 2005, **7**, 3297.
57 F. Weigend, *Phys. Chem. Chem. Phys.* 2006, **8**, 1057.
58 B. Metz, H. Stoll and M. Dolg, *J. Chem. Phys.* 2000, **113**, 2563.
59 D. L. Bergmann, L. Laaksonen and A. Laaksonen, *J. Mol. Graphics Mod.* 1997, **15**, 301.
60 G. M. Sheldrick, *Acta Crystallogr., Sect. A* 2015, **71**, 3; G. M. Sheldrick, *Acta Crystallogr., Sect. C* 2015, **71**, 3; O. V. Dolomanov, L. J. Bourhis, R. J. Gildea, J. A. K. Howard and H. Puschmann, *J. Appl. Crystallogr.* 2009, **42**, 339.

Ternary Mixed-Valence Organotin Copperselenide Clusters

Niklas Rinn,[a] Lukas Guggolz,[a] Jurek Lange,[b] Sangam Chatterjee,[b] Theresa Block,[c] Rainer Pöttgen,[c] and Stefanie Dehnen*[a]

[a] *Fachbereich Chemie und Wissenschaftliches Zentrum für Materialwissenschaften, Philipps-Universität Marburg, Hans-Meerwein-Straße 4, 35043 Marburg, Germany, E-mail: dehnen@chemie.uni-mabrug.de*
[b] *Department of Physics, Justus-Liebig University Gießen, Heinrich-Buff-Ring 16, 35392 Gießen, Germany*
[c] *Institut für Anorganische und Analytische Chemie, Westfälische Wilhelms-Universität Münster, Corrensstraße 30, 48149 Münster, Germany*

SUPPORTING INFORMATION

Crystal structure of 1·2 DCM

The highest peak of residual electron density on the difference Fourier map (0.83 $e^{-}/Å^3$) is found 1.058 Å apart from Sn2, on the bond between Sn2 and Se4. A picture of the crystals of **1**·2 DCM is shown in Figure S1, and a cutout of the crystal structure is shown in Figure S2.

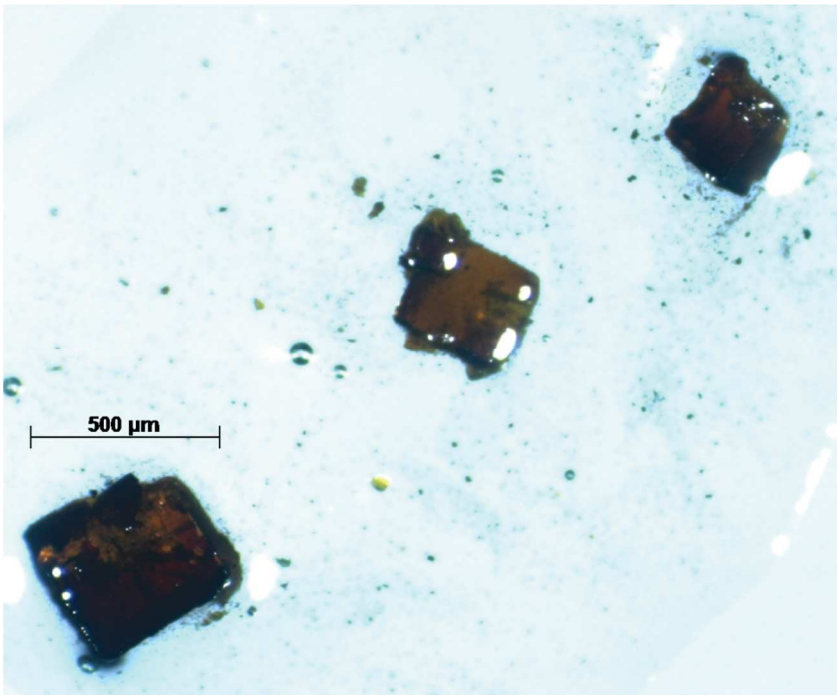

Figure S1: Crystals of **1**·2 DCM.

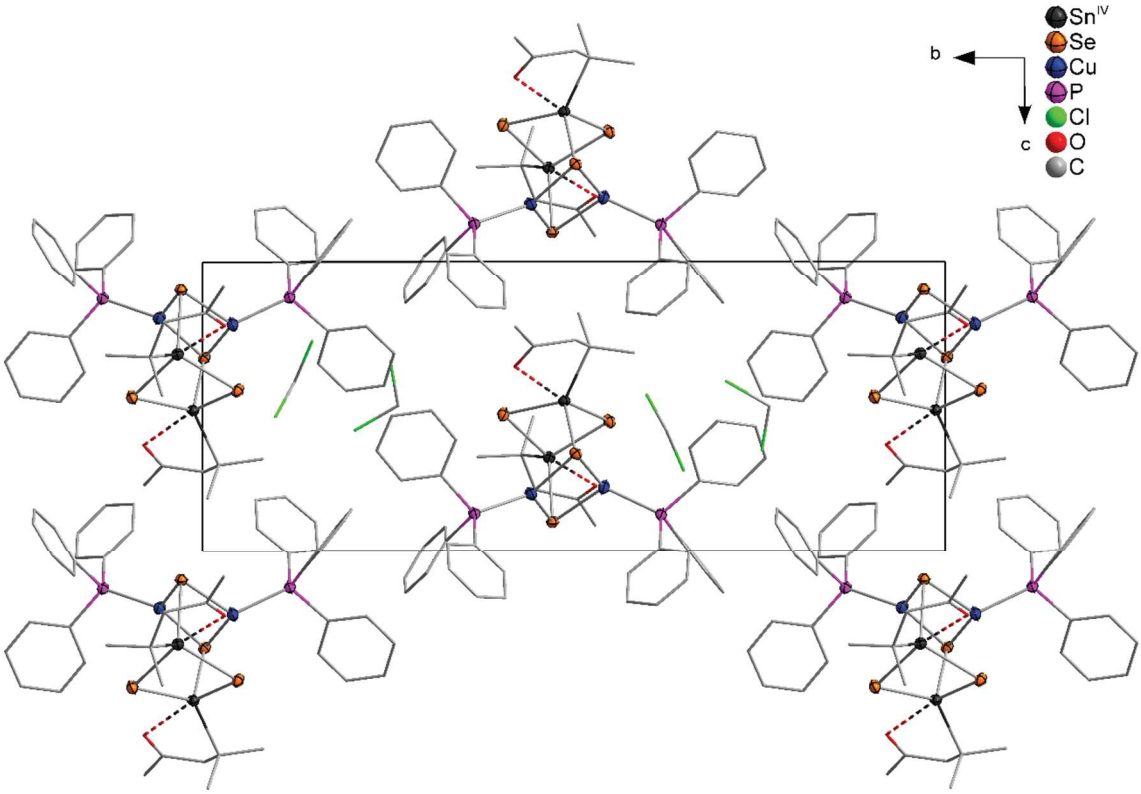

Figure S2: Cutout of the crystal structure of **1**·2 DCM viewed along the *a* axis.

Crystal structure of 2·1.5 DCM

The highest peak of residual electron density on the difference Fourier map (1.74 $e^{-}/Å^3$) is found 0.747 Å apart from Sn1B. The two molecules of **2** form alternating chains via H-bonds between N4A and N4B. A cutout of the crystal structure of **2**·1.5 DCM is shown in Figure S3.

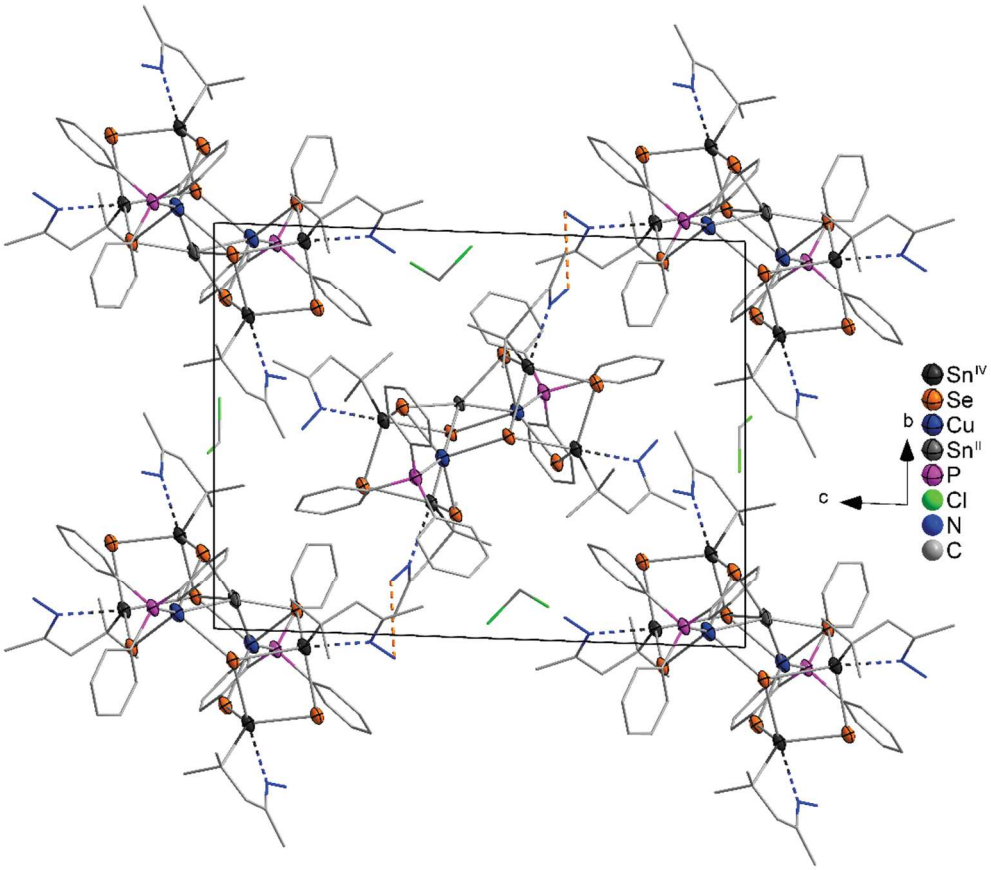

Figure S3: Cutout of the crystal structure of **2**·1.5 DCM viewed along the *a* axis. H-bonds are indicated by orange dashed line between the donor and acceptor atoms.

Sn1 and C32, a carbon atom of a DCM molecule, are disordered over two positions owing to the crystal symmetry, with an site occupation of 0.5 each. This disorder is illustrated in Figure S4.

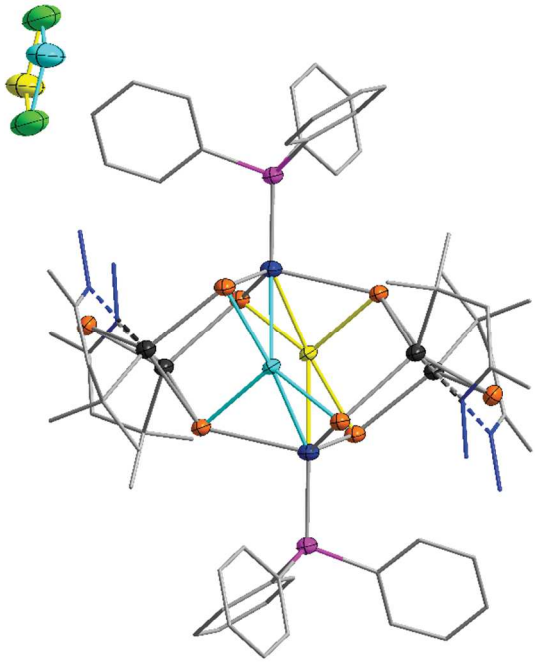

Figure S4: Disorder of Sn1A and C32 the in **2**·1.5 DCM. The disorder of Sn1B is analogous.

Crystal structure of 2·3 DCM

The highest peak of residual electron density on the difference Fourier map (1.96 $e^{-}/Å^3$) is found 0.579 Å apart from Sn1A. A picture of the crystals of **2**·3 DCM is shown in Figure S5, and a cutout of the crystal structure is shown in Figure S6.

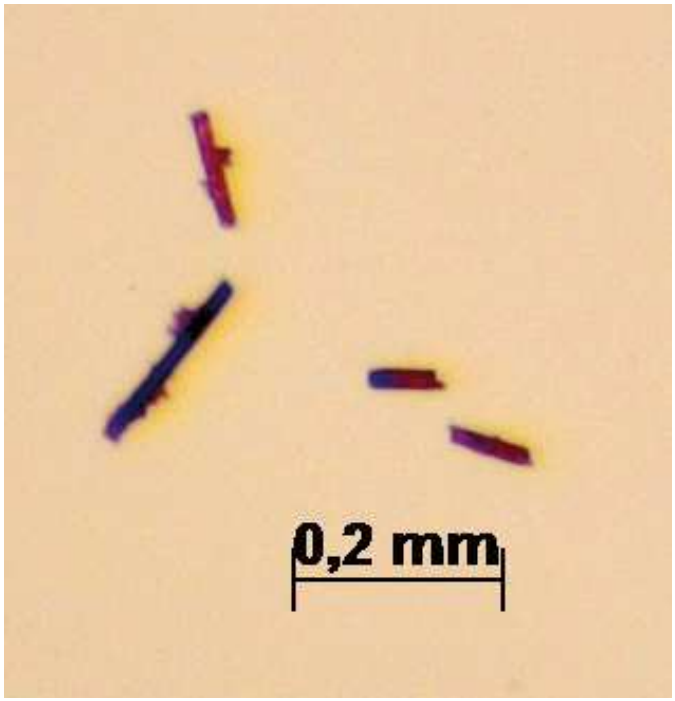

Figure S5: Crystals of **2**·3 DCM.

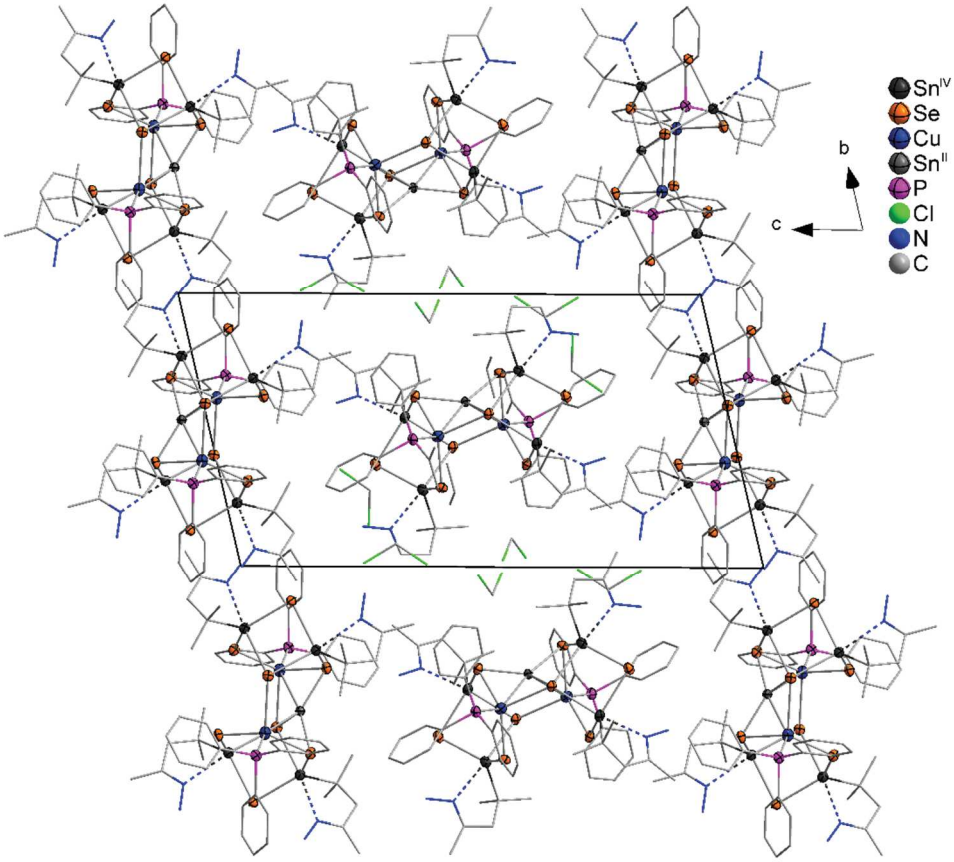

Figure S6: Cutout of the crystal structure of **2**·3 DCM viewed along the *a* axis.

Sn1 is disordered in an identical fashion to **2**·1.5 DCM. Additionally Cl6 is disordered on two positions Cl6A and Cl6B with an occupancy of 0.68 and 0.32 respectively.

Crystal structure of 3a

The highest peak of residual electron density on the difference Fourier map (1.78 $e^{-}/Å^3$) is found 0.1016 Å apart from Sn2 one the Sn2–Se2 bond. A small solvent accessible void of 316 $Å^3$ and 44 electrons was found in **3a** that could not be fitted to a solvent molecule model. It was removed using the SQUEEZE routine. A picture of the crystals of **3a** is shown in Figure S7, and a cutout of the crystal structure is shown in Figure S8.

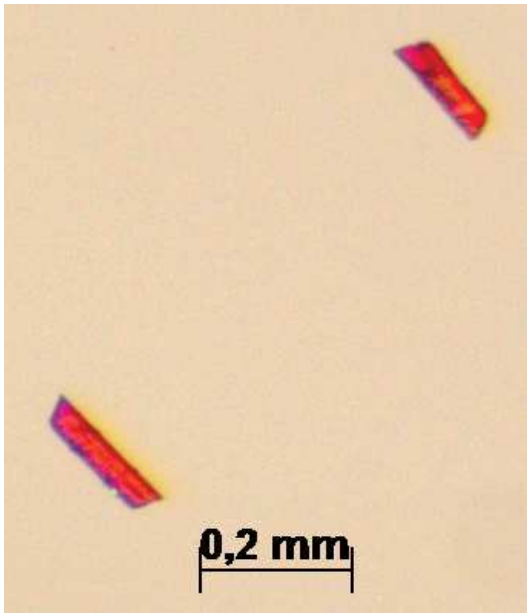

Figure S7: Crystals of **3a**.

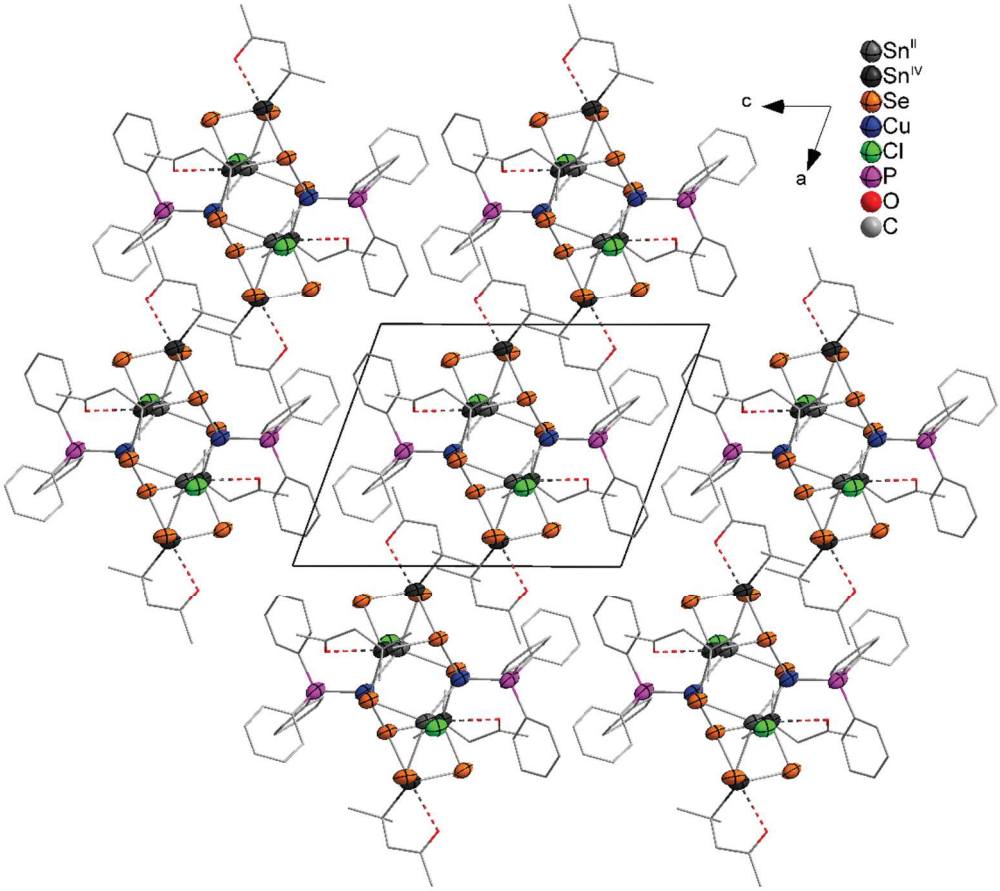

Figure S8: Cutout of the crystal structure of **3a** viewed along the *b* axis.

Crystal structure of 3a·2 DCM

The highest peak of residual electron density on the difference Fourier map (2.34 $e^{-}/Å^3$) is found 2.420 Å apart from Se2. A picture of the crystals of **3a**·2 DCM is shown in Figure S9, and a cutout of the crystal structure is shown in Figure S10.

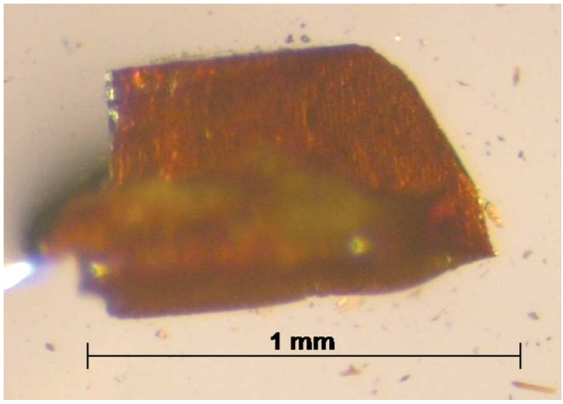

Figure S9: Crystals of **3a**·2 DCM.

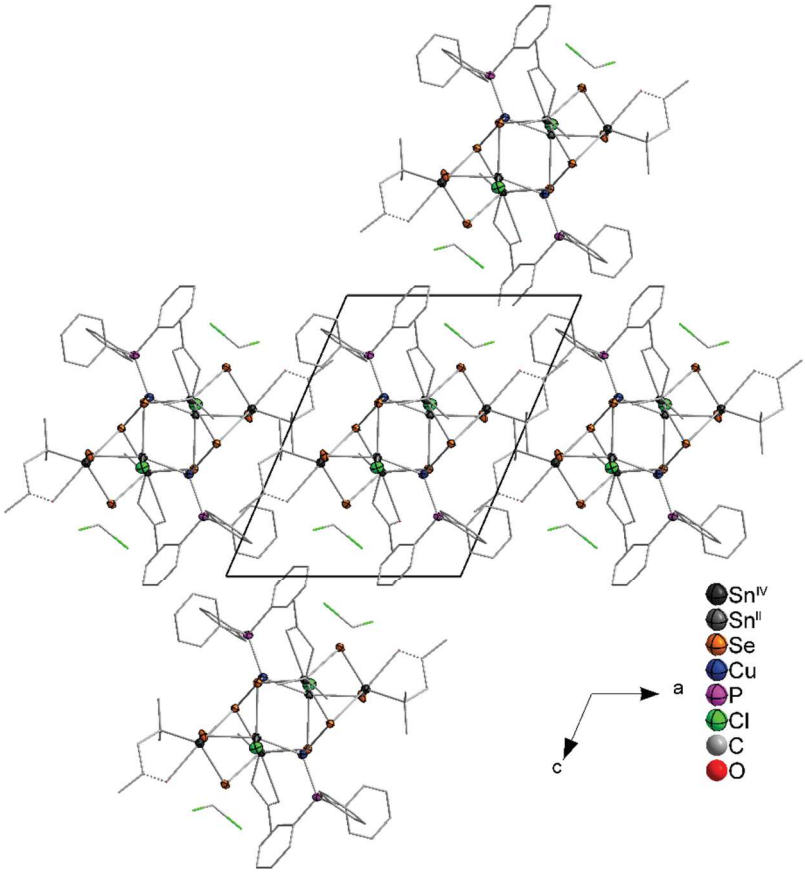

Figure S10: Cutout of the crystal structure of **3a**·2 DCM viewed along the *b* axis.

Crystal structure of 3a·B DCM

The highest peak of residual electron density on the difference Fourier map (1.39 $e^{-}/Å^3$) is found 0.977 Å apart from Se3. A picture of the crystals of **3a**·**B** is shown in Figure S11, and a cutout of the crystal structure is shown in Figure S12.

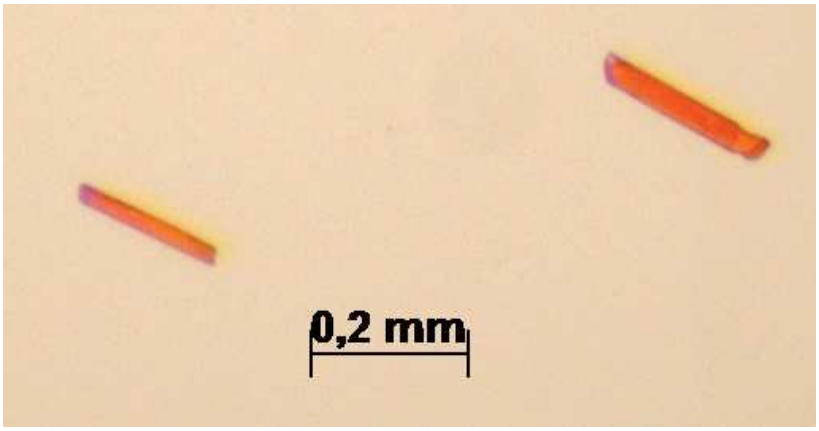

Figure S11: Crystals of **3a**·**B**.

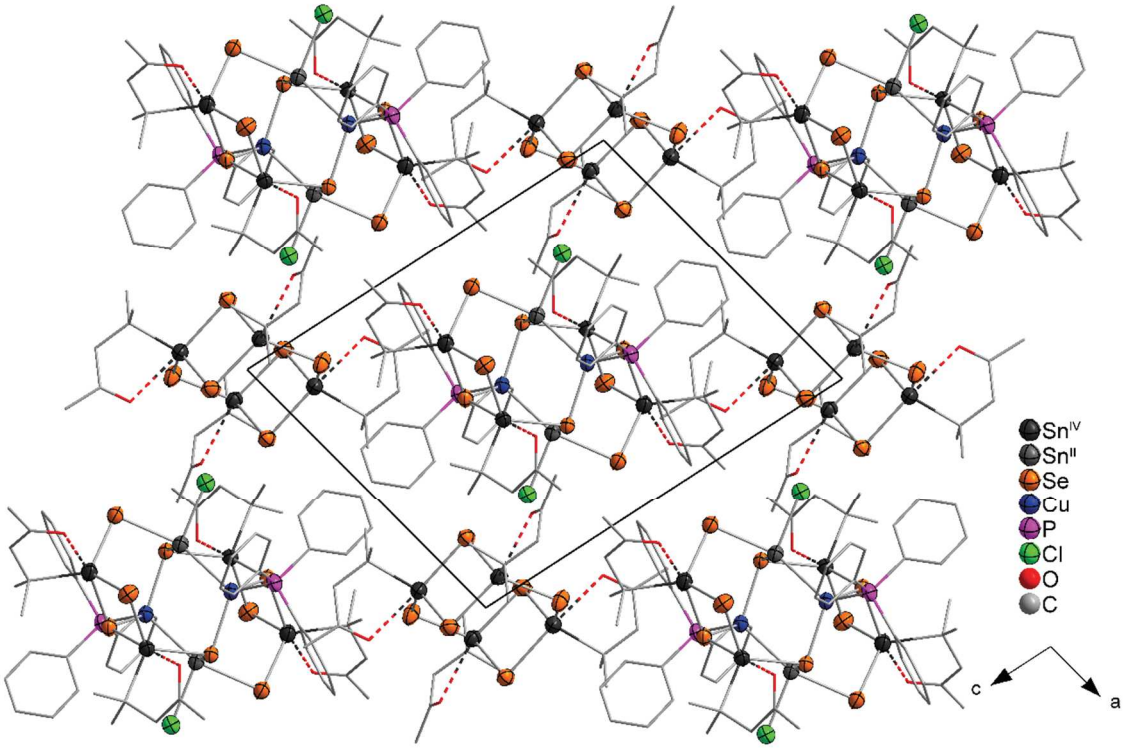

Figure S12: Cutout of the crystal structure of **3a**·**B** viewed along the *b* axis.

Crystal structure of 3c·3 DCM

The highest peak of residual electron density on the difference Fourier map (5.04 $e^{-}/Å^3$) is found 1.381 Å apart from Sn3. A cutout of the crystal structure of **3c**·3 DCM is shown in Figure S13.

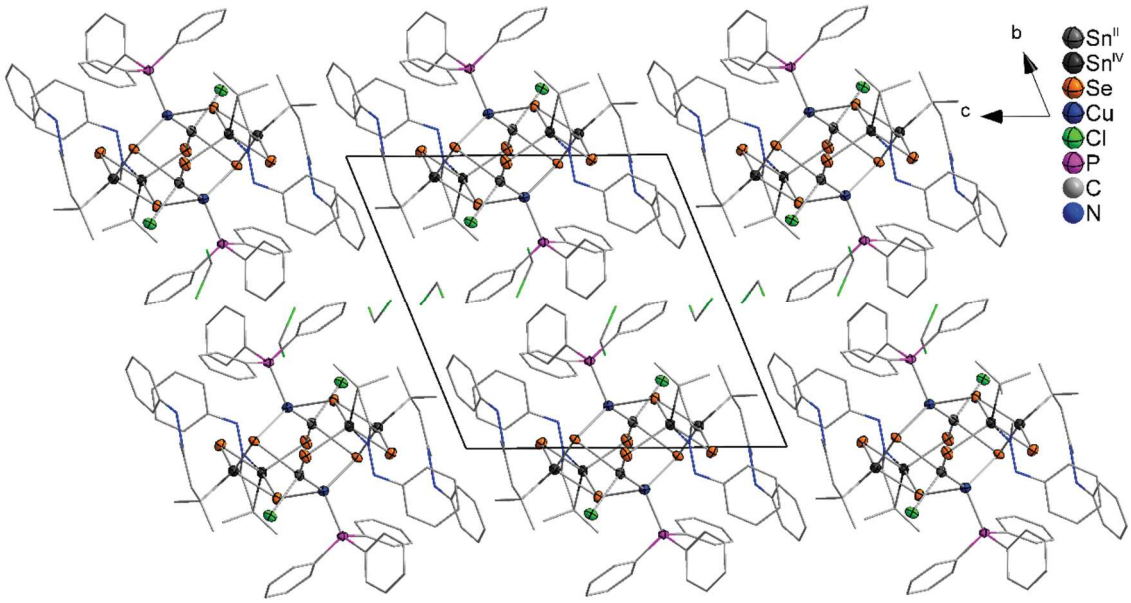

Figure S13: Cutout of the crystal structure of **3c**·3 DCM viewed along the *a* axis.

One DCM molecule has a total occupancy of 0.5, with the two chlorine atoms, Cl5 and Cl6, being disordered on two positions with an site occupation of 0.25 each.

Crystal structure of 4

The highest peak of residual electron density on the difference Fourier map (0.57 $e^{-}/Å^3$) is found 1.453 Å apart from Se1, on the bond between Sn1 and Se1. The atomic positions of one DCM molecule was found in the asymmetric unit with a large amount of residual electron density in solvent accessible voids that could not be fitted to a solvent molecule model. This solvent accessible void with a volume of 3744 $Å^3$, 956 electrons, and a barycenter at x = 0.088, y = 0.103 and z = 0.093 was removed using the SQUEEZE routine. 956 electrons would approximately correspond to about 23 / 6 additional molecules of DCM, 19 / 5 molecules of *n*-hexane or a mixture of both per unit cell / molecule. A picture of the crystals of **1a** is shown in Figure S14, and a cutout of the crystal structure is shown in Figure S15.

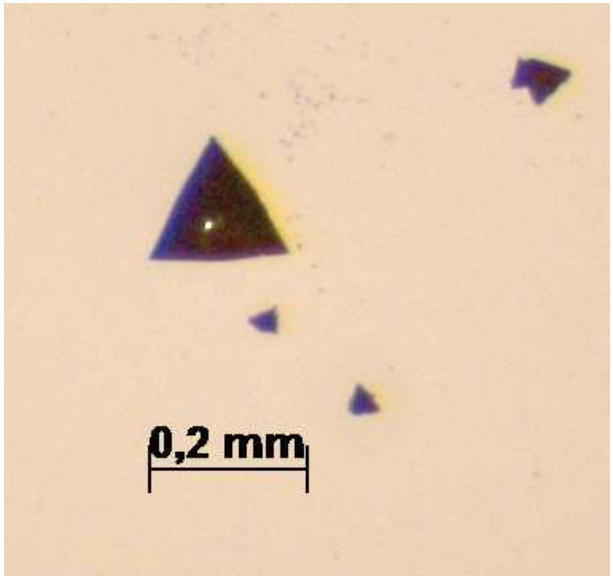

Figure S14: Crystals of **4**.

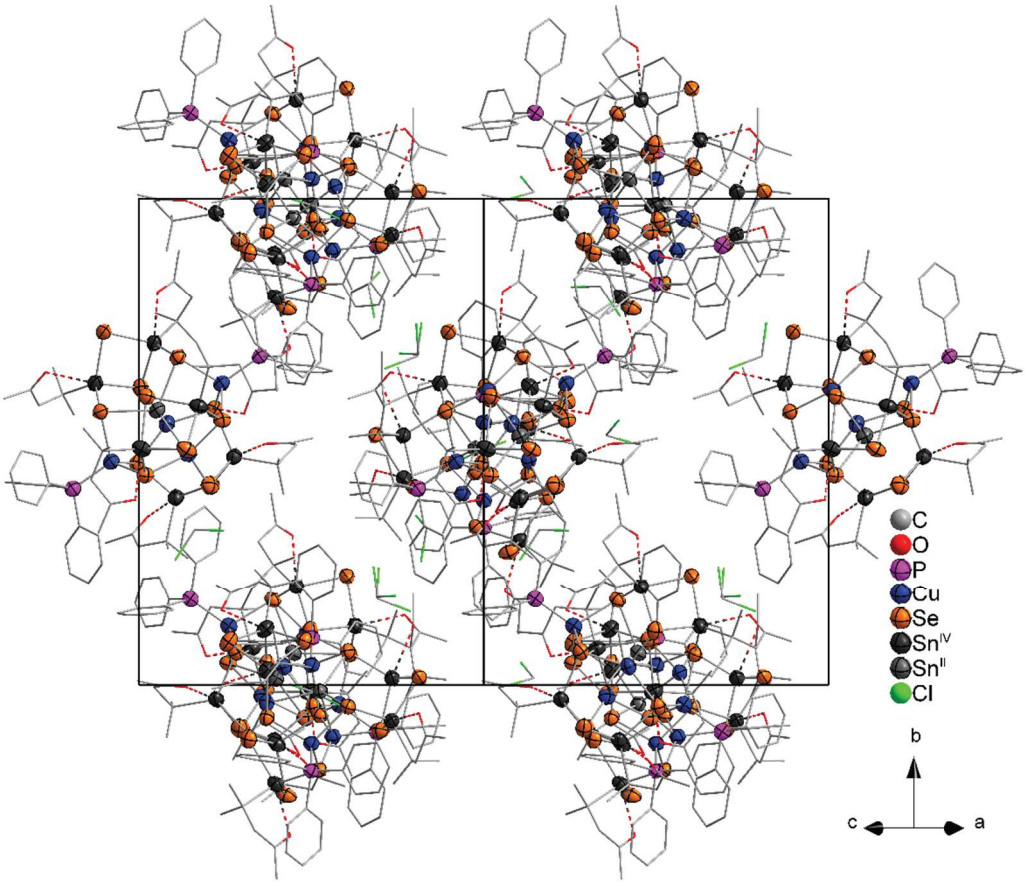

Figure S15: Cutout of the crystal structure of **4** viewed along the [101] axis.

The central Cu–Sn–Cu unit is disordered along the crystallographic C_3 axis in **4**. Figure S16 illustrates the three possible positions within the inorganic cluster core.

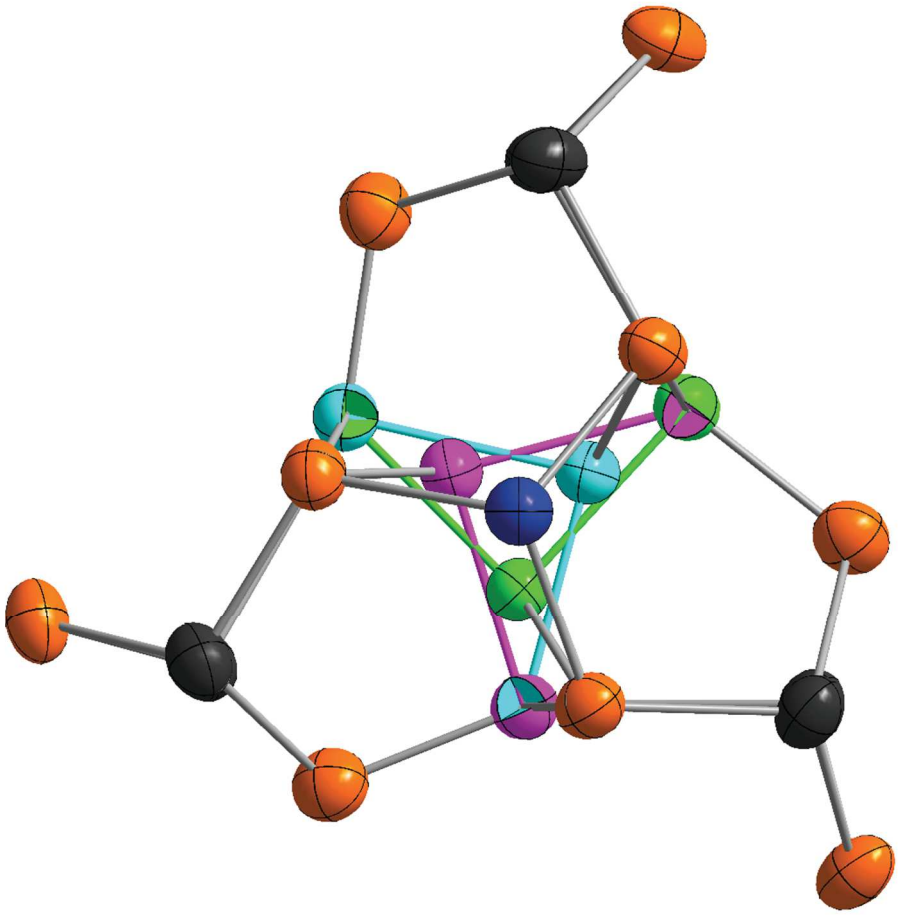

Figure S16: Disorder of the Cu–Sn–Cu subunit in **4** viewed along the C_3 axis thorugh Cu1 and Cu2. The three plausible parts are shown in cyan, green or pink respectively.

Crystal structure of 5

The highest peak of residual electron density on the difference Fourier map (3.62 $e^{-}/Å^3$) is found 1.182 Å apart from Cu1, between Cu1 and Sn1. A small solvent accessible void of 647 $Å^3$ and 57 electrons was found in **5** that could not be fitted to a solvent molecule model. It was removed using the SQUEEZE routine. 57 electrons would approximately correspond to one DCM or one molecule of *n*-hexane per unit cell. A picture of the crystals of **5** is shown in Figure S17, and a cutout of the crystal structure is shown in Figure S18. The disorder of the Cu–Sn–Cu unit accords to that found in **4**.

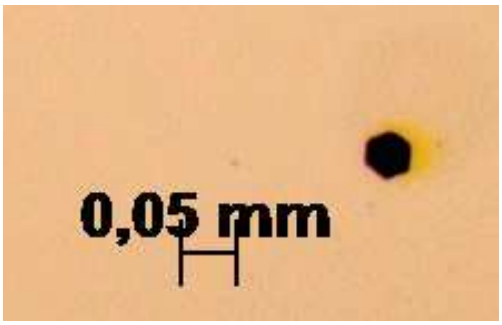

Figure S17: Crystals of **5**.

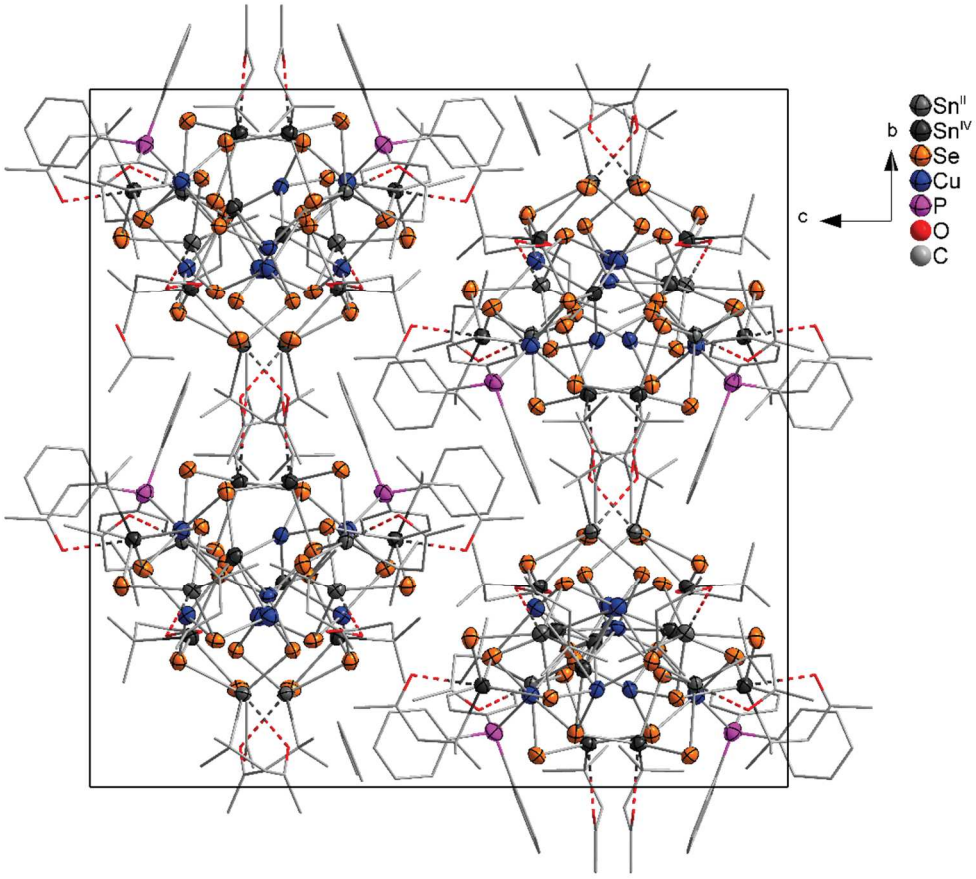

Figure S18: Cutout of the crystal structure of **5** viewed along the *a* axis.

Crystal structure of 5·0.5 hexane

The highest peak of residual electron density on the difference Fourier map (1.24 $e^{-}/Å^3$) is found 1.225 Å apart from Sn1, between Cu1 and Sn1. One heavily disordered *n*-hexane molecule was found that did not refine properly, however. For that, the SQUEEZE routine was used to remove 195 electrons from a volume of 733 $Å^3$. A picture of the crystals of **5**·0.5 hexane is shown in Figure S19, and a cutout of the crystal structure is shown in Figure S20.

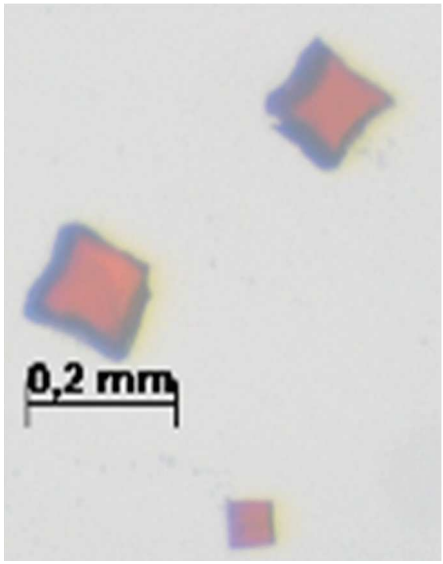

Figure S19: Crystals of **5**.

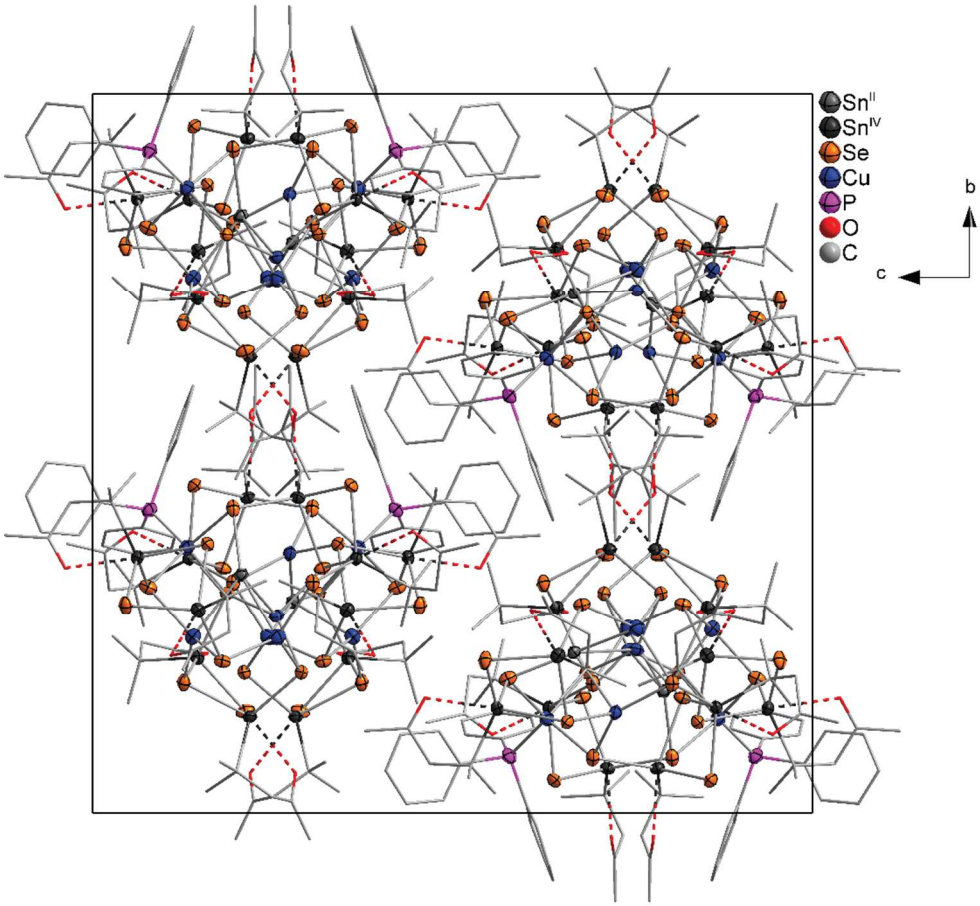

Figure S20: Cutout of the crystal structure of **5** viewed along the *a* axis.

Crystal structure of 6

The highest peak of residual electron density on the difference Fourier map (0.65 $e^{-}/Å^3$) is found 1.012 Å apart from Sn1. A picture of the crystals of **6** is shown in Figure S21, and a cutout of the crystal structure is shown in Figure S22.

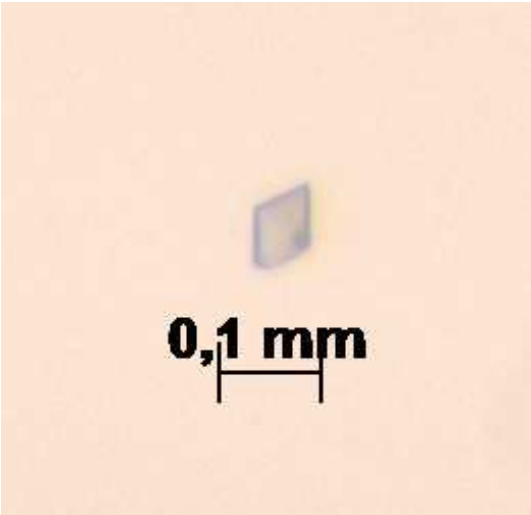

Figure S21: Crystals of **6**.

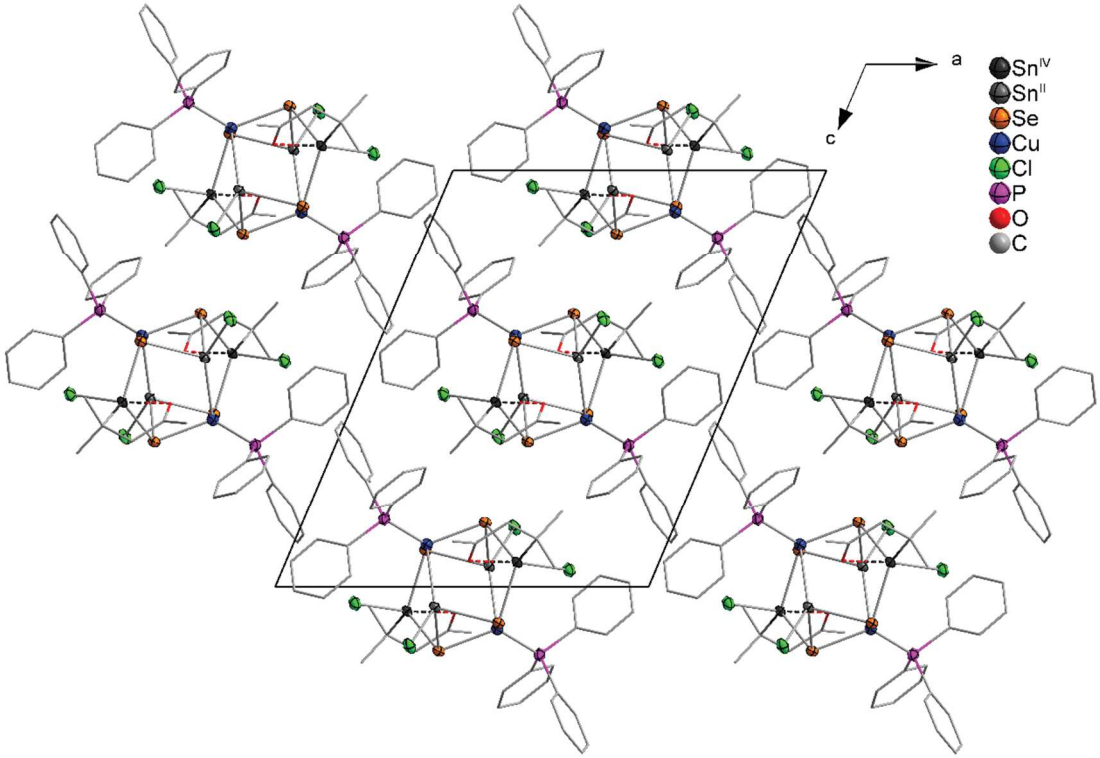

Figure S22: Cutout of the crystal structure of **6** viewed along the *b* axis.

One Phenyl unit is disordered on two positions (C19A-C25A and C19B-C25B) with site occupations of 0.52 and 0.48, respectively. The disorder is displayed in Figure 23.

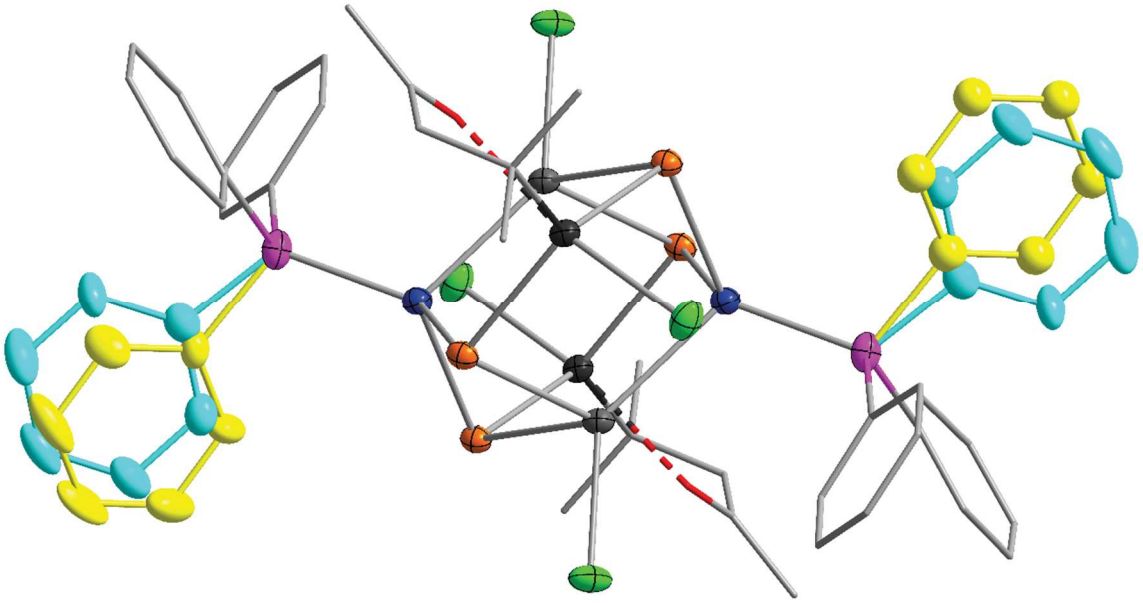

Figure S23: Disorder of a phenyl ring in **6**.

Table S1. Crystallographic data and refinement results of **2**·6 CH_2Cl_2, **3a,** .**3a**·**B** and **5.**

Compound	**2**·3 CH_2Cl_2	**3a**	**3a**·**B**	**5**
Empirical formula	$C_{126}H_{176}Cl_{12}Cu_4N_{16}P_4Se_{16}Sn_{10}$	$C_{60}H_{74}Cl_2Cu_2O_4P_2Se_8Sn_6$	$C_{84}H_{118}Cl_2Cu_2O_8P_2Se_{14}Sn_{10}$	$C_{54}H_{78}Cu_4O_6PSe_{12}Sn_7$
Fw / g·mol^{-1}	5168.52	2462.93	3808.04	2886.64
Crystal color and shape	orangish yellow block	dark red rhombohedron	orangish yellow plate	dark red hexagonal plates
Crystal size / mm^3	0.13x0.01x0.07	0.22×0.18×0.08	0.30x0.28x0.24	0.06x0.06x0.03
Crystal system	triclinic	triclinic	triclinic	cubic
Space group	$P\bar{1}$	$P\bar{1}$	$P\bar{1}$	$Pa\bar{3}$
a / Å	13.8312(5)	11.8131(12)	12.5759(7)	25.0225(3)
b / Å	14.2729(5)	13.2781(15)	15.4529(9)	a
c / Å	24.2698(8)	14.9270(7)	15.5066(8)	a
α / °	77.583(3)	76.150(9)	90.985(5)	90
β / °	89.058(3)	67.201(8)	101.783(4)	90
γ / °	65.297(3)	73.438(8)	100.855(5)	90
V / Å^3	4236.3(3)	2046.8(2)	2892.3(3)	15667.2(6)
Z	1	1	1	8
ρcalcd / g·cm^{-3}	2.03	2.00	2.19	2.45
μ(Mo Kα) / mm^{-1}	5.65	6.01	7.00	8.90
Absorption correction type	numerical	numerical	numerical	multi-scan
min. / max. transmission	0.629 / 0.693	0.066 / 0.134	0.141 / 0.185	0.587 / 0.792
2 θ range / deg	3.45 / 53.60	2.99 / 53.91	3.37 / 53.58	4.88 / 50.13
no. of meas. Reflns	37405	28456	24937	52569
R(int)	0.0843	0.0821	0.1017	0.1595
Indep. reflns	17815	8698	12146	4641
Indep. Reflns (I > 2σ(I))	10716	4731	7020	2641
no. of parameters	876	355	562	268
R1 (I > 2σ(I)) / wR2 (all data)	0.051 / 0.0906	0.0626 / 0.1563	0.0528 / 0.1085	0.0607 / 0.1324
S (all data)	0.877	1.007	0.898	1.057
Max. peak / hole / e$^-$· Å^3	1.96 / -1.45	1.78 / –1.43	1.39 / -1.72	3.53 / -1.77

Table S2. Selected atom distances in **1** – **6**.

Distances	**1** 2 CH_2Cl_2	**2**·1.5 CH_2Cl_2	**2**·3 CH_2Cl_2	**3a**	**3a**·2 CH_2Cl_2	**3a**·**B**	**3c**·3 CH_2Cl_2	**4**·3 CH_2Cl_2	**5**	**5**·0.5 C_6H_{14}	**6**
Sn2–Se1	2.6405(8)	2.513(1)/2.4953(9)	2.501(1)/2.496(1)	2.532(1)	2.5259(7)	2.533(1)	2.548(1)	2.498(1)	2.513(2)	2.5088(9)	2.5326(4)
Sn2–Se2	2.5363(8)	2.7152(9)/2.677(1)	2.6849(8)/2.7393(9)	2.602(2)	2.6001(6)	2.596(1)	2.563(1)	2.553(1)	2.541(2)	2.5427(9)	2.5364(5)
Sn2–Se3		2.5487(9)/2.5519(8)	2.539(1)/2.5602(9)	2.522(1)	2.5268(8)	2.526(1)	2.535(1)	2.624(1)	2.630(2)	2.6370(9)	
Sn2–Se4	2.4983(6)							2.553(1)	2.548(2)	2.5501(9)	
Sn3–Se2		2.6635(8)/2.7048(8)	2.686(1)/2.6328(8)	2.639(1)	2.6470(9)	2.626(1)	2.693(1)	2.601(1)	2.612(2)	2.6130(9)	
Sn3–Se3		2.5646(7)/2.5630(9)	2.5732(9)/2.558(1)	2.545(2)	2.5331(6)	2.547(1)	2.502(2)	2.553(1)	2.548(2)	2.5501(9)	
Sn3–Se4		2.5134(9)/2.5094(9)	2.497(1)/2.490(1)	2.496(2)	2.4977(7)	2.489(1)	2.564(1)	2.504(1)	2.511(2)	2.5133(9)	
Sn1–Se1	2.5508(8)	2.380(1)/2.394(2)	2.386(1)/2.490(1)	2.687(2)	2.6734(7)	2.669(1)	2.664(1)	2.756(2)	2.511(4)	2.502(2)	2.6788(4)
Sn1–Se2	2.6176(8)	2.551(2)/2.764(2)	2.608(1)/2.549				2.664(1)				
Sn1–Se2$^{i/ii/i/iii/i}$		3.448(1)/2.996(1)	3.337(2)/3.434(2)								2.6671(4)
Sn1–Se2$^{vi/ix/x}$								3.005(2)	2.905(4)	2.906(9)	
Sn1–Se3	2.4956(6)										
Sn1–Se4								2.744(2)	2.990(4)	3.021(2)	
Sn1–Se4$^{i/ii/i/iii/i/iv/v}$		2.381(1)/2.383(1)	2.368(1)/2.370(1)	2.602(1)	2.6099(7)	2.632(1)	2.608(1)				
Sn1–Cu1		2.757(1)/2.764(2)	2.747(2)/2.780(1)	2.599(2)	2.5831(8)	2.594(1)	2.561(1)	3.414(2)	3.116(4)	3.121(2)	2.6178(5)
Sn1–Cu1$^{i/ii/i/iii}$		2.552(1)/2.668(2)	2.585(1)/2.632(1)								
Sn1–Cu2								3.367(2)	2.658(4)	2.674(2)	
Sn1–Cu3$^{vi/viii/x}$								2.699(3)	2.761(5)	2.747(2)	
Sn1–Cu3$^{vii/ix/xi}$								2.748(3)	2.823(5)	2.825(2)	
Sn1–Cl1				2.469(3)	2.478(1)	2.473(2)	2.505(2)				2.440(1)

Sn1–O1	2.584(5)										
Sn1–C1	2.196(7)										
Sn2–O/N1	2.614(5)	2.430(7)/2.465(7)	2.468(6)/2.390(7)	2.68(1)	2.696(7)	2.593(7)	2.929(7)	2.606(7)	2.57(1)	2.560(5)	2.479(2)
Sn2–C	2.196(7)	2.199(6)/2.206(7)	2.18(1)/2.21(1)	2.20(1)	2.189(6)	2.185(9)	2.194(5)	2.22(1)	2.22(2)	2.196(8)	2.184(4)
Sn2–Cl2											2.4190(9)
Sn3–O2/N3		2.410(6)/2.425(6)	2.386(8)/2.552(7)	2.501(7)	2.517(5)	2.489(1)	2.358(5)	2.693(9)	2.67(2)	2.700(5)	
Sn3–C7		2.21(1)/2.185(9)	2.206(8)/2.176(9)	2.17(1)	2.190(5)	2.23(1)	2.201(6)	2.18(2)	2.20(2)	2.198(8)	
Cu1–P1	2.216(2)	2.269(2)/2.285(3)	2.271(3)/2.270(2)	2.268(3)	2.264(1)	2.260(3)	2.259(2)	2.267(3)	2.270(5)	2.260(2)	2.4957(6)
Cu2–P2	2.221(1)							2.266(3)			
Cu1–Se1	2.8222(8)	2.447(1)/2.460(1)	2.456(2)/2.431(2)					2.506(2)	2.517(3)	2.520(1)	
Cu1–Se1$^{i/i/iv/v/i}$				2.433(2)	2.4456(9)	2.444(1)	2.422(1)				2.4957(6)
Cu1-Se2				2.476(2)	2.4805(9)	2.488(2)	2.510(1)				2.5064(5)
Cu1-Se2$^{i/ii/i/iii}$		2.677(1)/2.697(1)	2.681(1)/2.718(2)								
Cu1-Se3	2.52(1)										
Cu1-Se4	2.542(1)	2.482(1)/2.497(1)	2.472(1)/2.465(1)								
Cu2-Se2	3.4004(8)										
Cu2-Se3	2.443(1)										
Cu2-Se4	2.416(1)							2.508(2)	2.428(3)	2.427(1)	
Cu1-Cu2	2.678(1)										
Cu3^{A}–Se1$^{vi/viii/x}$								2.403(2)	2.467(4)	2.473(2)	
Cu3^{A}–Se4$^{vi/viii/x}$								2.403(2)	2.383(4)	2.346(1)	
Cu3^{A}–Se2$^{vii/ix/xi}$								2.317(2)	2.348(4)	2.382(2)	

i = 1-X, 1-Y, 1-Z; ii = 1-X, 2-Y, 2-Z; iii = 1-X, 1-Y., 2-Z; iv = 1-X, -Y, 1-Z; v = 2-X, -Y., 1-Z; vi = +Y, +Z, +X; vii = +Z, +X, +Y; viii = ½+Z, 3/2-X, 1-Y; ix = 3/2-Y, 1-Z, -1/2+X; x = -½+Z, ½-X, 1-Y; xi = ½-Y, 1-Z, ½+X.

Table S3. Selected angles in **1** – **6**.

Angles	**1**·2 CH_2Cl_2	**2**·3 CH_2Cl_2	**2**·3 CH_2Cl_2	**3a**	**3a**·2 CH_2Cl_2	**3a**·**B**	**3c**·3 CH_2Cl_2	**4**·3 CH_2Cl_2	**5**	**5**·0.5 C_6H_{14}	**6**
Sn2–Se2–Sn3		81.25(3)/81.55(3)	81.29(3)/81.50(3)	84.47(4)	84.98(2)	84.68(4)	84.66(2)	82.73(4)	82.90(6)	82.99(3)	
Sn2–Se3–Sn3		86.46(3)/86.82(3)	86.35(3)/86.51(3)	88.10(5)	88.93(2)	87.79(4)	87.93(2)	85.11(4)	86.00(7)	86.16(3)	
Se2–Sn2–Se3		91.55(3)/92.60(3)	91.00(3)/88.98(3)	94.38(5)	93.64(2)	94.36(4)	95.56(2)	92.49(4)	92.03(7)	91.95(3)	
Se2–Sn3–Se3		92.40(3)/91.71(3)	90.24(3)/91.41(3)	92.93(5)	92.37(2)	93.13(4)	91.78(2)	91.95(4)	91.77(7)	91.56(3)	
Se1–Sn2–Sn3		100.96(2)/100.65(3)	101.34(3)/101.11(3)	123.28(4)	123.42(2)	124.82(3)	125.12(2)	102.18(3)	102.77(6)	102.81(2)	
Se4–Sn3–Sn2		99.26(2)/100.66(2)	100.05(3)/98.76(3)	118.62(4)	118.58(2)	118.93(4)	117.50(2)	103.84(3)	102.86(6)	102.68(2)	
Se1–Sn2–Se2	92.67(2)										
Sn1–Se1–Sn2	82.78(2)										
Sn1–Se2–Sn2	83.52(2)										
Se3–Sn1–Sn2	97.44(2)										
Se4–Sn2–Sn1	99.12(2)										
Se1–Sn2–$Se2^{i}$											112.14(2)
$Se1^{i}$–Sn1–$Se2^{i}$											86.91(1)
$Se1^{i}$–Sn1–Cu1											113.36(2)
$Se2^{i}$–Sn1–Cu1											113.70(2)
$Sn1^{i}$–Se1–Cu1											78.59(1)
$Sn1^{i}$–Se2–Cu1											78.63(1)
$Cu3^{vi/viii/x}$–Sn1–$Cu3^{vii/ix/xi}$								87.82(7)	83.5(1)	83.85(6)	
Cu1–Sn1–$Cu1^{i/ii/iii}$		118.14(5)/121.98(6)	119.12(5)/118.66(5)								
Se1–Sn1–Cu1				109.65(5)	109.73(2)	107.38(4)	109.47(2)				

Se4$^{i/i/iv/v}$–Sn1–Cu1				150.21(5)	151.59(3)	151.40(4)	148.39(3)				
Se1–Cu1–Se2$^{i/ii/i/iii}$		114.09(4)/108.12(4)	112.24(5)/113.83(5)								
Se1–Cu1–Se4		126.23(5)/127.21(5)	128.09(5)/127.67(6)								
Se2$^{i/ii/i/iii}$–Cu1–Se4		103.60(4)/104.34(4)	103.15(5)/100.84(5)								
Se1–Sn1–Se2	92.88(2)	93.33(4)/98.82(5)	106.10(5)/107.53(5)								
Se1–Sn1–Se2$^{i/ii/i/iii}$		107.71(4)/101.01(5)	94.97(4)/93.97(4)								
Se1–Sn1–Se4$^{i/ii/i/iii/i/i/v/v}$		130.71(5)/134.58(6)	132.07(6)/132.50(6)	90.51(5)	89.60(2)	89.96(4)	94.53(2)				
Se2$^{i/ii/i/iii}$–Sn1–Se2		128.36(4)/126.17(5)	127.60(5)/127.48(4)								
Se2–Sn1–Se4$^{i/ii/i/iii}$		128.36(4)/105.54(5)	108.44(5)/108.70(5)								
Se2$^{i/ii/i/iii}$–Sn1–Se4$^{i/ii/i/iii}$		86.46(4) / 94.74(5)	89.46(4)/87.62(4)								
Se1–Cu3–Se4								144.44(8)	142.4(2)	142.31(6)	
Se1–Cu3–Se2$^{vi/viii/x}$								107.99(7)	100.6(1)	99.39(5)	
Se2$^{vi/vii/x}$–Cu3–Se4								105.25(7)	112.5(1)	114.02(6)	
Se1–Cu1–Se1$^{vi/vii/x}$								105.13(5)	107.6(1)	106.82(4)	
Se4–Cu2–Se4$^{vi/vii/x}$								105.94(5)	119.9(1)	119.90(5)	
Se1–Cu1–Se2											94.62(2)
Se1–Cu1–Se2$^{i/i/iv/v}$				117.10(7)	116.65(3)	116.40(5)	114.29(3)				
Se1–Cu1–Sn1				114.53(7)	114.32(3)	119.07(6)	117.57(3)				101.93(2)
Se2–Cu1–Sn1											102.11(2)
Se2$^{i/i/iv/v}$–Cu1–Sn1				93.67(6)	94.44(3)	94.36(5)	95.66(3)				
Cu1–Se3–Cu2	65.57(3)										
Cu1–Se4–Cu2	65.33(3)										
Se3–Cu1–Se4	110.93(3)										

Se3–Cu2–Se4	117.55(4)									
Se1–Cu1–Cu2	108.06(3)									
Se2–Cu2–Cu1	92.07(3)									
Se2–Sn2–O1/N1		174.2(2)/173.0(2)	170.9(2)/169.9(2)	164.8(2)	164.64(9)	173(7)(2)	176.8(1)	161.4(2)	164.8(3)	164.1(1)
Se2–Sn3–O2/N1		171.0(2)/168.8(2)	167.7(2)/165.9(2)	171.0(2)	170.7(1)	164.8(2)	172.0(1)	170.1(2)	155.0(3)	153.7(1)
Se1–Sn2–O2	164.8(1)									
Se2–Sn1–O1	167.2(1)									
Cl2–Sn2–O1										168.81(6)

i = 1-X, 1-Y, 1-Z; ii = 1-X, 2-Y, 2-Z; iii = 1-X, 1-Y., 2-Z; iv = 1-X, -Y, 1-Z; v = 2-X, -Y., 1-Z; vi = +Y, +Z, +X; vii = +Z, +X, +Y; viii = ½+Z, 3/2-X, 1-Y; ix = 3/2-Y, 1-Z, -1/2+X; x = -½+Z, ½-X, 1-Y; xi = ½-Y, 1-Z, ½+X.

Quantum chemical investigations

The geometric structures and selected structural parameters of the quantum chemically optimized molecules are shown in Figures S24-S31 and Tables S4-S10, respectively.

Computationally optimized structure of compound 1

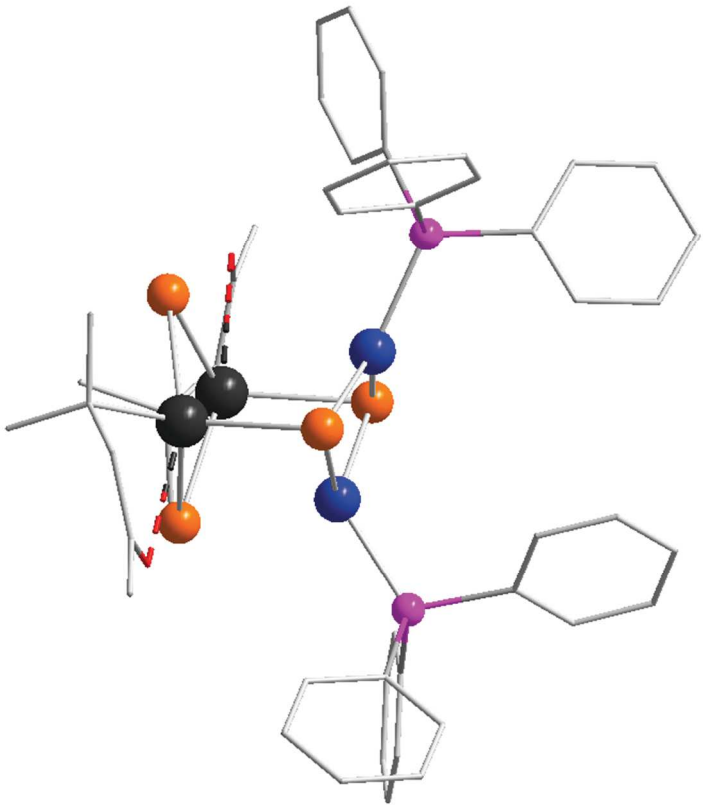

Figure S24. Computationally optimized structure of compound **1** (Cu: dark blue, Se: orange, Sn: dark grey, P: pink, O: red, C: light grey, H atoms are omitted for clarity).

Table S4. Ranges of interatomic distances and corresponding shared electron numbers of compound **1**.

	Interatomic distances / Å	SENs
Cu···Cu	2.58	0.05
Cu–Se	2.47 – 2.61	0.16 – 0.21
Cu–Sn	---	---
Sn–Se	2.53 – 2.68	0.82 – 1.04

Computationally optimized structure of compound 2

As can be seen in Figure S25, we were not able to reproduce the crystal structure of compound **2**, given in Figure 1, computationally. The found minimum structure differs significantly from the experimental data. This might be due effects within the crystal structure itself. We therefore do not discuss the results obtained by DFT methods for compound **2** any further.

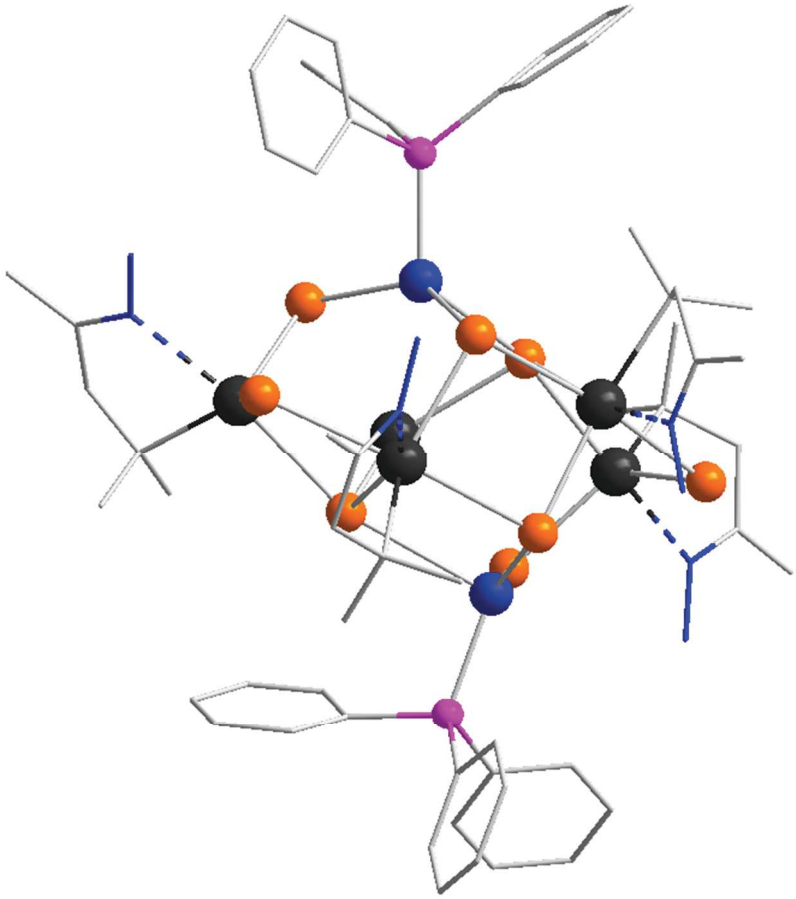

Figure S25. Computationally optimized structure of compound **2** (Cu: dark blue, Se: orange, Sn: dark grey, P: pink, N: blue, C: light grey, H atoms are omitted for clarity).

Computationally optimized structure of compound 3a

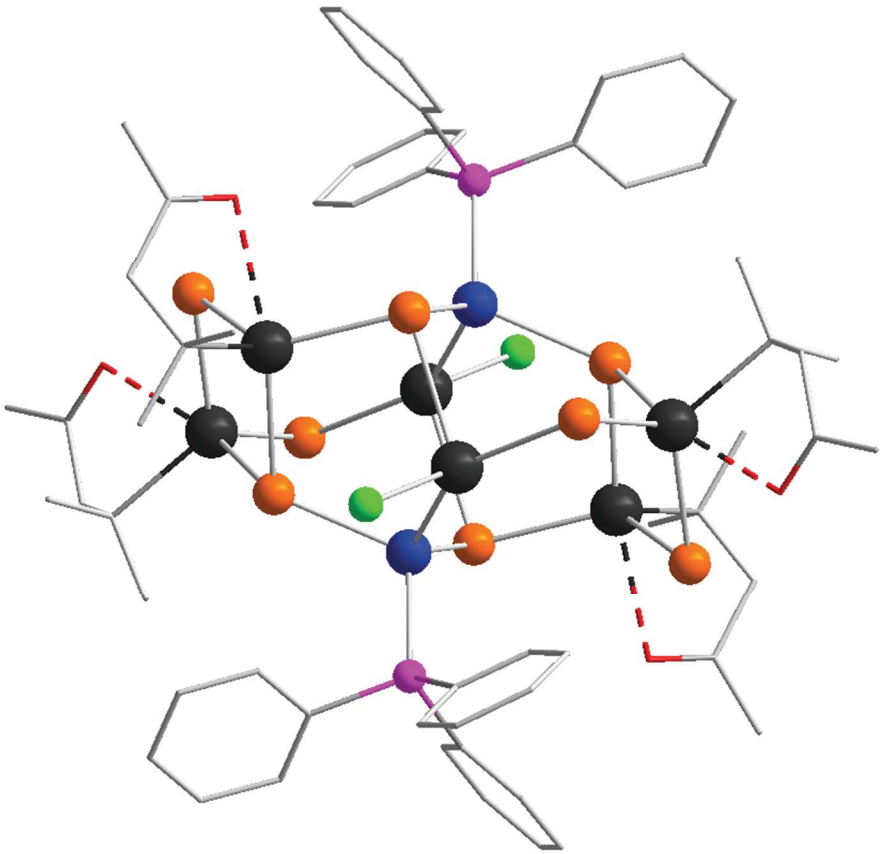

Figure S26. Computationally optimized structure of compound **3a** (Cu: dark blue, Se: orange, Sn: dark grey, P: pink, O: red, Cl: green, C: light grey, H atoms are omitted for clarity).

Table S5. Ranges of interatomic distances and corresponding shared electron numbers of compound **3a**.

	Interatomic distances / Å	**SENs**
Cu···Cu	4.35	---
Cu–Se	2.45 – 2.50	0.14 – 0.16
Cu–Sn	2.66	0.21
Sn–Se	2.56 – 2.69	0.69 – 1.02

Computationally optimized structure of compound 3b

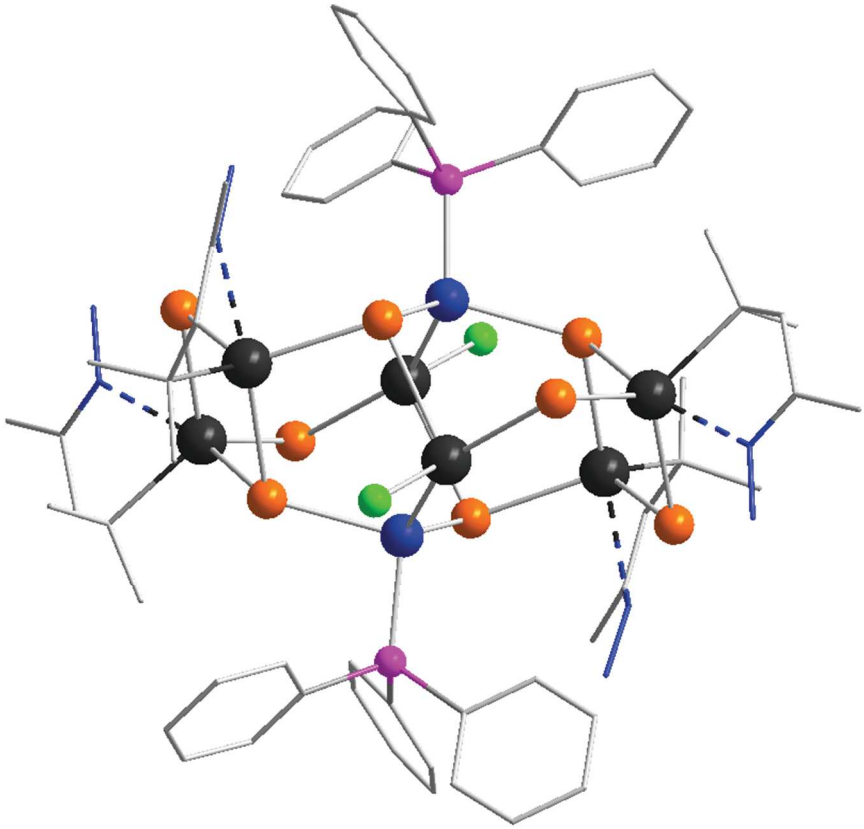

Figure S27. Computationally optimized structure of compound **3b** (Cu: dark blue, Se: orange, Sn: dark grey, P: pink, N: blue, Cl: green, C: light grey, H atoms are omitted for clarity).

Table S6. Ranges of interatomic distances and corresponding shared electron numbers of compound **3b**.

	Interatomic distances / Å	**SENs**
Cu···Cu	4.26	---
Cu–Se	2.45 – 2.49	0.14 – 0.16
Cu–Sn	2.64 – 2.67	0.20 – 0.22
Sn–Se	2.53 – 2.70	0.71 – 1.05

Computationally optimized structure of compound 3c

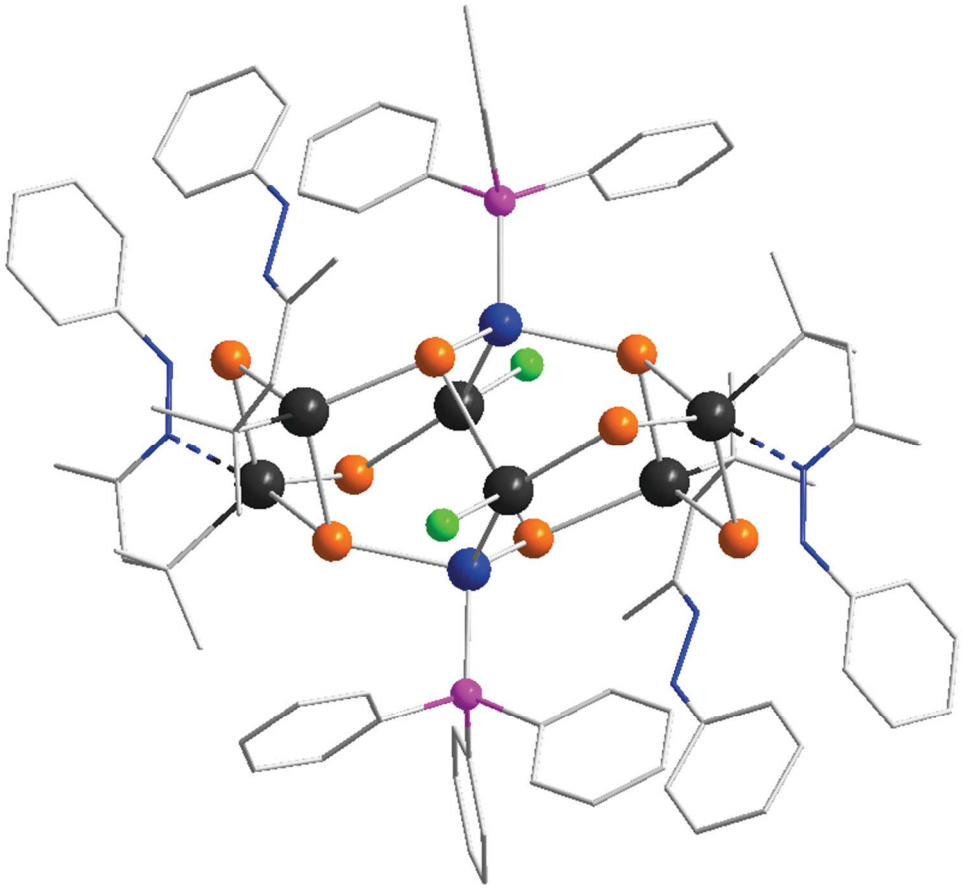

Figure S28. Computationally optimized structure of compound **3c** (Cu: dark blue, Se: orange, Sn: dark grey, P: pink, N: blue, Cl: green, C: light grey, H atoms are omitted for clarity).

Table S7. Ranges of interatomic distances and corresponding shared electron numbers of compound **3c**.

	Interatomic distances / Å	SENs
Cu···Cu	4.43	---
Cu–Se	2.44 – 2.50	0.12 – 0.16
Cu–Sn	2.68 – 2.70	0.19 – 0.21
Sn–Se	2.44 – 2.71	0.70 – 1.04

Computationally optimized structure of compound 4

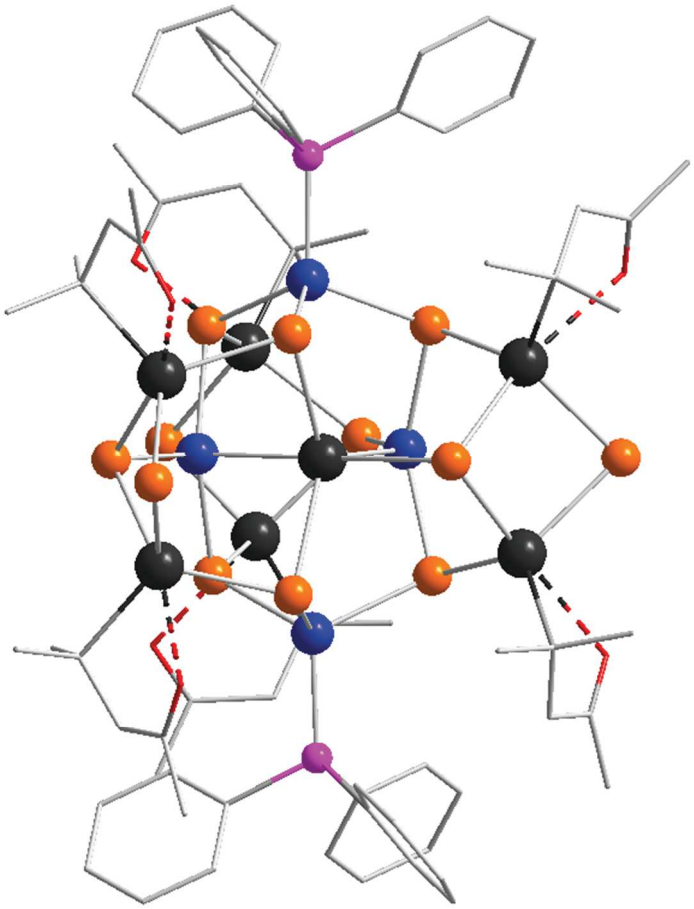

Figure S29. Computationally optimized structure of compound **4** (Cu: dark blue, Se: orange, Sn: dark grey, P: pink, O: red, C: light grey, H atoms are omitted for clarity).

Table S8. Ranges of interatomic distances and corresponding shared electron numbers of compound **4**.

	Interatomic distances / Å	SENs
Cu···Cu	3.86 – 3.95	---
Cu–Se	2.43 – 2.55	0.09 – 0.31
Cu–Sn	2.78 – 2.80	0.18 – 0.20
Sn–Se	2.54 – 2.69	0.51 – 0.98

Computationally optimized structure of compound 5

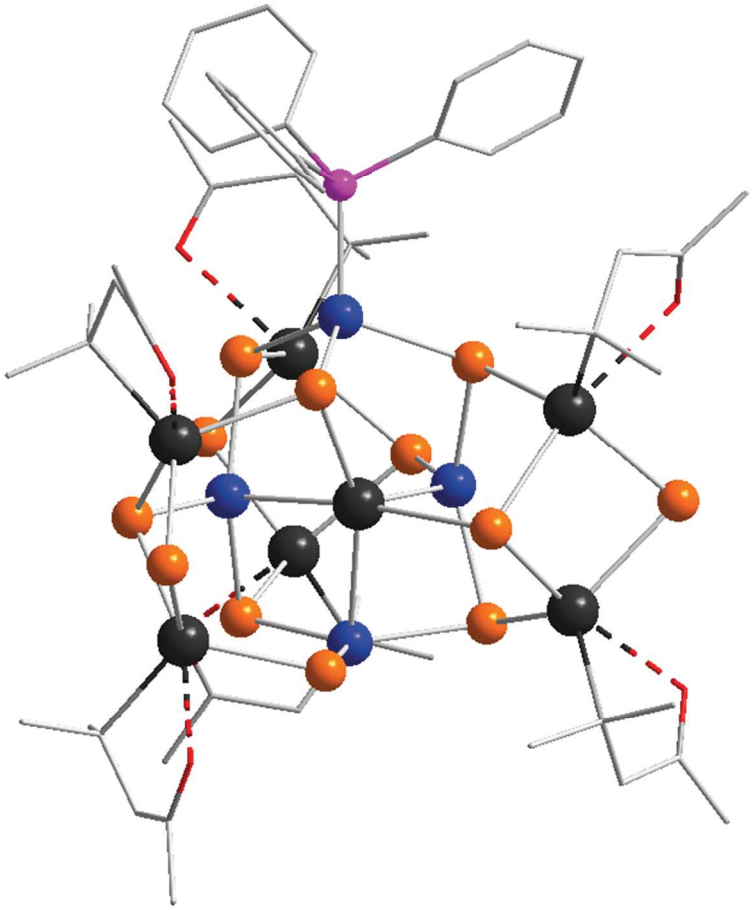

Figure S30. Computationally optimized structure of compound **5** (Cu: dark blue, Se: orange, Sn: dark grey, P: pink, O: red, C: light grey, H atoms are omitted for clarity).

Table S9. Ranges of interatomic distances and corresponding shared electron numbers of compound **5**.

	Interatomic distances / Å	SENs
Cu···Cu	3.06 – 4.03	---
Cu–Se	2.41 – 2.55	0.12 – 0.32
Cu–Sn	2.85 – 2.89	0.14 – 0.20
Sn–Se	2.54 – 2.69	0.11 – 0.99

Computationally optimized structure of compound 6

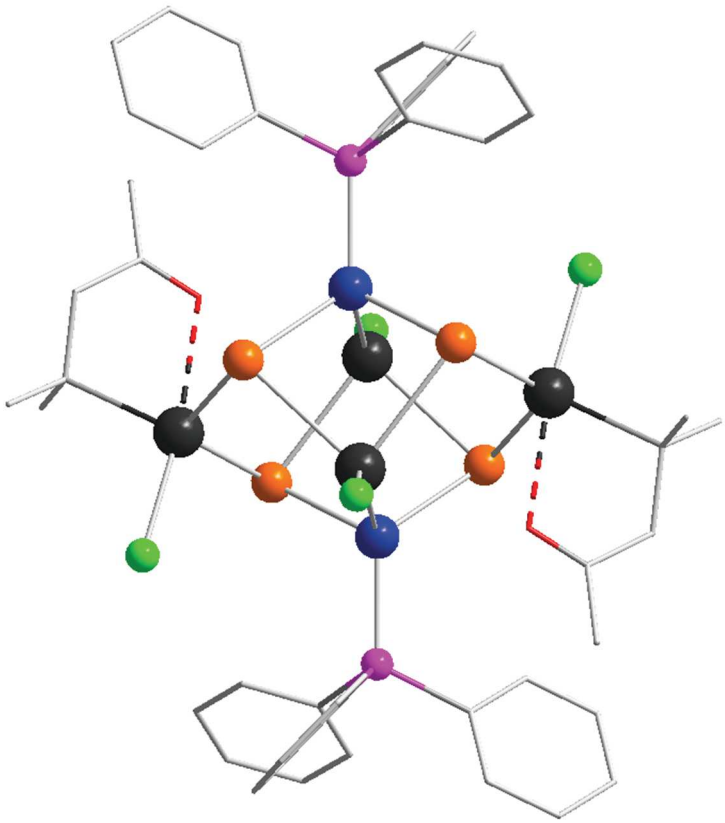

Figure S31. Computationally optimized structure of compound **6** (Cu: dark blue, Se: orange, Sn: dark grey, P: pink, O: red, Cl: green, C: light grey, H atoms are omitted for clarity).

Table S10. Ranges of interatomic distances and corresponding shared electron numbers of compound **6**.

	Interatomic distances / Å	SENs
Cu···Cu	4.48	---
Cu–Se	2.52 – 2.53	0.16
Cu–Sn	2.71	0.19
Sn–Se	2.55 – 2.78	0.64 – 0.96

Calculated HOMO LUMO gaps

Table S11 shows the HOMO LUMO gaps obtained during the simultaneous optimizations of geometric and electronic structures. Illustrations of the respective MOs are shown in Figures S32-S39.

Table S11. Calculated HOMO LUMO gaps

Compound	HOMO LUMO gap / eV
1	1.58
3a	2.01
3b	2.08
3c	2.10
4	1.77
5	1.75
6	2.16

Highest and lowest occupied molecular orbitals of compound 1

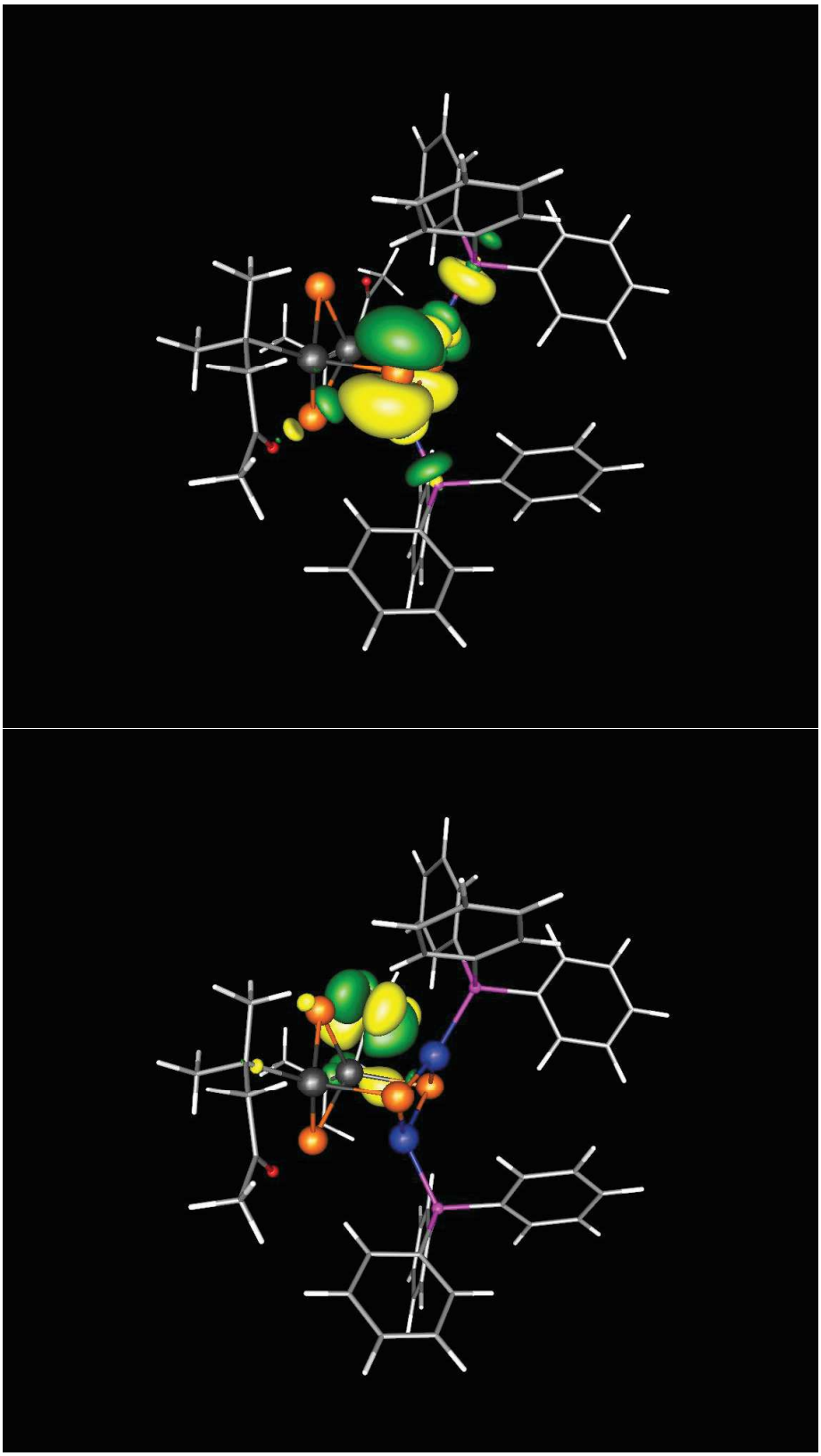

Figure S32. Highest occupied molecular orbital (HOMO, top) and lowest unoccupied molecular orbital (LUMO, bottom) of compound **1** (amplitudes drawn at ±0.03 a.u.).

Highest and lowest occupied molecular orbitals of compound 3a

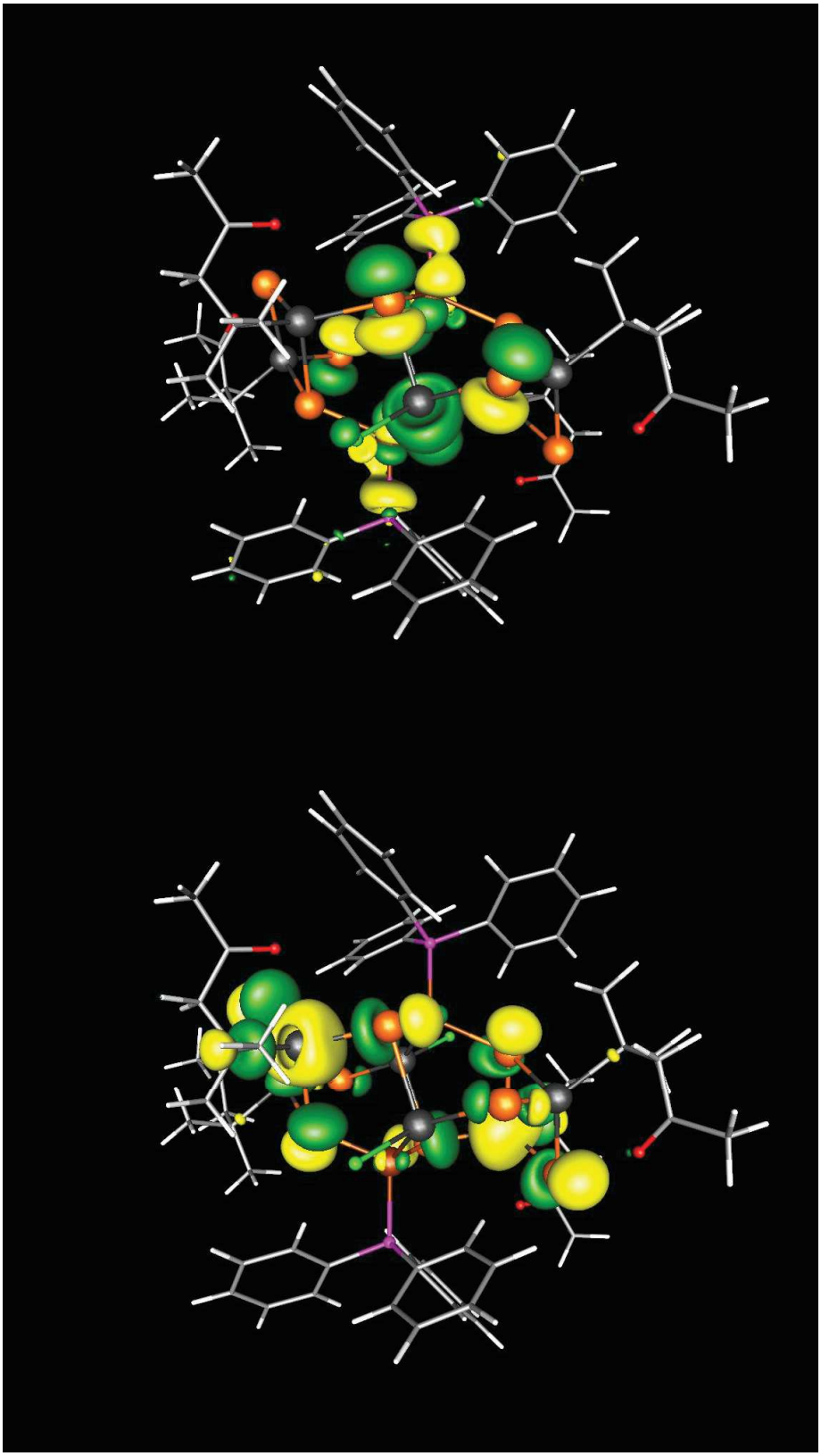

Figure S33. Highest occupied molecular orbital (HOMO, top) and lowest unoccupied molecular orbital (LUMO, bottom) of compound **3a** (amplitudes drawn at ±0.03 a.u.).

Highest and lowest occupied molecular orbitals of compound 3b

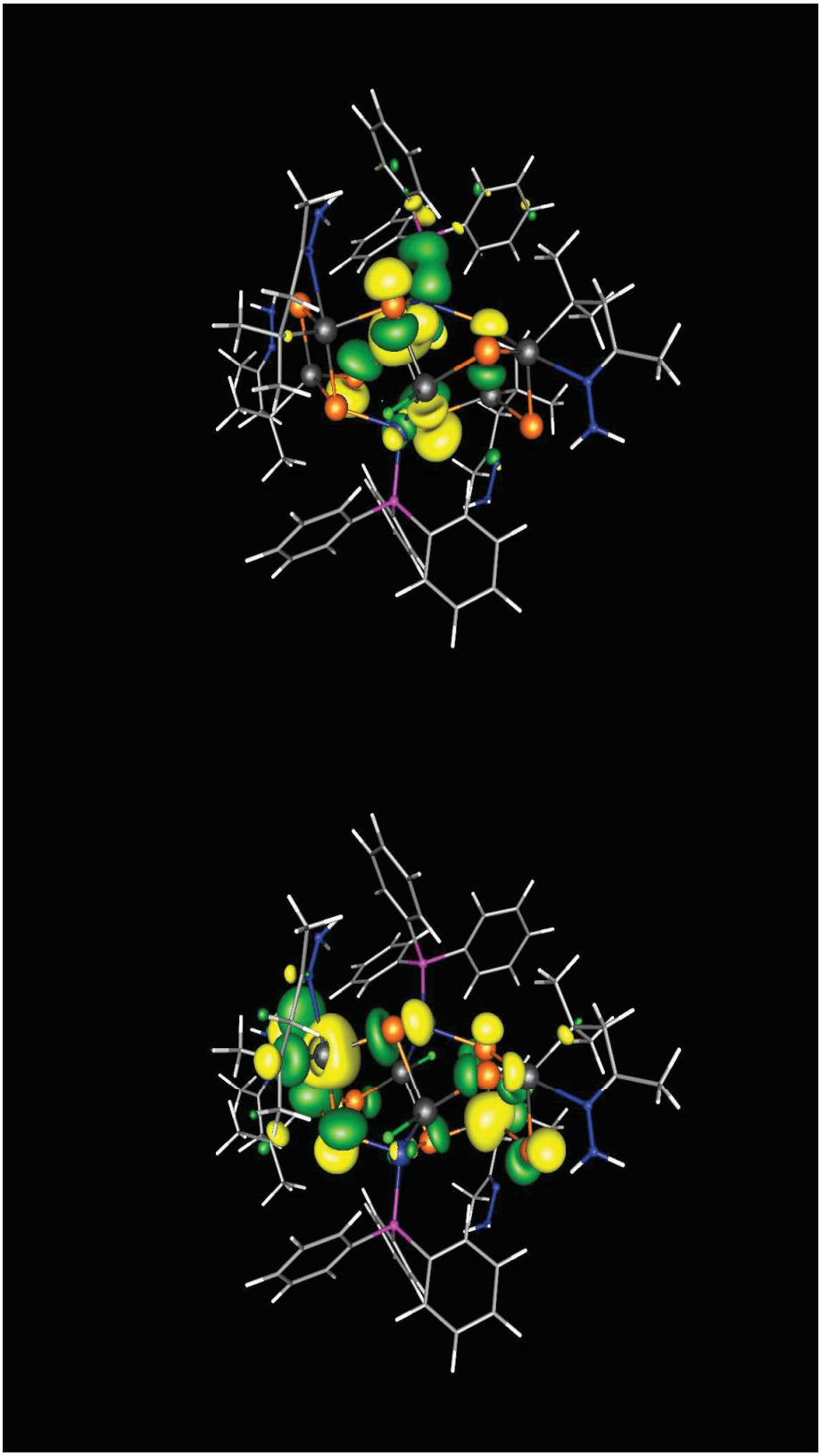

Figure S34. Highest occupied molecular orbital (HOMO, top) and lowest unoccupied molecular orbital (LUMO, bottom) of compound **3b** (amplitudes drawn at ±0.03 a.u.).

Highest and lowest occupied molecular orbitals of compound 3c

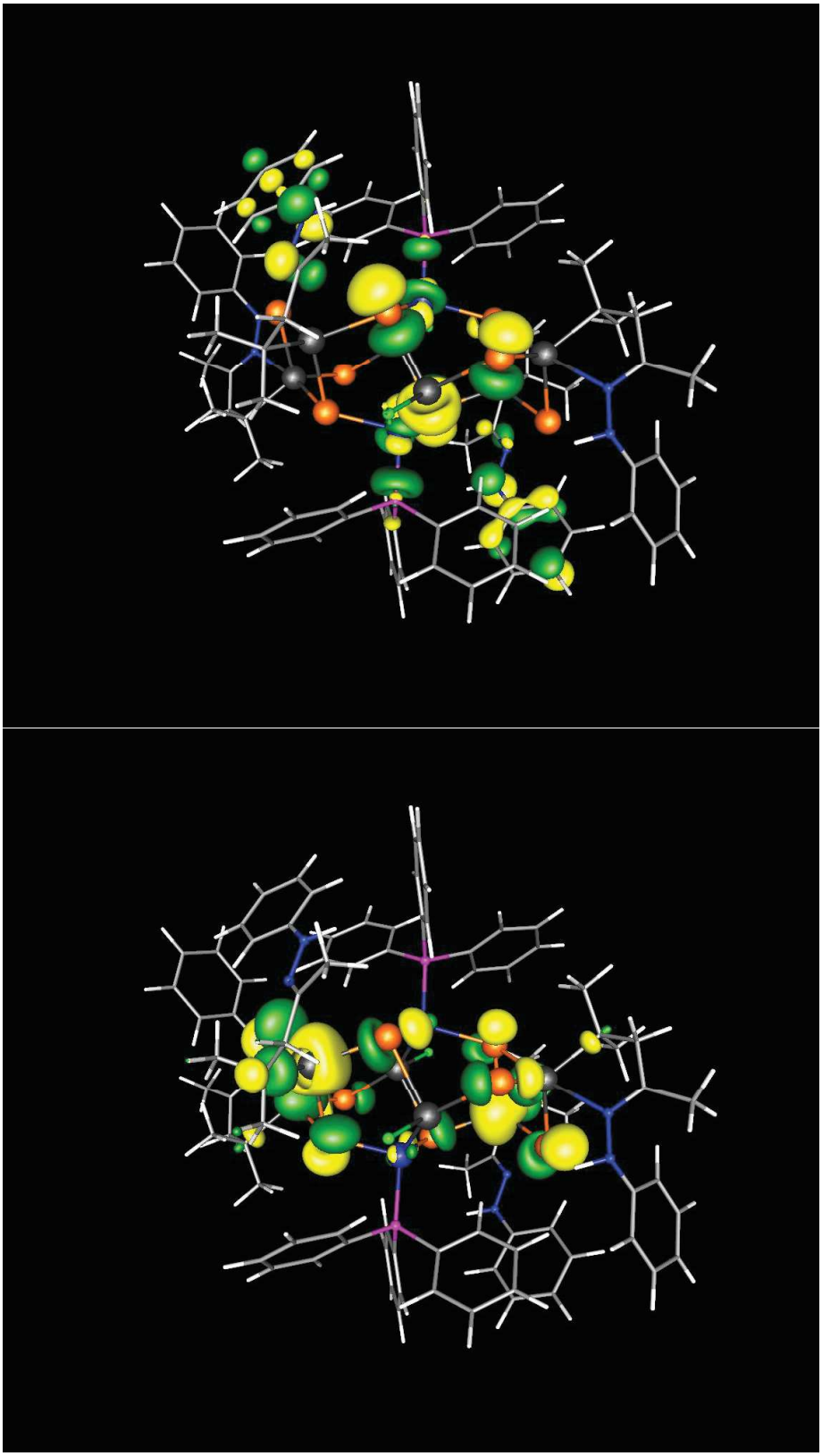

Figure S35. Highest occupied molecular orbital (HOMO, top) and lowest unoccupied molecular orbital (LUMO, bottom) of compound **3c** (amplitudes drawn at ±0.03 a.u.).

Highest and lowest occupied molecular orbitals of compound 4

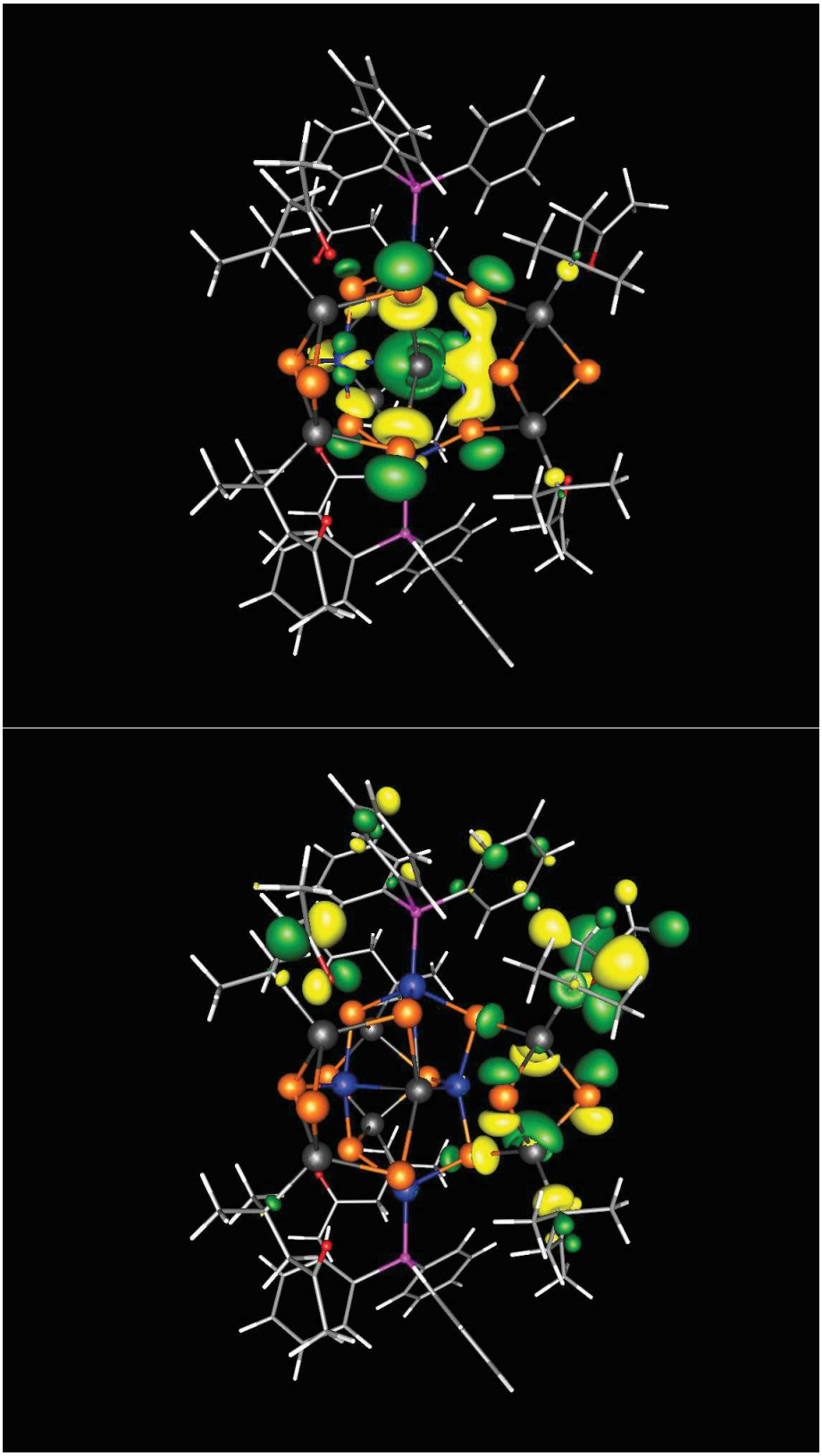

Figure S37. Highest occupied molecular orbital (HOMO, top) and lowest unoccupied molecular orbital (LUMO, bottom) of compound **4** (amplitudes drawn at ±0.03 a.u.).

Highest and lowest occupied molecular orbitals of compound 5

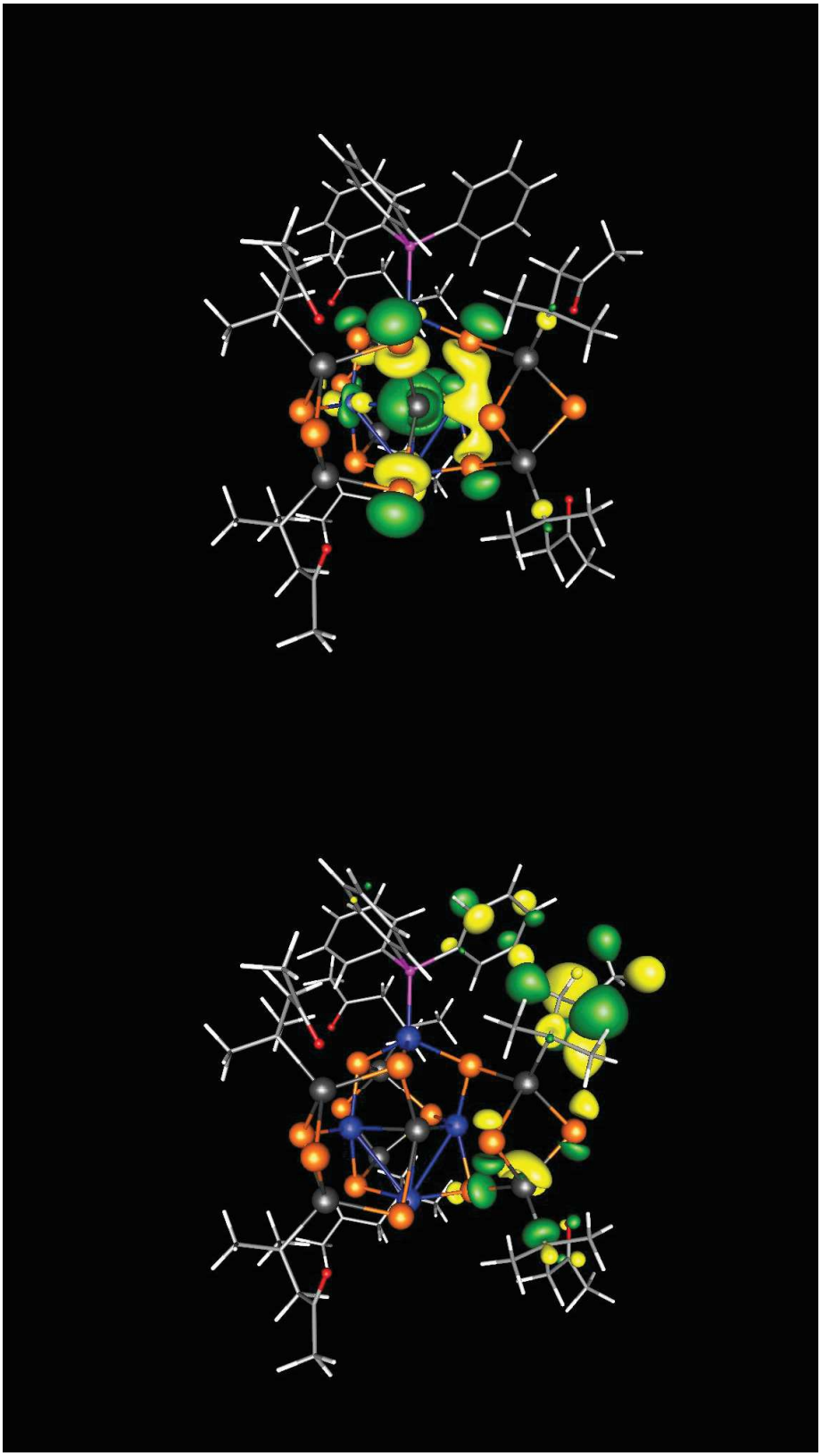

Figure S38. Highest occupied molecular orbital (HOMO, top) and lowest unoccupied molecular orbital (LUMO, bottom) of compound **5** (amplitudes drawn at ±0.03 a.u.).

Highest and lowest occupied molecular orbitals of compound 6

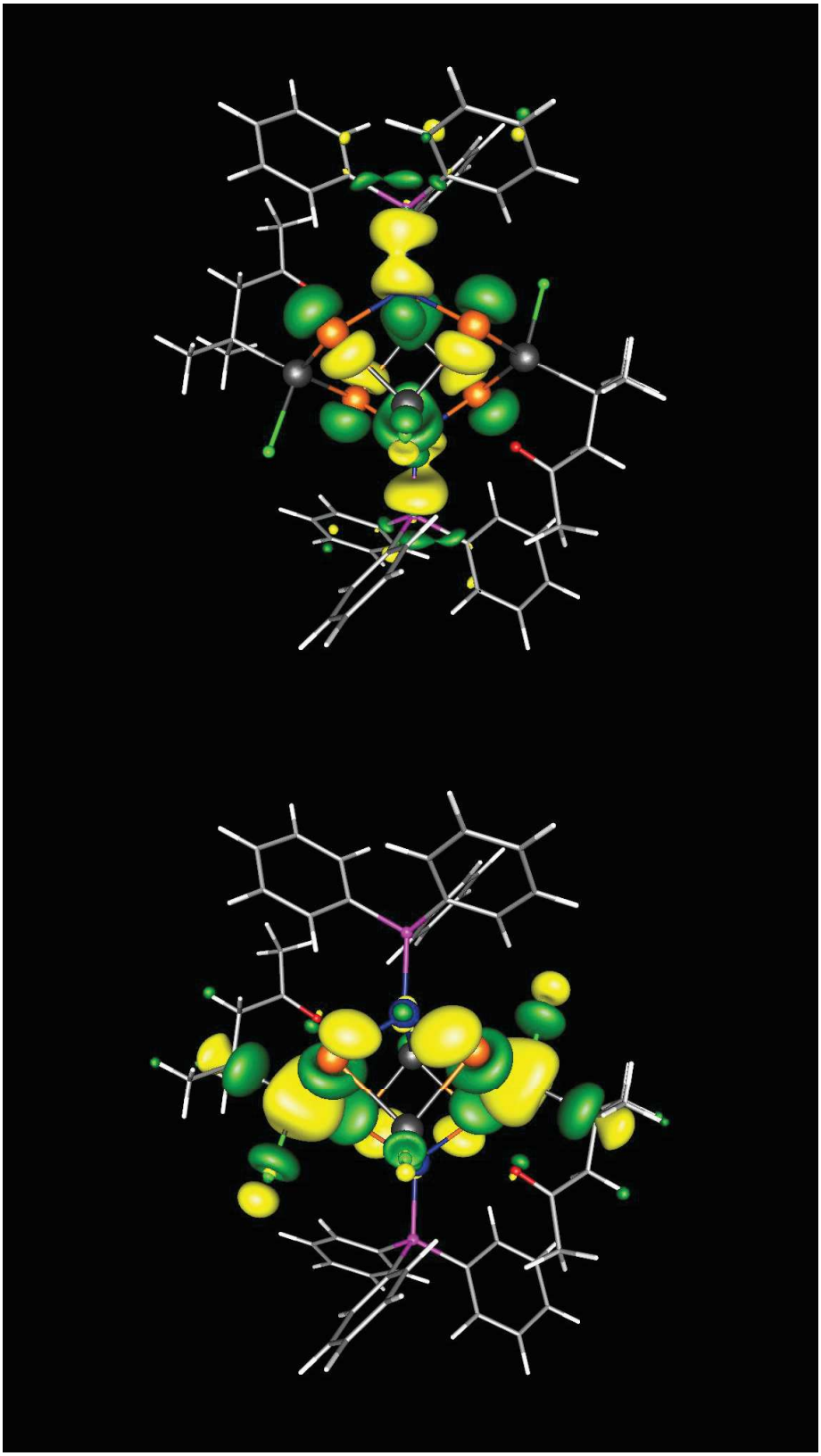

Figure S39. Highest occupied molecular orbital (HOMO, top) and lowest unoccupied molecular orbital (LUMO, bottom) of compound **6** (amplitudes drawn at ±0.03 a.u.).

3.3. Formation and Structural Diversity of Organo-Functionalized Silver-Tin-Selenide Clusters

Niklas Rinn, Lukas Guggolz, Katharina Gries, Kerstin Volz, Jürgen Senker und Stefanie Dehnen, *Chem. Eur. J.* **2017**, eingereichtes Manuskript.

Abstract: When reacting the organic functionalized tin selenide clusters $[(SnR^1)_3Se_4Cl]$ (**A**, $R^1 = CMe_2CH_2C(O)Me$) or $[(SnR^1)_4Se_6]$ (**B**) with $(TMS)_2Se$ and $[Ag(PPh_3)_3Cl]$ at –78°C in CH_2Cl_2, a microcrystalline, intermediate (compound **i**) precipitates, which was investigated by magic angle spinning (MAS) NMR spectroscopy, X-ray powder diffraction (PXRD), energy dispersive X-ray (EDX) spectroscopy, and quantum chemistry. From these studies, a suggestion about its identity was derived. Compound **i** re-dissolves under reorganization into the organo-functionalized Ag/Sn/Se cluster compound $[Ag_6(\mu_6\text{-}Se)(Ag_8Se_{12})\{(R^1Sn)_2Se_2\}_6]$ (**1**), or the mixed-valence cluster $[(AgPPh_3)_2(Sn^{II}Cl)_2Se_2\{(R^1Sn^{IV})_2Se_2\}_2]$ (**2**), depending on the presence or the exclusion of daylight, respectively. The addition of $N_2H_4{\cdot}H_2O$ to a solution of **i** yields selectively $[(\mu_7\text{-}Se)Ag_7Se_{12}\{(R^2Sn)_2Se_2\}_6]$ (**3**, $R^2 = CMe_2CH_2C(N_2H_2)Me$), the Ag/Sn/Se core of which is isomeric to that of **1**. **1** - **3** were characterized by X-ray diffraction. NMR spectroscopic studies on solutions of **i** indicate the co-existence of different species.

Inhaltsangabe: Die Umsetzung der Zinnselenidcluster $[(SnR^1)_3Se_4Cl]$ (**A**) und $[(SnR^1)_4Se_6]$ (**B**)[101] mit $[Ag(PPh_3)_3Cl]$ und $(SiMe_3)_2Se$ wurde untersucht. Hierbei konnte bei einer Reaktionsführung bei niedrigen Temperaturen unabhängig von dem eingesetzten Eduktcluster ein gelbliches, mikrokristallines Pulver **i** isoliert werden. Durch (MAS-)NMR-Spektroskopie, EDX und Röntgenpulverdiffraktometrie (RPD) ließen sich zwar Aussagen über die elementare Zusammensetzung von **i** machen, jedoch konnte kein sicherer Strukturvorschlag gemacht werden. Nach Umkristallisieren von **i** in Dichlormethan (DCM) durch Überschichtung mit *n*-Hexan unter Lichtausschluss entstehen Kristalle von $[(AgPPh_3)_2(Sn^{II}Cl)_2Se_2\{(R^1Sn^{IV})_2Se_2\}_2]$ (**2**), mit einer Topologie, die bereits von analogen Kupfer- und Schwefelclustern bekannt war.[96,102] Wiederholt man dieses Experiment, belichtet aber die Lösung von **i** für ca. 30 Minuten, so färbt sich diese rot, und es lassen sich nach Überschichten mit *n*-Hexan Kristalle von $[Ag_6(\mu_6\text{-}Se)(Ag_8Se_{12})\{(R^1Sn)_2Se_2\}_6]$ (**1**) isolieren. **1** besitzt eine neuartige Topologie mit einem Silberselenid-Kern und einer Organozinnselenid Hülle. Durch Zugabe von $N_2H_4{\cdot}H_2O$ vor dem Umkristallisieren, bildet sich die Verbindung $[(\mu_7\text{-}Se)Ag_7Se_{12}\{(R^2Sn)_2Se_2\}_6]$ (**3**) mit einem zu **1** isomeren anorganischen Grundgerüst, aber einer ungewöhnlich unsymmetrischen Clustertopologie. Die ungenügende Datenqualität erlaubte es nicht, dass die organischen Liganden in **3** per Differenz-Fourieranalyse lokalisiert werden konnten, jedoch konnte die Anwesenheit von Hydrazonliganden in **3** mittels ^{1}H-NMR-Spektroskopie nachgewiesen werden. Abbildung 3.3 zeigt alle hier besprochenen Molekülstrukturen.

Eigener Anteil: Alle Reaktionen wurden von mir geplant und alle analytischen Daten wurden von mir ausgewertet. Alle Reaktionen wurden von mir durchgeführt, bis auf diese diejenigen, die zur Bildung von **2** und **3** führten. Diese wurden unter meiner Anleitung von Tobias Schwarz im Rahmen eines Forschungspraktikums bei mir durchgeführt. Elektronenmikroskopische Aufnahmen und energiedispersive Röntgenabsorptionsspektren (energy-dispersive X-ray absorption spectroscopy, EDX spectroscopy) wurden von Dr. Katharina Gries durchgeführt. Die quantenchemischen Berechnungen wurden von Lukas Guggolz durchgeführt. MAS-NMR-Spektroskopie wurde von der Arbeitsgruppe von Prof. Dr. Jürgen Senker an der Universität Bayreuth betrieben. Das Manuskript habe ich in Kooperation mit Prof. Dr. Stefanie Dehnen geschrieben. Die Co-Autoren haben jeweils kurze Abschnitte über ihre Beiträge eingefügt oder die von uns vorgeschlagenen Abschnitte dazu überarbeitet.

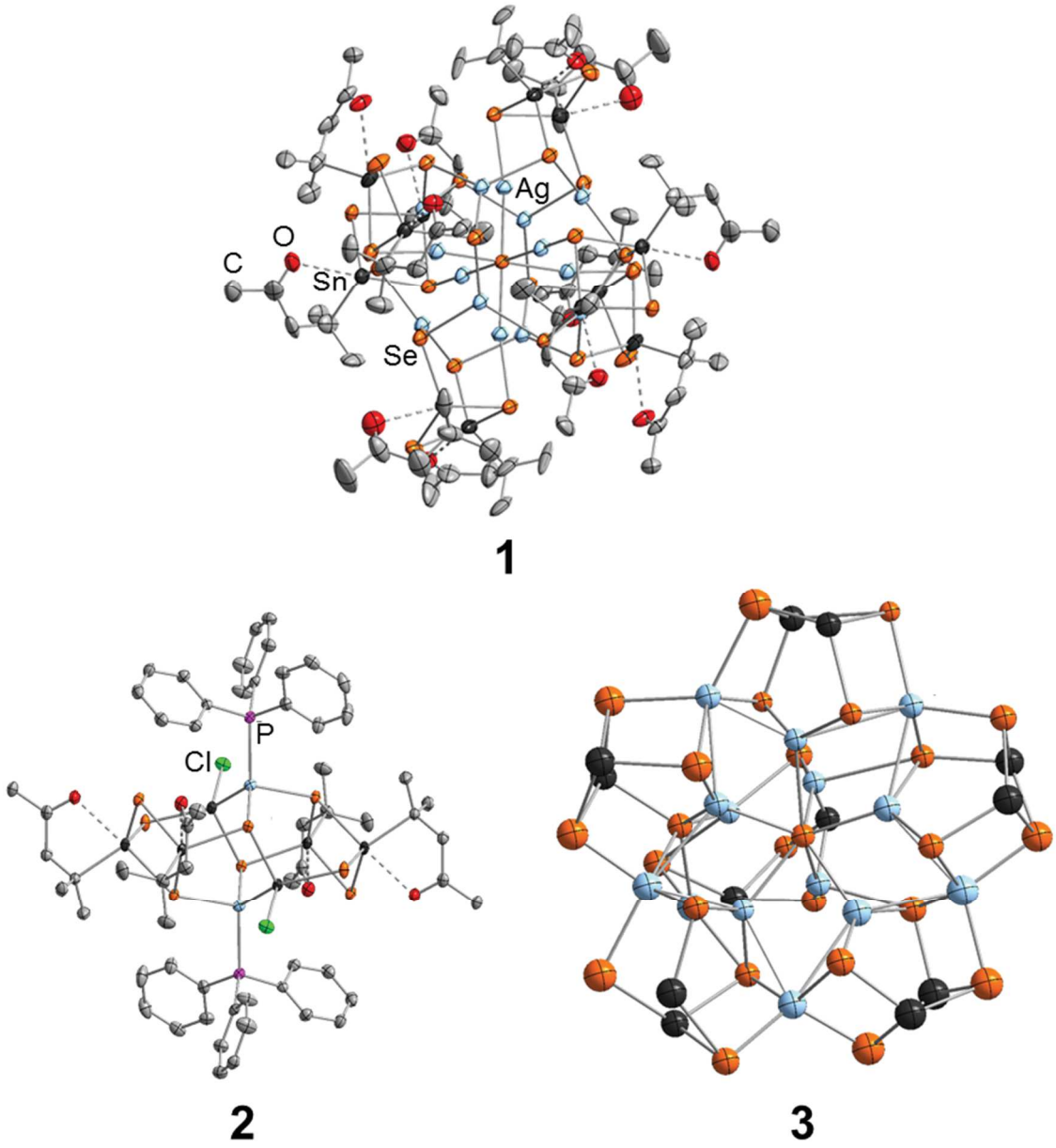

Abbildung 3.3: In „Formation and Structural Diversity of Organo-Functionalized Silver-Tin-Selenide Clusters" beschriebene Molekülstrukturen. Wasserstoffatome wurden aus Übersichtlichkeitsgründen nicht angezeigt.

COMMUNICATION

Formation and Structural Diversity of Organo-Functionalized Tin-Silver Selenide Clusters

Niklas Rinn,[a,c], Lukas Guggolz,[a,c] Katharina Gries,[b,c] Kerstin Volz,[b,c] Jürgen Senker,[d] and Stefanie Dehnen*[a,c]

When reacting the organic functionalized tin selenide clusters $[(SnR^1)_3Se_4Cl]$ (**A**, R^1 = $CMe_2CH_2C(O)Me$) or $[(SnR^1)_4Se_6]$ (**B**) with $(SiMe_3)_2Se$ and $[Ag(PPh_3)_3Cl]$ at –78°C in CH_2Cl_2, a microcrystalline, intermediate (compound **i**) precipitates, which was investigated by magic angle spinning (MAS) NMR spectroscopy, powder X-ray diffraction (PXRD), energy dispersive X-ray (EDX) spectroscopy, and quantum chemistry. From these studies, a suggestion about its identity was derived. Compound **i** re-dissolves under reorganization into the organo-functionalized Ag/Sn/Se cluster compound $[Ag_6(\mu_6\text{-}Se)(Ag_8Se_{12})\{(R^1Sn)_2Se_2\}_6]$ (**1**), or the mixed-valence cluster $[(AgPPh_3)_2(Sn^{II}Cl)_2Se_2\{(R^1Sn^{IV})_2Se_2\}_2]$ (**2**), depending on the presence or the exclusion of daylight, respectively. The addition of $N_2H_4{\cdot}H_2O$ to a solution of **i** yields selectively $[(\mu_7\text{-}Se)Ag_7Se_{12}\{(R^2Sn)_2Se_2\}_6]$ (**3**, R^2 = $CMe_2CH_2C(N_2H_2)Me$), the Ag/Sn/Se core of which is isomeric to that of **1**. **1** - **3** were characterized by X-ray diffraction. NMR spectroscopic studies on solutions of **i** indicate the co-existence of different species.

The first organo-functionalized tin sulfide clusters has been known since 1903,[1] fully characterized since 1968.[2] Recently, these studies, which mainly focused on inert ligands,[3–5] were further extended towards organic ligands with reactive sites such as keto groups, to enable further functionalization through complementary organic chemistry.[6–9] This way, clusters with both different ligands shells and different inorganic cores were accessed. In the presence of organic ligands R that do not undergo intramolecular coordination to the Sn atom, a hetero-adamantane-like $[(RSn)_4S_6]$ architecture (AD) is preferred, while ligands R^F that are functionalized with Lewis basic donor atoms lead stabilize an isomeric sesquisulfide cluster, $[(R^FSn)_4S_6]$ with a "double-decker"-type topology (DD). Here, two four membered $[Sn_2S_2]$ rings are connected via two μ-S bridges. By accordingly adjusting the Sn:S ratio during the reaction, or by enforced product precipitation prior to the formation of the less soluble DD-type cluster later on in the formation cascade, the R^F ligands also enable the isolation of defect-heterocubane-type clusters (DC) with a 3:4 Sn:S ratio, $[(RSn)_3S_4Cl]$.[10,11]

The chemistry of functionalized organotin and homologous organogermanium sulfide clusters was also varied by introducing another metal atom type into the cluster network. A straight-forward approach for this is the simultaneous addition of excess sulfide, to break up the intra-cluster bonds, and a transition metal compound. This way, Cu, Ag, and Au atoms were successfully introduced into functionalized organotin sulfide clusters.[7,9,12–16]

Both approaches were only recently transferred to functionalized organotin selenide and organotin telluride clusters for the first time.[10] In the case of the selenide compounds, the DC-type and the DD-type clusters $[(R^1Sn)_3Se_4Cl]$ (**A**, R^1 = $CMe_2CH_2C(O)Me$) and $[(R^1Sn)_4Se_6]$ (**B**) were reported.[10,17] According reactions with transition metal compounds have remained rare, however, with $[(CuPPh_3)_2(R^1Sn)_2Se_4]$ (**C**) being the only known example so far.[18]

Aiming at the formation of compounds with an Ag/Sn/Se elemental combination, we recently studied reactions of the precursor clusters **A** or **B** with $(SiMe_3)_2Se$ and $[Ag(PPh_3)_3Cl]$. The reaction solutions turned out to be much more sensitive to temperature and light. Upon optimization of the reaction conditions, three organo-functionalized $Ag_xSn_ySe_z$ clusters were obtained as single-crystals. $[Ag_6(\mu_6\text{-}Se)(Ag_8Se_{12})\{(R^1Sn)_2Se_2\}_6]$ (**1**, CCDC 1562670) and $[(AgPPh_3)_2(Sn^{II}Cl)_2Se_2\{(R^1Sn^{IV})_2Se_2\}_2]$ (**2**, CCDC 1562671) form from a microcrystalline intermediate (**i**) under identical conditions except the presence/absence of daylight. Upon addition of $N_2H_4{\cdot}H_2O$ to the re-dissolved intermediate **i**, $[(\mu_7\text{-}Se)Ag_7Se_{12}\{(R^2Sn)_2Se_2\}_6]$ (**3**, R^2 = $CMe_2CH_2C(N_2H_2)Me$) is obtained selectively, with a cluster core isomeric to that of **1**. Herein, we describe and discuss the syntheses and analyses of the uncommon compounds.

Upon addition of two equivalents of $[Ag(PPh_3)_3Cl]$ and four equivalents of $(SiMe_3)_2Se$ to a solution of **A** or **B**, respectively, in DCM at –78 °C, and slow warming to room temperature during four hours under exclusion of light, a light yellow powder of compound **i** precipitates. The powder proved to be microcrystalline, consisting of fine needles (Figure 1).

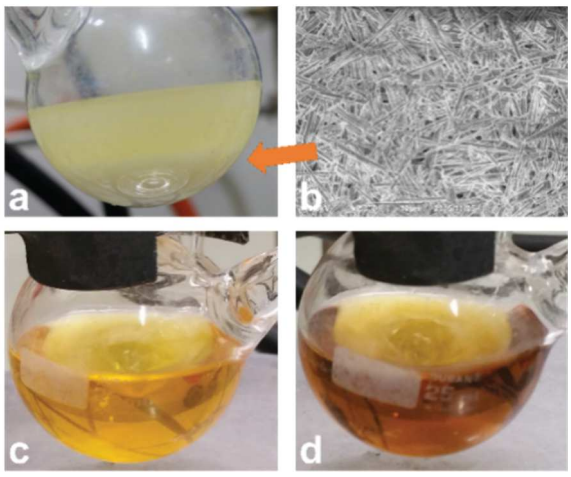

Figure 1. Reaction solution after precipitation of **i** (a); scanning electron microscopy (SEM) image of solid **i** (b); solution of **i** in DCM directly after dissolving at room temperature (c), and after 30 minutes (d).

[a] N. Rinn, L. Guggolz, Dr. S. Dehnen
Fachbereich Chemie, Philipps-Universität Marburg
Hans-Meerwein-Straße 4, 35043 Marburg (Germany)
E-mail: dehnen@chemie.uni-marburg.de
[b] Fachbereich Physik, Philipps-Universität Marburg, Renthof 7, 35032 Marburg (Germany)
[c] Wissenschaftliches Zentrum für Materialwissenschaften (WZMW), Philipps-Universit.t Marburg, Hans-Meerwein-Straße, 35043 Marburg (Germany)
[d] Department of Chemistry, University of Bayreuth, Universitätsstraße 30, 95447 Bayreuth (Germany)

Supporting information for this article is given via a link at the end of the document

Energy-dispersive X-ray (EDX) analyses revealed the heavy element composition of **i** to be approximately 1P:2Ag:2Sn:4Se (Figure S1 and Table S1). A relatively poor quality of the powder X-ray diffraction diagram (Figure S2) did not allow for assignment of the reflections, but MAS NMR spectroscopy of solid **i** (Figures S6 and S7) revealed the presence of two inequivalent Sn and four inequivalent Se sites in agreement with the EDX data.

When dissolving the poorly soluble **i** in DCM at room temperature in light, the yellow solution turns orange-red within 30 minutes. Layering of this solution with *n*-hexane yields red blocks of single-crystalline compound **1** which were analyzed by X-ray diffraction.

1 crystallizes in the monoclinic space group $P2_1/n$ together with partially disordered DCM molecules (5.3 molecules on average per formula unit). The inversion-symmetric molecule can be described as consisting of an Se-centered $[Ag_{14}Se_{12}]$ unit, hence an inner $[Ag_{14}Se_{13}]$ cluster core, which is coordinated by six $[(SnR^1)_2Se_2]$ moieties (Figure 2).

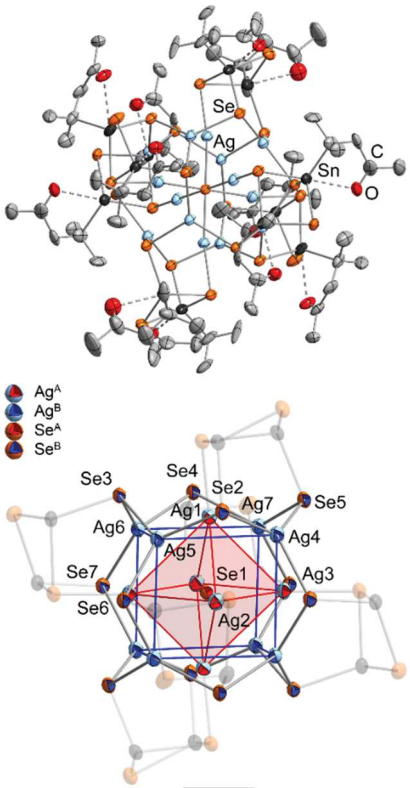

Figure 2. Top: molecular structure **of 1**. Ellipsoids are drawn at the 50% probability level; hydrogen atoms are omitted for clarity. Different positions of the Ag and Se atoms are indicated by different colors, see legend. Selected structural parameters [Å, °]: Se^A–Ag^A 2.640(1)–2.705(1), Se^B–Ag^B 2.612(2)–2.649(2), Se^C–Ag^A 2.633(2)–2.678(2), Se^B–Sn 2.508(2)–2.525(2), Se^C–Sn 2.598(2)–2.647(2), Se^D–Sn 2.518(2)–2.564(2), $Ag^A\cdots Ag^A$ 3.698(2)-3.845(2), $Ag^B\cdots Ag^B$ 4.055(2)-4.213(2), $Ag^A\cdots Ag^B$ 2.915(2)-3.236(2), Sn···O 2.55(1)–2.76(1), Ag^A–Se^A–Ag^A: 88.89(4)–92.47(3), Ag^B–Se^B–Ag^B: 111.29(6)–128.69(6). Bottom: $[Ag_{14}Se_{13}]$ core of **1**, emphasizing the $[Ag^A_6]$ and $[Ag^B_8]$ polyhedra and their connection to the μ_6-Se^A and μ_3-Se^B atoms.

There are two types of Ag atoms (Ag^A and Ag^B) and four types of Se atoms ($Se^{A\text{-}D}$), which differ in their chemical environment. The inorganic core is based on a μ_6-Se atom (Se^A) inside an (non-bonding) $[Ag_6]$ octahedron (Ag^A), which is trapped inside a distorted (non-bonding) $[Ag_8]$ cube (Ag^B). Each of the cube's edges are capped by a μ_3-Se atom (Se^B) that at the same time binds to one tin atom of external $[(SnR^1)_2Se_2]$ units. Besides coordination by the central μ_6-Se atom, the Ag atoms of the central octahedron are coordinated by one Se atoms (Se^C) of the $[(SnR^1)_2Se_2]$ units in a linear fashion, while the remaining Se atoms of the four membered $[Sn_2Se_2]$ rings only bind to their two Sn neighbors (Se^D).

The closest Ag···Ag contacts are found between Ag^A and Ag^B, atoms, hence between the octahedral and the cubic subunits (2.894(2) - 3.034(2) Å), with the exception of the significantly longer Ag(2)···Ag(4) distance of 3.236(2) Å). The Ag···Ag distances within these subunits are 3.698(2) - 3.861(2) Å ($Ag^A\cdots Ag^A$) and 4.055(2) - 4.253(2) Å ($Ag^B\cdots Ag^B$), respectively.

Quantum chemical calculations were undertaken to rationalize the experimental findings and to gain insight into possible Ag···Ag interactions. We simultaneously optimized the geometric and electronic structures by using density functional theory (DFT) methods[18–21] employing Grimme's B97-D functional[22] within the program system TURBOMOLE (V7.0.1).[23] Further technical details are given in the Supporting Information.

In agreement with the experimental results, the calculations for **1** were performed in C_i symmetry to reduce the computational effort. During the geometry optimization, the $Ag^A\cdots Ag^B$ distances were increased by up to 0.13 Å (0.06 Å on average), except for Ag(2)···Ag(4), which was decreased by 0.09 Å as a consequence of a slight relaxation of the structure. The calculated $Ag^A\cdots Ag^B$ distances range from 2.996 Å to 3.145 Å (Table S5). We ascribe the observed differences to slight conformational changes of the organic ligands during the calculations. However, the overall structures are extremely similar (see Figure S11). Both a population analysis based on occupation numbers (PABOON)[24] and the inspection of the canonical and localized[25] MOs point to notable Ag···Ag interactions[26] between the octahedral and the cubic subunits (Table S5). The $Ag^A\cdots Ag^A$ distances of the octahedral moiety range from 3.756 to 3.796 Å. As in the experiment, the $Ag^B\cdots Ag^B$ distances within the cubic subunit span a slightly larger range (4.166 - 4.347 Å). As expected, within each of the subunits, no signs of any argentophilic interactions are observed.

The $[Ag_{14}E_{13}]$ motif is well known for clusters with E = S, Se and Te.[27–34] However, in all of these reported compounds, the μ_3-E atoms corresponding to the Se^B sites are coordinated by terminal organic groups, while all of the Ag atoms are coordinated by terminal phosphine ligands. This leads to the general formula of $[(\mu_6\text{-}EAg_6)(AgPR_3)_8(\mu_3\text{-}ER)_{12}]$, except for some cases, in which two phosphine ligands or the central chalcogenide atom are missing. Comparison of the $[Ag_{14}Se_{13}]$ core in **1** with those in the three selenide analogs $[(\mu_6\text{-}SeAg_6)_{1\text{-}x}(AgPPh_3)_8(\mu_3\text{-}SeR)_{12}]^{-2x}$ (**C**, x = 0, R = Ph; **D**, x = 0.5, R = Ph; **E**, x = 0.5, R = Cy), indicates a much larger distortion of the underlying halite-like topology in the reported compounds. The Ag^A – Se^B distances, in particular, are significantly shorter in **C** – **E** (2.514(2) Å - 2.674(2) Å; **C:** 2.541(2) – 2.674(2) Å, **D** 2.514(2) – 2.554(1) Å, **E** 2.520(4)-2.549(4) Å) as compared to the corresponding bond lengths in **1** (3.148(2) Å - 3.467(2) Å). The Ag^A – Ag^B distances however are much longer, and show a much broader range (2.996 - 4.382 Å; **C**: 3.161 –

4.274 Å, **D**: 2.996-4.382 Å, **E**: 3.006 4.225 Å), again illustrating the notable deviation from an ideal halite-type architecture of the cluster cores.

Upon dissolving compound **i** in DCM under exclusion of light and layering with *n*-hexane, compound **2** is isolated as colorless blocks besides crystals of **B**, but without any crystals of **1**. Compound **2** crystallizes in the triclinic space group $P\bar{1}$. Its molecular structure (Figure 3) is topologically identical with that of the homologous sulfide,[14] but naturally differs in details regarding distances and angles. **2** seems to decompose in solution, thereby forming an equilibrium of different, so far unidentified species, as suggested by ^{1}H spectra of re-dissolved crystals of **2** (Figure S4).

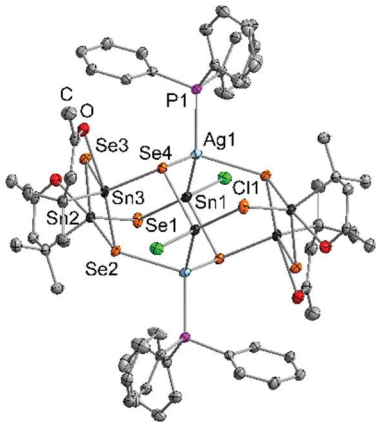

Figure 3. Molecular structure of **2**. Ellipsoids are drawn at the 50% probability level; hydrogen atoms are omitted for clarity. Selected structural parameters [Å, °]: Ag1–Sn1 2.7246(5), Ag1–Se 2.6590(4)–2.7507(4), Ag1–P1 2.4687(7) Sn–Se 2.5235(4)–2.6441(4), Sn1–Cl1 2.4729(7), Sn···O 2.470(2)–2.775(2), Sn–Se–Sn 84.13(1)–96.57(1), Se–Sn–Se 93.22(1)–115.96(1), Se4–Ag1–Se2^i 110.68(1). i = –x + 2, –y + 1, –z + 2.

To explore the availability and reactivity of the external C=O groups in **1** and/or **2** for condensation reactions, we added hydrazine hydrate to the reactive solution, from which **1** and **2** were crystallized. As we did not exclude light, we expected the *in situ*-formed cluster of **1** to undergo the derivatization reaction. Upon layering with *n*-hexane, the solution turned dark yellow and afforded golden needles of compound **3** after three days, however with very poor X-ray diffraction capability. None of the collected data sets led to a satisfying crystal structure refinement, such that even the best one has to be understood as a topological study. Hence structural details like interatomic distances will not be discussed at this point. However, as we were in the position to localize the atomic positions of heavy atoms, we report on this structural model herein. Due to the poor data, the organic ligands could not be localized on the difference Fourier map, but the presence of hydrazine units were confirmed by means of ^{1}H-NMR spectroscopy (δ = 5.6…5.7 ppm), indicating a successful conversion of the keto group in **3** to hydrazine units

. According to the analyses, the cluster core of **3** represents a structural isomer of the $[Ag_{14}Se_{25}Sn_{12}]$ core in **1** (Figure S10). As in **1**, the structure comprises a central Se atom (Se^A). However, different from the cluster structure of **1**, the central atom is surrounded by a pentagonal, star-shaped unit of ten Ag atoms (Ag^A for the next five atoms, Ag^B for the tips of the star). The edges of this star are capped by Se atoms alternatively pointing below (Se^B) and above (Se^C) the nearly flat plane of the star. Each pair of neighboring Se^B and Se^C atoms is capped by one of the external $[(R^2Sn)_2Se_2]$ units. Se^A is markedly displaced above the plane of the pentagonal star and coordinated by two additional Ag atoms, leading to a μ_7-bridging situation altogether. Above these Ag atoms and the Se^B sites is an asymmetrical unit of Ag_2Se_2 capped by a further $(R^2Sn)_2Se_2$ four membered ring.

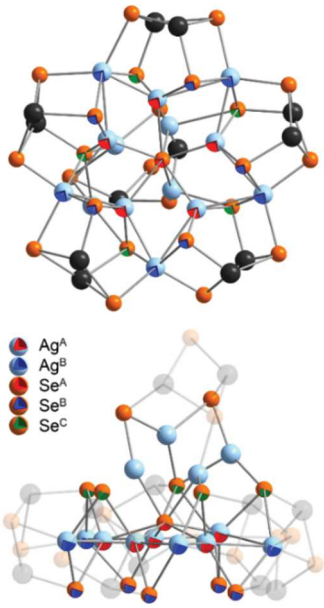

Figure 4. Topological model of the heavy atom cluster core in **3**, shown with arbitrary atomic radii. The different positions of the Ag and Se atoms are indicated by different colors according to the legend (see text). Top: View onto the pentagonal star-like $[Ag_{14}Se_{25}Sn_{12}]$ core along the idealized C_5 axis. Bottom: Side view of the $[Ag_{14}Se_{25}Sn_{12}]$ core. Preliminary structural data [Å]: Se^A–Ag^A 2.88–2.60, Se^B–Ag^A 2.45–2.72, Se^B–Ag^B 2.48–2.80, Se^C–Ag^A 2.48–2.74, Se^C–Ag^B 2.67–2.82, Se^B–Sn 2.48–2.79, Se^C–Sn 2.45–2.58, Ag^A···Ag^A 2.84–3.20 Ag^A Ag^A···Ag^B 2.71–3.36.

In a computational study, the organic ligands R^2 were added manually to the Sn atoms (details are given in the Supporting Information). The resulting structure is a minimum on the energy hypersurface, but shows a slight deviation of the Ag^B arrangement, two of which are situated below the mean Ag^A/Ag^B plane (Figure S14). $Ag^{A,B}$···$Ag^{A,B}$ distances range from 2.905 Å to 3.521 Å, thus longer than the experimental data, as typical for the treatment of weak interactions by means of DFT methods. The calculated shared electron numbers (SEN) again indicate argentophilic interactions with the largest values found between 0.37 and 0.46 within the two asymmetrical Ag_2Se_2 units (Table S5).

For a comparison of the isomeric structures, a derivative of compound **1** with R^2 ligands and a derivative of compound **3** with R^1 ligands were calculated. For both ligand types, the structural motif in **1** turned out to be energetically favored over that in **3**, ΔE = –134 kJ·mol^{-1} for R^1, and –117 kJ·mol^{-1} for R^2 (Table S7). Hence, **3** might be a kinetic product that can only be isolated if the ligands cause a significantly lower solubility such that the compound crystallizes prior to its isomerization into the thermodynamically preferred cluster. The fact that clusters with

hydrazone ligands R^2 possess lower solubilities than identical clusters with ketone ligands R^1 correlates with all our previous findings. Combined with the already extremely low solubility of **i** and **1,** the crystalline yield did not allow for extensive spectroscopic analyses of **1**. This holds also for compound **3**.

The syntheses of **1** - **3** can be viewed as an extension of the chemistry of phosphine stabilized Ag/S and Ag/Se clusters, such as reported extensively by *Fenske et al*., if the organic protection of such binary clusters is replaced conceptually by (RSn)/Se units. However, the latter seem to better stabilize the cluster cores than relatively weakly bound phosphine ligands, such that the ternary clusters do not grow to the giant extensions as their binary relatives that have been known in sizes of between 4 to 490 Ag atoms.[35–41]

In conclusion, we have successfully extended the chemistry of organotin chalcogenide clusters to ternary $[Ag_xSn_ySe_z]$ cluster cores by reactions of binary precursor clusters with $(SiMe_3)_2Se$ and $[Ag(PPh_3)_3Cl]$. Upon optimization of the reaction conditions regarding temperature and the presence/absence of light, three new cluster compounds were selectively obtained from solutions of a not yet fully characterized microcrystalline intermediate **i**, which is based on a P:2Ag:2Sn:4Se elemental composition. $[Ag_6(\mu_6\text{-}Se)(Ag_8Se_{12})\{(R^1Sn)_2Se_2\}_6]$ (**1**, R^1 = $CMe_2CH_2C(O)Me$) exhibits an unprecedented core-shell-shell architecture, with an $[Ag_{14}Se_{12}]$ core surrounded by six $[Sn_2Se_2]$ units and an outer shell of twelve R^1 ligands. $[(AgPPh_3)_2(Sn^{II}Cl)_2Se_2\{(R^1Sn^{IV})_2Se_2\}_2]$ (**2**) possesses the same topology as its sulfide homolog. Upon addition of $N_2H_4{\cdot}H_2O$ to **i**, $[(\mu_7\text{-}Se)Ag_7Se_{12}\{(R^2Sn)_2Se_2\}_6]$ (**3**, R^2 = $CMe_2CH_2C(Me)N_2H_2$) crystallizes, the again unprecedented, irregular cluster core of which is isomeric to that of **1**.

Acknowledgement

This work was supported by the Deutsche Forschungsgemeinschaft within the framework of SFB 1083.

Keywords: cluster chemistry • isomers • silver • organotin • selenium

[1] P. Pfeiffer, R. Lehnardt, *Ber. Dtsch. Chem. Ges.* **1903**, *36*, 3027–3030.

[2] C. Dorfelt, A. Janeck, D. Kobelt, E. F. Paulus, H. Scherer, *J. Organomet. Chem.* **1968**, *14*, P22–P24.

[3] H. Berwe, A. Haas, *Chem. Ber.* **1987**, *120*, 1175–1182.

[4] D. Kobelt, E. F. Paulus, H. Scherer, *Acta Cryst. B* **1972**, *28*, 2323–2326.

[5] C. Wagner, C. Raschke, K. Merzweiler, *Appl. Organomet. Chem.* **2004**, *18*, 147–147.

[6] Z. Hassanzadeh Fard, M. R. Halvagar, S. Dehnen, *J. Am. Chem. Soc.* **2010**, *132*, 2848–2849.

[7] Z. Hassanzadeh Fard, L. Xiong, C. Müller, M. Hołyńska, S. Dehnen, *Chem. Eur. J.* **2009**, *15*, 6595–6604.

[8] B. E. K. Barth, B. A. Tkachenko, J. P. Eußner, P. R. Schreiner, S. Dehnen, *Organometallics* **2014**, *33*, 1678–1688.

[9] B. E. K. Barth, E. Leusmann, K. Harms, S. Dehnen, *Chem. Comm.* **2013**, *49*, 6590–6592.

[10] J. P. Eußner, B. E. K. Barth, E. Leusmann, Z. You, N. Rinn, S. Dehnen, *Chem. Eur. J.* **2013**, *19*, 13792–13802.

[11] Z. Hassanzadeh Fard, M. Hołyńska, S. Dehnen, *Inorg. Chem.* **2010**, *49*, 5748–5752.

[12] K. Merzweiler, R. Hauser, *Z. Anorg. Allg. Chem.* **2002**, *628*, 905–906.

[13] M. R. Halvagar, Z. Hassanzadeh Fard, S. Dehnen, *Chem. Comm.* **2010**, *46*, 4716–4718.

[14] J. P. Eußner, S. Dehnen, *Chem. Comm.* **2014**, *50*, 11385–11388.

[15] J. P. Eußner, B. E. K. Barth, U. Justus, N. W. Rosemann, S. Chatterjee, S. Dehnen, *Inorg. Chem.* **2015**, *54*, 22–24.

[16] M. R. Halvagar, Z. Hassanzadeh Fard, L. Xiong, S. Dehnen, *Inorg. Chem.* **2009**, *48*, 7373–7377.

[17] N. Rinn, J. P. Eußner, W. Kaschuba, X. Xie, S. Dehnen, *Chem. Eur. J.* **2016**, *22*, 3094–3104.

[18] F. Weigend, R. Ahlrichs, *Phys. Chem. Phys Chem.* **2005**, *7*, 3297.

[19] F. Weigend, *Phys. Chem. Chem. Phys.* **2006**, *8*, 1057–1065.

[20] D. Andrae, U. Häußermann, M. Dolg, H. Stoll, H. Preub, *Theor Chim Acta* **1990**, *77*, 123–141.

[21] B. Metz, H. Stoll, M. Dolg, *J. Chem. Phys.* **2000**, *113*, 2563–2569.

[22] S. Grimme, *J. Comput. Chem.* **2006**, *27*, 1787–1799.

[23] TURBOMOLE V7.0.1 2015, a Development of University of Karlsruhe and Forschungszentrum Karlsruhe GmbH, 1989-2007, TURBOMOLE GmbH, since 2007, Available from Http://www.turbomole.com.

[24] C. Ehrhardt, R. Ahlrichs, *Theor. Chim. Acta* **1985**, *245*, 231–245.

[25] F. S. Boys, *Quantum Theory of Atoms, Molecules and the Solid State*, Academic Press, New York, **1966**.

[26] H. Schmidbaur, A. Schier, *Angew. Chem. Int. Ed.* **2015**, *54*, 746–784.

[27] J.-X. Chen, Q.-F. Xu, Y. Zhang, Z.-N. Chen, Jian-Ping Lang, *J. Organomet. Chem.* **2004**, *689*, 1071–1077.

[28] X. Jin, K. Tang, W. Liu, H. Zeng, H. Zhao, Y. Ouyang, Y. Tang, *Polyhedron* **1996**, *15*, 1207–1211.

[29] C. Xu, J. Zhang, Q. Chen, T. Duan, W. Leung, Q. Zhang, *Inorg. Chem. Commun.* **2012**, *21*, 1–3.

[30] R. Langer, B. Breitung, L. Wünsche, D. Fenske, O. Fuhr, *Z. anorg. allg. Chem.* **2011**, *637*, 995–1006.

[31] J. F. Corrigan, D. Fenske, W. P. Power, *Angew. Chem. Int. Ed.* **1997**, *36*, 1176–1179.

[32] D. G. Macdonald, A. Eichhöfer, C. F. Campana, J. F. Corrigan, *Chem. Eur. J.* **2011**, *17*, 5890–5902.

[33] C. Xu, X. Yi, T. Duan, Q. Chen, Q. Zhang, *Polyhedron* **2011**, *30*, 2637–2643.

[34] H. P. Nayek, W. Massa, S. Dehnen, *Inorg. Chem.* **2010**, *49*, 144–149.

[35] D. Fenske, N. Zhu, T. Langtepe, *Angew. Chem. Int. Ed.* **1998**, *37*, 2639–2644.

[36] D. Fenske, T. Langtepe, *Angew. Chem. Int. Ed.* **2002**, *41*, 300–304.

[37] C. E. Anson, A. Eichöfer, I. Issac, D. Fenske, O. Fuhr, P. Sevillano, C. Persau, D. Stalke, J. Zhang, *Angew. Chem. Int. Ed.* **2008**, *47*, 1326–1331.

[38] O. Fuhr, S. Dehnen, D. Fenske, *Chem. Soc. Rev.* **2013**, *42*, 1871–1906.

[39] X. Yang, I. Isaac, C. Persau, R. Ahlrichs, O. Fuhr, D. Fenske, *Inorganica Chim. Acta* **2014**, *421*, 233–245.

[40] S. Bestgen, X. Yang, I. Issac, O. Fuhr, P. W. Roesky, *Chem. Eur. J.* **2016**, 9933–9937.

[41] S. Bestgen, O. Fuhr, B. Breitung, V. S. K. Chakravadhanula, G. Guthausen, F. Hennrich, W. Yu, M. M. Kappes, P. W. Roesky, D. Fenske, *Chem. Sci.* **2017**, *8*, 2235–2240.

Entry for the Table of Contents

COMMUNICATION

Two organotin silverselenide clusters with isomeric ternary cluster cores are obtained depending on whether the organic groups are keto-functionalized or further transferred into hydrazine units. We report on the formation of these two clusters and a third, mixed valence species from the same intermediate under different reaction conditions. The intermediate and the products were studied by a variety of experimental and quantum chemical methods.

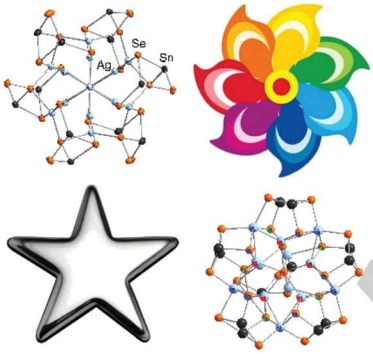

*N. Rinn, L. Guggolz, K. Gries, K. Volz, J. Senker, S. Dehnen**

Page No. – Page No.

Formation and Structural Diversity of Organo-Functionalized Tin-Silver Selenide Clusters

1. Synthesis Details

1.1 Synthesis of i

Compound **A** (202 mg, 0.20 mmol) was dissolved in 5 mL of CH_2Cl_2 and cooled down to −78 °C. This solution was added to a suspension of $[Ag(PPh_3)_3Cl]$ (359 mg, 0.40 mmol) in 5 mL of CH_2Cl_2 at −78 °C. $(TMS)_2Se$ (181 mg, 0.80 mmol) was added and the mixture was stirred under exclusion of daylight at room temperature for 4 hours. Compound **i** (225 mg) was isolated by filtration

1.2 Synthesis of $[(\mu_6\text{-}SeAg_6)(Ag_8\mu_3\text{-}Se_{12})\{(R^1Sn)_2Se_2\}_6]$ (1)

Compound **i** was dissolved in CH_2Cl_2 and exposed to ambient light for 30 minutes. The resulting orange-red solution was layered with n-hexane and stored under exclusion of daylight, allowing red crystalline blocks of **1** to grow in approximately 10% yield after one week.

1.3 Synthesis of $[\{(R^1Sn^{IV})_2Se_2\}_2(AgPPh_3)_2(Sn^{II}Cl)_2(\mu_3\text{-}Se)_2]$ (2)

Compound **i** was dissolved in CH_2Cl_2 and layered with n-hexane under exclusion of daylight. After one week, colorless blocks of **2** form alongside of colorless blocks of **B** in yields of approximately 20% for both species.

1.4 Synthesis of $[\mu_7\text{-}SeAg_7Se_{12}\{(R^2Sn)_2Se_2\}_6]$ (3)

Compound **i** was dissolved in CH_2Cl_2, two droplets of $N_2H_4{\cdot}H_2O$ were added, and the mixture was exposed to daylight for 30 minutes. The solution turned orange, whereupon it was layered with *n*-hexane and stored in the dark. Red crystalline blocks of **1** appeared after one week in approximately 10% yield.

2. Energy dispersive X-ray spectroscopy (EDX)

EDX experiments were carried out in a scanning electron microscope (SEM) to elucidate the elemental composition of **i**. For this purpose **i** was ground in a mortar under Ar atmosphere and suspended in n-hexane. A carbon coated copper grid was immersed in the suspension and attached on an aluminum SEM sample holder using carbon conductive tape. EDX spectra were recorded using a Bruker XFlash 5010 energy-dispersive X-ray detector attached to a JEOL JIB-4601F SEM (implemented in a SEM/focused ion beam dual beam system) operating at 15kV. A background corrected spectrum is shown in Figure S1. The different colors highlight the deconvoluted signals of the different elements present in the sample. The results of the quantification of the elements located in **i** are given in Table S1.

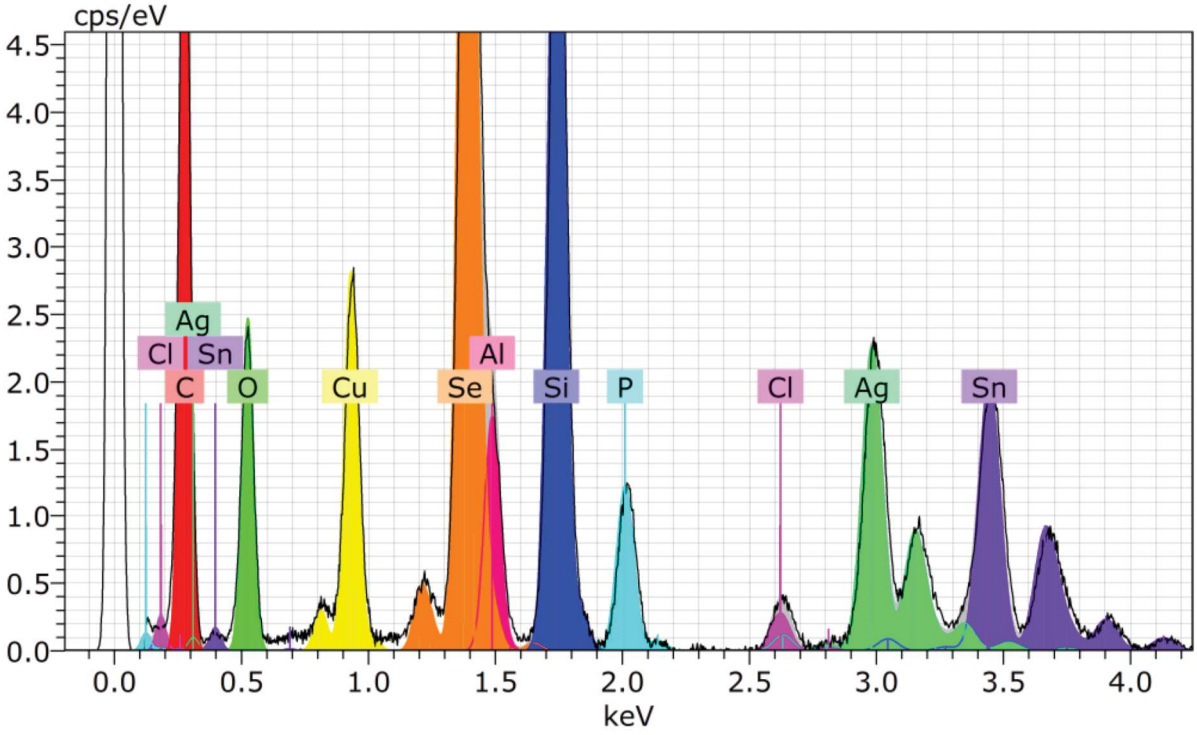

Figure S1. EDX spectrum of **i**. The copper and aluminum signals derive from the sample holder. The small chlorine impurity is most likely caused by residues of the used solvent (DCM). The silicon signal originates from silicon vacuum grease that was partially dissolved in the solvent.

Table S1. Quantified and normalized results of the EDX measurement of i.

	Detected counts	Series used for Quantification	Ratio [wt. %]	Error 1 σ [wt. %]	Ratio [at. %]	Ratio [normalized]
P	32934	K-series	3.99	0.13	11	1
Cl	8538	K-series	1.11	0.05	3	0.3
Se	256244	L-series	40.36	1.35	44	4
Ag	111485	L-series	24.20	0.53	19	2
Sn	114521	L-series	30.33	0.64	22	2

3. Powder X-Ray Diffraction (PXRD)

The powder X-ray diffraction pattern of **i** (Figure S2) was measured on a Stoe StadiMP diffractometer system equipped with a Mythen 1K silicon strip detector and a Cu-Kα (λ = 1.54056 Å) radiation source. The microcrystalline powder was filled into a 0.6 mm mark tube which was then sealed air-tight with soft wax. The tube was then mounted onto the goniometer head using wax (horizontal setup) and rotated throughout the measurement.

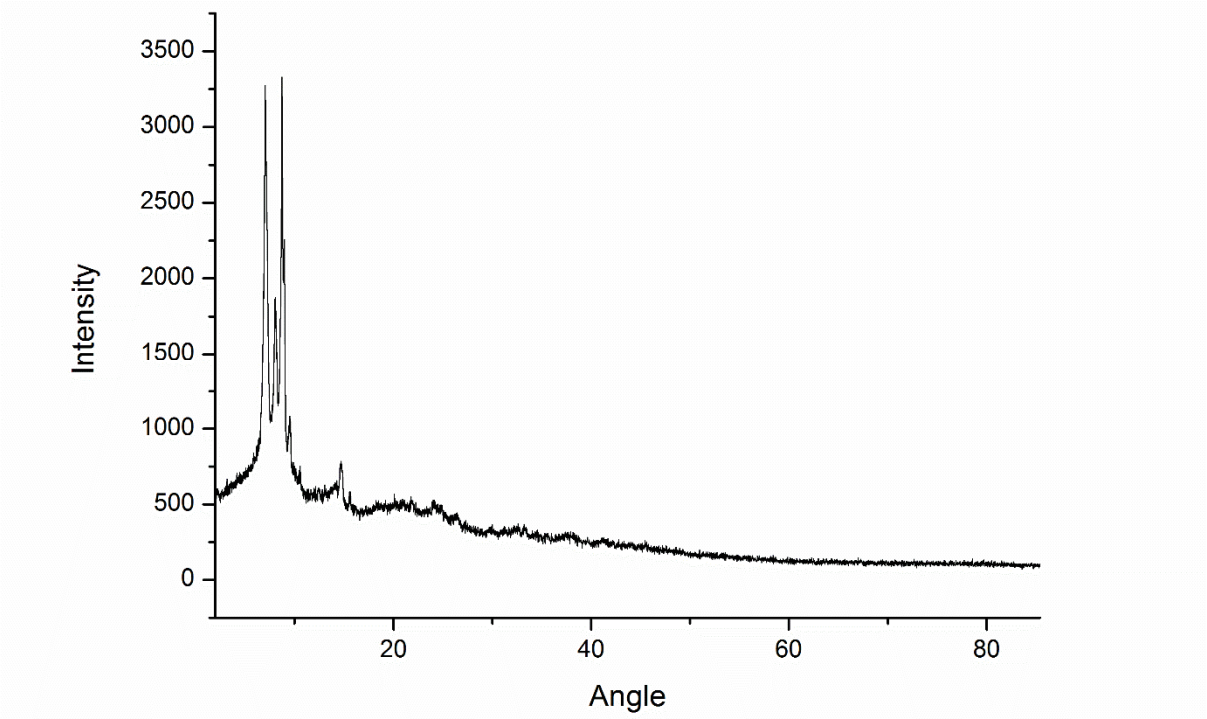

Figure S2. PXRD diagram of **i**.

4. NMR spectroscopy

4.1 Temperature-Dependent ^{1}H NMR Spectroscopy

^{1}H NMR measurements of **i** were carried out by using a Bruker DRX 300 MHz spectrometer. The solvent used was CD_2Cl_2 in all cases. Figure S3 shows the results.

The first spectrum (from bottom to top) was recorded at room temperature using a sample prepared with **B** under exclusion of daylight.

The next three spectra were recorded at different temperatures from a batch produced from precursor **A** under exclusion of daylight. **I** was dissolved at 273 K, and the spectra were subsequently recorded with rising temperature. THF and water impurities are visible. Three main signals at 1.27 ppm, 2.21 ppm and 2.71 ppm can be attributed to the organic ligand R^1 in **B**, which indicates a formation of **B** after dissolving **i**. This is consistent with the isolation of crystals of **B** alongside crystals of **1**.

The fourth spectrum shows a spectrum of **i** produced from precursor **A** at room temperature after exposure to daylight for 4 hours. The fifths and topmost spectrum shows the same sample after exposure to daylight for 24 hours. This lead to the rise of signals at 1.87 ppm, 2.10 ppm and 2.12 ppm, most likely intermediates towards decomposition to binary selenides and elements like **1**.

In conclusion, neither variation of the reactants (**A** versus **B**) nor variation of the temperature lead to a disparity in the spectra. Light irradiation leads to the occurrence of new signals, but eventually to decomposition of the sample: if stored for 48 hours under daylight, one observes the precipitation of selenides and metal elements.

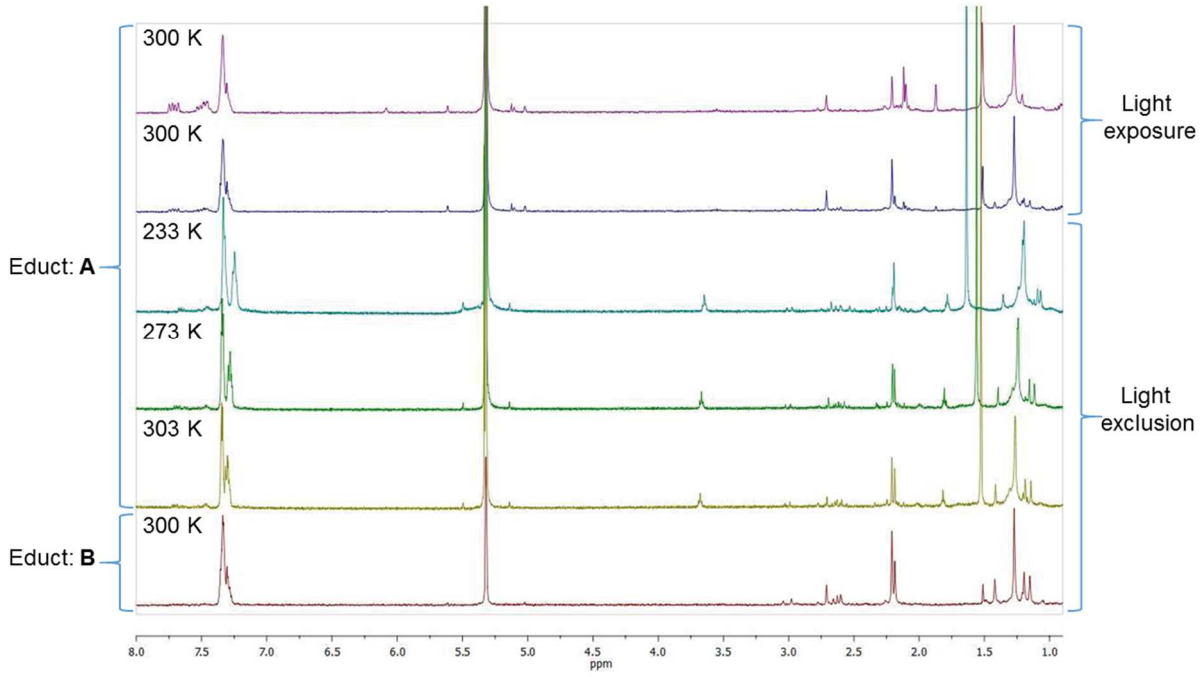

Figure S3. ^{1}H NMR spectra of **i** in CD_2Cl_2.

Crystals of **2** were dissolved and ^{1}H NMR experiments were carried out. The resulting spectrum is shown in Figure S4. However, the obtained signals do not seems to correspond to a single set corresponding to the R^{1} ligand, typically found around 1.3 ppm, 2.2 ppm and 2.7 ppm with integral ratios of 6 to 3 to 2, thus pointing to an equilibrium of various species in solution.

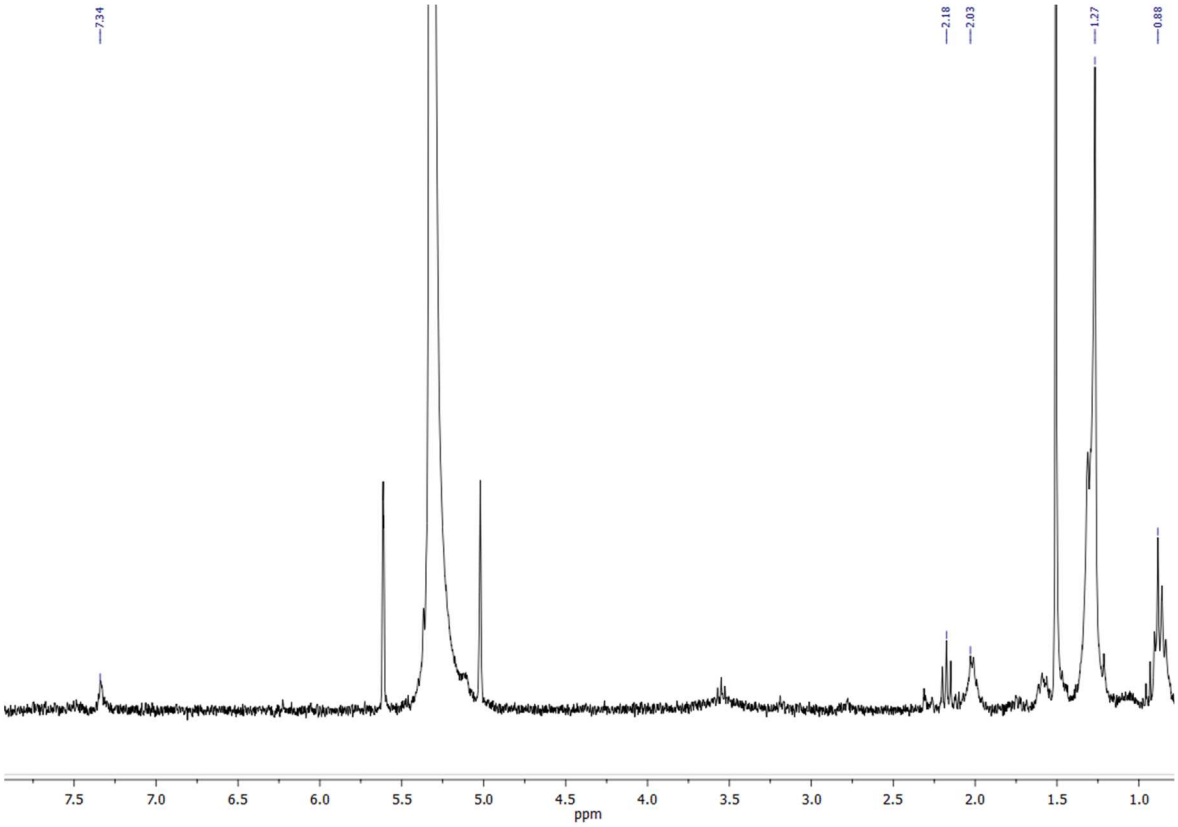

Figure S4. ^{1}H NMR spectra of **2** in CD_2Cl_2.

Crystals of **3** were dissolved in CD_2Cl_2 to record NMR spectra. The solution turned from golden yellow to orange red within 20 seconds. The resulting ^1H NMR spectrum is shown in Figure S5. The individual signals could not be identified, but three ranges (ca. 1.0 to 1.4 ppm, 1.7 to 2.1 ppm, and 2.2 to 2.7 ppm) show signals that can be attributed to the organic ligand, which is typically used in our chemistry. Additional, newly arising signals at 5.60 and 5.68 ppm hint towards the presence of hydrazone groups and thus a successful condensation reaction between the ketone in R^1 and hydrazine hydrate.

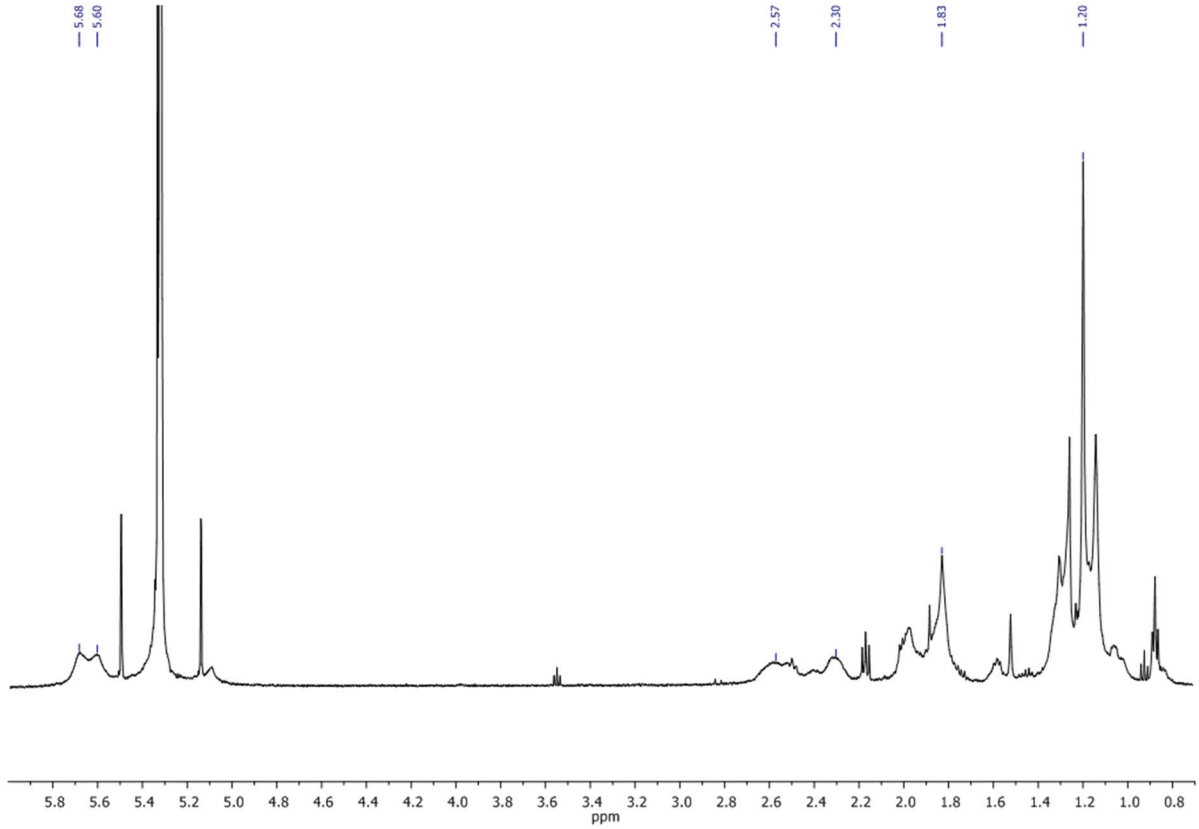

Figure S5. ^1H NMR spectrum of a solution of **3** in CD_2Cl_2.

4.2 MAS NMR spectroscopy

All solid-state NMR spectra were acquired on a Bruker Avance-II spectrometer operating at a B_0 field of 7.4 T. ^{77}Se ($_0$ = 57.24 MHz) and ^{119}Sn ($_0$ = 111.89 MHz) high-resolution spectra were acquired with a ramped cross-polarization (CP)[1] experiment where the nutation frequency $_{nut}$ on the proton channel was varied linearly by 30%. The samples were spun at 10 and 12.5 kHz in a 4 mm MAS triple resonance probe (Bruker), respectively. The sample was packed in a glove box and handled strictly inert gas atmosphere. The corresponding $_{nut}$ on the X channel and the contact time were adjusted to 70 kHz and 3.0 ms. Proton broadband decoupling with spinal-64[2] was applied during acquisition with a nutation frequency of 50 kHz. The ^{77}Se and ^{119}Sn spectra are referenced with respect to Me_2Se and $SnMe_4$ using secondary standards.

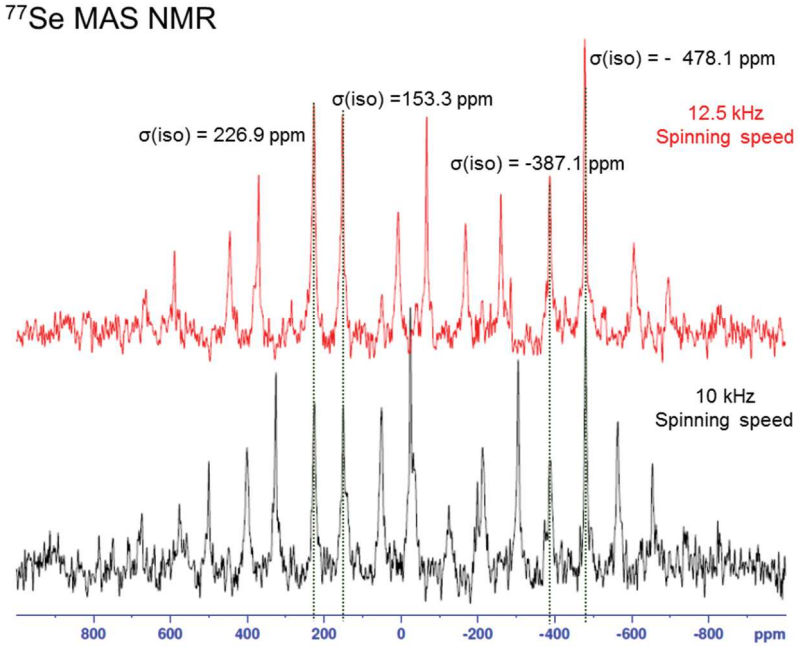

Figure S6. ^{77}Se MAS NMR spectrum of **i** at spinning speeds of 10 kHz and 12.5 kHz. Three chemically different Se sites are detected.

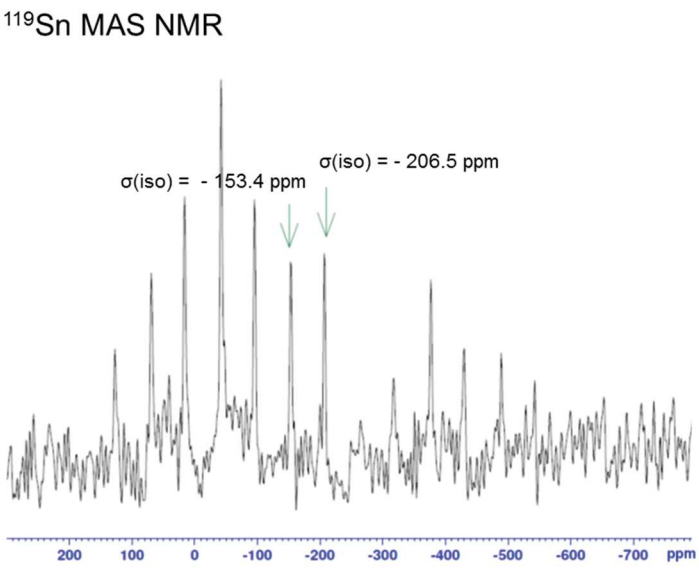

Figure S7. ^{119}Sn MAS NMR spectrum of **i**. Two chemically different Se sites could be detected.

5 Details of the X-ray diffraction measurements and refinements

5.1 Methods

All single-crystal X-ray diffraction studies were performed on Stoe IPDS2/2T diffractometers at 100 K, using a Mo-K_α X-ray source (λ = 0.71073 Å). The structures were solved by direct methods in SHELXS97 and refined by full-matrix-least-squares refinement against F^2 in and SHELX2013.[1] Methyl and methylene hydrogen atoms were added assuming ideal geometry on their carbon parent atom, with U_{eq} = nU_{eq} (parent atom), n = 1.2 for methylene and 1.5 for methyl groups. All structures are shown with thermal ellipsoids drawn at 50% probability. Hydrogen atoms are omitted for clarity in the structure figures. More detailed crystallographic data are available in Table S2 and from the CIF.

Table S2. Crystallographic data and refinement results of **1** and **2**.

	1·5.25 DCM	**2**·2 DCM
Empirical formula	$C_{77.3}H_{139.5}O_{12}Cl_{10.5}Se_{25}Sn_{12}Ag_{14}$	$C_{62}H_{78}Cl_6P_2Se_8Sn_6Ag_2$
Fw / g·mol^{-1}	6297.32	2721.44
Crystal color and shape	red block	colorless block
Crystal size / mm^3	0.108×0.105×0.078	0.454×0.195×0.167
Crystal system	Monoclinic	triclinic
Space group	$P2_1/n$	$P\bar{1}$
a / Å	17.7232(6)	12.9934(4)
b / Å	19.5772(4)	14.0644(5)
c / Å	22.4737(8)	14.1006(5)
α / °	90	90.145(3)
β / °	92.021(3)	112.437(3)
γ / °	90	116.178(3)
V / Å^3	7792.9(4)	2091.6(2)
Z	2	1
ρ_{calcd} / g·cm^{-3}	2.76	2.161
μ(Mo K_α) / mm^{-1}	9.655	5.969
Absorption correction type	Numerical	Numerical
Min. / max. transmission	0.3486 / 0.5469	0.1936 / 0.4646
2 θ range / deg	2.76 / 53.69	3.298 / 58.506
No. of measured reflns	93528	43266
R(int)	0.2081	0.1231
Indep. Reflns	16539	11250
Indep. Reflns ($I > 2\sigma(I)$)	8342	9881
No. of parameters	704	412
R_1 ($I > 2\sigma(I)$) / wR_2 (all data)	0.0605 / 0.1175	0.0282 / 0.0663
S (all data)	0.841	0.997
Max. peak / hole / e$^-$·Å^3	2.63 / –1.16	1.04/ –1.50
CCDC number	CCDC 1562670	CCDC 1562671

5.2 Crystal structure of 1

The highest peak of residual electron density on the difference Fourier map (2.63 $e^{-}\cdot Å^{-3}$) is found 1.063 Å apart from Sn1 on the bond between Sn1 and Se11. The atomic positions of three molecules of CH_2Cl_2 were found in the asymmetric unit, one being only partially occupied with a freely refined site occupancy of 0.63. A cutout of the crystal structure of **1** is shown in Figure S8. Some structural parameters are given in Table S3.

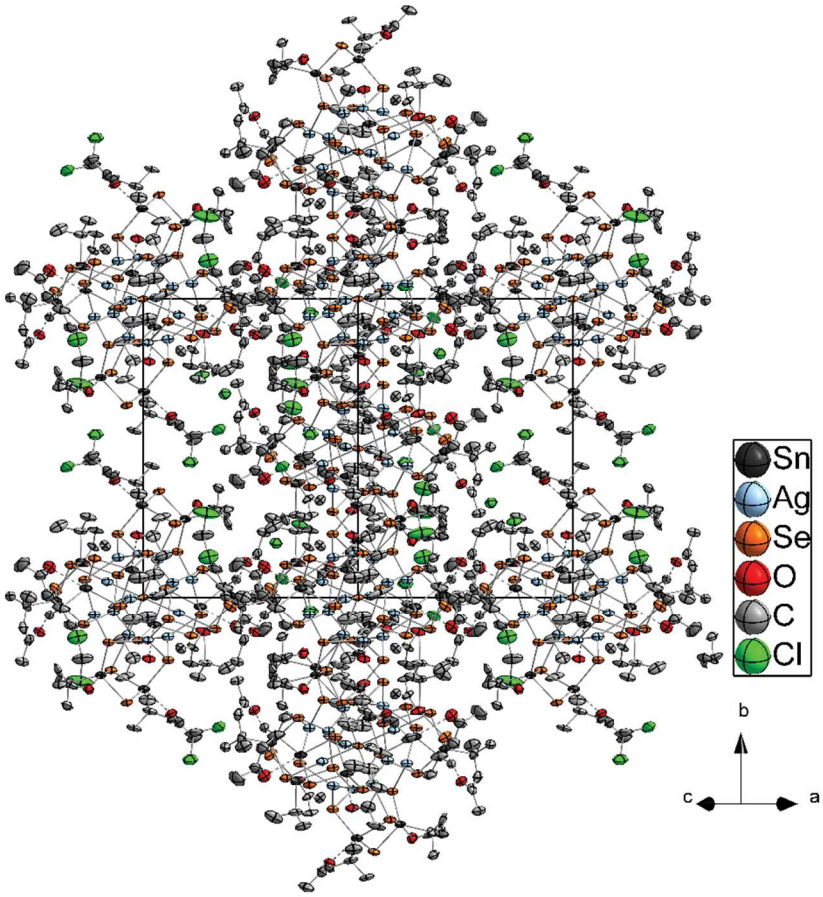

Figure S8. Cutout of the crystal structure of **1** viewed along the [101] axis. **1** crystallizes in the monoclinic space group $P2_1/n$.

In a simplified manner, the structure can be viewed as a body centered cubic packing of **1**. Intramolecular hydrogen bonds can be formulated between the O1 and C36 sites with a donor–acceptor distance of 3.20(2) Å and a C–H···O angle of 122.77°.

Table S3. Selected structural parameters of **1.** a = –x + 2, –y + 1, –z + 2

Parameter	Value [Å / °]	Parameter	Value [Å / °]	Parameter	Value [Å / °]
Se1–Ag1	2.640(1)	Sn2–Se2	2.512(2)	Ag2···Ag4	3.236(2)
Se1–Ag2	2.692(1)	Sn2–Se8	2.598(2)	Ag2···Ag5	2.974(2)
Se1–Ag3	2.705(1)	Sn2–Se11	2.547(2)	Ag2···Ag6[a]	3.019(2)
Se8–Ag1	2.633(2)	Sn2–C7	2.20(2)	Ag2···Ag7[a]	2.954(2)
Se9[a]–Ag2	2.677(2)	Sn2···O2	2.76(1)	Ag3···Ag4[a]	2.949(2)
Se10–Ag3	2.678(2)	Sn3–Se3	2.508(2)	Ag3···Ag5	3.034(2)
Ag4–Se2	2.643(2)	Sn3–Se10	2.601(2)	Ag3···Ag6	2.914(1)
Ag4–Se5	2.623(2)	Sn3–Se13	2.541(2)	Ag3···Ag7[a]	3.003(2)
Ag4–Se7[a]	2.649(2)	Sn3–C13	2.16(2)	Ag1–Se1–Ag2	91.11(4)
Ag5–Se2	2.633(2)	Sn3···O3	2.71(1)	Ag1–Se1–Ag2[a]	88.89(4)
Ag5–Se3	2.632(2)	Sn4–Se7	2.520(2)	Ag1–Se1–Ag3	92.47(3)
Ag5–Se6	2.612(2)	Sn4–Se10	2.624(2)	Ag1–Se1–Ag3[a]	87.53(3)
Ag6–Se3	2.647(2)	Sn4–Se13	2.555(2)	Se1–Ag1–Se8	170.61(6)
Ag6–Se4	2.634(2)	Sn4–C19	2.22(2)	Se1–Ag2–Se9[a]	171.50(6)
Ag6–Se7	2.619(2)	Sn4···O4	2.56(1)	Se1–Ag3–Se10	175.28(7)
Ag7–Se4	2.625(2)	Sn5–Se6	2.522(2)	Se5–Ag4–Se2	128.65(6)
Ag7–Se5	2.628(2)	Sn5–Se9	2.647(2)	Se5–Ag4–Se7[a]	119.76(7)
Ag7–Se6[a]	2.636(2)	Sn5–Se12	2.518(2)	Se7[a]–Ag4–Se2	111.29(6)
Se2–Sn2	2.512(2)	Sn5–C25	2.19(2)	Se2–Ag5–Se3	116.86(6)
Se3–Sn3	2.508(2)	Sn5···O5	2.62(1)	Se2–Ag5–Se6	122.75(6)
Se4–Sn6	2.525(2)	Sn6–Se4	2.525(2)	Se3–Ag5–Se6	119.32(6)
Se5–Sn1	2.518(2)	Sn6–Se9	2.610(2)	Se3–Ag6–Se4	112.22(6)
Se6–Sn5	2.522(2)	Sn6–Se12	2.521(2)	Se3–Ag6–Se7	128.70(6)
Se7–Sn4	2.520(2)	Sn6–C31	2.21(1)	Se4–Ag6–Se7	118.44(7)
Sn1–Se5	2.518(2)	Sn6···O6	2.68(1)	Se4–Ag7–Se5	120.29(7)
Sn1–Se8	2.627(2)	Ag1···Ag4	2.894(2)	Se4–Ag7–Se6[a]	126.19(7)
Sn1–Se11	2.564(2)	Ag1···Ag5	3.009(2)	Se5–Ag7–Se6[a]	113.31(6)
Sn1–C1	2.23(2)	Ag1···Ag6	3.031(2)		
Sn1···O1	2.56(1)	Ag1···Ag7	3.000(2)		

5.3 Crystal structure of 2

The highest peak of residual electron density on the difference Fourier map (1.04 e^{-}·Å^{-3}) is found 98.9 pm apart from Sn2 on the bond between Sn2 and Se3. Two molecules of CH_2Cl_2 were found in the asymmetric unit. A cutout of the crystal structure of **2** is shown in Figure S9. Some structural parameters are given in Table S4.

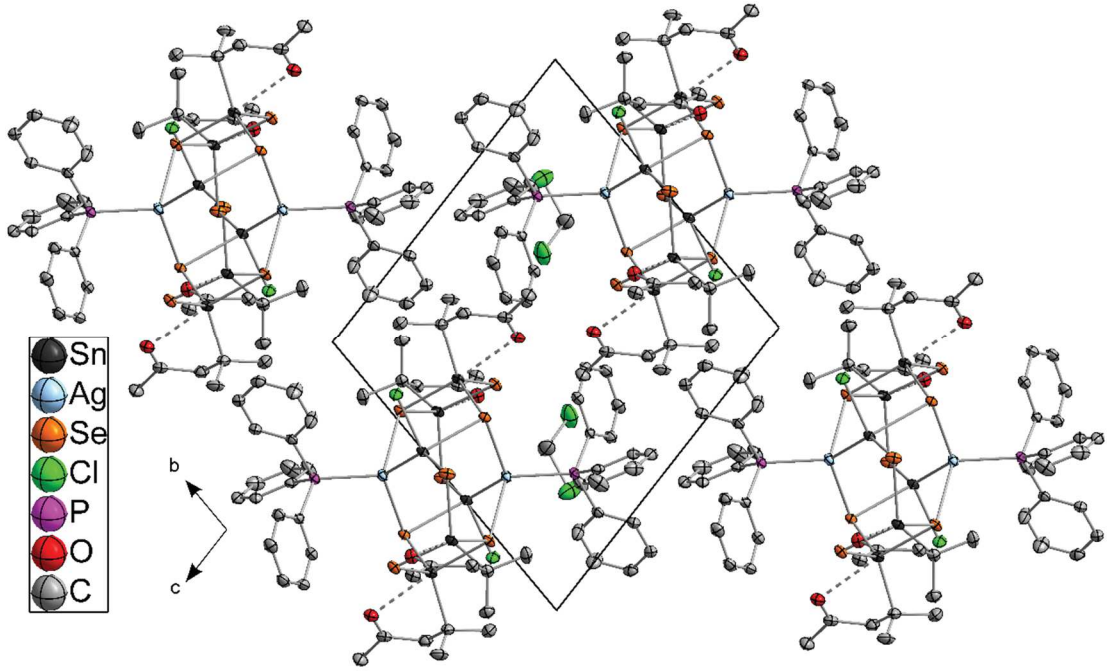

Figure S9. Cutout of the crystal structure of **2** viewed along the crystallographic *a* axis. **2** crystallizes in the triclinic space group $P\bar{1}$.

Table S4. Selected structural parameters of **2**. A = –x + 2, –y + 1, –z + 2.

Parameter	Value [Å / °]	Parameter	Value [Å / °]	Parameter	Value [Å / °]
Sn1–Ag1	2.7246(5)	Ag1–Se2[a]	2.7507(4)	Se2–Sn3–O2	172.35(5)
Sn1–Cl1	2.4729(7)	Ag1–Se4	2.6590(4)	Sn1–Se1–Sn2	93.22(1)
Sn1–Se1	2.5941(5)	Ag1–P1	2.4687(6)	Sn2–Se2–Sn3	84.13(1)
Sn1–Se4[a]	2.6441(4)	Ag1–Sn1–Se1	141.80(1)	Sn2–Se2–Ag1	122.27(1)
Sn2–Se1	2.5098(4)	Ag1–Sn1–Se4[a]	113.95(1)	Sn3–Se2–Ag1	112.25(1)
Sn2–Se2	*2.6381(4)*	Ag1–Sn1–Cl1	110.90(2)	Sn2–Se3–Sn3	87.43(1)
Sn2–Se3	2.5379(5)	Se4[a]–Sn1–Se1	94.30(1)	Sn1–Se4–Sn3	96.57(1)
Sn2···O1	2.470(2)	Se3–Sn2–Se1	115.96(1)	Sn1–Se4–Ag1	89.92(1)
Sn2–C1	2.182(4)	Se3–Sn2–C1	124.14(8)	Sn3–Se4–Ag1	99.27(1)
Sn3–Se2	2.5823(4)	C1–Sn2–Se1	109.89(8)	Sn1–Ag1–Se2[a]	90.28(1)
Sn3–Se3	2.5235(4)	Se2–Sn2–O1	165.35(6)	Sn1–Ag1–Se4	120.02(1)
Sn3–Se4	2.5345(5)	Se3–Sn3–Se4	112.73(1)	Se4–Ag1–Se2[a]	110.68(1)
Sn3···O2	2.775(2)	Se3–Sn3–C7	115.44(8)	Sn1–Ag1–P1	120.45(2)
Sn3–C7	2.193(3)	C7–Sn3–Se4	114.95(8)		

5.4 Preliminary crystal structure data of 3

The single-crystal X-ray diffraction of the crystals of **3** yielded data with subpar quality (R_{int} = 0.2017, R_1 = 0.2625, $2\theta_{max}$ = 26.508°). We decided to use the isotropically refined heavy atom inorganic core as the basis for a preliminary discussion of the topology **3**, which does not intend to be a discussion of its actual molecular structure. The arrangement of the discussed cluster fragments in the crystal structure is shown in Figure S10.

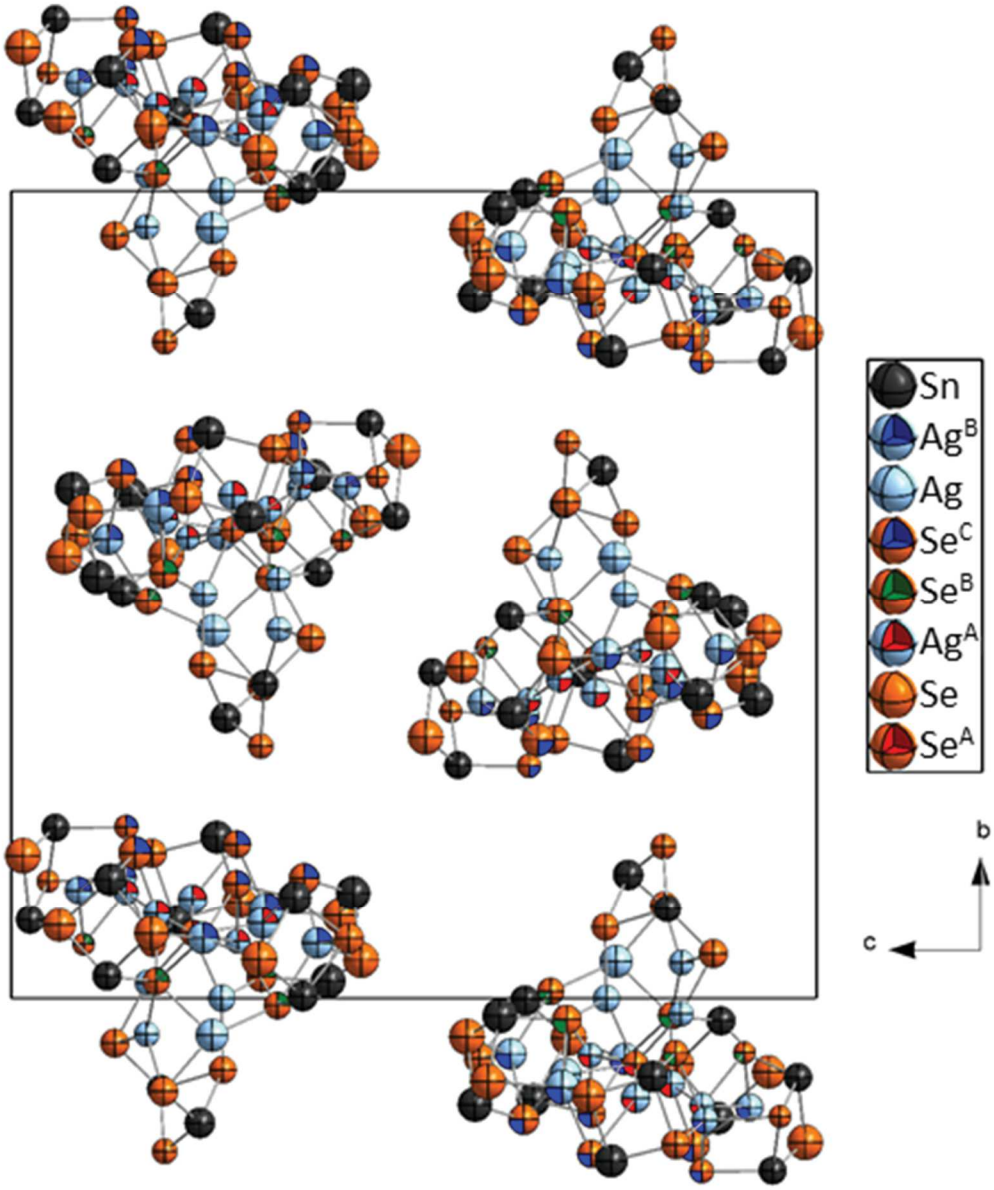

Figure S10. Cutout of the preliminary crystal structure of **3**.

6. Quantum Chemical Studies

6.1 Methods

The quantum chemical calculations were undertaken by employing the program system TURBOMOLE V7.0.1,[3] using the B97-D functional[4] (grid size m3) with dispersion correction DFT-D3[5] and BJ-damping,[6] def2-TZVP basis sets[7] with the corresponding auxiliary bases,[8] and effective core potential at the Ag and Sn atoms.[9,10] The organic groups (R^2) of compound **3** were added with the Z-matrix editor of the program MOLDEN.[11] The chemical shifts were calculated by means of the module MPSHIFT[12] as implemented in TURBOMOLE. The localization of the MOs was obtained *via* Boys' method.[13] In Tables S4 and S5, the calculated Ag···Ag distances and shared electron numbers are shown, respectively. The shared electron numbers (SEN) were calculated *via* a population analysis based on occupation numbers (PABOON).[14]

6.2 Computational study of compound 1

The cluster structure was first optimized based on the data of the single-crystal structure, *i. e.*, considering keto-functionalized R^1-type organic ligands at the Sn atoms. The resulting structures of **1**^{calc} and **1** differ only relatively slightly, as illustrated in Figures S11 and S12, and in Tables S5 and S6.

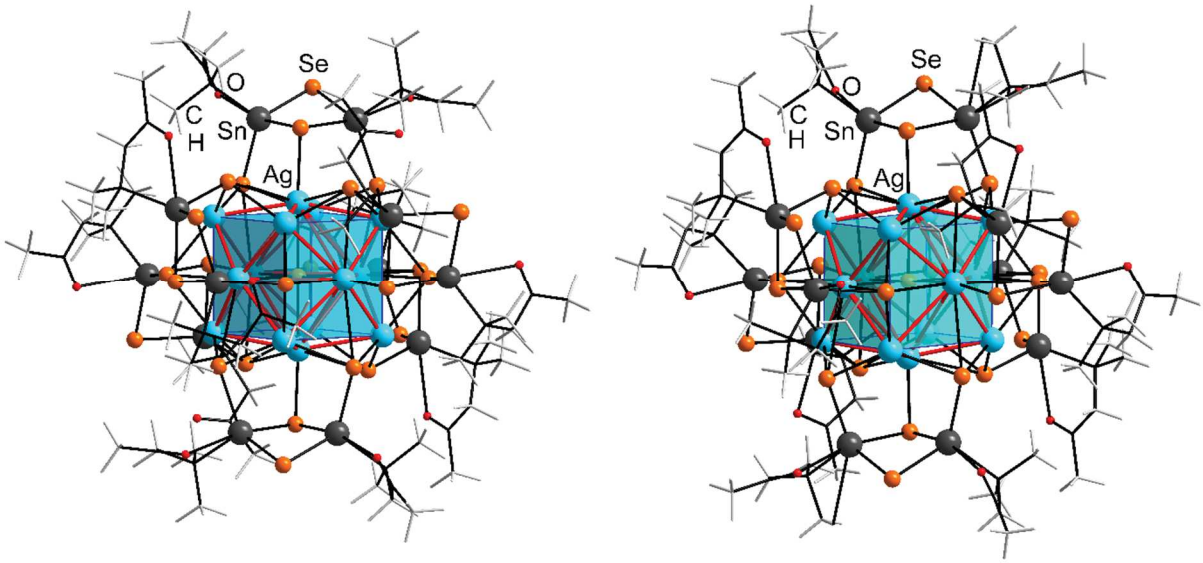

Figure S11. Comparison of the calculated structure of **1**^{calc} (left) with the experimentally found one in **1** (right). Comparison of the structural data are given in Tables S4 and S5.

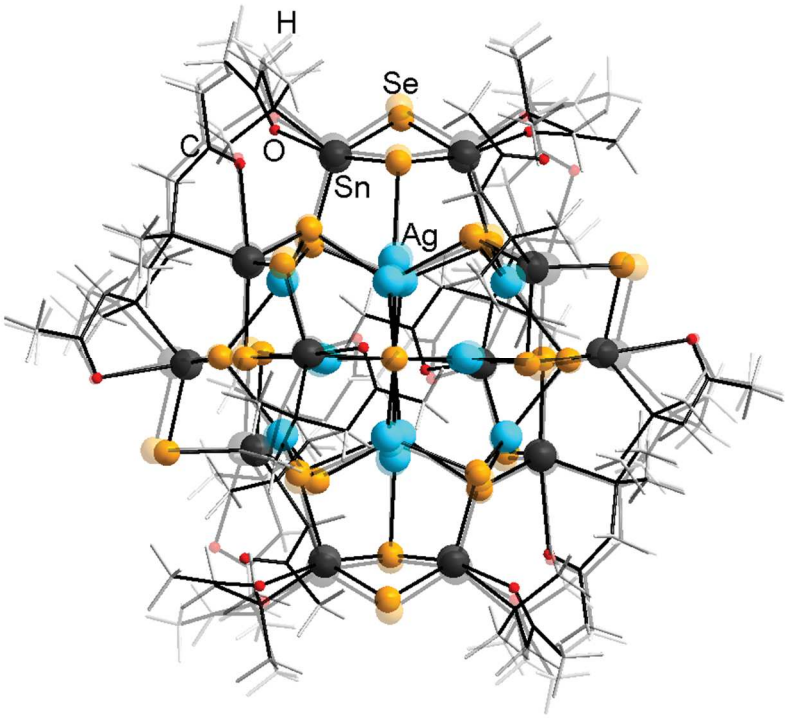

Figure S12. Overlay of the computed structure of **1**^{calc} (solid) with the experimentally found one in **1** (semi-transparent) to illustrate the slightly oriented organic groups upon geometry optimization using DFT methods.

Table S5. Calculated and experimentally observed $Ag^{A}\cdots Ag^{B}$ distances, and corresponding SENs of **1**^{calc} in C_i symmetry.

	Distance [Å] in 1^{calc} (calculated)	**Distance [Å] in 1 (experimental)**	**SEN in 1^{calc}**
Ag1···Ag4	3.002	2.894(2)	0.3664
Ag1···Ag5	3.065	3.009(2)	0.1028
Ag1···Ag6	3.075	3.031(2)	0.1161
Ag1···Ag7	3.102	3.000(2)	0.0819
Ag2···Ag4	3.145	3.236(2)	0.1176
Ag2···Ag5	3.069	2.974(2)	0.0907
Ag2···Ag6a	3.086	3.019(2)	–
Ag2···Ag7a	3.031	2.954(2)	0.4427
Ag3···Ag4a	3.012	2.949(2)	–
Ag3···Ag5	3.041	3.034(2)	–
Ag3···Ag6	2.996	2.914(1)	0.4391
Ag3···Ag7a	3.028	3.003(2)	0.1368

Table S4 further shows the calculated SENs obtained *via* a PABOON analysis. Although not all SENs correlate with the Ag···Ag distances in a strict way, it is reasonable to indicate argentophilic interactions. The largest SEN is observed for the shortest Ag···Ag distance. The other values range in the same order as the respective distances.

For a comprehensive comparison with the structural isomer in compound **3**, and to answer the question whether the ligands play any structure-directing role, the cluster core of **1** was also calculated in an R^2 ligand environment. The resulting structure of the cluster, denoted as $\mathbf{1}^{\mathbf{calc'}}$, is shown in Figure S13.

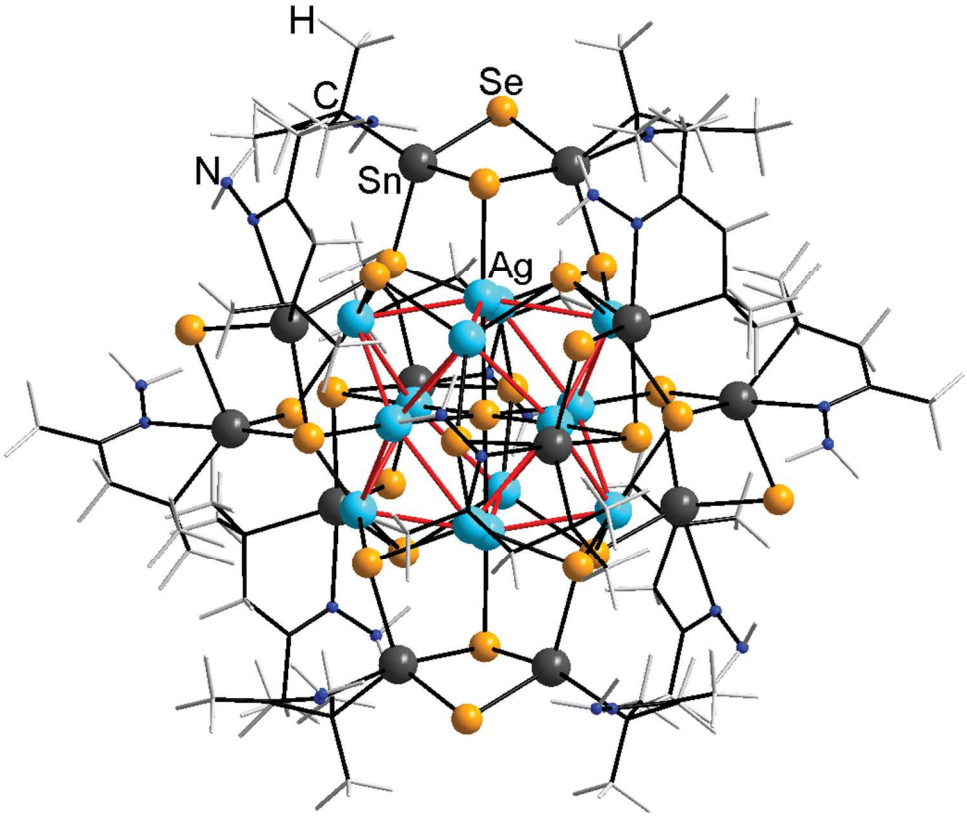

Figure S13. Structure of $\mathbf{1}^{\mathbf{calc'}}$ upon replacement of the C=O groups in the structure of $\mathbf{1}^{\mathbf{calc}}$ with C=N–NH_2 groups. Energetics are documented below.

The overall structure does not change significantly upon substitution of hydrazone for keto groups. As typically observed, the intramolecular Sn···N distances in the structure of $\mathbf{1}^{\mathbf{calc'}}$ are slightly shorter than the Sn···O distances in the calculated structure of $\mathbf{1}^{\mathbf{calc}}$. However, as these slight changes occur at twelve tin atoms altogether, the formation of this cluster with hydrazone groups is favored with respect to the one with R^1 ligands, according to the following reaction scheme [eq. (S1)]:

$$\mathbf{1}^{\mathbf{calc}} + 12\ H_2NNH_2 \rightarrow \mathbf{1}^{\mathbf{calc'}} + 12\ H_2O \qquad | \Delta E = -746\ \text{kJ/mol} \qquad \text{(S1)}$$

It should be noted that the reaction scheme also accounts for a change from a total of 24 N–H bonds in the reactant on the left hand side to 24 O–H bonds in the by-product on the right hand side (ΔE = –66 kJ/mol in favor of O per bond). Hence, the ΔE value is to be corrected about this difference, which leads to a corrected reaction energy ΔE = +838 kJ/mol.

6.3 Computational study of compound 3

As the positions of the organic R^2 ligands at the cluster core could not be determined by X-ray crystallography, the cluster was modelled with both R^1 and R^2 ligands, and compared. The resulting structures of **3**$^{calc'}$ and **3**^{calc} differ only relatively slightly, as illustrated in Figure S14 and in Table S5.

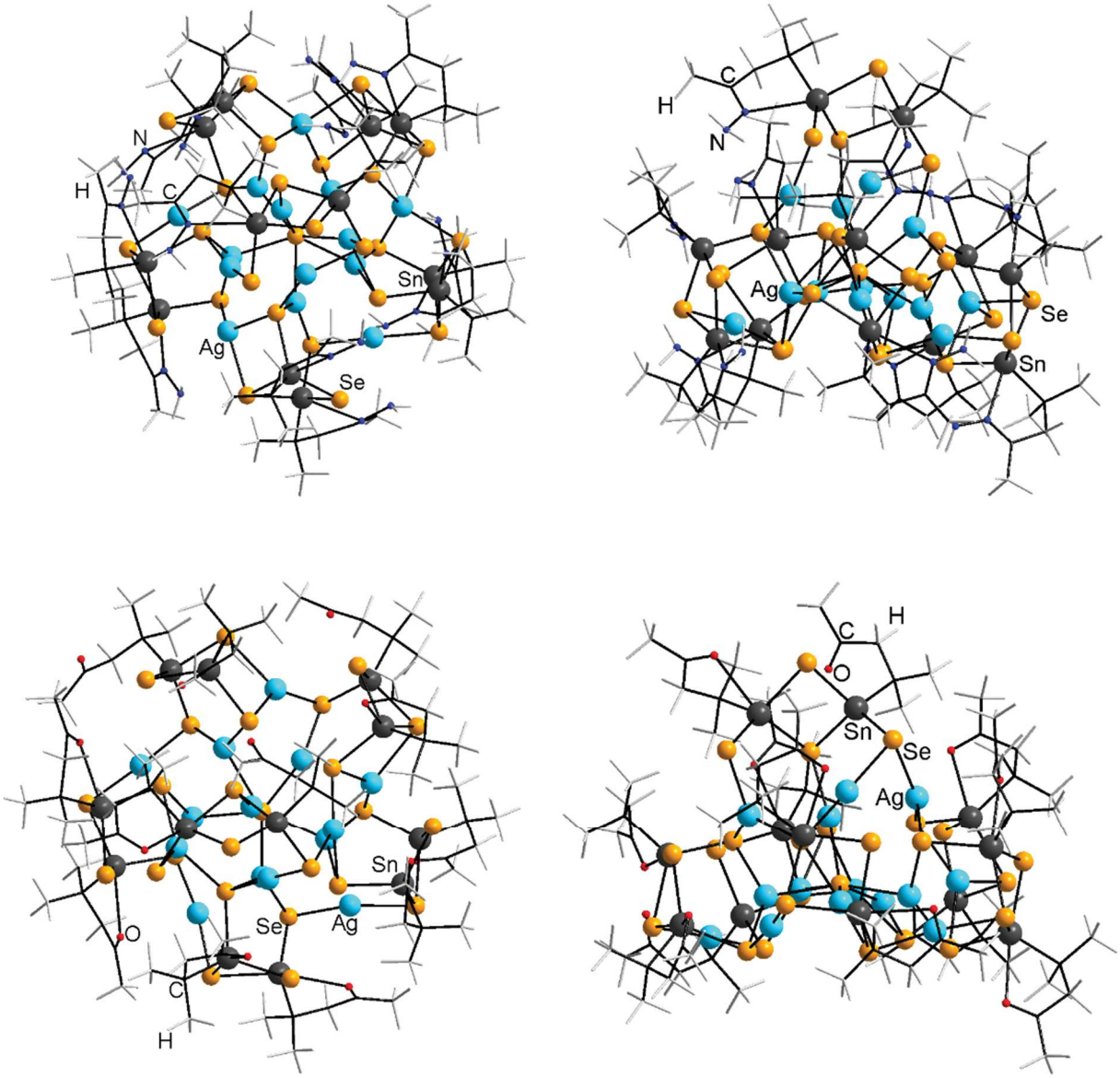

Figure S14. Top views (left) and side views (right) of the pentagonal star-shaped structure of **3**^{calc}, exhibiting R^2 ligands (top), and **3**$^{calc'}$, exhibiting R^1 ligands (bottom), after optimization of the geometric structures in C_1 symmetry. For clarity, Ag···Ag contacts are not drawn.

Table S6. Calculated Ag···Ag distances (< 3.6. Å) and corresponding SENs of **3**^{calc} and **3**$^{calc'}$. Ag1 - Ag4 are within the Ag_2Se_2 units. Ag5 - Ag9 are of the type Ag^A and Ag10 - Ag14 are of the type Ag^B. Comparison to experimental values are omitted due to the uncertainty of the latter.

	Distance [Å] in **3**^{calc}	SEN in **3**^{calc}	Distance [Å] in **3**$^{calc'}$	SEN in **3**$^{calc'}$
Ag1···Ag2	3.150	0.3674	3.030	0.4344
Ag1···Ag3	3.092	0.4574	---	---
Ag1···Ag4	3.009	0.2378	3.182	0.2600
Ag2···Ag3	3.259	0.1977	3.338	0.2065
Ag2···Ag4	2.992	0.1438	3.376	0.1439
Ag2···Ag5	---	---	3.598	0.2064
Ag3···Ag6	---	---	3.236	0.1702
Ag5···Ag6	---	---	2.986	0.1181
Ag5···Ag9	---	---	3.267	0.1201
Ag5···Ag10	3.521	0.1658	---	---
Ag5···Ag14	3.108	0.2118	3.024	0,2837
Ag6···Ag11	3.065	0.1223	---	---
Ag7···Ag8	2.915	0.1213	2.895	0.1622
Ag8···Ag9	---	---	3.267	0.1451
Ag8···Ag12	3.046	0.1409	---	---
Ag8···Ag13	---	---	2.905	0.2920
Ag9···Ag13	2.905	0.1630	2.932	0.3827
Ag9···Ag14	2.912	0.1864	2.975	0.2857

The obtained SENs again indicate significant Ag···Ag interactions. As already shown for compound **1**^{calc}, the largest SENs in **3**^{calc} and **3**$^{calc'}$ are observed for the shortest Ag···Ag distances. The other values range in the same order as the respective distances. It should be noted, that a correlation between atom distances and SENs is only given for each respective structure, *i. e.* a comparison between the SENs in **3**^{calc} with the SENs in **3**$^{calc'}$ is difficult.

Although there are some shifts in the Ag···Ag distances, the overall structure does not change significantly upon substitution of keto for hydrazone groups. As expected, the intramolecular Sn···N distances in the structure of **3**^{calc} are slightly shorter than the Sn···O distances in the calculated structure of **3**$^{calc'}$. However, this has no significant effect on the reaction enthalpy ΔE, according to the following reaction scheme [eq. (S2)]:

$$\mathbf{3}^{calc} + 12\ H_2O \rightarrow \mathbf{3}^{calc'} + 12\ H_2NNH_2 \qquad | \Delta E = -763\ kJ/mol \qquad (S2)$$

It should be noted that the reaction scheme also accounts for a change from a total of 24 O–H bonds in the reactant on the left hand side to 24 N–H bonds in the by-product on the right hand side (ΔE = –66 kJ/mol in favor of O per bond). Hence, the ΔE value is to be corrected about this difference, which leads to a corrected reaction energy ΔE = +821 kJ/mol and thus to **3**^{calc} being energetically favored compared to **3**$^{calc'}$.

6.4 Comparison of the isomeric structures in 1 and 3

For a statement on the relative energies of clusters with R^1 versus R^2 ligands in the two isomeric forms, we have additionally compared the total energies of the isomeric pairs $\mathbf{1}^{calc}/\mathbf{3}^{calc'}$ and $\mathbf{1}^{calc'}/\mathbf{3}^{calc}$. The clusters of the first pair are surrounded by R^1 ligands (according with the experimentally observed structure of **1**), while the second cluster pair exhibits R^2 ligands (according with the anticipated situation in the experimental cluster structure of **3**). A final summary of relative energies is given in Table S7.

Table S7. Comparison of the total energies (in kJ/mol) of isomeric clusters with R^1 ligands, $\mathbf{1}^{calc}$ versus $\mathbf{3}^{calc'}$, (top) and $\mathbf{1}^{calc'}$ versus $\mathbf{3}^{calc}$ (bottom), with R^1 or R^2 ligands, respectively. Cluster types with different ligands are not compared here; according reaction energies are provided above (equations (S1) and (S2), respectively).

	Isomer type 1	**Isomer type 3**
R^1 ligands	0 ($\mathbf{1}^{calc}$)	+134 ($\mathbf{3}^{calc'}$)
R^2 ligands	0 ($\mathbf{1}^{calc'}$)	+117 ($\mathbf{3}^{calc}$)

The values given in Table S7 indicate that the more symmetric isomer is preferred for both ligand types, however, more significantly in the case of R^1 ligands. Thus, we assume that the star-shaped isomer in **3** was observed as a kinetic product, hence an intermediate, as its more rapid crystallization was promoted by the hydrazone groups, in agreement with the overall lower solubility of hydrazone derivatives as compared with keto derivatives of organotin chalcogenide clusters. In the case of **1**, the better solubility apparently allowed for the formation of the thermodynamic product prior to crystallization.

7. References for the Supporting Information

[1] A. Pines, M. G. Gibby, J. S. Waugh, *J. Chem. Phys.* **1973**, *59*, 569–590.
[2] B. M. Fung, A. K. Khitrin, K. Ermolaev, *J. Magn. Reson.* **2000**, *142*, 97–101.
[3] TURBOMOLE V7.0.1 2015, a development of University of Karlsruhe and Forschungszentrum Karlsruhe GmbH, 1989-2007, TURBOMOLE GmbH, since 2007; available from http://www.turbomole.com.
[4] S. Grimme, *J. Comput. Chem.* **2006**, *27*, 1787–1799.
[5] S. Grimme, J. Antony, S. Ehrlich, H. Krieg, *J. Chem. Phys.* **2010**, *132*, 154104.
[6] S. Grimme, S. Ehrlich, L. Goerigk, *J. Comput. Chem.* **2011**, *32*, 1456–1465.
[7] F. Weigend, R. Ahlrichs, *Phys. Chem. Chem. Phys.* **2005**, *7*, 3297–3305.
[8] F. Weigend, *Phys. Chem. Chem. Phys.* **2006**, *8*, 1057–1065.
[9] D. Andrae, U. Haeussermann, M. Dolg, H. Stoll, H. Preuss, *Theor. Chim. Acta* **1990**, *77*, 123–141.
[10] B. Metz, H. Stoll, M. Dolg, *J. Chem. Phys.* **2000**, *113*, 2563-2569.
[11] G. Schaftenaar, J. H. Nordik, *J. Comput.-Aided Mol. Design* **2000**, *14*, 123-134.
[12] a) G. Schreckenbach, T. Ziegler, *J. Phys. Chem.* **1995**, *99*, 606-611; b) M. Kollwitz, J. Gauss, *Chem. Phys. Lett.* **1996**, *260*, 639–646.
[13] S. F. Boys, in: P.-O. Löwdin (Ed.), *Quantum Theory of Atoms, Molecules and the Solid State*, Academic Press, New York **1966**, 253–262.
[14] C. Ehrhardt, R. Ahlrichs, *Theor. Chim. Acta* **1985**, *68*, 231–245.

3.4. Trigonal Bipyramidal Metalselenide Clusters with Palladium and Tin Atoms in Various Positions

Niklas Rinn, Lukas Guggolz, Katharina Hanau und Stefanie Dehnen, *Z. Anorg. Allg. Chem.* **2017**, eingereichtes Manuskript.

Abstract: The reaction of $[(R^1Sn)_3Se_4Cl]$ ($R^1 = CMe_2CH_2COMe$) with $[Pd(PPh_3)_2Cl_2]$, $(SiMe_3)_2Se$ and hydrazine hydrate yields a new Pd/Se cluster, $[Pd_3(PPh_3)_5(SeH)(\mu_3\text{-}Se)_2][SnCl_3]$ (**1**). Using $[(R^1Sn)_4Se_6]$ as reactant and varying the reaction conditions as well as the addition of $(SiMe_3)_2Se$ and hydrazine hydrate, $[Pd_3(PPh_3)_5(SnCl_3)(\mu_3\text{-}Se)_2][SnCl_3]$ (**2**) and $[Pd_2(PPh_3)_3Cl\{SnR^2Cl_2\}(\mu_3\text{-}Se)_2]$ (**3**) can be isolated. **3** is the first compound based on a $[Pd_2SnSe_2]$ moiety, which furthermore exhibits a functional organic group at the tin atom. Its photoluminescence and absorption spectra are discussed as well. All compounds were characterized via single-crystal X-ray diffraction, indicating a bipyramidal structure. Mass spectrometric analyses of the reactive solutions provide some insight into the formation of the clusters.

Inhaltsangabe: Umsetzungen der Zinnselenidcluster $[(SnR^1)_3Se_4Cl]$ (**A**) beziehungsweise $[(SnR^1)_4Se_6]$ (**B**)[101] mit $[Pd(PPh_3)_2Cl_2]$ und $(SiMe_3)_2Se$ wurden untersucht. Hierbei konnten zwar in Reaktionen mit beiden Eduktclustern massenspektrometrisch Fragmente der Formel $[Se_2Pd_3(PPh_3)_xCl]$ (x = 2-5) gefunden, es ließen sich aber keine Einkristalle für eine Strukturbestimmung erhalten. Setzt man jedoch $N_2H_4{\cdot}H_2O$ zu entsprechenden Umsetzungen mit dem **A** zu, so lässt sich die Verbindung $[(Pd_3(PPh_3)_5Se_2SeH][SnCl_3]\cdot$(**1**) einkristallin isolieren. Diese Verbindung ist alternativ durch eine analoge Umsetzung mit **B** ohne Schutzgasatmosphäre zugänglich. Weitere Umsetzungen mit diesem Eduktcluster mit $N_2H_4{\cdot}H_2O$ Zusatz, allerdings wiederum unter Luft- und Wasserausschluss, führten zur Bildung eines roten Niederschlags, welcher durch Lösen und Überschichten mit *n*-Hexan Kristalle von $[Pd_3(PPh_3)_5Se_2SnCl_3][SnCl_3]\cdot$(**2**) lieferte, in einer roten Lösung, aus der ebenfalls durch Überschichtung mit *n*-Hexan Kristalle von $[Se_2Pd_2(PPh_3)_3Cl\{SnR^2Cl_2\}]$ (**3**) isoliert werden können. Da $N_2H_4{\cdot}H_2O$ diese Reaktionen ermöglicht, aber in **1** und **2** nicht explizit vorliegt, ist davon auszugehen, dass seine reduzierende Wirkung für die Bildung dieser beiden Verbindungen essentiell ist. Tatsächlich treten in **1** und **2** eine beziehungsweise zwei $[SnCl_3]^-$-Einheit(en) auf, die Sn(II) enthalten. Die Molekülstrukturen der drei Vorgestellten Verbindungen sind in Abbildung 3.4 gezeigt.

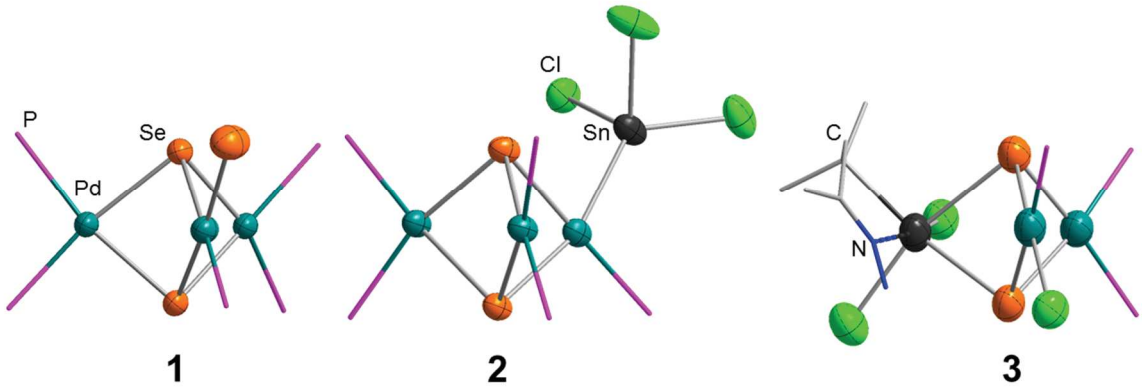

Abbildung 3.4: In „Trigonal Bipyramidal Metalselenide Clusters with Palladium and Tin Atoms in Various Positions" beschriebene Molekülstrukturen. Die Phenylgruppen und Wasserstoffatome wurden aus Übersichtlichkeitsgründen nicht angezeigt.

Eigener Anteil: Alle Reaktionen wurden von mir geplant und alle analytischen Daten wurden von mir ausgewertet. Alle Reaktionen wurden von Luomo Li im Rahmen eines Forschungspraktikums bei mir unter meiner Anleitung durchgeführt. Alle massenspektrometrischen Experimente wurden von der zentralen Abteilung für

Massenspektrometrie und Elementaranalyse der Philipps-Universität Marburg durchgeführt. NMR-Spektren wurden von der zentralen NMR-Abteilung des Fachbereichs Chemie an der Philipps-Universität Marburg gemessen. Das Manuskript wurde in Kooperation mit Katharina Hanau und Stefanie Dehnen geschrieben. Weitere Co-Autoren haben jeweils kurze Abschnitte über ihre Beiträge eingefügt oder die von uns vorgeschlagenen Abschnitte dazu überarbeitet.

Trigonal Bipyramidal Metalselenide Clusters with Palladium and Tin Atoms in Various Positions

Niklas Rinn,[a] Katharina Hanau,[a] Lukas Guggolz,[a] Andre Rinn,[b] Sangam Chatterjee,[c] and Stefanie Dehnen*[a]

Dedicated to Professor Wolfgang Schnick on the occasion of his 60th birthday.

Abstract: The reaction of [(R^{1}Sn)$_3$Se$_4$Cl] (R^1 = CMe$_2$CH$_2$COMe) with [Pd(PPh$_3$)$_2$Cl$_2$], (SiMe$_3$)$_2$Se and hydrazine hydrate yields a new Pd/Se cluster, [Pd$_3$(PPh$_3$)$_5$(SeH)(μ$_3$-Se)$_2$][SnCl$_3$] (**1**). Using [(R^{1}Sn)$_4$Se$_6$] as reactant and varying the reaction conditions as well as the addition of (SiMe$_3$)$_2$Se and hydrazine hydrate, [Pd$_3$(PPh$_3$)$_5$(SnCl$_3$)(μ$_3$-Se)$_2$][SnCl$_3$] (**2**) and [Pd$_2$(PPh$_3$)$_3$Cl{SnR^{2}Cl$_2$}(μ$_3$-Se)$_2$] (**3**) can be isolated. **3** is the first compound based on a [Pd$_2$SnSe$_2$] moiety, which furthermore exhibits a functional organic group at the tin atom. Its photoluminescence and absorption spectra are discussed as well. All compounds were characterized via single-crystal X-ray diffraction, indicating a bipyramidal structure. Mass spectrometric analyses of the reactive solutions provide some insight into the formation of the clusters.

Metal chalcogenide clusters, including virtually all kinds of binary and ternary elemental combinations within discrete, ligand-protected or ligand-free clusters or extended cluster networks, have been in the focus of many research teams worldwide because of their rich structure chemistry and interesting and finely tunable opto-electronic properties.[1,2]

Less attention has been paid to clusters that comprise a reactive organic ligand shell. However, as this generally allows for further extension of the cluster surface and attachment to solid substrates, one of our current aims is the synthesis and thorough investigation of metal chalcogenide clusters that comprise ligands with functional groups.[3–8]

For accessing ternary, organo-functionalized chalcogenide clusters, in which main group (semi-)metal atoms are combined with transition metal atoms for an even finer tunable electronic situation, the use of organotetrel chalcogenide clusters like [(R^{1}T)$_3$E$_4$Cl] or [(R^{1}T)$_4$E$_6$] (R^1 = CMe$_2$CH$_2$C(O)Me, T = Ge, Sn; E = S, Se, Te) has proven an efficient and versatile way.[5,9–14]

Yet, most reactions so far were carried out with coinage metal complexes, while combinations with other transition metals have remained a challenge. The only exceptions so far are the cluster [{R^{2}GeS$_3$}$_4$Pd$_6$] (R^2 = CMe$_2$CH$_2$C(NNH$_2$)Me)[15] and a network of [(R^{3}Ge)$_4$S$_6$] (R^3 = CH$_2$CH$_2$COO$^-$) clusters linked by Mn^{2+} ions.[16] The combination of Pd with group 14 elements is known to be catalytically highly active in nanoparticles, for which this elemental combination caught our interest.[17]

Herein, we report on a recent study, in which previous reactions of organogermanium sulfide clusters with Pd complexes were transferred to organotin selenide clusters. For this, the precursors shown in Scheme 1, [(R^{1}Sn)$_3$Se$_4$Cl] (**A**) and [(R^{1}Sn)$_4$Se$_6$] (**B**) were reacted with [Pd(PPh$_3$)$_2$Cl$_2$] under different conditions.

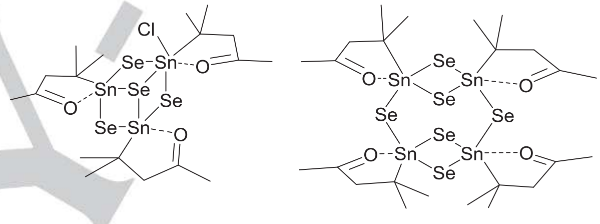

[(R^{1}Sn)$_3$Se$_4$Cl] (**A**) [(R^{1}Sn)$_4$Se$_6$] (**B**)

Scheme 1. Structural diagram of the organofunctionalized tinselenide clusters used as starting materials, [(R^{1}Sn)$_3$Se$_4$Cl] (**A**, R^1 = CMe$_2$CH$_2$COMe) and [(R^{1}Sn)$_4$Se$_6$] (**B**).

As indicated in Scheme 2, the reaction of **A** with (SiMe$_3$)$_2$Se, [Pd(PPh$_3$)$_2$Cl$_2$], and hydrazine hydrate under inert conditions yields a red solution. Upon layering of this solution with *n*-hexane, single crystals of [Pd$_3$(PPh$_3$)$_5$(SeH)(μ$_3$-Se)$_2$][SnCl$_3$]·3CH$_2$Cl$_2$ (**1**·3CH$_2$Cl$_2$) are isolated. **1** can also be synthesized by reacting **B** with [Pd(PPh$_3$)$_2$Cl$_2$] in air, while a reaction of **B** with [Pd(PPh$_3$)$_2$Cl$_2$] and hydrazine hydrate leads to another result. A red solution is obtained as well as a red solid. The solid can be redissolved in CH$_2$Cl$_2$ and layered with n-hexane to form single crystals of [Pd$_3$(PPh$_3$)$_5$(SnCl$_3$)(μ$_3$-Se)$_2$][SnCl$_3$]·2CH$_2$Cl$_2$ (**2**·2CH$_2$Cl$_2$). Layering of the residual solution with *n*-hexane yields single crystals of [Pd$_2$(PPh$_3$)$_3$Cl{SnR^{2}Cl$_2$}(μ$_3$-Se)$_2$]·CH$_2$Cl$_2$ (**3**·CH$_2$Cl$_2$, R^2 = CMe$_2$CH$_2$CMeNNH$_2$).

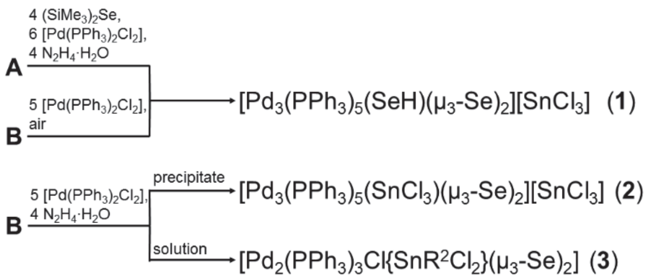

Scheme 2. Reaction scheme for the synthesis of compounds **1** - **3**.

[a] N. Rinn, K. Hanau, L. Guggolz, Prof. Dr. S. Dehnen
Fachbereich Chemie und Wissenschaftliches Zentrum für Materialwissenschaften (WZMW)
Philipps-Universität Marburg
Hans-Meerwein-Str. 4, 35043 Marburg (Germany)
E-mail: dehnen@chemie.uni-marburg.de

[b] A. Rinn
Faculty of Physics and Materials Sciences Center,
Philipps-Universität Marburg, Renthof 5, 35037 Marburg (Germany)

[c] Prof. S. Chatterjee, Ph.D.
Institute of Experimental Physics I, Justus-Liebig-University Giessen
Heinrich-Buff-Ring 16, 35392 Giessen (Germany)

Supporting information for this article is given via a link at the end of the document.

1, **2** and **3** were analyzed by single-crystal X-ray diffraction (see Experimental Section and Supporting Information). The molecular structures of compounds **1** – **3** are shown in Figure 1. Relevant structural parameter are given in Table 1.

Compounds **1** and **2** comprise a $[Pd_3(\mu_3\text{-}Se)_2]^{2+}$ bipyramidal cluster core, with one Pd atom bonded to an $(SeH)^-$ ligand in **1**, or an in situ-formed $[SnCl_3]^-$ unit in **2**, respectively. As reported previously,[12,18] the $[Sn^{II}Cl_3]^-$ anion originates from (partial) decomposition of the $[(R^1Sn)_xSe_yCl_z]$ starting material, initiated typically by water from the condensation reaction with hydrazine, or (as indicated for the alternative formation of **1**) by moisture from air. The remaining coordination sites at the Pd atoms of both clusters are occupied by PPh_3 ligands. This way, the overall charge of the clusters is +1, which is compensated by (further) $[SnCl_3]^-$ anions in both compounds.

The proton at the terminal Se atom in **1** could not be satisfyingly refined from the difference Fourier map, although some residual electron density was observed at a reasonable distance from the Se atom. We assume that the relatively high mobility of the (SeH) ligand, reflected in a relatively large thermal displacement parameter, inhibits a better refinement. However, related clusters comprising $(SeH)^-$ groups, $[Pd_2Au_2Se_2(SeH)_2(PPh_3)_4]$[19] or $[Pd_7Se_6(SeH)Cl(PPh_3)_7]$,[20] overall charge neutrality of **1** and reasonable structural data (see Table 1) indicate the assignment of a correct composition.

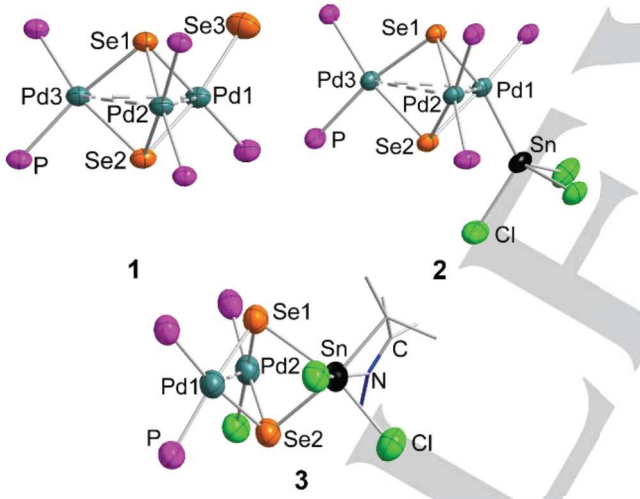

Figure 1. Molecular structures of **1**, **2**, and **3**. Phenyl groups, H atoms at organic groups, and counterions are omitted for clarity. Thermal ellipsoids are drawn at 50% probability. Selected structural parameters are given in Table 1.

The structural motif of a $[Pd_3Se_2]^{2+}$ bipyramid has been described for one further cluster, $[Pd_3Se_2(SeSiMe_3)_2(PPh_3)_4]$, with very similar structural features, yet within a neutral molecule.[21] Moreover, **3** is a neutral cluster, and it has an analogous topology, yet it unprecedentedly comprises two Pd atoms and one Sn atom within the trigonal bipyramidal cluster core. Besides coordination by three PPh_3 ligands, the formally cationic $[Pd_2Se_2Sn]^{4+}$ cluster core requires charge compensation, which is realized by three Cl substituents (one at Pd2, two at the Sn atom) and one R^2 ligand (at the Sn atom). The presence of a functionalized organic ligand is unique for this elemental combination.

Trigonal bipyramidal clusters are well-known for many elemental combinations, preferably combining the group 10 metals nickel, palladium, and platinum with sulfur atoms. Examples are $[Ni_3S_2Cl_2(PPh_3)_4]$, $[Pd_3S_2Cl_2(PPh_3)_4]$, or $[Ni_3Se_2(SeSiMe_3)_2(P(C_2H_4Ph)_3)_4]$.[20] Also, further palladium selenide clusters beside those quoted above have been published, such as $[Pd_5Se_4Cl_2(PPh_3)_6I]$, $[Pd_5Se_5(PPh_3)_5]$, $[Pd_6Se_4Cl_4(PPh_3)_6]$, $[Pd_8Se_8(PPh_3)_8]$, or $[Pd_8Se_8Cl(PPh_3)_8]^-$.[21] However, trigonal bipyramidal metal chalcogenide clusters, in which transition metal atoms are combined with tin atoms, are very rare. The only examples known to date are clusters of the general type $[(ML_z)_2(R_xSnX_y)(\mu_3\text{-}Se)_2]$ (M = Co, Ru, Os, Pt) or clusters, in which $[R_2SnSe_x]$ moieties are combined with $[(ML_z)_2(\mu_3\text{-}Se)_2]$ units, such as $[Pt_2(PPh_3)_4(SnMe_2Cl)(\mu_3\text{-}Se)]^+$,[22] $[Ru_3(CO)_7(H_2O)(\mu_3\text{-}Se)_2(Sn(Tb)Tip)Se_2]$ (Tb = 2,4,6,-tris[bis(trimethylsilyl)methyl; Tip = 2,4,6-tri(isopropyl)phenyl) and $[Ru_3(CO)_8Se_3(Sn(Tb)Tip)]$.[23]

Table 1: Selected structure parameters within the molecular structures of **1**, **2**, and **3**.

Distances [Å] and Angles [°]	**1**	**2**	**3**
Pd1–Se1	2.433(1)	2.442(2)	2.441(4)
Pd2–Se1	2.452(1)	2.456(2)	2.398(8)
Pd3–Se1	2.429(1)	2.435(2)	–
Pd1–Se2	2.439(1)	2.470(2)	2.481(3)
Pd2–Se2	2.433(1)	2.436(2)	2,478(3)
Pd3–Se2	2.453(1)	2.459(2)	–
Pd1–Se3	2.4134(16)	–	–
Se1···Se2	3.090(2)	3.088(2) Å	3.183(4)
Pd···Pd	3.201(1) – 3.382(1)	3.175(1) – 3.470(1)	3.222(3)
Pd–Sn, Pd···Sn	–	2.546(2)	3.541(3), 3.478(3)
Pd–Se–Pd	82.35(4) – 87.73(4)	80.80(5) – 90.37(6)	80.58(9), 81.49(9)
Se–Pd–Se	78.48(4) – 78.75(4)°	78.23(5) – 77.89(5)	81.03(9)
Se–Sn–Se	–	–	72.08(8)
Pd–Se–Sn	–	–	85.40(9) – 88.44(9)
Pd···Pd···Pd	57.94(2) – 63.58(2)	57.57(3) – 65.83(3)	–
Pd···Sn···Pd	–	–	54.65(5)
Sn···Pd···Pd	–	–	61.68(5) – 63.67(5)

Owing to the unsymmetrical coordination sphere at the Pd atoms, the Se–Pd distances vary much more distinctly than those in **1** and **2**. Further, the replacement of one Pd atom by an $[SnR^2Cl_2]$ unit naturally causes a distortion of the bipyramid, which is

reflected by more obtuse Se–Pd–Se angles of 80.58(9) and 81.49(9)° (opposed to 78.48(4) - 78.75(4)° in **1** or 78.23(5) - 77.89(5)° in **2**). In all compounds, the Pd···Pd distances are considerably longer than the sum of the covalent radii. In turn, the Se···Se distances are significantly shorter than the sum of the van der Waals radii, which has been observed before in such arrangements with long metal-metal distances.

Several compounds have been known featuring Pd–$SnCl_3$ moieties similar to that in **2**, e.g., [$(Cl_3Sn)Pd(PPh_3)(\eta^3\text{-}C_3H_5)$] (2.564 Å),[24] [$(Cl_3Sn)Pd(PPh_3)_2Cl$] (2.574 Å),[25] or [$(Cl_3Sn)Pd(\eta^3\text{-}CH_2C(CH_3)CH_2)(\eta^2\text{-}C_2H_3Ph)$] (2.554 Å),[26] featuring bond lengths similar to that observed in **2**. In order to examine the nature of the Pd–Sn bond present in compound **2**, we performed quantum chemical calculations using density functional theory (DFT) methods within the program system Turbomole.[27] Localization of molecular orbitals into LMOs indicated the presence of a relatively homopolar bond between both metal atoms, mainly resulting from interaction of the Pd $5d_{x2-y2}$ orbital and the 5p orbital-dominated HOMO of the $[SnCl_3]^-$ ligand (see Figure 2). Hence, a description as Pd^{II}–Sn^{II} seems reasonable here. The trigonal bipyramidal cluster itself is held together mainly by three-center Pd–Se–Pd bonds. This is also observed for the cluster in **1** and in **3**, the latter also including a Se–Sn–Se three-center bond.

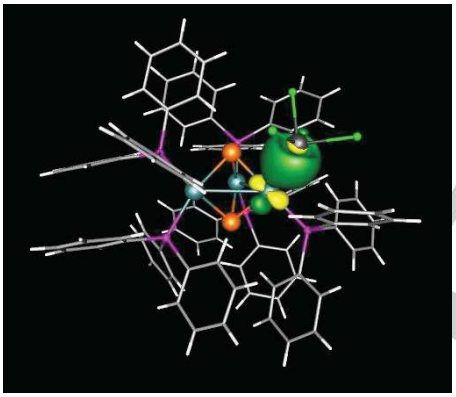

Figure 2. Localized molecular orbital (LMO) representing the Pd–Sn bond in **2**.

Mössbauer spectroscopy on a series of palladium stannyl-arsyl complexes like [$Pd_2Br\{\kappa_2(Sn,As)\text{-}2\text{-}MeBrSnC_6F_4AsPh_2\}_2$] have recently indicated a situation better described Pd^0–Sn^{IV}.[28] The bond length in the quoted complex (2.50 Å), however, is somewhat smaller than in **2**, pointing towards a notable heteropolarity.

To elucidate the optical properties of the mixed-metal selenide cluster compound **3**, its photoluminescence and linear absorption were determined on a single-crystal sample. The results are shown in Figure 3. The visual impression of the crystals color, red, is quantified as a broad absorption band between 1.77 and 3.5 eV. A more detailed analysis reveals two absorption features at 2.26 and 3.0 eV, respectively. Similarly, two discrete emission bands are observed at 1.77 and 2.78 eV. The luminescence signals peak at lower energies than the corresponding absorption bands as expected according to the Franck-Condon principle. Notably, the lower-energy emission at 1.77 eV matches the absorption edge belonging to the broad absorption peak at 2.26 eV and no significant Stokes shift is observed here. As we excited primarily at the higher-energy absorption, but still observed a lower-energy signal, we assume a coupling between both absorption levels, likely due to the different chromophores present in the cluster that comprises Pd and Sn atoms within their respective coordination spheres.

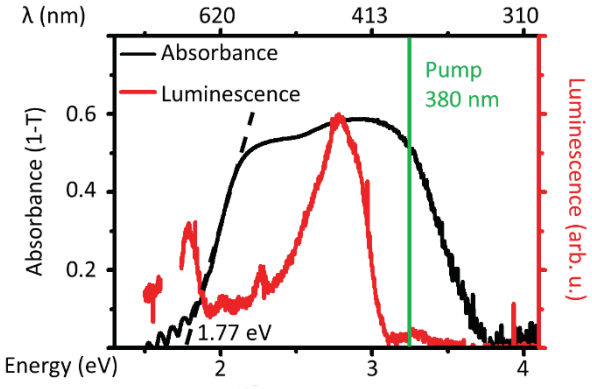

Figure 3. Absorbance (black) and luminescence (red) of a single-crystal of **3**.

A multitude of further reactions of **A** and **B** with $[Pd(PPh_3)_2Cl_2]$, $(SiMe_3)_2Se$ and $N_2H_4{\cdot}H_2O$ in different ratios and permutations were carried out. ESI(+) mass spectra of the reactive solutions and the sometimes resulting redissolved precipitates indicate the formation of cations of the general formula $[Pd_3Se_2(PPh_3)_xCl]^+$ (x = 2 - 5). Such compounds, most likely clusters with a trigonal bipyramidal topology, are also detected in ESI-MS experiments upon reactions of **A** or **B** with $[Pd(PPh_3)_2Cl_2]$ in different stoichiometries without further addition of hydrazine hydrate or $(SiMe_3)_2Se$. This suggests that $[Pd_3Se_2(PPh_3)_xCl]^+$ might play a key role in the formation of the clusters **1** – **3** presented herein. However, the corresponding compound could never be isolated. We assume that crystallization only occurs upon formation of the $[Sn^{II}Cl_3]^-$ anions in the way described above.

In summary, we described the synthesis and characterization of three new clusters that are related in that they contain palladium and selenium atoms in trigonal bipyramidal cluster cores, and comprise one or two tin atoms in different positions within or beside the clusters. The structural motif of an $[Pd_3(\mu_3\text{-}Se)_2]^{2+}$ bipyramid found in **1** and **2** has been already known, yet not with $(SeH)^-$ or $[SnCl_3]^-$ groups as ligands. The $[Pd_2\{SnRCl_2\}(\mu_3\text{-}Se)_2]^+$ bipyramid in **3** has not been reported to date. Similar clusters were described with Pt or Co instead of Pd, yet none of them comprising functionalized organic groups such as the R^2 ligand in **3**, the derivatization of which is subject to future work in our group. Measurements of the opto-electronic properties of single-crystals of **3** reflect the mixed-metal situation within this metal selenide cluster.

Experimental Section

General: All syntheses were performed under exclusion of air and moisture using standard Schlenk techniques. All solvents were dried and freshly distilled prior to use. $[(R^1Sn)_4Se_6]$, $[(R^1Sn)_3Se_4]Cl$, and $(SiMe_3)_2Se$

were prepared according to literature procedures.[12,29] Further chemicals were purchased from Sigma Aldrich. ^{1}H and ^{31}P NMR spectra were recorded with a Bruker ARX 300 spectrometer. ESI mass spectra were recorded with a Finnigan LTQ-FT mass spectrometer.

$[Pd_3(PPh_3)_5Se_2SeH][SnCl_3]$ (1): $[(R^1Sn)_3Se_4]Cl$ (101 mg, 0.10 mmol) and $[Pd(PPh_3)_2Cl_2]$ (430 mg, 0.61 mmol) were dissolved in 20 mL CH_2Cl_2 and $(SiMe_3)_2Se$ (94 mg, 0.42 mmol) and $N_2H_4{\cdot}H_2O$ (19 mg, 0.38 mmol) were added subsequently. The reaction mixture was stirred at room temperature for 16 h, filtered, and the filtrate was layered with *n*-hexane to afford red crystals of **1** (212 mg, 0.092 mmol, 32% compared to $[(R^1Sn)_3Se_4]Cl$]).

Alternative Synthesis of 1: $[(R^1Sn)_4Se_6]$ (100 mg, 0.07 mmol) and $[Pd(PPh_3)_2Cl_2]$ (228 mg, 0.32 mmol) were dissolved in 20 mL CH_2Cl_2 under air. After stirring for 16 h, and filtering, the solution was layered with *n*-hexane to afford red crystals of **1** (172 mg. 0,072 mmol, 20% compared to $[(R^1Sn)_4Se_6]$). NMR spectra could not be recorded due to very low solubility of the salt.

$[Pd_3(PPh_3)_5Se_2SnCl_3][SnCl_3]$ (2): $[(R^1Sn)_4Se_6]$ (97 mg, 0.07 mmol) and $[Pd(PPh_3)_2Cl_2]$ (248 mg, 0.35 mmol) were dissolved in 20 mL CH_2Cl_2 and $N_2H_4{\cdot}H_2O$ (14 mg, 0.28 mmol) was added. The solution was stirred at room temperature for 16 h, and a red powder precipitated. Upon re-dissolving the powder in CH_2Cl_2, red crystals of **2** crystallized by layering with *n*-hexane (44 mg. 0,022 mmol, 16% compared to $[(R^1Sn)_4Se_6]$). NMR spectra could not be recorded due to very low solubility of the salt.

$[Pd_2(PPh_3)_3Se_2SnR^2Cl_3]$ (3): $[(R^1Sn)_4Se_6]$ (97 mg, 0.07 mmol) and $[Pd(PPh_3)_2Cl_2]$ (248 mg, 0.35 mmol) were dissolved in 20 mL CH_2Cl_2 and $N_2H_4{\cdot}H_2O$ (14 mg, 0.28 mmol) was added. The solution was stirred at room temperature for 16 h, and a red precipitate was filtered off. The filtrate was layered with *n*-hexane to afford red crystals of 3 (78 mg. 0,049 mmol, 18% compared to $[(R^1Sn)_4Se_6]$). ^{1}H NMR (300 MHz, $CDCl_3$, 25 °C): δ = 1.55 (s, 6H, C(CH_3)$_2$), 1.75 (s, 3H, CCH_3), 2.01 (s, 2H, CH_2), 7.02 – 7.76 (m, 45H, PPh_3) ppm. ^{31}P NMR (121.5 MHz, $CDCl_3$, 25 °C): δ = 20.3 (s, $PdPPh_3Cl$), 24.2 (d, $^{2}J_{PP}$ = 29.8 Hz, $Pd(PPh_3)_2$), 26.9 (d, $^{2}J_{PP}$ = 36.2 Hz, $Pd(PPh_3)_2$) ppm.

Single Crystal X-ray Diffraction: Crystals suitable for X-ray diffraction analyses were investigated with a STOE IPDS-2T (**1**) or IPDS-II (**2** and **3**) diffractometer at 100 K using Mo-K_α radiation and a graphite monochromator (λ = 0.71073 Å). Upon numerical absorption correction (STOE X-AREA), the structure solution was performed by direct methods, followed by full-matrix-least-squares refinement against F^2, using SHELXT15, SHELXL15, and OLEX2 software.[30]

Crystallographic data (excluding structure factors) for the structures reported in this paper have been deposited with the Cambridge Crystallographic Data Centre as supplementary publication no. CCDC 1564626-1564628. Copies of the data can be obtained free of charge on application to CCDC, 12 Union Road, Cambridge CB2 1EZ, UK [fax.: (internat.) + 44 1223/336-033; e-mail: deposit@ccdc.cam.ac.uk].

Computational Details: The quantum chemical investigations were performed within the program system Turbomole V7.0.1.[27] We used the functional B97-D[31] with dispersion correction[32] and BJ-damping.[33] We applied the def2-TZVP basis set[34] with auxiliary bases[35] and effective core potentials (ECPs) at the Pd atoms.[36] Localization of MOs was done following the procedure by Boys.[37]

Acknowledgements

This work was supported by the Deutsche Forschungsgemeinschaft (DFG) within the framework of GRK 1782 “Functionalization of Semiconductors”. SC also acknowledges the Heisenberg program of the DFG (CH660/2).

Keywords: Clusters • Tin • Palladium • Selenium • Functional Ligands

[1] (a) O. Fuhr, S. Dehnen, D. Fenske, *Chem. Soc. Rev.* **2013**, *42*, 1871–1906; (b) S. Santner, J. Heine, S. Dehnen, *Angew. Chem. Int. Ed.* **2016**, *55*, 876–893.

[2] P. Feng, X. Bu, N. Zheng, *Acc. Chem. Res.* **2005**, *38*, 293–303.

[3] Z. Hassanzadeh Fard, C. Müller, T. Harmening, R. Pöttgen, S. Dehnen, *Angew. Chem. Int. Ed.* **2009**, *48*, 4441–4444.

[4] N. W. Rosemann, J. P. Eußner, A. Beyer, S. W. Koch, K. Volz, S. Dehnen, S. Chatterjee, *Science* **2016**, *352*, 1301–1305.

[5] M. R. Halvagar, Z. Hassanzadeh Fard, S. Dehnen, *Chem. Commun.* **2010**, *46*, 4716–4718.

[6] S. Heimann, M. Hołyńska, S. Dehnen, *Chem. Commun.* **2011**, *47*, 1881–1883.

[7] Z. Hassanzadeh Fard, M. R. Halvagar, S. Dehnen, *J. Am. Chem. Soc.* **2010**, *132*, 2848–2849.

[8] J. P. Eußner, B. E. K. Barth, E. Leusmann, Z. You, N. Rinn, S. Dehnen, *Chem. Eur. J.* **2013**, *19*, 13792−13802.

[9] J. P. Eußner, S. Dehnen, *Chem. Comm.* **2014**, *50*, 11385–11388.

[10] Z. Hassanzadeh Fard, L. Xiong, C. Müller, M. Hołyńska, S. Dehnen, *Chem. Eur. J.* **2009**, *15*, 6595–6604.

[11] I. Schellenberg, C. Pöhlker, R. Pöttgen, S. Dehnen, *Chem. Comm.* **2010**, *46*, 2605–2607.

[12] N. Rinn, J. P. Eußner, W. Kaschuba, X. Xie, S. Dehnen, *Chem. Eur. J.* **2016**, *22*, 3094–3104.

[13] B. E. K. Barth, E. Leusmann, K. Harms, S. Dehnen, *Chem. Comm.* **2013**, *49*, 6590–6592.

[14] E. Leusmann, E. Geringer, B. Weinert, S. Dehnen, *Dalt. Trans.* **2016**, *45*, 15298–15302.

[15] M. R. Halvagar, Z. Hassanzadeh Fard, L. Xiong, S. Dehnen, *Inorg. Chem.* **2009**, *48*, 7373–7377.

[16] Z. Hassanzadeh Fard, R. Clérac, S. Dehnen, *Chem. Eur. J.* **2010**, *16*, 2050–3.

[17] S.J. Freakley, Q. He, J. H. Harrhy, L. Lu, D. A. Crole, D. J. Morgan, E. N. Ntainjua, J. K. Edwards, A. F. Carley, A. Y. Borisevich, C. J. Kiely, G. J. Hutchings, *Science* **2016**, *351*, 965–968.

[18] (a) J. P. Eußner, R. O. Kusche, S. Dehnen, *Chem. Eur. J.* **2015**, *21*, 12376–12388. (b) S. Heimann, M. Hołynska, S. Dehnen, *Z. Anorg. Allg. Chem.* **2012**, *638*, 1663–1666.

[19] P. D. Harvey, A. Eichhöfer, D. Fenske, *J. Chem. Soc., Dalt. Trans.* **1998**, 3901–3903.

[20] D. Fenske, H. Fleischer, H. Krautscheid, J. Magull, C. Oliver, *Z. Naturforsch. B* **1991**, *46*, 1384–1394.

[21] D. Fenske, H. Fleischer, H. Krautscheid, J. Magull, *Z. Naturforsch.* **1990**, *45b*, 127–133.

[22] J. S. L. Yeo, J. J. Vittal, T. S. A. Hor, W. Henderson, *Dalt. Trans.* **2001**, 315–321.

[23] Y. Matsuhashi, N. Tokitoh, R. Okazaki, *Organometallics* **1994**, *13*, 4387–4397.

[24] R. Mason, P. O. Whimp, *J. Chem. Soc. A* **1969**, 2709–2717.

[25] E. Wachtler, R. Gericke, L. Zhechkov, T. Heine, T. Langer, B. Gerke, R. Pöttgen, J. Wagler, *Chem. Commun.* **2014**, *50,* 5382–5384.

[26] A. Musco, R. Pontellini, M. Grassi, A. Sironi, S. V. Meille, H. Ruegger, C. Ammann, P. S. Pregosin, *Organometallics* **1988**, *7*, 2130–2137.

[27] TURBOMOLE V7.0.1 2015, a Development of University of Karlsruhe and Forschungszentrum Karlsruhe GmbH, 1989-2007, TURBOMOLE GmbH, since 2007, Available from http://www.turbomole.com.

[28] N. Mirzadeh, M. Bennett, J. Wagler, E. Wächtler, B. Gerke, R. Pöttgen,

S. Bhargava, *Eur. J. Inorg. Chem.* **2013**, 1997–2001.
[29] M. R. Detty, M. D. Seidler, *J. Org. Chem.* **1982**, *47*, 1354–1356.
[30] a) G. M. Sheldrick, *Acta Crystallogr., Sect. A* **2015**, *71*, 3–8. b) G. M. Sheldrick, *Acta Crystallogr., Sect. C* **2015**, *71*, 3–8. c) O. V. Dolomanov, L. J. Bourhis, R. J. Gildea, J. A. K. Howard, H. Puschmann, *J. Appl. Crystallogr.* **2009**, *42*, 339–341.
[31] S. Grimme, *J. Comput. Chem.* **2006**, *27*, 1787–1799.
[32] S. Grimme, J. Antony, S. Ehrlich, H. Krieg, *J. Chem. Phys.* **2010**, *132*, 154104.
[33] S. Grimme, S. Ehrlich, L. Goerigk, *J. Comput. Chem.* **2011**, *32*, 1456-1465.
[34] F. Weigend, R. Ahlrichs, *Phys. Chem. Chem. Phys.* **2005**, *7*, 3297–3305.
[35] F. Weigend, *Phys. Chem. Chem. Phys.* **2006**, *8*, 1057–1065.
[36] D. Andrae, U. Haeussermann, M. Dolg, H. Stoll, H. Preuss, *Theor. Chim. Acta* **1990**, *77*, 123–141.
[37] (a) S. F. Boys, *Rev. Mod. Phys.* **1960**, *32*, 296–299; (b) J. M. Foster, S. F. Boys, *Rev. Mod. Phys.* **1960**, *32*, 300–302.

Entry for the Table of Contents (Please choose one layout)

COMMUNICATION

Syntheses and structures of three new compounds are presented that are based on trigonal bipyramidal palladium selenide cluster cores with one or two tin atoms in different positions within or beside the clusters. One of them is the first ternary Pd/Sn/Se cluster (see Figure), and it also comprises a functional organic ligand. The opto-electronic properties reflect the mixed-metal situation.

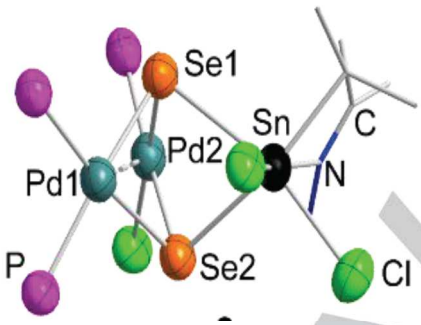

*Niklas Rinn, Katharina Hanau, Lukas Guggolz, Andre Rinn, Sangam Chatterjee, Stefanie Dehnen**

Page No. – Page No.

Trigonal Bipyramidal Metalselenide Clusters with Palladium and Tin Atoms in Various Positions

Metalselenide Clusters with Palladium and Tin Atoms in Various Positions

Niklas Rinn,[a] Katharina Hanau,[a] Lukas Guggolz,[a] Andre Rinn,[b] Sangam Chatterjee,[c] and Stefanie Dehnen*[a]

[a] N. Rinn, K. Hanau, L. Guggolz, Prof. Dr. S. Dehnen
Fachbereich Chemie und Wissenschaftliches Zentrum für Materialwissenschaften (WZMW)
Philipps-Universität Marburg
Hans-Meerwein-Str. 4, 35043 Marburg (Germany)
E-mail: dehnen@chemie.uni-marburg.de
[b] A. Rinn
Faculty of Physics and Materials Sciences Center,
Philipps-Universität Marburg, Renthof 5, 35037 Marburg (Germany)
[c] Prof. S. Chatterjee, Ph.D.
Institute of Experimental Physics I, Justus-Liebig-University Giessen
Heinrich-Buff-Ring 16, 35392 Giessen (Germany)

SUPPORTING INFORMATION

1. Details of the X-ray diffraction measurements and refinements

General: All X-ray crystal structures were measured using Stoe IPDS2/2T diffractometers. All measurements were carried out at 100 K using a Mo-Kα X-ray source. The structures were solved by intrinsic Phase methods in SHELXT and refined by full-matrix-least-squares refinement against F^2 in SHELXL using the Olex2 user interface.[1] Methyl and methylene hydrogen atoms were added assuming ideal geometry on their carbon parent atom, with Ueq = n·Ueq (parent atom), n = 1.2 for methylene and 1.5 for methyl groups. Hydrogen atoms at hydrazone moieties were likewise added with n = 1.2. All structures are shown with thermal ellipsoids at 50% probability. Hydrogen atoms are omitted for clarity in the structure figures.

Crystal structure of 1·3 DCM

The highest peak of residual electron density on the difference Fourier map (2.00 $e^-/Å^3$) is found at 0.958 Å apart from Pd1. A fragment of the crystal structure of **1**·3 DCM is shown in Figure S1.

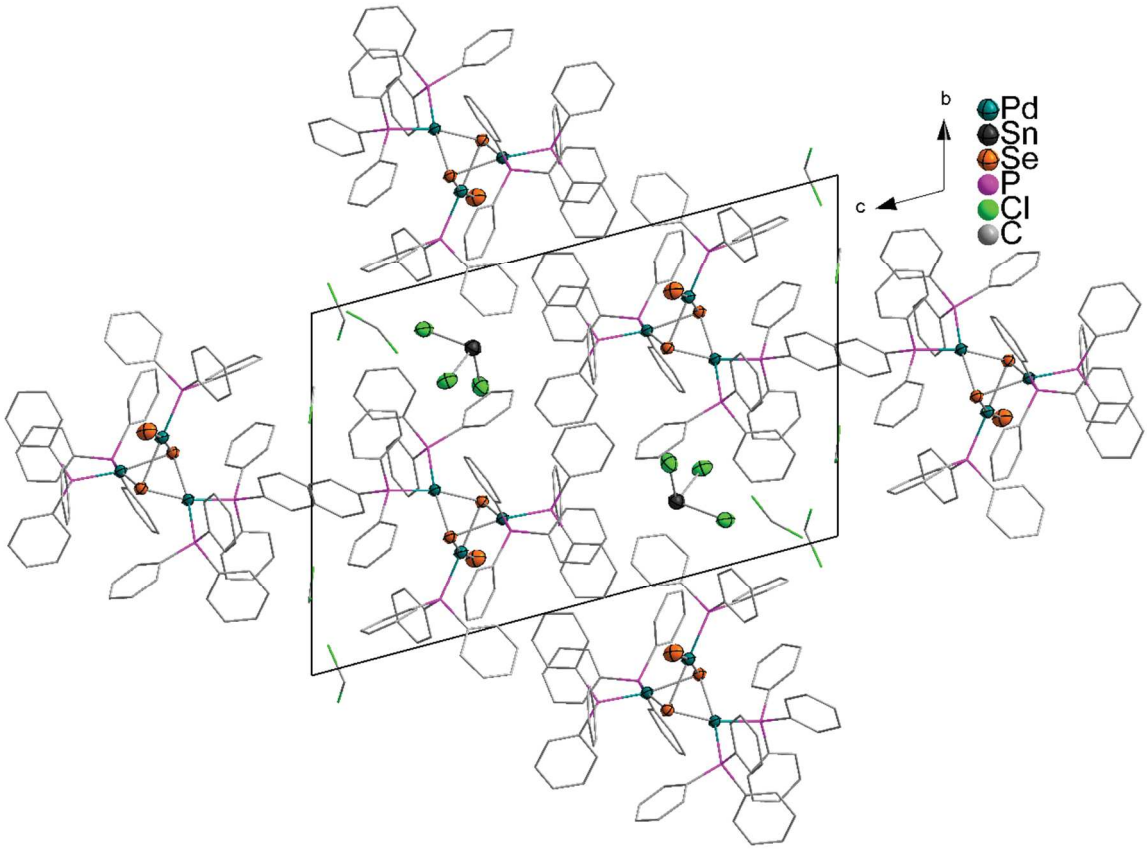

Figure S1: Fragment of the crystal structure of **1**·3 DCM viewed along the *a* axis.

Crystal structure of 2·2 DCM

The highest peak of residual electron density on the difference Fourier map (2.01 $e^{-}/Å^3$) is found at 1.573 Å apart from Cl4. A fragment of the crystal structure of **2**·2 DCM is shown in Figure S2.

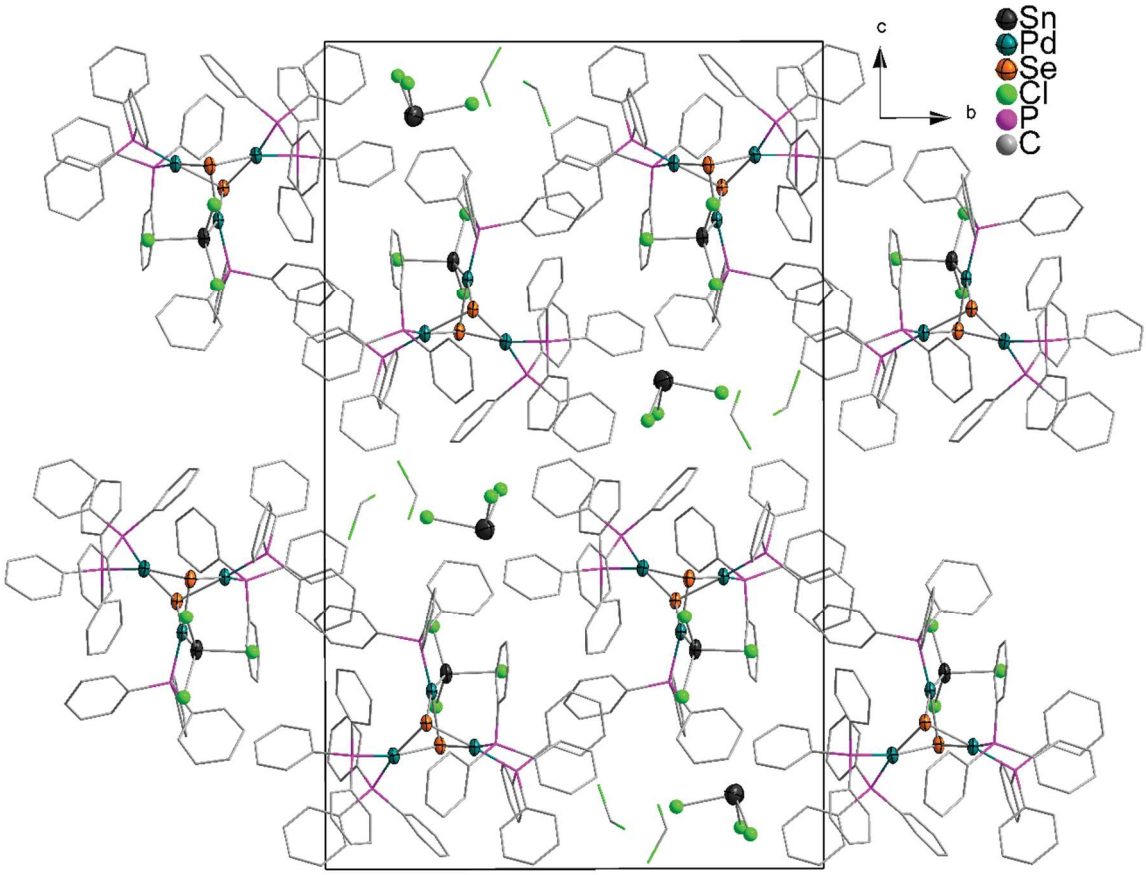

Figure S2: Fragment of the crystal structure of **2**·2 DCM viewed along the *a* axis.

Crystal structure of 3·DCM

The highest peak of residual electron density on the difference Fourier map (0.22 $e^{-}/Å^3$) is found at 1.106 Å apart from Pd1, on the bond between Pd1 and Se1. A fragment of the crystal structure of **3**·DCM is shown in Figure S3.

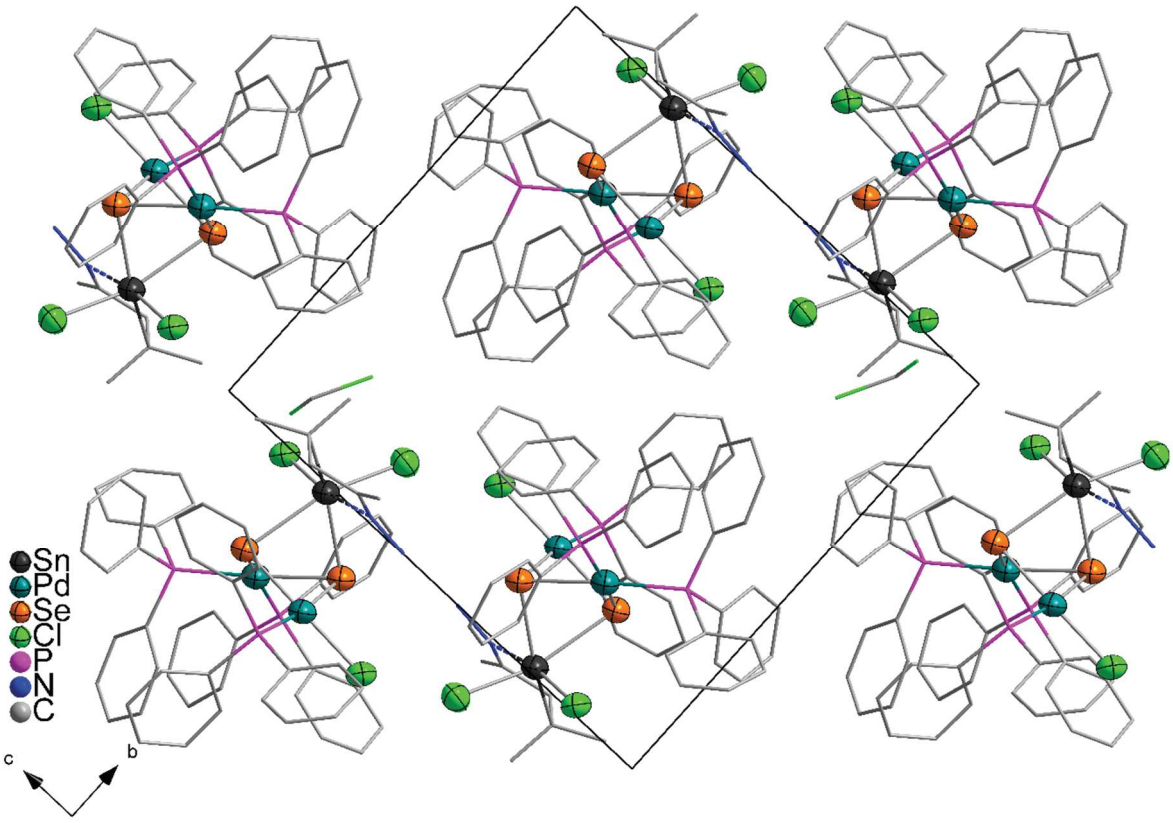

Figure S3: Fragment of the crystal structure of **3**·DCM viewed along the *a* axis.

Table S1. Selected distances and angles in **1** – **3**.

Distances [Å]	**1**·3 CH_2Cl_2	**2**·2 CH_2Cl_2	**3**·CH_2Cl_2	Angles [°]	**1**·3 CH_2Cl_2	**2**·2 CH_2Cl_2	**3**·CH_2Cl_2
Se1–Pd1	2.433(1)	2.442(2)	2.441(4)	Se1–Pd1–Se2	78.75(4)	77.89(5)	80.58(9)
Se1–Pd2	2.452(1)	2.456(2)	2.398(8)	Se1–Pd2–Se2	78.48(4)	78.28(5)	81.49(9)
Se1–Pd3	2.429(1)	2.435(2)		Se1–Pd3–Se2	78.54(4)	78.23(5)	
Se2–Pd1	2.439(1)	2.470(2)	2.481(3)	Se1–Sn1–Se2			72.08(8)
Se2–Pd2	2.433(1)	2.436(2)	2,478(3)	Pd1–Se1–Pd2	82.45(4)	80.80(5)	83.50(9)
Se2–Pd3	2.453(1)	2.459(2)		Pd1–Se1–Pd3	82.35(4)	82.32(5)	
Se1–Sn1			2.805(3)	Pd2–Se1–Pd3	87.73(4)	90.37(6)	
Se1–Sn2			2.598(3)	Sn1–Se1–Pd1			82.74(8)
Pd1–P1	2.285(3)	2.321(4)	2.296(6)	Sn1–Se1–Pd2			85.40(9)
Pd1–P2			2.342(8)	Pd1–Se2–Pd2	82.72(4)	80.63(5)	81.05(9)
Pd1–Se3	2.413(2)				81.74(4)	81,27(5)	
Pd1–Sn1		2.546(1)			87.61(4)	90.28(6)	
Pd2–P2	2.318(3)	2.331(4)		Sn1–Se2–Pd1			86.41(9)
Pd2–P3	2.330(3)	2.324(4)		Sn1–Se2–Pd2		2.291(7)	88.44(9)
Pd2–Cl1			2.368(5)	Se1–Pd1–Se3	90.81(5)		
Pd3–P4	2.319(3)	2.308(4)		Se2–Pd1–Se3	169.56(5)		
Pd3–P5	2.291(3)	2.324(4)		Se1–Pd1–Sn1		161.74(6)	
Sn1–Cl1		2.374(5)		Se2–Pd1–Sn1		84.95(5)	
Sn1–Cl2		2.374(4)	2.460(6)	Se1–Sn1–Cl2			164.6(2)
Sn1–Cl3		2.375(4)	2.499(5)	Se2–Sn1–C1			159.6(6)
Sn1–C1			2.19(3)	Cl3–Sn1–N1			170.6(5)
Sn1–N1			2.42(2)	Pd1–Pd2–Pd3	57.94(2)	57.57(3)	
Pd1–Pd2	3.219(1)	3.175(1)	3.222(3)	Pd1–Pd3–Pd2	58.47(2)	56.59(3)	
Pd1–Pd3	3.201(1)	3.210(1)		Pd2–Pd1–Pd3	63.58(2)	65.83(3)	
Pd2–Pd3	3.382(1)	3.470(1)		Pd1–Sn1–Pd2			54.65(5)
Se1–Se2	3.090(2)	3.088(2)	3.183(3)	Sn1–Pd1–Pd2			63.67(5)
				Sn1–Pd2–Pd1			61.68(5)

Table 1. Crystallographic data and refinement results of **1** – **3.**

Compound	**1**·3 CH_2Cl_2	**2**·2 CH_2Cl_2	**3**·CH_2Cl_2
Empirical formula	$C_{93}H_{81}Cl_9P_5Se_3SnPd_3$	$C_{92}H_{79}Cl_{10}P_5SeSnPd_3$	$C_{61}H_{60}Cl_5N_2P_3Se_2SnPd_2$
Fw / g·mol^{-1}	2347.24	2408.40	1580.68
Crystal color and shape	red block	red block	red block
Crystal size / mm^3	0.4×0.2×0.1	0.3x0.2x0.1	0.72×0.25×0.12
Crystal system	triclinic	monoclinic	triclinic
Space group	$P\bar{1}$	$P2_1/c$	$P\bar{1}$
a / Å	12.092(2)	12.4336(3)	14.089(3)
b / Å	16.031(3)	21.1025(6)	14.804(3)
c / Å	24.268(5)	35.0448(9)	16.264(3)
α / °	104.40(3)	90	83.64(3)
β / °	97.18(3)	92.466(2)	69.35(3)
γ / °	92.93(3)	90	74.62(3)
V / Å^3	4504.3(17)	9186.5(4)	3060.2(13)
Z	2	4	2
ρ_{calcd} / g·cm^{-3}	1.731	1.741	1.715
μ(Mo Kα) / mm^{-1}	2.477	2.328	2.513
Absorption correction type	numerical	numerical	numerical
min. / max. transmission	0.438 / 0.811	0.5480 / 0.7654	0.536 / 0.794
2 θ range / deg	2.632 / 50.994	5.038 / 42.998	2.75 / 52.58
no. of meas. Reflns	54968	45083	29851
R(int)	0.1167	0.1103	0.1816
Indep. Reflns	16768	10541	8964
Indep. Reflns (I > 2σ(I))	10744	7568	2592
no. of parameters	1027	1003	689
R1 (I > 2σ(I)) / wR2 (all data)	0.0776 / 0.2183	0.0909 / 0.2355	0.0821 / 0.1894
S (all data)	1.005	1.007	0.683
Max. peak / hole / e$^-$· Å^3	2.00 / –2.32	7.41 / –2.30	2.02 / –0.88

2. Mass Spectrometry

Multiple spectra from reactive solutions of with varying reactants and ratios and re-dissolved precipitates were taken using ESI^+ ionization method. All of them show signals that can be attributed to $[(Se_2Pd_3(PPh_3)_xCl]$ (x = 2, 3, and up to 4 in some spectra). Two exemplary spectra are shown in Figures S4 and S5.

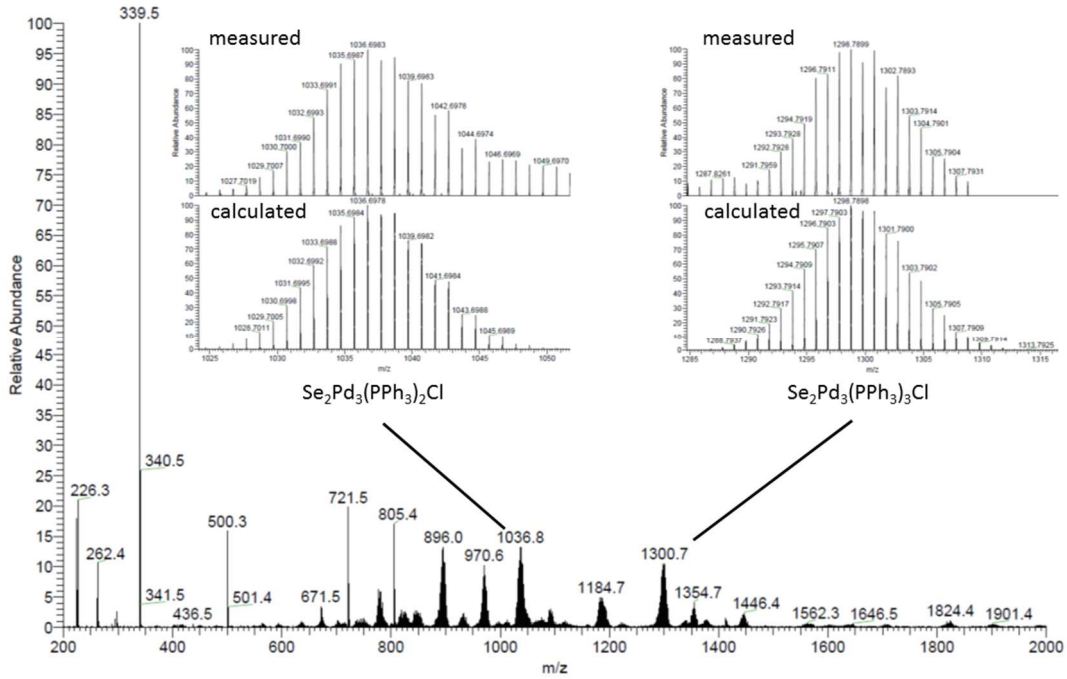

Figure S4: ESI^+ mass spectrum of the re-dissolved precipitate from a reaction of $[(SnR^1)_4Se_6]$ + 6 $[Pd(PPh_3)_2Cl_2]$ + 4 N_2H_4 H_2O.

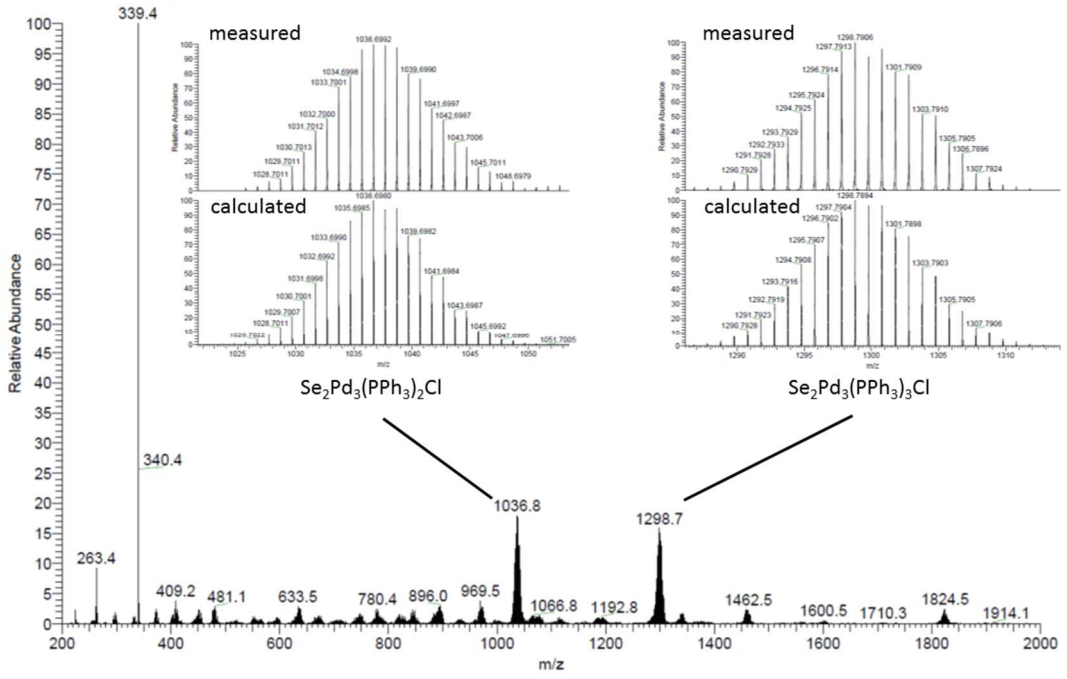

Figure S5: ESI^+ mass spectrum of a reactive mixture of $[(SnR^1)_3Se_4Cl]$ + 2 $[Pd(PPh_3)_2Cl_2]$.

3. Optical Spectroscopy

Absorption spectra in the solid state are obtained using a setup with all reflective optics to avoid chromatic aberrations. The sample in illuminated in transmission geometry using a standard tungsten-halogen source. The transmission is imaged by a 36x, 0.5 NA Schwarzschild reflective microscope objective. A pinhole (25 µm diameter) is placed in the image plane and used to select a nearly diffraction-limited spot on individual single crystals. The light transmitted through the pinhole is relayed onto the entrance slit of a grating monochromator where it is spectrally dispersed and detected by a thermoelectrically cooled scientific charge-coupled device camera (Roper Scientific, HAM 1024x128). To obtain information on the exact position of the measured spot, a removable beam splitter images a part of the light onto an additional camera.

Emission spectra are obtained in confocal geometry. The 100-fs pulses from a Ti:saphire laser oscillator are frequency doubled to 380 nm using a β-Bariumborate crystal. The sample is illuminated through a 36x 0.5 NA Schwarzschild reflective microscope objective and are collected in reflectance through the same optics. The emission is selected by a beam splitter and is focused on the entrance slit of a grating spectrometer after passing through a dielectric filter to eliminate scattered laser light. The light is detected by a cooled scientific CCD camera (Andor DU 440 BU). A removable mirror can be places between the focusing lens and the entrance slit of the spectrometer to image the sample on a CMOS camera for a direct image of the exciting laser spot on the sample. A spatial resolution of 10 µm is achieved, enough to excite individual crystals.

4. Literature

[1] a) G. M. Sheldrick, *Acta Crystallogr., Sect. A* **2015**, *71*, 3–8. b) G. M. Sheldrick, *Acta Crystallogr., Sect. C* **2015**, *71*, 3–8. c) O. V. Dolomanov, L. J. Bourhis, R. J. Gildea, J. A. K. Howard, H. Puschmann, *J. Appl. Crystallogr.* **2009**, *42*, 339–341.

3.5. Peptide – Functionalized Organotin Sulfide Clusters

Niklas Rinn, Jan-Philipp Berndt, Annikka Kreher, Radim Hrdina, Matthias Reinmuth, Peter R. Schreiner, Stefanie Dehnen, *Organometallics*, **2016**, *35* (18), 3215-3220.

Abstract: We report the first successful attachment of peptides to tin sulfide clusters. For proof of principle, H-L-Phe hydrazide and Boc-protected dipeptide hydrazides (Boc-L-Ala-L-Ala hydrazide and Boc-L-Val-L-Phe hydrazide) were reacted with keto-functionalized tin sulfide clusters $[(R^1Sn)_4S_6]$ (**A**; R^1 = $CMe_2CH_2C(O)Me$) and $[(R^1Sn)_3S_4Cl]$ (**B**). In the first case, we obtained single crystals of an amino acid functionalized Sn/S cluster, $[R^2{}_2Sn_4S_5]$ (**1**; R^2 = $(CMe_2CH_2C(Me)\text{-}N_2C(O)CH(CH_2Ph)NC(Me)CH_2CMe_2)$, formed after inorganic cluster rearrangement and intramolecular condensation of the amino acid ligand. By means of NMR spectroscopic investigations and ESI/LIFDI mass spectrometry, we demonstrate that both dipeptides are attached to **B** under retention of the original cluster architecture to yield $[(R^3Sn)_3S_4Cl]$ (**2**; R^3 = $CMe_2CH_2C(NNH\text{-}Ala\text{-}Ala\text{-}Boc)Me$) and $[(R^4Sn)_3S_4Cl]$ (**3**; R^4 = CMe2CH2C(NNH-Phe-Val-Boc)Me), as evident from mass spectrometric data of their cations $[(R^3Sn)_3S_4]^+$ (**2**$^+$) and $[(R^4Sn)_3S_4]^+$ (**3**$^+$).

Inhaltsangabe: Keto-funktionalisierte Zinnsulfidcluster wurden mit Phenylalaninhydrazid und Dipeptidhydraziden umgesetzt. Hierbei bildete sich in einer Reaktion des DD-Typ-Clusters $[(SnR^1)_4S_6]$ mit Phenylalaninhydrazid nach langsamem Verdampfen des Lösungsmittels die Verbindung $[R^{Phe}{}_2Sn_4S_5]$ (**1**; R^{Phe} = $(CMe_2CH_2C(Me)\text{-}N_2C(O)CH(CH_2Ph)NC(Me)CH_2CMe_2)$ mit einer durch Einkristallstrukturanalyse bestimmten neuartigen Clustertopologie (siehe Abbildung 3.5). Eine weitere Umsetzung von $[(SnR^1)_4S_6]$ oder der DHK-Typ-Verbindung $[(SnR^1)_3S_4Cl]$ mit dem Dipeptidhydrazid Boc-L-Ala-L-Ala-Hydrazid führte jeweils zum gleichen Produkt mit DHK-Typ-Topologie $[(SnR^{Ala})_3S_4Cl]$ (**2**; R^{ala} = $CMe_2CH_2C(NNH\text{-}Ala\text{-}Ala\text{-}Boc)Me$) (Boc = *tert*-Butyloxycarbonyl; Ala = Alanin). Diese Verbindung konnte NMR-spektroskopisch und als Kation $[(SnR^{Ala})_3S_4]^+$ (**2**$^+$) auch massenspektrometrisch nachgewiesen werden. Eine analoge Reaktion ließ sich mit $[(SnR^1)_3S_4Cl]$ und Boc-L-Val-L-Phe-Hydrazid (Val = Valin; Phe = Phenylalanin) realisieren, wobei das Produkt $[(R^{Val}Sn)_3S_4Cl]$ (**3**; R^{val} = CMe2CH2C(NNH-Phe-Val-Boc)Me) ebenfalls durch NMR-Spektroskopie und als Kation **3**$^+$ massenspektrometrisch nachgewiesen werden konnte.

Eigener Anteil: Ich habe in Kooperation mit Stefanie Dehnen und Jan-Philipp Berndt das Manuskript verfasst. Weitere Co-Autoren haben jeweils kurze Abschnitte über ihre Beiträge eingefügt oder die von uns vorgeschlagenen Abschnitte dazu überarbeitet. Zudem war ich bei der Charakterisierung von **1** sowie bei der Synthese und Charakterisierung von **2** und **3** beratend tätig. Verbindung **1** wurde von Matthias Reinmuth synthetisiert und charakterisiert. Die Verbindungen **2** und **3** wurden unter meiner Anleitung von Annikka Kreher dargestellt und charakterisiert. Hierbei wurden alle massenspektrometrischen Experimente von der zentralen Abteilung für Massenspektrometrie und Elementaranalyse der Philipps-Universität Marburg durchgeführt. Die Dipeptid-Liganden Boc-L-Ala-L-Ala-Hydrazid und Boc-L-Val-L-Phe-Hydrazid wurden von Jan-Philipp Berndt synthetisiert und weiter charakterisiert.

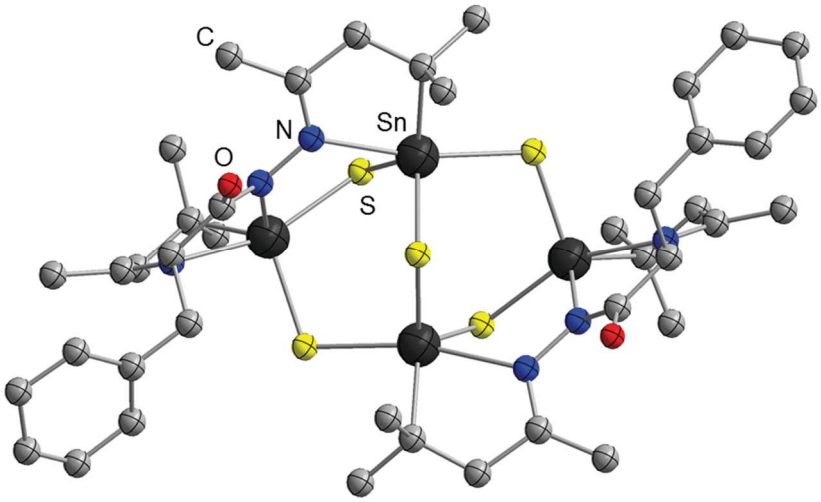

Abbildung 3.5: Molekülstruktur des Clusters [$R^{Phe}_2Sn_4S_5$] aus „Peptide-Functionalized Organotin Sulfide Clusters". Wasserstoffatome wurden aus Übersichtlichkeitsgründen nicht angezeigt.

ORGANOMETALLICS

Article

pubs.acs.org/Organometallics

Peptide-Functionalized Organotin Sulfide Clusters

Niklas Rinn,[§] Jan-Philipp Berndt,[‡] Annikka Kreher,[§] Radim Hrdina,[‡] Matthias Reinmuth,[§] Peter R. Schreiner,[‡] and Stefanie Dehnen*[,§]

[§]Department of Chemistry and Wissenschaftliches Zentrum für Materialwissenschaften (WZMW), Philipps-Universität Marburg, 35037 Marburg, Germany

[‡]Institute of Organic Chemistry, Justus-Liebig University, Heinrich-Buff-Ring 17, 35392 Giessen, Germany

Supporting Information

ABSTRACT: We report the first successful attachment of peptides to tin sulfide clusters. For proof of principle, H-L-Phe hydrazide and Boc-protected dipeptide hydrazides (Boc-L-Ala-L-Ala hydrazide and Boc-L-Val-L-Phe hydrazide) were reacted with keto-functionalized tin sulfide clusters $[(R^1Sn)_4S_6]$ (**A**; R^1 = $CMe_2CH_2C(O)Me$) and $[(R^1Sn)_3S_4Cl]$ (**B**). In the first case, we obtained single crystals of an amino acid functionalized Sn/S cluster, $[R^2{}_2Sn_4S_5]$ (**1**; R^2 = $(CMe_2CH_2C(Me)N_2C(O)CH(CH_2Ph)NC(Me)CH_2CMe_2)$, formed after inorganic cluster rearrangement and intramolecular condensation of the amino acid ligand. By means of NMR spectroscopic investigations and ESI/LIFDI mass spectrometry, we demonstrate that both dipeptides are attached to **B** under retention of the original cluster architecture to yield $[(R^3Sn)_3S_4Cl]$ (**2**; R^3 = $CMe_2CH_2C(NNH\text{-}Ala\text{-}Ala\text{-}Boc)Me$) and $[(R^4Sn)_3S_4Cl]$ (**3**; R^4 = $CMe_2CH_2C(NNH\text{-}Phe\text{-}Val\text{-}Boc)Me$), as evident from mass spectrometric data of their cations $[(R^3Sn)_3S_4]^+$ (**2**$^+$) and $[(R^4Sn)_3S_4]^+$ (**3**$^+$).

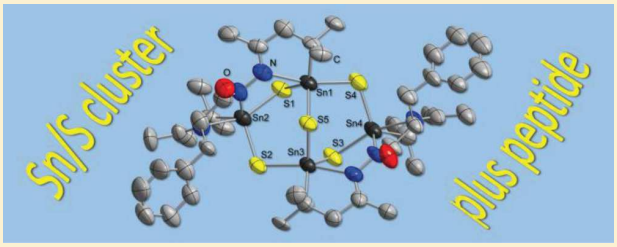

INTRODUCTION

The formation of hybrid compounds that exhibit biopatterns attached to inorganic clusters or nanoparticles are attractive due to the combination of the optoelectronic properties of the inorganic (semimetal) cores with that of the organic decoration featuring molecular interaction patterns (including chiral information), fluorescence, or further reactivity or that affect the overall cluster or particle solubility. Previous reports include the use of transition metal clusters as fluorophores for biological imaging[1−4] and biotemplating of semiconductor nanoparticles for a vast variety of applications.[5−7] The coordination behavior of amino acids as ligands on heteroatomic clusters has been examined for several lanthanide,[8,9] transition metals,[10−13] and transition metal chalcogenides,[14,15] as well as for a few bismuth oxo-clusters.[16]

As a particular class of heteroatomic systems, which has also been studied extensively in cluster chemistry,[17−19] tin chalcogenides are desirable materials owing to their semi- or ion-conductivity[20−22] and the catalytic activity of related nanosized particles.[21,23] The properties of nanosized tin chalcogenide particles and clusters can be further varied by the presence of organic ligands, regarding both the physical and chemical properties and their bioactivity. The latter ranges from the high toxicity of triorganotin compounds[24] that allows for applications as fungicides[25] and insecticides,[26] through the secondary effect of their environmental abundance, for instance, on the cardiovascular activity in mammals,[27] to antitumor applications that were explored for mono- or multinuclear organotin compounds.[28−30]

Notably, to date no attempts have been made to tune both biocompatibility and bioactivity of tin chalcogenide clusters by their functionalization with biomolecules. If this was realized, then a specific delivery of the polar and potentially hydrolyzable tin chalcogenide moieties into cells would come into sight for targeted use as enzyme inhibitors or cytotoxic agents.

Based on our experience with the organic functionalization of tin chalcogenide complexes and clusters,[31−42] we are currently investigating the attachment of biomolecules to Sn/E scaffolds (E = S, Se, and Te) by condensation reactions with a pre-existing ligand shell. As a first proof of principle, we herein present our most recent results that indicate the successful introduction of amino acid and dipeptide molecules to medium-sized Sn/S clusters, starting from organo-functionalized clusters $[(R^1Sn)_4S_6]$ (**A**; R^1 = $CMe_2CH_2C(O)Me$)[35] and $[(R^1Sn)_3S_4Cl]$ (**B**).[34]

RESULTS AND DISCUSSION

Keto-functionalized tin sulfide cluster **A** was reacted with phenylalanine hydrazide in a 1:4 ratio. Upon removal of the solvent *in vacuo*, a white powder formed that could be redissolved in larger amounts of $CHCl_3$. Upon slow evaporation of the solvent, we obtained single crystals of $[R^2{}_2Sn_4S_5]$ (**1**; R^2 = $(CMe_2CH_2C(Me)N_2C(O)CH(CH_2Ph)NC(Me)CH_2CMe_2)$, as outlined in Scheme 1. According to single-crystal X-ray diffraction and structure analysis, the

Received: July 14, 2016
Published: September 7, 2016

DOI: 10.1021/acs.organomet.6b00561
Organometallics 2016, 35, 3215−3220

Scheme 1. Synthesis of 1 by Reaction of Organotin Sulfide Cluster A with Phenylalanine Hydrazide in a 1:4 Ratio

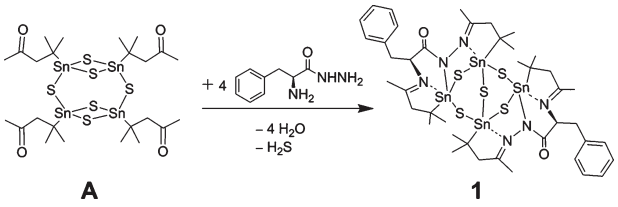

inorganic cluster core underwent an unprecedented rearrangement during the formation of **1**. Furthermore, the hydrazide groups of the phenylalanine hydrazide reacted with two of the four keto groups of the original R^1 ligands via hydrazone formation, whereas the two other keto groups were involved in an imine formation with the amino functionalities of the two amino acid molecules.

We assume that this reaction occurring under additional release of one equivalent of H_2S competes with the formation of "$[(R^{2a}Sn)_4S_6]$" [R^{2a} = $(CMe_2CH_2C(Me)NNHC(O)CH(NH_2)CH_2Ph)$] which we originally expected to be the product of the simple 1:4 condensation reaction. NMR studies of the redissolved white powder indeed indicated the formation of the latter, as we observed only one signal at δ = −99.36 ppm, in accordance with the reported chemical shift of another hydrazide-functionalized Sn_4S_6 cluster.[43] However, this compound did not crystallize, presumably owing to the high flexibility of the rather extended organic ligands. In contrast, the solubility and hence concentration of **1** is apparently too low to allow for its detection via NMR, but due to its rigid ligand environment, this compound crystallizes. The molecular structure of **1** is shown in Figure 1; the arrangement of the molecules within the unit cell is illustrated in Figure S1.

Compound **1** crystallizes in the orthorhombic space group $P2_12_12_1$. The unit cell contains a large amount of crystal water, of which only three molecules were unambiguously located during the structure refinement, whereas the others had to be modeled using the SQUEEZE routine in SHELXL (see Experimental Section and Supporting Information). The inorganic core underwent a rearrangement into a *pseudo*-C_2-symmetric bicyclic system of two six-membered $[Sn_3S_3]$ rings that share a common Sn_2S unit. Owing to the condensation reaction of the hydrazine and amine moieties of the amino acid with two of the keto groups each of the ligands at the tin atoms, Sn1 and Sn2 as well as Sn3 and Sn4 are connected through organic bridges. All Sn atoms show a distorted trigonal bipyramidal coordination environment by one S and one N atom in the axial positions and another three atoms (S, S, and C at Sn1 and Sn3; S, N, and C at Sn2 and Sn4) in equatorial positions. All sulfur atoms act as μ^2-bridges between Sn atoms. A detailed view of the ligand situation at Sn1 and Sn2, as an example, is presented in Figure 2.

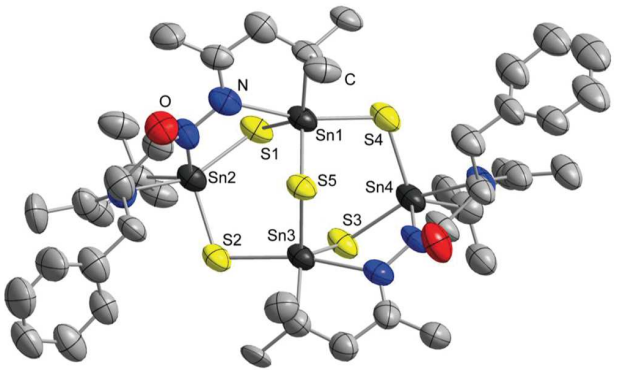

Figure 1. Molecular structure of **1**. Ellipsoids are drawn at 50% probability, and hydrogen atoms were omitted for clarity. Ranges of selected bond lengths and angles [Å; °]: Sn(1,3)−S 2.396(4)−2.500(4), Sn(2,4)−S 2.365(4)−2.449(4), Sn(1,3)−C 2.20(1)−2.21(2), Sn(2,4)−C 2.16(2)−2.19(2), Sn(1,3)···N 2.35(1)−2.39(1), Sn(2,4)···N 2.14(1)−2.30(1); Sn−S(1,2,3,4)−Sn 98.8(1)−107.5(1), Sn−S5−Sn 105.8(1), S−Sn−S 101.6(1)−114.6(1), S−Sn−C 96.0(4)−126.4(4), S−Sn···N 80.8(3)−168.6(3), C−Sn···N 72.6(5)−121.6(6).

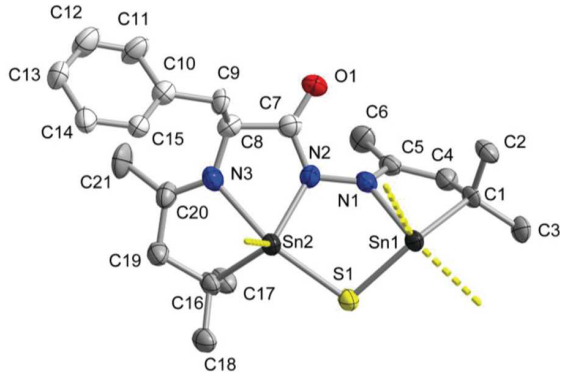

Figure 2. Fragment of the molecular structure of compound **1** with emphasis on the organic ligand. For clarity, thermal ellipsoids are drawn at the 25% probability level; hydrogen atoms were omitted for clarity. C atoms that belong to the phenylalanine unit are drawn in a lighter gray color than those of the original R^1 ligands. Further Sn−S bonds at the tin atoms are indicated by dashed yellow lines.

Sn−S distances range from 2.365(4) to 2.500(4) Å, with the longest distances (Sn1−S4, Sn3−S2, Sn2−S1, and Sn4−S3) found in the *trans*-position of N atoms. Accordingly, the corresponding angles tend toward linearity for N1−Sn1−S4 (167.3(3)°), N4−Sn3−S2 (168.6(3)°), N3−Sn2−S1 (156.7(4)°), and N6−Sn4−S3 (159.7(4)°), with the more acute angles correlating with shorter Sn−S bonds. The Sn−S−Sn angles range from 98.7(1) to 108.9(1)°, with the smallest angles Sn1−S1−Sn2 (98.7(1)°) and Sn3−S3−Sn4 (99.5(1)°) being part of the five-membered ring formed by coordination of the hydrazone moieties to two tin atoms.

Both organic ligands are oriented toward the same side of the cluster in a pseudo-*cis* conformation. The Sn···N distances range from 2.14(1) Å (Sn−$N_{hydrazone}$ bond) to 2.40(1) and 2.35(1) Å (Sn···N_{amine} contact in axial positions). The hydrazide derivative of **A**, $[(R^NSn)_4S_6]$ ($\mathbf{A^N}$; R^N = $CMe_2CH_2C(Me)NNH_2$),[44] shows a very similar range of Sn−S distances (2.391(2) to 2.514(2) Å), with the longer bonds opposite of the Sn···N interactions with the hydrazone groups. The Sn−S angles in $\mathbf{A^N}$ are more acute within the planar four-membered Sn−S−Sn−S rings (88.67(7)−89.17(7)°) than those in **1**, even more acute than Sn1−S1−Sn2 or Sn3−S3−Sn4 in **1**, while the angles at the bridging S atoms between the four-membered rings in $\mathbf{A^N}$ are quite similar to the angles between unbridged Sn atoms in **1**. The Sn···hydrazone distances in $\mathbf{A^N}$ are significantly longer (2.454(6)−2.470(6) Å) when compared to

DOI: 10.1021/acs.organomet.6b00561
Organometallics 2016, 35, 3215−3220

Scheme 2. Treatment of Organotin Sulfide Cluster A with Boc-Protected Hydrazine Dipeptide Derivatives Boc-L-Ala-L-Ala-N_2H_3 (C) in $CHCl_3$ (1:4, top) or Treatment of Cluster B with C or Boc-L-Val-L-Phe-N_2H_3 (4) in CH_2Cl_2 (1:3, bottom) to Afford Clusters 2^+ and 3^+

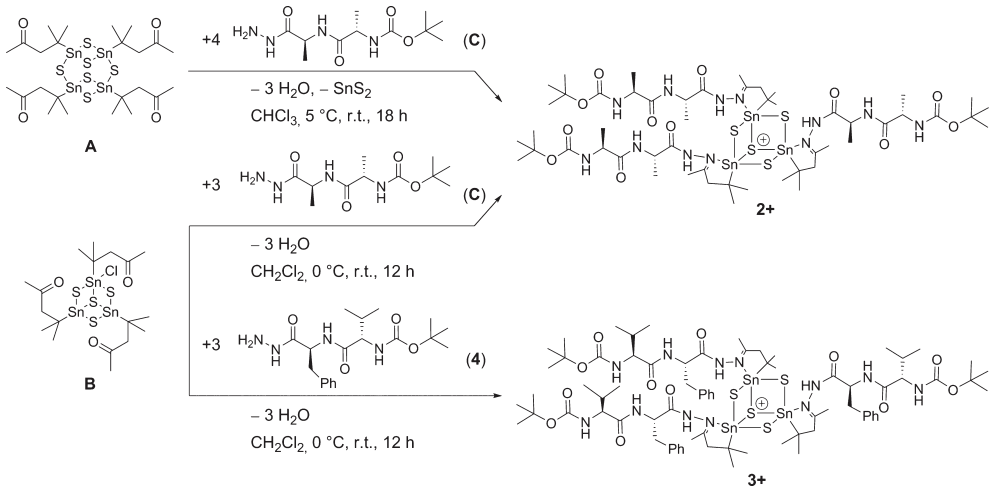

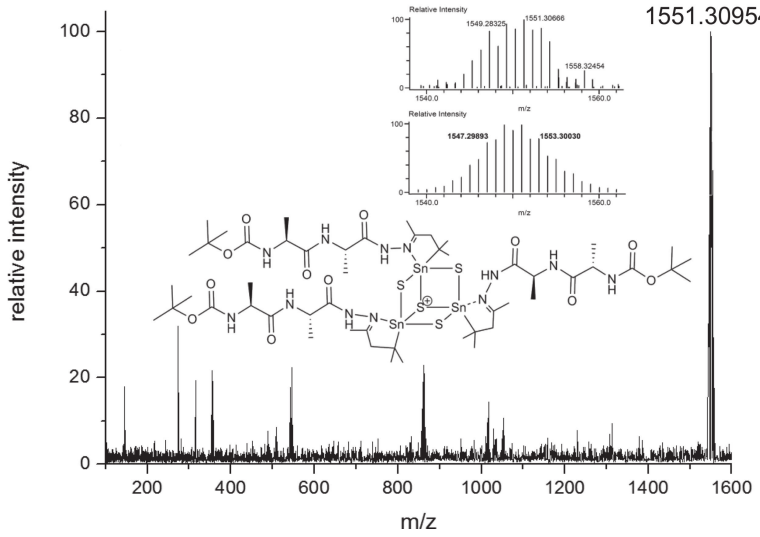

Figure 3. LIFDI(+) mass spectrum of the product obtained from the reaction of **B** with **C**, investigated as fresh solution in CH_2Cl_2. The major product, $\mathbf{2}^+$, is found at m/z 1551.3, according to $[Sn_3S_4C_{51}H_{93}N_{12}O_{12}]^+$ (see simulation in the inset).

those in **1**, most likely due to the intramolecular condensation of the hydrazone to two tin atoms in **1**.

However, with the long-term goal to bring the Sn/S clusters into the environment of a biomolecule, for instance, by peptide formation starting from the amino acid functionalized cluster, the amino function needs to be retained. Ongoing research is therefore currently undertaken with Boc-protected amino acids.

In a parallel study, we tested the utilization of Boc-protected hydrazine derivatives of dipeptides for integration into the ligand shell of organotin sulfide clusters. Although single crystals were not obtained from these reactions, we could prove the successful attachment of the dipeptide units by mass spectrometry and NMR spectroscopy. Scheme 2 illustrates the corresponding reactions that are described and discussed in detail below.

Upon reaction of **A** with Boc-L-Ala-L-Ala-N_2H_3 (**C**) in a 1:4 ratio in $CHCl_3$ and removal of the solvent *in vacuo*, one obtains a white powder that is soluble in dichloromethane. Electrospray ionization (ESI) mass spectrometry indicates a mixture of clusters with either the original $[Sn_4S_6]$ moiety (minority) or a $[Sn_3S_4]$ unit (predominant), both possessing three organic ligands. Although the minority component indeed represents the desired extension of **A**, upon loss of a ligand, major component $[(R^3Sn)_3S_4]^+$ ($\mathbf{2}^+$; R^3= CMe_2CH_2C(NNH-L-Ala-L-Ala-Boc)Me) may be viewed as a derivative of the first upon loss of 1 equiv of SnS_2 (Figure S2). As the product mixtures thus contain considerable amounts of the cluster with an $[Sn_3S_4]$ core, we performed the reactions directly starting out from **B** that possesses this very tin sulfide scaffold. Upon reaction of **B** with 3 equiv of **C** in CH_2Cl_2, liquid injection field desorption ionization (LIFDI) mass spectrometry shows a signal that is in agreement with the m/z value of the cationic derivative of targeted product $[(R^3Sn)_3S_4]^+$ ($\mathbf{2}^+$; Figure 3). Signals of relatively smaller abundance (below 30% relative intensity) hint at partial decomposition of **2** under mass spectrometry conditions.

DOI: 10.1021/acs.organomet.6b00561
Organometallics 2016, 35, 3215–3220

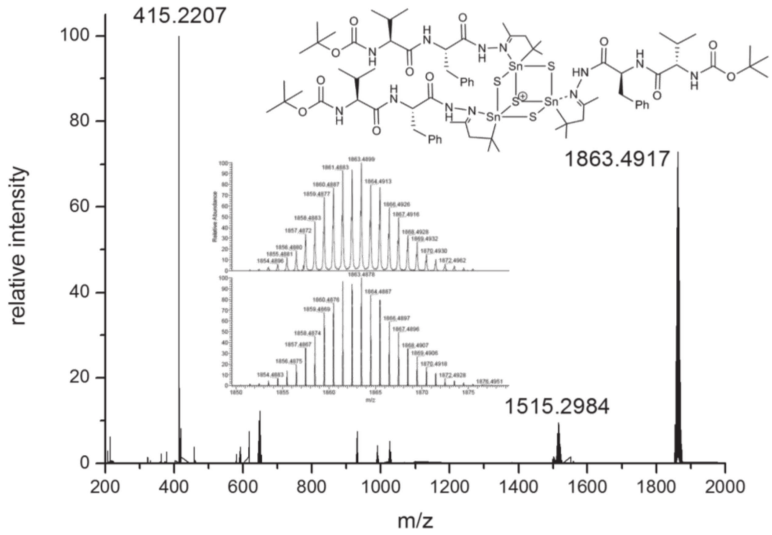

Figure 4. ESI(+) mass spectrum of the product obtained from the reaction of **B** with **4**, investigated as fresh solution in CH_2Cl_2. Major product $\mathbf{3}^+$ is found at m/z 1863.5, according to $[Sn_3S_4C_{75}H_{117}N_{12}O_{12}]^+$ (see simulation in the inset). The smaller peak at m/z 1515.3 $[Sn_3S_4C_{56}H_{91}N_{10}O_8]^+$ is in accord with a fragment of $\mathbf{3}^+$ upon loss of one of the peptide ligands under retention of the hydrazone moiety (the larger signal at 415.2 is a $K_1C_{18}H_{36}N_2O_6^+$ residue that is trapped in the spectrometer upon previous measurements of samples of our colleagues).

2D HMQC NMR measurements prior to the MS experiment indicated that fragmentation does not occur in solution, and ^{1}H NMR spectroscopy points to the presence of a chloride ligand at one of the tin moieties: Smaller signals with half integral intensity were found next to the signals for the CH_2 and C(NR)CH_3 groups, respectively, reflecting the influence of the chloride ligand on the chemical shift values of one of the ligands. In the ^{119}Sn NMR spectrum, one obtains a broad signal at −112 ppm, which is asymmetric due to a smaller shoulder to the high field, in agreement with the known, very slight difference of the ^{119}Sn chemical shifts observed for $[(RSn)_3S_4Cl]$ clusters like **B** and its derivatives.[34] All data hence correspond with the presence of neutral **2**, $[(R^3Sn)_3S_4Cl]$, in solution. The NMR spectra are provided in the Supporting Information. Similar results were obtained in a reaction of **B** with Boc-L-Val-L-Phe-N_2H_3 (**4**; 1:3 in CH_2Cl_2) to form $[(R^4Sn)_3S_4Cl]$ (**3**; R^4 = CMe_2CH_2C(NNH-L-Ala-L-Ala-Boc)Me; Figure 4).

Again, the NMR data strongly suggest the presence of a chloride ligand and thus of neutral **3** in solution (see the Supporting Information). We are currently exploring the possibility to grow crystals of **2** or **3** to study their solid-state structures.

CONCLUSIONS

Reactions between organotin sulfide clusters and hydrazide derivatives of phenylalanine and Boc-protected dipeptides led to an attachment of the latter to different Sn/S cluster units, namely, $[Sn_4S_5]$, $[Sn_4S_6]$, and $[Sn_3S_4]$. The amine group of the unprotected phenylalanine derivative underwent condensation with $[(R^1Sn)_4S_6]$ (**A**; R^1 = CMe_2CH_2C(O)Me) cluster precursor, hence not being available for further peptide growth on the cluster. Consequently, future work will be dealing with the Boc-protected derivatives that proved to be useful and promising in the second part of the study. Here, **C** and **4** were successfully reacted with **B** and attached to its organic ligand, as demonstrated by means of mass spectrometry and NMR spectroscopy.

EXPERIMENTAL SECTION

Syntheses. *General.* All manipulations were performed under an argon atmosphere. All solvents were dried and freshly distilled prior to use. Dipeptides Boc-L-Ala-L-Ala-OMe **C** and Boc-L-Val-L-Phe-OMe **4** were prepared according to liquid-phase peptide synthesis. Analytical data are in agreement with literature.[45,46]

*Synthesis of $[R^2{}_2Sn_4S_5]$ (**1**).* First, 0.072 g of phenylalanine hydrazide (0.402 mmol) was dissolved in 10 mL of $CHCl_3$ and added dropwise to a solution of 0.105 g of **A** (0.099 mmol) in 10 mL of $CHCl_3$ at −5 °C. The reaction mixture was warmed to room temperature and stirred for 18 h. The solvent was removed *in vacuo* to afford a white powder. The product was redissolved in of $CHCl_3$. By slow solvent evaporation, few crystals of **1** could be obtained after 2 weeks.

*Synthesis of $[(R^3Sn)_3S_4Cl]$ (**2**).* First, 0.100 g of **B** (0.122 mmol) was dissolved in 10 mL of CH_2Cl_2 and added to a solution of 0.999 g of **C** (0.367 mmol) in 6 mL of CH_2Cl_2 at 0 °C. The solution was stirred for 12 h at room temperature. The solvent was removed *in vacuo* to afford a white powder. The reaction was quantitative.

^{1}H NMR (300 MHz, $CDCl_3$) δ = 1.3−1.5 (m, 63H, Me), 1.95 (s, 6H, C(NNHR)CH_3), 2.05 (s, 3H, C(NNHR)CH_3 @SnCl), 2.74 (s, 4H, CH_2), 2.83 (s, 2H, CH_2 @SnCl), 4.20 (m, 3H, C*H*), 4.68 (m, 3H, C*H*), 5.60 (d, 3H, NH, ^3J = 19 Hz), 7.36 (d, 3H, N*H*, ^3J = 26 Hz), 9.90 (br s, 3H, NN*H*) ppm; ^{13}C NMR (75 MHz, $CDCl_3$) δ = 18.18 (SnCMe_2), 18.53 (ClSnCMe_2), 21.63 (C(NNR)*Me*), 26.12 (Me-Ala), 26.90 (Me-Ala), 28.46 (Boc Me), 47.93 (*CH*), 48.52 (*CH*), 50.35 (SnC(Me$_2$)CH_2), 50.66 (ClSnC(Me$_2$)CH_2), 80.11 (SnC), 80.37 (ClSn*C*), 155.64 (C_{quart}), 168.60 (C_{quart}), 173.35 (C_{quart}), 173.68 (C_{quart}) ppm; ^{119}Sn NMR (187 MHz, CD_2Cl_2) δ = −112 ppm (br, s).

HRMS (LIFDI+) m/z calcd: 1553.29847 $[M - Cl]^+$. Found: 1553.29848.

Anal. Calcd for $C_{51}H_{93}O_{12}N_{12}S_4Sn_3Cl$: C, 38.62; H, 5.91; N, 10.60; S, 8.08. Found: C, 38.31; H, 5.96; N, 10.53; S, 8.06.

*Synthesis of $[(R^4Sn)_3S_4Cl]$ (**3**).* First, 0.100 g of **B** (0.122 mmol) was dissolved in 10 mL of CH_2Cl_2 and added to a solution of 0.139 g of **4** (0.367 mmol) in 6 mL of CH_2Cl_2 at 0 °C. The solution was stirred for 12 h at room temperature. The solvent was removed *in vacuo* to quatitatively afford a white powder.

^{1}H NMR (300 MHz, $CDCl_3$) δ = 0.82 (m, 18H, SnCMe_2), 1.42 (s, 45H, OCMe_3 and $CHMe_2$), 1.87 (m, 3H, *CH*Me$_2$), 1.94 (s, 6H, C(NNHR)CH_3), 2.09 (s, 3H, C(NNHR)CH_3 @SnCl), 2.74 (m, 6H, CH_2Ph), 2.88 (s, 2H, ClSnC(Me$_2$)CH_2), 3.21 (s, 4H, SnC(Me$_2$)CH_2),

DOI: 10.1021/acs.organomet.6b00561
Organometallics 2016, 35, 3215−3220

3.95 (d, 3H, NC*H* Val, ^3J = 42 Hz), 5.03 (d, 3H, NC*H* Phe, ^3J = 22 Hz), 6.74 (br s, 3H, N*H*), 7.22 (m, 15H, Ph), 7.64 (br s, 3H, N*H*), 9.94 (br s, 3H, NN*H*) ppm; ^{13}C NMR (75 MHz, $CDCl_3$) δ = 19.4 (SnC*Me*$_2$), 19.5 (ClSnC*Me*$_2$), 19.7 (C(NNR)*Me* @SnCl), 21.7 (C(NNR)*Me*), 28.0 (CH*Me*$_2$), 28.5−28.6 (Boc Me), 38.0 (SnC-(Me$_2$)C*H*$_2$), 50.6 (*CH*$_2$Ph), 54.0 (NC*H* Phe), 60.4 (NC*H* Val), 127.0−129.7 (Ph), 133.1 (C$_{quart}$), 135.4 (C$_{quart}$), 156.1 (C$_{quart}$) ppm; ^{119}Sn NMR (187 MHz, CD_2Cl_2) δ = −112 ppm (br, s).

HRMS (ESI+) m/z calcd: 1863.4878 [M − Cl]$^+$. Found: 1863.4899.

Anal. Calcd for $C_{75}H_{117}O_{12}N_{12}S_4Sn_3Cl$: C, 47.45; H, 6.21; N, 8.85; S, 6.75. Found: C, 47.06; H, 6.27; N, 8.79; S, 6.71.

*Synthesis of Boc-L-Ala-L-Ala-N$_2$H$_3$ (**C**).* First, 1.00 g (3.65 mmol) of dipeptide Boc-L-Ala-L-Ala-OMe, 0.355 mL (7.30 mmol) of $(NH_2)_2\cdot H_2O$, and 1.83 mL of MeOH were stirred for 18 h at 25 °C. After evaporation of the solvent, 0.987 g of (3.60 mmol, 99%) of a colorless solid of **C** was obtained and characterized.

^{1}H NMR (200 MHz, DMSO-d_6) δ = 1.19−1.12 (m, 6 C*H*$_3$-Ala), 1.37 (s, 9H, C*H*$_3$-Boc), 3.94 (quint, 1H, J = 6.9 Hz), 4.30−4.16 (m, 3H), 6.96 (d, 1H, J = 7.4 Hz), 7.81 (d, 1H, J = 7.7 Hz), 9.05 (br s, 1H) ppm; ^{13}C NMR (101 MHz, DMSO-d_6) δ = 18.0, 18.7, 28.2, 46.7, 49.7, 78.2, 155.2, 171.5, 172.2 ppm.

HRMS (ESI) m/z = 297.1539 [M + Na$^+$]$^+$ (calcd for $C_{11}H_{22}N_4O_4Na^+$ 297.1533).

IR (ATR) $\tilde{\nu}$ (cm^{-1}) = 3291, 3066, 2981, 2931, 1694, 1672, 1641, 1614, 1522, 1448, 1390, 1364, 1274, 1255, 1228, 1166, 1094, 1055, 1030, 972, 910, 861, 780, 668, 647, 582.

Reported analytical data are in agreement.[47,48]

*Synthesis of Boc-L-Val-L-Phe-N$_2$H$_3$ (**4**).* First, 1.38 g (3.64 mmol) of dipeptide Boc-L-Val-L-Phe-OMe, 0.72 mL (14.8 mmol) of $(NH_2)_2\cdot H_2O$, and 4 mL of MeOH were stirred for 18 h at 25 °C. After evaporation of the solvent, 1.47 g (3.64 mmol, >99%) of a colorless solid of **4** was obtained and fully characterized.

R_f = 0.71 (CH_2Cl_2/MeOH, 10:1).

^{1}H NMR (400 MHz, DMSO-d_6, Figure S9) δ = 0.65−0.71 (m, 6H), 1.38 (br s, 9H), 1.74−1.84 (m, 1H, C*H*-Val), 2.76−2.94 (m, 2H), 3.72 (t, 1H), 4.18 (br s, 2H), 4.47−4.54 (m, 1H), 6.66 (d, 1H, J = 9.0 Hz), 7.14−7.25 (m, 5H), 7.88 (d, 1H, J = 8.5 Hz), 9.13 (br s, 1H) ppm; ^{13}C NMR (101 MHz, DMSO-d_6, Figure S10) δ = 18.1 (CH$_3$-Val), 19.0 (CH$_3$-Val), 28.1 (3C, CH$_3$-Boc), 30.4 (CH-Val), 38.1 (CH$_2$), 52.3(CH), 60.1 (CH), 78.1 (C$_q$-Boc), 126.2 (C$_{Ar}$), 128.0 (2C, C$_{Ar}$), 129.1 (2C, C$_{Ar}$), 137.5 (C$_{Ar}$), 155.3 (OCONH), 170.1 (CONH), 170.8 (CONH) ppm.

HRMS (ESI) m/z = 401.2164 [M + Na$^+$]$^+$ (calcd for $C_{19}H_{30}N_4O_4Na^+$ 401.2159).

IR (ATR) $\tilde{\nu}$ (cm^{-1}) = 3289, 2966, 2871, 1689, 1650, 1526, 1454, 1390, 1367, 1342, 1303, 1247, 1231, 1173, 1116, 1080, 1046, 1023, 988, 928, 877, 844, 804, 773, 756, 731, 692, 562, 543.

Analytical Methods. *X-ray Diffraction.* Data collection was performed on a STOE IPDS2 diffractometer using graphite-monochromatized Mo Kα radiation (λ = 71.073 pm) at 100 K. Structure solution and refinement was done by direct methods and full-matrix-least-squares on F^2, respectively, using SHELXTL software.[49] Details of the measurements, structure solutions, and refinements are provided in the Table S1. CCDC 1470530 contains the supplementary crystallographic data for this paper. These data are provided free of charge by The Cambridge Crystallographic Data Centre.

Nuclear Magnetic Resonance Spectroscopy. ^{1}H NMR (300 MHz) and ^{13}C NMR (75 MHz) measurements were carried out using a Bruker Avance II spectrometer at 25 °C. ^{1}H NMR (400 MHz, 200 MHz) and ^{13}C NMR (101 MHz) measurements for dipeptides were carried out using a Bruker Avance II spectrometer at 25 °C. The chemical shifts were quoted in parts per million (ppm) relative to the residual protons of deuterated DMSO or chloroform (Figures S2−S10).

Infrared Spectroscopy. IR spectra were recorded on an ALPHA spectrometer from Bruker Optics.

Mass Spectrometry. ESI(+) MS measurements were performed on a Thermo Fischer Scientifics Finnigan LTQ-FT by using the solvent (DCM/chloroform mixture) as the carrier gas. LIFDI(+) measurements were carried out on a JEOL AccuTOF-GCv spectrometer in DCM (for compound **2**$^+$, see Figure S1). ESI(+) MS measurements for the dipeptides were performed on a Bruker Mikro-TOF by using methanol as the carrier gas.

Elemental Analyses. Combustion analyses were performed with a vario Micro cube from Elementar in CHN(S) modus.

■ ASSOCIATED CONTENT

Supporting Information

The Supporting Information is available free of charge on the ACS Publications website at DOI: 10.1021/acs.organomet.6b00561.

Crystallographic details for **1**, mass spectrum of product obtained from the reaction of **A** with **C**, and NMR spectroscopic data of compounds **2**−**4** (PDF)

Crystallographic information file of **1** (CIF)

■ AUTHOR INFORMATION

Corresponding Author

*E-mail: dehnen@chemie.uni-marburg.de. Web: http://www.uni-marburg.de/fb15/ag-dehnen.

Author Contributions

N.R. and J.-P.B. are considered equal first authors of this work.

Notes

The authors declare no competing financial interest.

■ ACKNOWLEDGMENTS

This work was financially supported by LOEWE "SynChem-Bio".

■ REFERENCES

(1) Richards, C. I.; Choi, S.; Hsiang, J. C.; Antoku, Y.; Vosch, T.; Bongiorno, A.; Tzeng, Y. L.; Dickson, R. M. *J. Am. Chem. Soc.* **2008**, *130*, 5038−5039.

(2) Chen, J.; Ji, X.; Tinnefeld, P.; He, Z. *ACS Appl. Mater. Interfaces* **2016**, *8*, 1786−1794.

(3) Tanaka, S. I.; Miyazaki, J.; Tiwari, D. K.; Jin, T.; Inouye, Y. *Angew. Chem., Int. Ed.* **2011**, *50*, 431−435.

(4) Dereza, P. Y.; Krytchankou, I. S.; Krupenya, D. V.; Gurzhiy, V. V.; Koshevoy, I. O.; Melnikov, A. S.; Tunik, S. P. *Z. Anorg. Allg. Chem.* **2013**, *639*, 398−402.

(5) Kumar, A.; Kumar, V. *Chem. Rev.* **2014**, *114*, 7044−7078.

(6) Li, X.; Coffer, J. L. *Chem. Mater.* **1999**, *11*, 2326−2330.

(7) Kumar, A.; Jakhmola, A. *J. Phys. Chem. C* **2009**, *113*, 9553−9559.

(8) Tang, X. L.; Wang, W. H.; Dou, W.; Jiang, J.; Liu, W. S.; Qin, W. W.; Zhang, Q. L.; Zhang, H. R.; Yu, K. B.; Zheng, L. M. *Angew. Chem., Int. Ed.* **2009**, *48*, 3499−3502.

(9) Wang, R.; Zheng, Z.; Jin, T.; Staples, R. J. *Angew. Chem., Int. Ed.* **1999**, *38*, 1813−1815.

(10) Yoshinari, N.; Tatsumi, K.; Igashira-Kamiyama, A.; Konno, T. *Chem. - Eur. J.* **2010**, *16*, 14252−14255.

(11) Birker, P. J.; Freeman, H. C. *J. Am. Chem. Soc.* **1977**, *99*, 6890−6899.

(12) Lee, P. S.; Igashira-Kamiyama, A.; Kuwamura, N.; Yoshinari, N.; Konno, T. *Chem. - Eur. J.* **2014**, *20*, 6646−6649.

(13) Yoshinari, N.; Konno, T. *Dalton Trans.* **2011**, *40*, 12191−12200.

(14) Ama, T.; Rashid, M.; Sarker, A. K.; Miyakawa, H.; Yonemura, T.; Kawaguchi, H.; Yasui, T. *Bull. Chem. Soc. Jpn.* **2001**, *74*, 2327−2333.

(15) Sokolov, M. N.; Adonin, S. A.; Virovets, A. V.; Abramov, P. A.; Vicent, C.; Llusar, R.; Fedin, V. P. *Inorg. Chim. Acta* **2013**, *395*, 11−18.

(16) Mansfeld, D.; Miersch, L.; Rüffer, T.; Schaarschmidt, D.; Lang, H.; Böhle, T.; Troff, R. W.; Schalley, C. a; Müller, J.; Mehring, M. *Chem. - Eur. J.* **2011**, *17*, 14805−14810.

DOI: 10.1021/acs.organomet.6b00561
Organometallics 2016, 35, 3215−3220

(17) Santner, S.; Heine, J.; Dehnen, S. *Angew. Chem., Int. Ed.* **2016**, *55*, 876−893.
(18) Heine, J.; Dehnen, S. *Z. Anorg. Allg. Chem.* **2012**, *638*, 2425−2440.
(19) Dehnen, S.; Melullis, M. *Coord. Chem. Rev.* **2007**, *251*, 1259−1280.
(20) Zai, J.; Wang, K.; Su, Y.; Qian, X.; Chen, J. *J. Power Sources* **2011**, *196*, 3650−3654.
(21) Gou, X.; Chen, J.; Shen, P. *Mater. Chem. Phys.* **2005**, *93*, 557−566.
(22) Ning, J.; Men, K.; Xiao, G.; Zou, B.; Wang, L.; Dai, Q.; Liu, B.; Zou, G. *CrystEngComm* **2010**, *12*, 4275−4279.
(23) Fakhri, A.; Behrouz, S. *Sol. Energy* **2015**, *117*, 187−191.
(24) Krigman, M. R.; Silverman, A. P. *Neurotoxicology* **1984**, *5*, 129−139.
(25) Pellerito, L.; Nagy, L. *Coord. Chem. Rev.* **2002**, *224*, 111−150.
(26) Ahmad, N. W.; Mohd, S.; Balabaskaran, S.; Das, V. G. K. *Appl. Organomet. Chem.* **1993**, *7*, 583−591.
(27) Nath, M. *Appl. Organomet. Chem.* **2008**, *22*, 598−612.
(28) Martins, M.; Baptista, P. V.; Mendo, A. S.; Correia, C.; Videira, P.; Rodrigues, A. S.; Muthukumaran, J.; Santos-Silva, T.; Silva, A.; Guedes da Silva, M. F. C.; Gigante, J.; Duarte, A.; Gajewska, M.; Fernandes, A. R. *Mol. BioSyst.* **2016**, *12*, 1015−1023.
(29) Gielen, M. *Coord. Chem. Rev.* **1996**, *151*, 41−51.
(30) Hong, M.; Geng, H.; Niu, M.; Wang, F.; Li, D.; Liu, J.; Yin, H. *Eur. J. Med. Chem.* **2014**, *86*, 550−561.
(31) Fard, Z. H.; Halvagar, M. R.; Dehnen, S. *J. Am. Chem. Soc.* **2010**, *132*, 2848−2849.
(32) Halvagar, M. R.; Fard, Z. H.; Dehnen, S. *Chem. Commun.* **2010**, *46*, 4716−4718.
(33) Barth, B. E. K.; Leusmann, E.; Harms, K.; Dehnen, S. *Chem. Commun.* **2013**, *49*, 6590−6592.
(34) Eußner, J. P.; Barth, B. E. K.; Leusmann, E.; You, Z.; Rinn, N.; Dehnen, S. *Chem. - Eur. J.* **2013**, *19*, 13792−13802.
(35) Hassanzadeh Fard, Z.; Müller, C.; Harmening, T.; Pöttgen, R.; Dehnen, S. *Angew. Chem., Int. Ed.* **2009**, *48*, 4441−4444.
(36) Fard, Z. H.; Xiong, L.; Müller, C.; Hołyńska, M.; Dehnen, S. *Chem. - Eur. J.* **2009**, *15*, 6595−6604.
(37) Pöhlker, C.; Schellenberg, I.; Pöttgen, R.; Dehnen, S. *Chem. Commun.* **2010**, *46*, 2605−2607.
(38) Hassanzadeh Fard, Z.; Hołyńska, M.; Dehnen, S. *Inorg. Chem.* **2010**, *49*, 5748−5752.
(39) Halvagar, M. R.; Hassanzadeh Fard, Z.; Dehnen, S. *Chem. - Eur. J.* **2011**, *17*, 4371−4374.
(40) You, Z.; Dehnen, S. *Inorg. Chem.* **2013**, *52*, 12332−12334.
(41) Eußner, J. P.; Dehnen, S. *Chem. Commun.* **2014**, *50*, 11385−11388.
(42) Eußner, J. P.; Barth, B. E. K.; Justus, U.; Rosemann, N. W.; Chatterjee, S.; Dehnen, S. *Inorg. Chem.* **2015**, *54*, 22−24.
(43) You, Z.; Fenske, D.; Dehnen, S. *Dalton Trans.* **2013**, *42*, 8179−8182.
(44) Rinn, N.; Eußner, J. P.; Kaschuba, W.; Xie, X.; Dehnen, S. *Chem. - Eur. J.* **2016**, *22*, 3094−3104.
(45) Rella, M. R.; Williard, P. G. *J. Org. Chem.* **2007**, *72*, 525−531.
(46) Rzepecki, P.; Schrader, T. *J. Am. Chem. Soc.* **2005**, *127*, 3016−3025.
(47) Teno, N.; Tsuboi, S.; Shimamura, T.; Okada, Y.; Yanagida, Y.; Yoshinaga, M.; Ohgi, K.; Irie, M. *Chem. Pharm. Bull.* **1987**, *35*, 468−478.
(48) Götz, M. G.; James, K. E.; Hansell, E.; Dvořák, J.; Seshaadri, A.; Sojka, D.; Kopáček, P.; McKerrow, J. H.; Caffrey, C. R.; Powers, J. C. *J. Med. Chem.* **2008**, *51*, 2816−2832.
(49) Sheldrick, G. M. *Acta Crystallogr., Sect. A: Found. Crystallogr.* **2008**, *64*, 112−122.

DOI: 10.1021/acs.organomet.6b00561
Organometallics 2016, 35, 3215−3220

SUPPORTING INFORMATION

Peptide-Functionalized Organotin Sulfide Clusters

Niklas Rinn,[§] Jan-Philipp Berndt,[‡] Annikka Kreher,[§] Radim Hrdina,[‡] Matthias Reinmuth,[§] Peter R. Schreiner,[‡] and Stefanie Dehnen[*,§]*

‡ Department of Chemistry and Wissenschaftliches Zentrum für Materialwissenschaften (WZMW), Philipps-Universität Marburg, 35037 Marburg, Germany

§ Institute of Organic Chemistry, Justus-Liebig University, Heinrich-Buff-Ring 17, 35392 Giessen, Germany

Contents:

1. Crystallographic details of **1**

Table S1 lists the crystallographic data for structure solution and refinement of compound **1**.

Table S1. Crystallographic data for compound **1**.

Empirical formula	$C_{42}H_{60}N_6O_2S_5Sn_4 \cdot 2H_2O$
Fw / g·mol^{-1}	1364.02
Crystal color and shape	colorless block
Crystal size / mm^3	0.12×0.10×0.08
Crystal system	orthorhombic
Space group	$P2_12_12_1$
a / Å	11.1594(3)
b / Å	18.4601(5)
c / Å	32.6848(10)
α / deg	90
β / deg	90
γ / deg	90
V / Å^3	90
Z	4
ρ_{calcd} / g·cm^{-3}	1.346
μ(Mo K$_\alpha$) / mm^{-1}	1.657
Absorption correction type	numerical
min./max. transmission	0.8015 / 0.9044
2 θ range / deg	2.5 / 46.74
no. of meas. reflns	52091
R(int)	0.1320
Indep. reflns	14240
Indep. Reflns ($I > 2\sigma(I)$)	8450
no. of parameters	571
R_1 ($I > 2\sigma(I)$) / wR_2 (all data)	0.0611 / 0.1482
S (all data)	0.901
Max. peak / hole / e$^-$· Å^3	1.052 / –1.436

The SQUEEZE[1] routine was utilized to remove a volume of 1682 Å (421 electrons) of disordered crystal solvent molecules. Some water molecules (formed as by-product of the reaction) were localized on the difference Fourier map, as indicated in Figure S1.

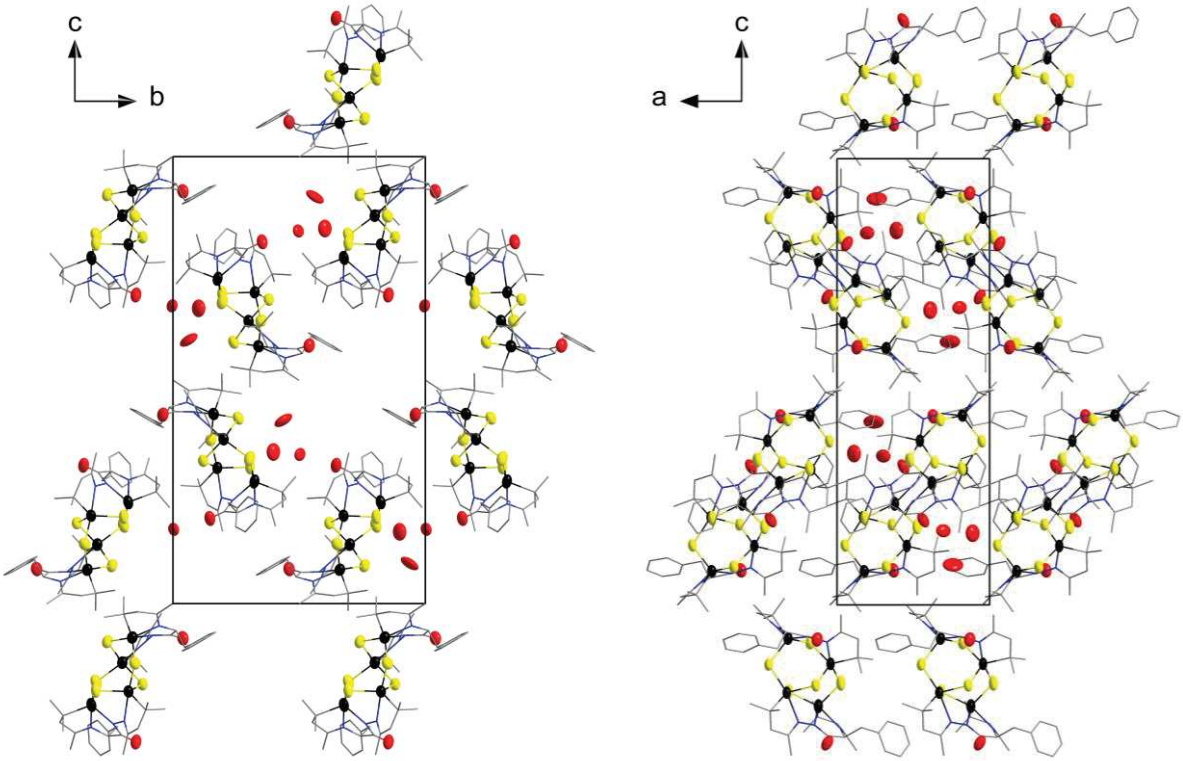

Figure S1. Fragment of the crystal structure of **1** viewed down the crystallographic *a* axis (left) and *b* axis (right). The large voids are filled with crystal solvent molecules. Sn, Sn and O atoms are shown as ellipsoids (50% probability), C and N atoms as wires, H atoms are omitted for clarity. Color code: Sn, black; S, yellow; O, red; C, grey; N, blue.

2. Reaction of **A** with **C**

Upon reaction **A** with **C** at –5 °C in $CHCl_3$ and removal of the solvent, a colorless residue was obtained that was shown to be a mixture of different compounds in ESI(+) mass spectrometry (Figure S2). Clean NMR data could not be obtained.

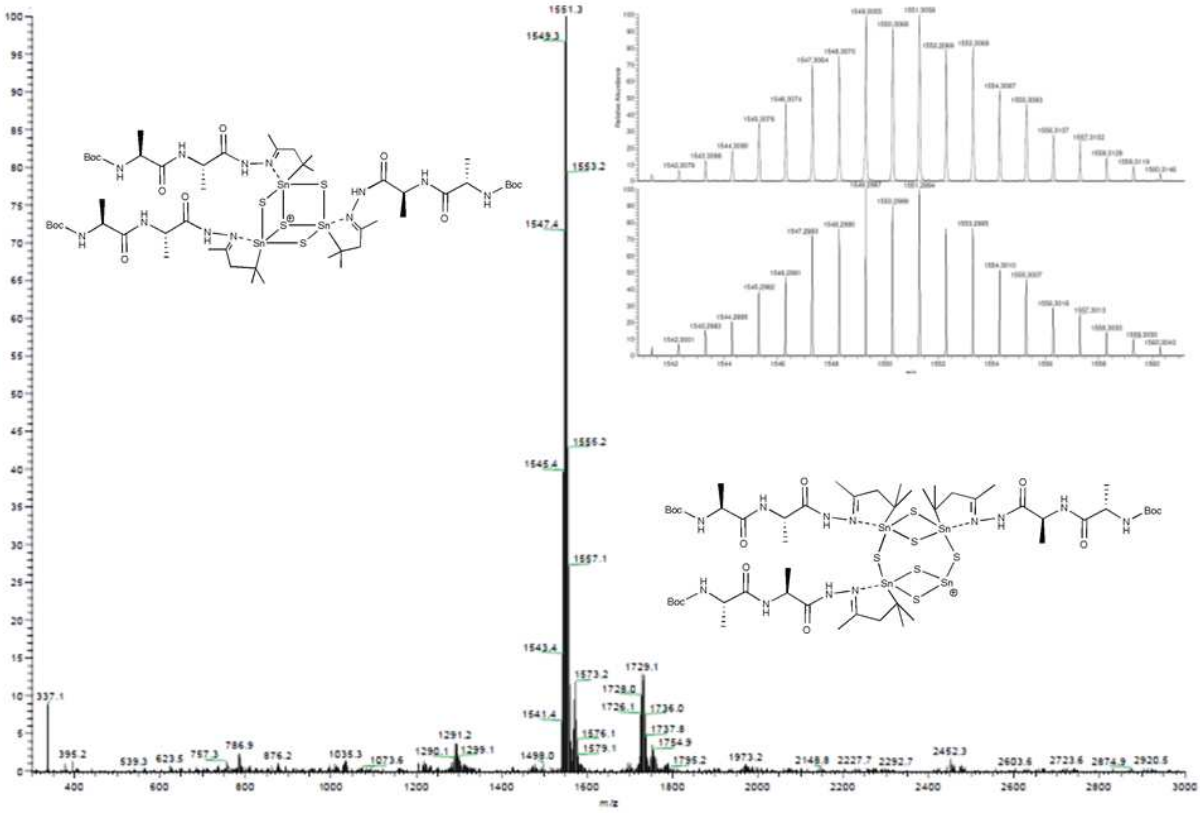

Figure S2. ESI(+) mass spectrum of the product obtained from the reaction of **A** with **C**. The major product, $\mathbf{2}^+$, is found at m/z 1550.3, according to $[Sn_3S_4C_{51}H_{93}N_{12}O_{12}]^+$ (see simulation in the zoom; Boc = $C_5H_9O_2$). The smaller peak at m/z 1732.1 accords with an $[Sn_4S_6]$ composition of the starting material **A**, however with only three instead of four ligands, $[Sn_4S_6C_{51}H_{93}N_{12}O_{12}]^+$.

3. NMR Spectroscopy

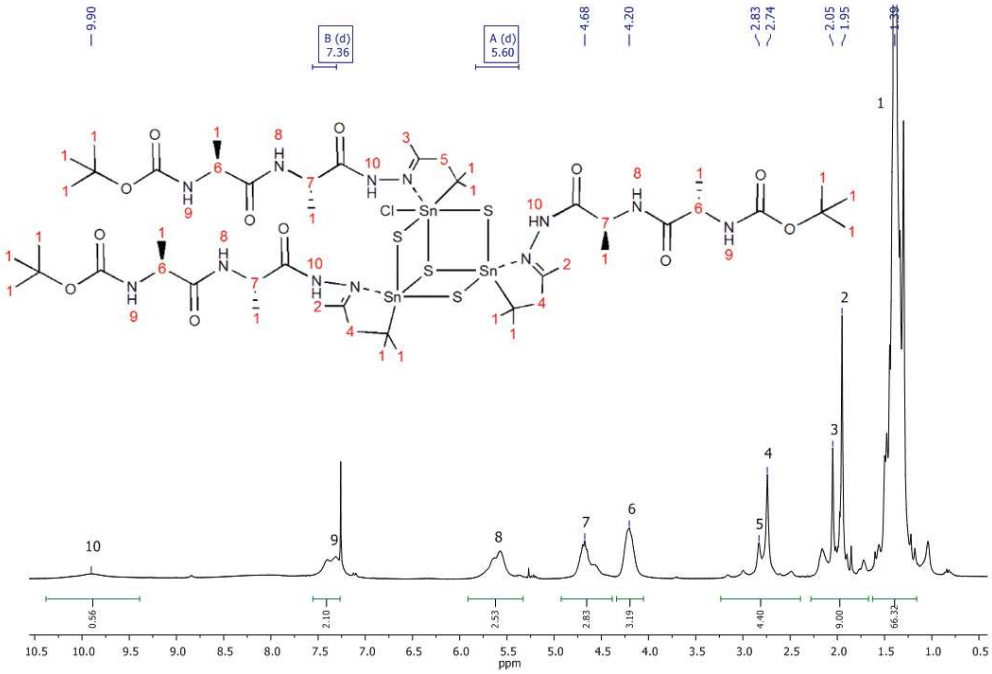

Figure S3. ^{1}H NMR spectrum of compound **2**.

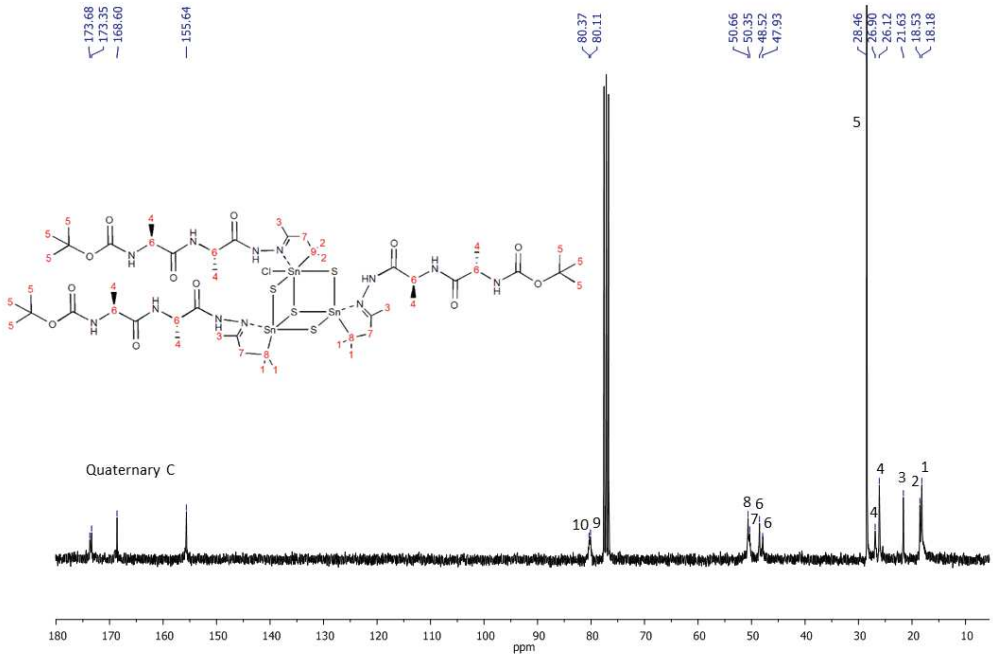

Figure S4. ^{13}C NMR spectrum of compound **2**. Note that the numbers correlate with the indicated signals and not with those given in Figure S3.

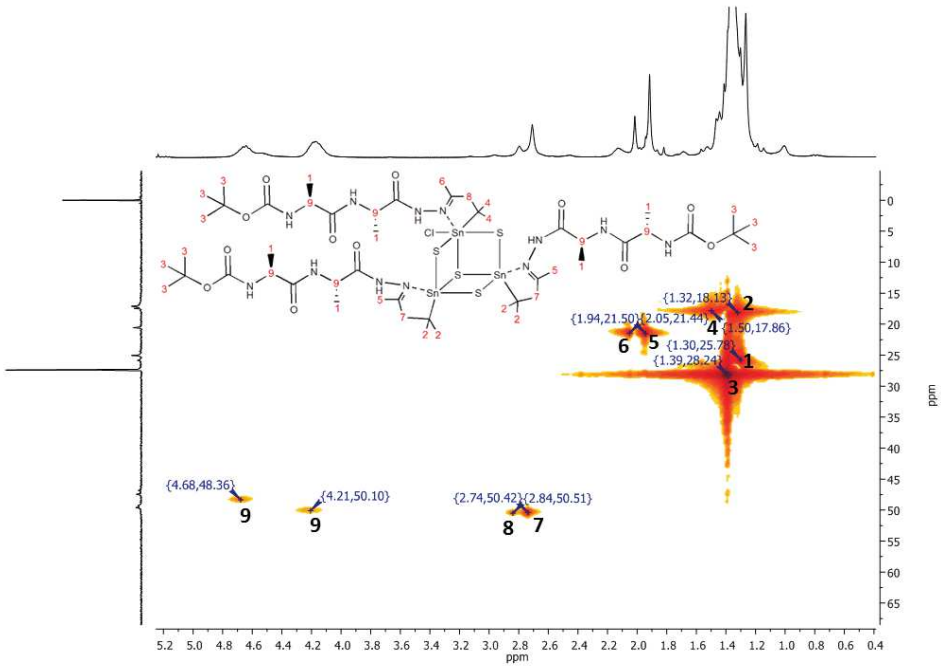

Figure S5. HMQC spectrum of compound **2**. Note that the numbers correlate with the indicated cross signals and not with those given in Figure S3.

The spectra of **3** show a small impurity of grease (long aliphatic hydrocarbons) overlapping with the signals for **1** and **2** in the ^{1}H NMR.

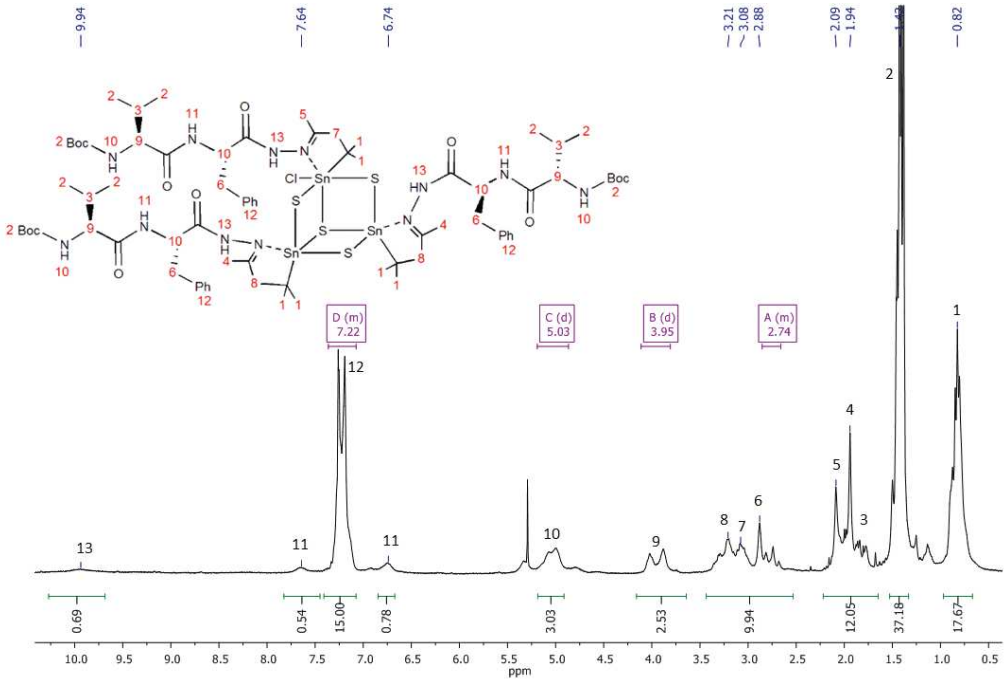

Figure S6. ^{1}H NMR spectrum of compound **3**.

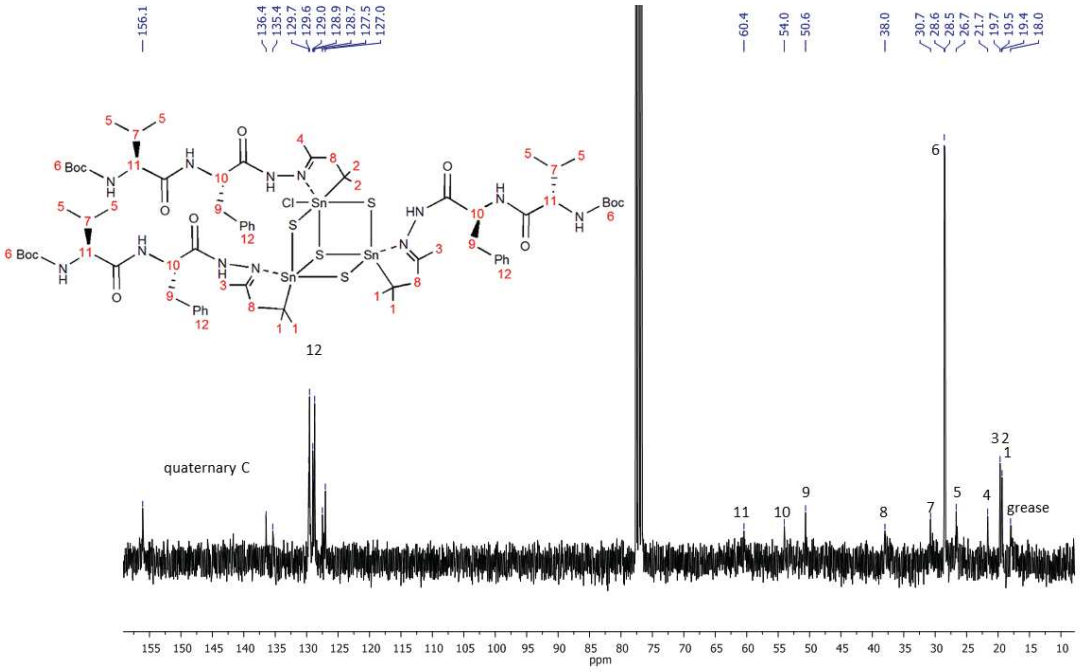

Figure S7. ^{13}C NMR spectrum of compound **3**. Note that the numbers correlate with the indicated signals and not with those given in Figure S6.

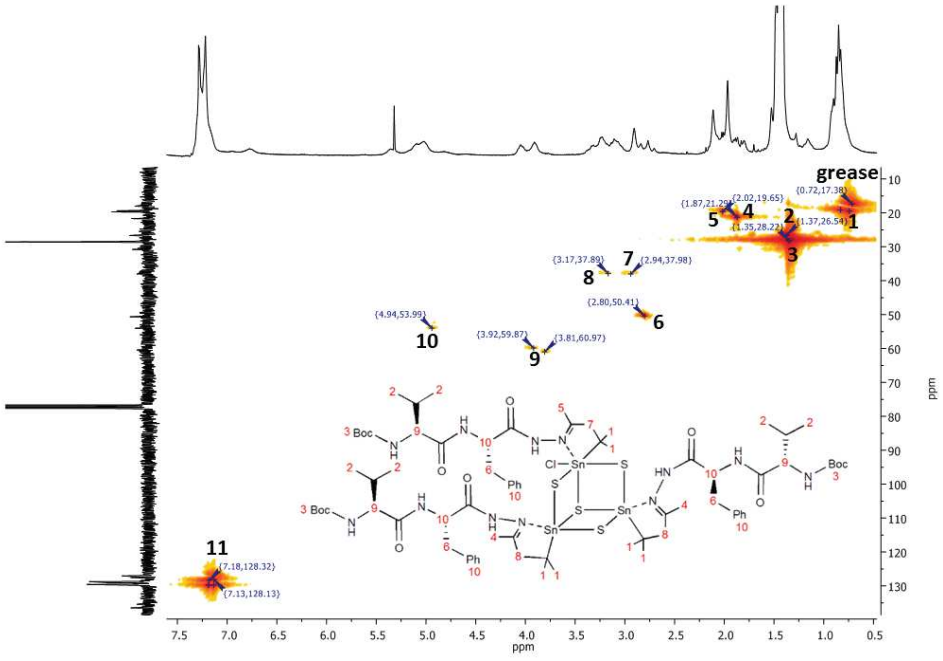

Figure S8. HMQC spectrum of compound **3**. Note that the numbers correlate with the indicated cross signals and not with those given in Figure S6.

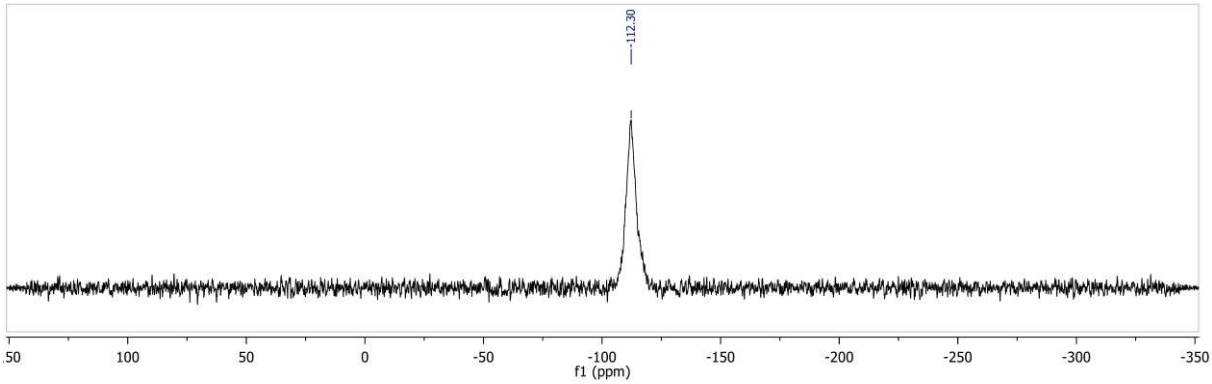

Figure S9. ^{119}Sn NMR spectrum of compound **2**.

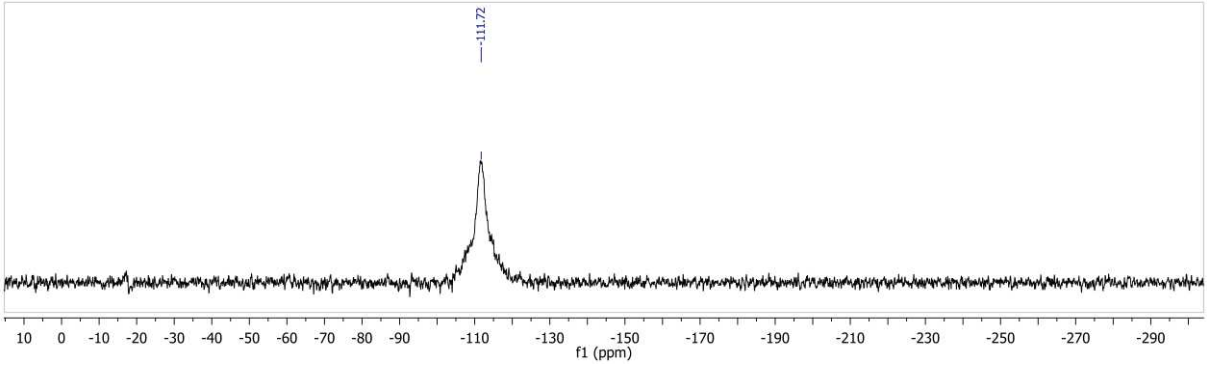

Figure S10. ^{119}Sn NMR spectrum of compound **3**.

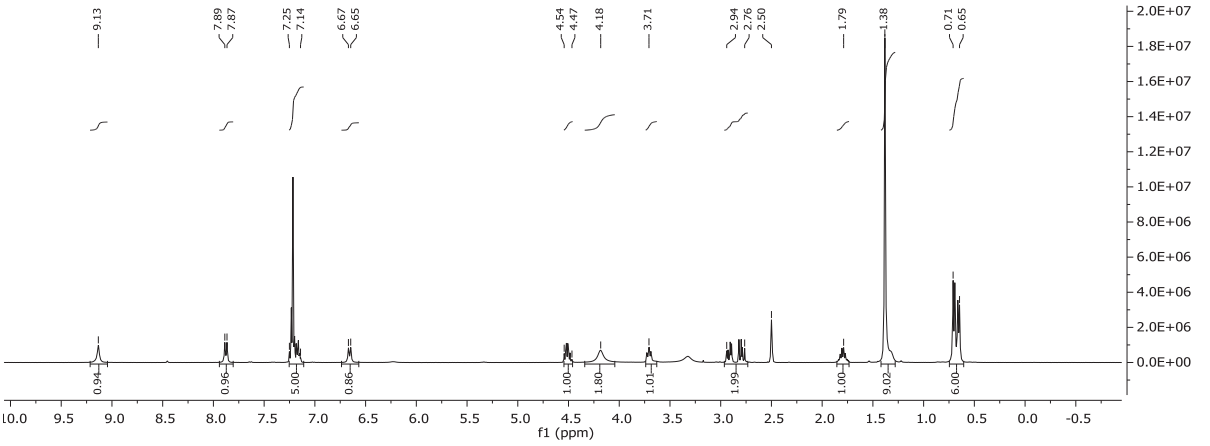

Figure S11. ^{1}H NMR spectrum of Boc-L-Val-L-Phe-N_2H_3 (**4**).

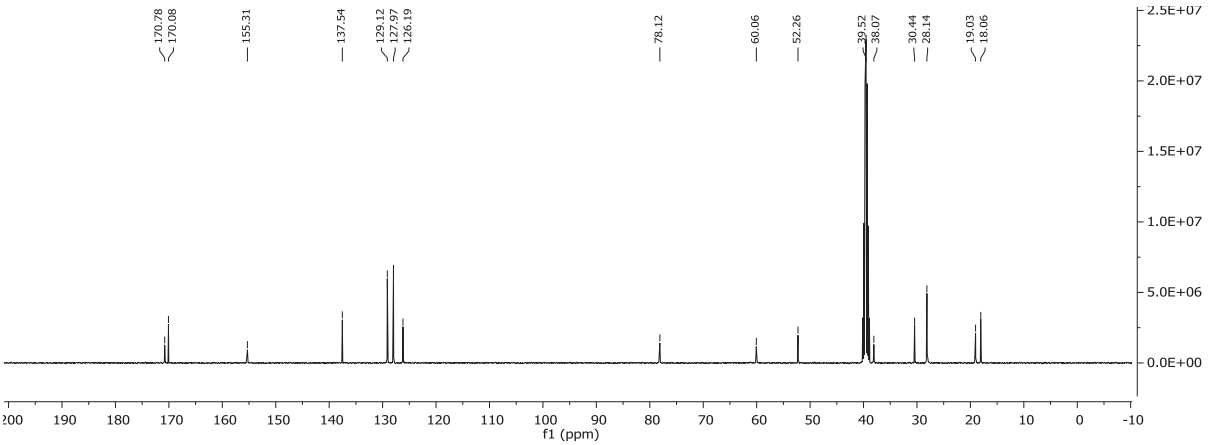

Figure S12. ^{13}C NMR spectrum of Boc-L-Val-L-Phe-N_2H_3 (**4**).

4. References

[1] A. L. Speck, *Bijvoet Center for Biomolecular Research, University Utrecht*

4. Zusammenfassung

Im Rahmen meiner Doktorarbeit beschäftigte ich mich mit der gezielten Synthese und weiteren Derivatisierung von Organozinnselenidclustern des allgemeinen Typs $[(RSn)_xSe_y]$. Hier konnte ich den bislang für diese Elementkombination unbekannten Doppeldecker-Typ $[(SnR^1)_4Se_6]$ (**1**, $R^1 = CMe_2CH_2C(O)Me$) darstellen und diesen sowie seine bereits bekannten Vorläuferverbindungen $[(SnR^1)_2SeCl_4]$ und $[(SnR^1)_2Se_2Cl_2]$ durch Zugabe von Hydrazinen weiter derivatisieren (**2**-**4**). Weiterhin wurden Gleichgewichte dieser drei Verbindungen sowie des ebenfalls in vorherigen Arbeiten synthetisierten Defektheterokuban-artigen Clusters $[(SnR^1)_3Se_4Cl]$ (**A**) in Lösung mit und ohne Zugabe von $(SiMe_3)_2Se$ untersucht.

A und **1** wurden zudem mit Übergangsmetallkomplexen zu Reaktion gebracht, wodurch einige neuartige Clusterverbindungen dargestellt werden konnten. Verwendet man hierfür die Kupferkomplexe $[Cu(PPh_3)_{4-x}Cl_x]$ (x = 1-2) in Gegenwart eines Überschusses an $(SiMe_3)_2Se$, so lassen sich strukturell verwandte Verbindungen der Art $[(CuPPh_3)_2\{(SnR)Se_4\}_x(ML)_y]$ (**5**: x = 1, y = 0, R = R^1; **6**: x = 2, y = 2, R = R^1, ML = SnCl) isolieren. Bei Reaktionen in konzentrierter Lösung konnte durch Fällung ein Cluster ähnlich zu $[(CuPPh_3)_2\{(SnR)Se_4\}_3(SnCu_2)]$ (**B**) isoliert werden, der jedoch im Rahmen eines dynamischen Gleichgewichts in Lösung einen PPh_3-Liganden verloren hat (**7;** x = 3, y = 1, R = R^1, ML = $SnCu_2$). Reaktionen mit Hydrazin oder Hydrazinderivaten können hier in einigen Fällen zu einer Umlagerung des anorganischen Grundgerüstes führen (**8**: x = 2, y = 1, R = $R^2 = CMe_2CH_2C(NNH_2)Me$, ML = Sn; **9**: x = 2, y = 2, R = $R^3 = CMe_2CH_2C(NNHPh)Me$, ML = SnCl) . **A** reagiert darüber hinaus mit $[Cu(PPh_3)_2Cl_2]$ auch ohne den Zusatz von $(SiMe_3)_2Se$ zu einem Cluster, welcher mit $[(CuPPh_3)_2\{(SnR^1)Se_2\}_2(SnCl)_2]$ (**10**) einen leicht anderen Aufbau als die vorher besprochenen Verbindungen besitzt. Dieser beinhaltet an Stelle von $[(SnR^1)_2Se_2]$-Baugruppen die etwas kleineren $[ClSnR^1]$-Einheiten. Die damit einhergehende Veränderung der elektronischen Struktur führt zu einer Vergrößerung des energetischen HOMO-LUMO-Abstandes, weswegen dieser Cluster im Vergleich zu allen anderen hier gezeigten kupferhaltigen Verbindungen nicht orange, sondern farblos ist.

Setzt man **A** oder **1** mit $[Ag(PPh_3)_3Cl]$ und $(SiMe_3)_2Se$ bei –78 °C um, so erhält man in beiden Fällen einen gelblichen Niederschlag der das Elementverhältnis P:Sn:Ag:Se = 1:2:2:4 besitzt. Mittels Festkörper-NMR-Studien (in Kooperation mit der Arbeitsgruppe Senker, Bayreuth) konnte gezeigt werden, dass in dieser Substanz zwei verschiedene Sn- und vier verschiedenen Se-Positionen im Festkörper vorliegen. Diese Verbindung ließ sich jedoch nicht genauer strukturell charakterisieren, da sie sich durch Auflösen in neuartige Verbindungen umwandelt. Umkristallisieren unter Lichtausschluss führt hierbei zur Bildung der Verbindung $[(AgPPh_3)_2\{(SnR^1)Se_4\}_2(SnCl)_2]$ (**11**), einem Cluster, der isotyp zur Verbindung **6** aufgebaut ist. Wiederholt man das Umkristallisieren nach einer 30-minütigen Lichteinstrahlung, so verfärbt sich die Lösung rot, und man kann anschließend Kristalle einer anderen Verbindung, $[Ag_6(\mu_6\text{-}Se)(Ag_8Se_{12})\{(R^1Sn)_2Se_2\}_6]$ (**12**), erhalten, in deren anorganischem Grundgerüst mit der Zusammensetzung $[Ag_{14}Sn_{12}Se_{25}]$ ein $[Ag_{14}Se_{13}]$-Kern von sechs $[(SnR^1)_2Se_2]$-Fragmenten umgeben wird. Zusatz von $N_2H_4{\cdot}H_2O$ führt zur Bildung von $[(\mu_7\text{-}Se)Ag_7Se_{12}\{(R^2Sn)_2Se_2\}_6]$ (**13**) ($R^2 = CMe_2CH_2C(NNH_2)Me$), einem Cluster welcher ebenfalls einen $[Ag_{14}Sn_{12}Se_{25}]$ Clusterkern aufweist, der jedoch isomer zu dem in Verbindnug **12** und völlig unsymmetrisch aufgebaut ist.

Umsetzungen von **1** und **A** mit $[Pd(PPh_3)_2Cl_2]$ und $(SiMe_3)_2Se$ führen nicht zu isolierbaren Verbindungen. Der Zusatz von $N_2H_4{\cdot}H_2O$ zu den Reaktionslösungen bewirkt jedoch, dass nach einer Überschichtung kristalline Produkte erhalten werden können. Hierbei handelt es sich um Clusterverbindungen mit trigonal-bipyramidalem Aufbau, die Selenatome in den apikalen Positionen besitzen. Durch Reaktionen mit **A** lässt sich dabei $[\{Pd(PPh_3)_2\}_2\{Pd(PPh_3)SeH\}Se_2][SnCl_3]$ (**14**) darstellen. Setzt man **1** jedoch mit $[Pd(PPh_3)_2Cl_2]$ und $(SiMe_3)_2Se$ unter Zugabe von $N_2H_4{\cdot}H_2O$ um, so erhält man neben einem Niederschlag, welcher sich durch Lösen und Überschichten mit *n*-Hexan in Kristalle von $[\{Pd(PPh_3)_2\}_2\{Pd(PPh_3)SnCl_3\}Se_2][SnCl_3]$ (**15**) umwandeln lässt, den Palladium-

Organozinnselenidcluster $[\{Pd(PPh_3)_2\}_2\{Pd(PPh_3)Cl\}(Cl_2SnR^2)Se_2]$ (**16**) nach Überschichten der Reaktionslösung mit *n*-Hexan. Es wird bei allen Reaktionen mit Palladiumkomplexen davon ausgegangen, dass $N_2H_4 \cdot H_2O$ aufgrund seiner reduzierenden Wirkung gegenüber Sn^{IV} auch bei solchen Reaktionen benötigt wird, in denen die Hydrazingruppe anschließend nicht im Produkt beobachtet werden kann.

Alle Organozinn-(Metall)Selenidcluster aus dieser Arbeit sind in Abbildung 4.1 gezeigt.

An die zu **A** und **1** analogen Schwefelverbindungen $[(SnR^1)_4S_6]$ und $[(SnR^1)_3S_4Cl]$ lassen sich zudem Aminosäure- und Dipeptidderivate anbinden. $[(SnR^1)_4S_6]$ reagiert mit Phenylalaninhydrazid zu der Clusterverbindung, $[R^{Phe}{}_2Sn_4S_5]$ (R^{Phe} = $(CMe_2CH_2C(Me)N_2C(O)CH(CH_2Ph)NC(Me)CH_2CMe_2)$, bei der sowohl die Hydrazid- als auch die Amingruppe an Zinnatome des Clusters binden. Durch Massenspektrometrie und nuklearmagnetische Resonanz-Spektroskopie konnte zudem die Anbindung von Dipeptiden an $[(SnR^1)_3S_4Cl]$ belegt werden. Dieser Teil der Arbeit entstand in Kooperation mit Annikka Kreher.

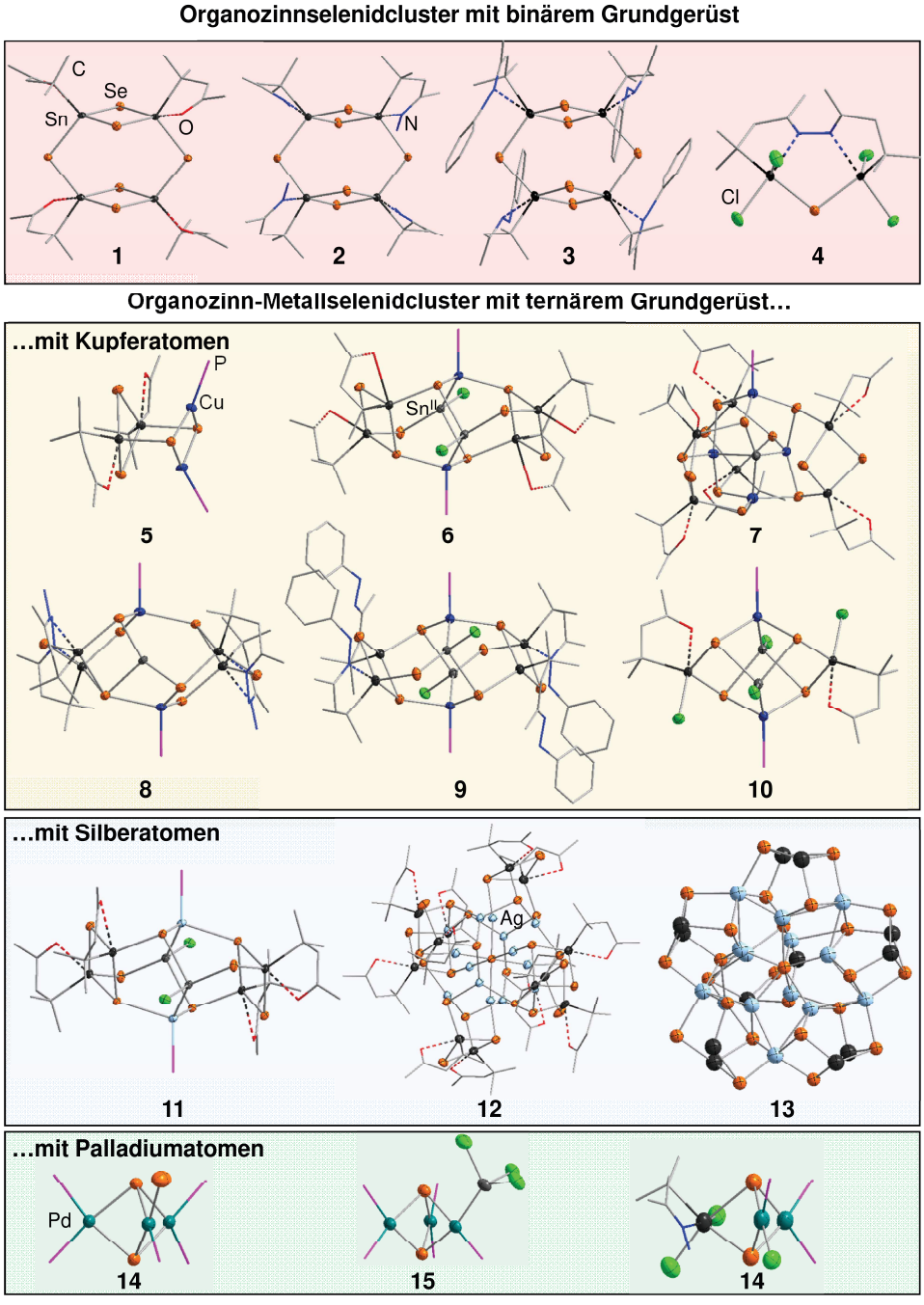

Abbildung 4.1: Sämtliche im Rahmen dieser Arbeit strukturell charakterisierte Organozinn-(Metall)Selenidcluster.

5. Summary

I isolated the double-decker-type cluster compound $[(SnR^1)_4Se_6]$ (**1**, $R^1 = CMe_2CH_2C(O)Me$), which was to date unknown for the tin selenium elemental combination. I further treated **1** and its precursor compounds $[(SnR^1)_2SeCl_4]$ and $[(SnR^1)_2Se_2Cl_2]$ with hydrazines to achieve different organic functionality (**2**-**4**). These three compounds as well as the defect-hetero-cubane-type compound $[(SnR^1)_3Se_4Cl]$ (**A**) were found to be part of a dynamic equilibrium, which could be perturbed by addition of $(SiMe_3)_2Se$.

The clusters **A** and **1** were shown to react with certain metal complexes towards novel cluster compounds with ternary inorganic cores. When using the copper complexes $[Cu(PPh_3)_{4-x}Cl_x]$ (x = 1-2) and an excess of $(SiMe_3)_2Se$, structurally related compounds $[(CuPPh_3)_2\{(SnR)Se_4\}_x(ML)_y]$ (**5**: x = 1, y = 0, $R = R^1$; **6**: x = 2, y = 2, $R = R^1$, ML = SnCl) were obtained. Through synthesis in concentrated solutions, it is possible to precipitate a cluster (**7**) that is similar to **B** (x = 3, y = 1, $R = R^1$, $ML = SnCu_2$), but lacking one PPh_3 unit due to an equilibrium by release and re-attachment of PPh_3 to the cluster. Addition of hydrazines to the compounds leads not only to a conversion of the organic ligand (**8**: x = 2, y = 1, $R = R^2 = CMe_2CH_2C(NNH_2)Me$, ML = Sn; **9**: x = 2, y = 2, $R = R^3 = CMe_2CH_2C(NNHPh)Me$, ML = SnCl), but in some cases also to a rearrangement of the inorganic core. When adding $[Cu(PPh_3)_2Cl_2]$ to a solution of **A** without $(SiMe_3)_2Se$, the cluster $[(CuPPh_3)_2\{(SnR^1)Se_2\}_2(SnCl)_2]$ (**10**) is formed, which deviates from the general buildup of the previous compounds by replacement of a $[(SnR^1)_2Se_2]$ unit with $[ClSnR^1]$. This leads to a change in the electronic situation and a colorless compound, as opposed to the former compounds featuring an orange/red color.

By treating **A** or **1** with $[Ag(PPh_3)_3Cl]$ and $(SiMe_3)_2Se$ at –78 °C, a pale yellow, microcrystalline precipitate was isolated in both cases. Its structure could not be determined, but its elemental composition was shown to be P:Sn:Ag:Se = 1:2:2:4, and two distinct Sn and four distinct Se sites were determined by solid-state nuclear magnetic resonance spectroscopy (NMR-spectroscopy). Due to rapid rearrangement in solution, this compound could not be further characterized. When trying to recrystallize it under light exclusion, $[(AgPPh_3)_2\{(SnR^1)Se_4\}_2(SnCl)_2]$ (**11**) was isolated instead, a compound that is isostructural to a previously reported copper compound **6**. By repeating this process, but exposing the solution to daylight for 30 minutes, the color turns from yellow to red, and another cluster forms, $[Ag_6(\mu_6\text{-}Se)(Ag_8Se_{12})\{(R^1Sn)_2Se_2\}_6]$ (**12**). In its inorganic $[Ag_{14}Sn_{12}Se_{25}]$ core, an $[Ag_{14}Se_{13}]$ moiety is surrounded by six $[(SnR^1)_2Se_2]$ units. Upon addition $N_2H_4{\cdot}H_2O$, the compound $[(\mu_7\text{-}Se)Ag_7Se_{12}\{(R^2Sn)_2Se_2\}_6]$ ($R^2 = CMe_2CH_2C(NNH_2)Me$; **13**) was obtained, which is based on an isomeric $[Ag_{14}Sn_{12}Se_{25}]$ inorganic core, albeit with an atypical asymmetric connectivity.

When adding **A** or **1** to a solution of $[Pd(PPh_3)_2Cl_2]$ with an excess of $(SiMe_3)_2Se$, no compounds could be isolated. However, in the presence of $N_2H_4{\cdot}H_2O$, clusters with a trigonal bipyramidal inorganic core with selenium in the apical positions were obtained after layering. By using **A** as the starting material, $[\{Pd(PPh_3)_2\}_2\{Pd(PPh_3)SeH\}Se_2][SnCl_3]$ (**14**) is found to be the product cluster. In contrast, reactions with **1** afford a precipitate, which could be dissolved and layered with *n*-hexane to afford crystals of $[\{Pd(PPh_3)_2\}_2\{Pd(PPh_3)SnCl_3\}Se_2][SnCl_3]$ (**15**) and a red solution, which yields $[\{Pd(PPh_3)_2\}_2\{Pd(PPh_3)Cl\}(Cl_2SnR^2)Se_2]$ (**16**) after a likewise layering. It can be deduced that $N_2H_4{\cdot}H_2O$ is required in the reactions leading to **1** and **2**, although it is not incorporated in the products themselves, as it serves to reduce the tin atoms, which is required to form the $[SnCl_3]^-$ units observed in **1** and **2**. All organotin (metal) selenide clusters structurally described in this work are shown in figure 5.1.

$[(SnR^1)_4S_6]$ und $[(SnR^1)_3S_4Cl]$, the lower sulfide congeners of **A** and **1** respectively, can be linked to amino acids and dipeptide derivatives. $[(SnR^1)_4S_6]$ reacts with phenylalanin hydrazide to form $[R^{Phe}{}_2Sn_4S_5]$ ($R^{Phe} = (CMe_2CH_2C(Me)\text{-}N_2C(O)CH(CH_2Ph)NC(Me)CH_2CMe_2)$, a cluster with a novel topology, in which the ligand coordinates to two Sn moieties upon condensation of its hydrazide and amine groups. Through mass spectroscopy and NMR it was further shown that dipeptides could be linked to these clusters.

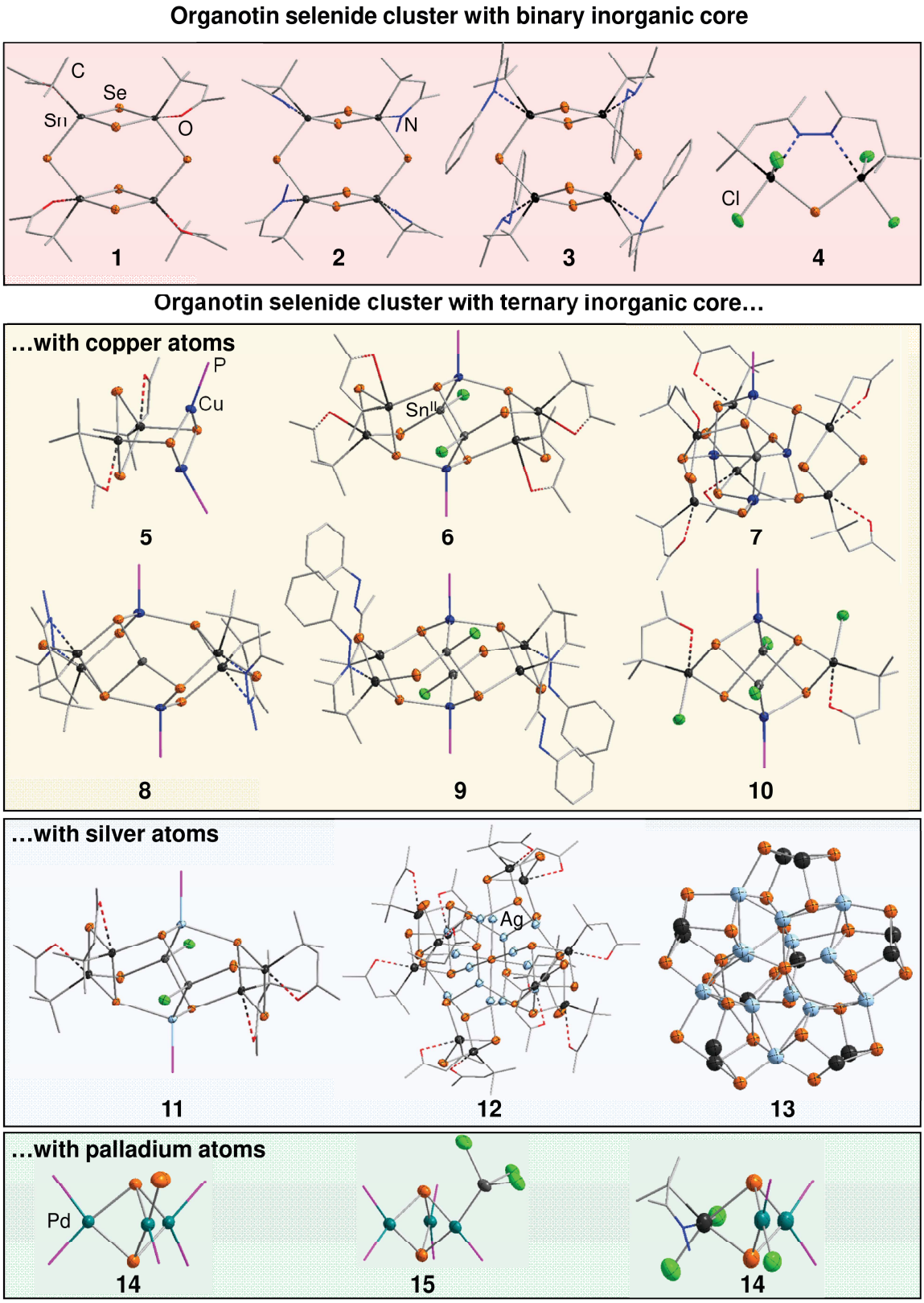

Figure 5.1: All molecular structures of organotin (metal) selenide clusters structurally characterized in this work.

6. Abkürzungsverzeichnis

AD	Adamantan
Ala	Alanin
BDHK	Bisdefektheterokuban
Bipy	2,2´-Bipyridyl
Boc	*tert*-Butyloxycarbonyl
CH	Chevrel
Cp	Cyclopentadienyl
Cp*	Pentamethylcyclopentadienyl
DCM	Dichlormethan
DD	Doppeldecker
DHK	Defektheterokuban
dppe	Bis(diphenylphosphanyl)ethan
dppp	Bis(diphenylphosphanyl)propan
E	Chalkogen
EDX	Energiedispersive Röntgenspektroskopie
Fc	Ferrocenyl
HK	Heterokuban
IR	Infrarot
L	Ligand
M	Metall
NMR	nuklearmagnetische Resonanz
Ph	Phenyl
Phe	Phenylalanin
R	Organischer Ligand
R^1	$CMe_2CH_2C(O)Me$
R^2	$CMe_2CH_2C(NNH_2)Me$
R^3	$[CMe_2CH_2CMe(NH)]_2$
R^4	$CMe_2CH_2C(NNHPh)Me$
R^{ala}	CMe2CH2C(NNH-Ala-Ala-Boc)Me
R^{CH}	$(CMe_2CH_2CMeNNH)_2CO$
R^{COOH}	CH_2CH_2COOH

R^N	Hydrazonhaltiger Ligand
R^{Phe}	$CMe_2CH_2C(Me)\text{-}N_2C(O)CH(CH_2Ph)NC(Me)CH_2CMe_2$
R^{Val}	CMe2CH2C(NNH-Phe-Val-Boc)Me
RPD	Röntgenpulverdiffraktometrie
SR	Schaufelrad
Tb	2,4,6,-tris[bis(trimethylsilyl)methyl
Tip	2,4,6-triisopropylphenyl
Val	Valin
X	Anion

7. Literaturverzeichnis

[1] F. A. Devillanova, W.-W. du Mont, *Handbook of Chalcogen Chemistry*, RSC Publishing, **2013**.

[2] A. F. Hollemann, N. Wiberg, E. Wiberg, *Lehrbuch Der Anorganischen Chemie*, De Gruyter, Berlin, New York, **2007**.

[3] C. H. Griffiths, H. Sang, *Mater. Res. Bull.* **1967**, *2*, 515–519.

[4] P. Cherin, P. Unger, *Acta Cryst. B* **1972**, *28*, 313–317.

[5] J. Beck, *Z. Anorg. Allg. Chem.* **1995**, *621*, 131–136.

[6] A. Baumann, J. Beck, T. Hilbert, *Z. Naturforsch. B* **1999**, *54*, 1253–1259.

[7] J. Beck, T. Hilbert, *Z. Anorg. Allg. Chem.* **2000**, *626*, 837–844.

[8] J. Beck, A. Fischer, *Z. Anorg. Allg. Chem.* **1997**, *623*, 780–784.

[9] T. Klapötke, J. Passmore, *Acc. Chem. Res* **1989**, *22*, 234–240.

[10] V. Müller, C. Grebe, U. Müller, K. Dehnicke, *Z. Anorg. Allg. Chem.* **1993**, *619*, 416–420.

[11] D. Fenske, G. Krauter, K. Dehnicke, *Angew. Chem. Int. Ed.* **1990**, *29*, 390–391.

[12] J. Dietz, U. Müller, V. Müller, K. Dehnike, *Z. Naturforsch.* **1991**, *46b*, 1296–1299.

[13] W. S. Sheldrick, H. G. Braunbeck, *Z. Naturforsch. B* **1989**, *44*, 1397–1401.

[14] T. Chen, F. Lo, M. Tsai, K. Shih, G. Lee, W. Liaw, *Inorganica Chim. Acta* **2006**, *359*, 2525–2533.

[15] N. Albrecht, E. Weiss, *J. Organomet. Chem.* **1988**, *355*, 89–98.

[16] U. Müller, M.-L. Ha-Eierdanz, G. Kräuter, K. Dehnicke, *Z. Naturforsch. B* **1990**, *45*, 1128–1132.

[17] A. Kromm, Y. Geldmacher, W. S. Sheldrick, *Z. Anorg. Allg. Chem.* **2008**, *634*, 2191–2198.

[18] M. Herberhold, G. Jina, A. L. Rheingold, *Z. Naturforsch. B* **1996**, *51*, 681–685.

[19] J. M. McConnachie, M. A. Ansari, J. A. Ibers, *Inorg. Chem.* **1993**, *32*, 3250–3255.

[20] C. Feldmann, A. Okrut, *Z. Anorg. Allg. Chem.* **2009**, *635*, 1807–1811.

[21] A. L. Rheingold, B. S. Haggerty, *Z. Naturforsch. B* **1991**, *46*, 500–506.

[22] S. Nagao, H. Seino, T. Okada, M. Hidai, *J. Chem. Soc., Dalt. Trans.* **2000**, 3546–3553.

[23] M. G. Kanatzidis, S. Dhingra, *Inorg. Chem.* **1989**, *28*, 2024–2026.

[24] D. Freedman, J. H. Melman, T. J. Emge, J. G. Brennan, *Inorg. Chem.* **1998**, *37*, 4162–4163.

[25] L. Song, H. Cheng, Q. Hu, *Organometallics* **2004**, *23*, 1072–1080.

[26] M. Sokolov, J. A. Gavin, P. Esparza, R. Hernandez-Molina, J. G. Platas, A. Mederos, R. Llusar, C. Vicent, *Inorg. Chem.* **2005**, *44*, 1132–1141.

[27] M. Reyes-lezama, H. Höpfl, N. Zúniga-Villarreal, *Organometallics* **2010**, *29*, 1537–

1540.

[28] O. A. Efremova, Y. V Mironov, K. A. Brylev, V. E. Fedorov, H. Pietzsch, H. Stephan, *Polyhedron* **2009**, *28*, 2973–2976.

[29] M. A. Bobrik, E. J. Laskowski, W. W. Johnson, W. O. Gillum, J. M. Berg, K. O. Hodgson, R. H. Holm, *Inorg. Chem.* **1978**, *17*, 1402–1410.

[30] E. J. Houser, S. Dev, A. E. Ogilvy, T. B. Rauchfuss, S. R. Wilson, *Organometallics* **1993**, *12*, 4678–4681.

[31] D. Fenske, J. Ohmer, J. Hachgenei, *Angew. Chem. Int. Ed.* **1985**, *24*, 993–995.

[32] S. Schulz, M. Andruh, T. Pape, T. Heinze, H. W. Roesky, L. Haming, A. Kuhn, R. Herbst-Irmer, *Organometallics* **1994**, *13*, 4004–4007.

[33] J. M. McConnachie, M. A. Ansari, J. A. Ibers, *J. Am. Chem. Soc.* **1998**, *113*, 7078–7079.

[34] S. Schulz, H. W. Roesky, H. J. Koch, G. M. Sheldrick, D. Stalke, A. Kuhn, *Angew. Chem. Int. Ed.* **1993**, *32*, 1729–1731.

[35] W. Uhl, M. Benter, W. Saak, P. G. Jones, *Z. Anorg. Allg. Chem.* **1998**, *624*, 1622–1628.

[36] Y. Zhang, Z. Lei, J. Jiang, Q. Zhu, X. Zhang, G. Bian, J. Dai, *Inorganica Chim. Acta* **2011**, *376*, 645–650.

[37] J. Campbell, H. P. A. Mercier, D. P. Santry, R. J. Suontamo, H. Borrmann, G. J. Schrobilgen, *Inorg. Chem.* **2001**, *40*, 233–254.

[38] J. Beck, S. Schlüter, N. Zotov, *Z. Anorg. Allg. Chem.* **2004**, *630*, 2512–2519.

[39] B. Bechlars, I. Issac, R. Feuerhake, R. Clérac, O. Fuhr, D. Fenske, *Eur. J. Inorg. Chem.* **2008**, *2008*, 1632–1644.

[40] A. G. Algarra, M. N. Sokolov, J. González-Platas, M. J. Fernández-Trujillo, M. G. Basallote, R. Hernández-Molina, *Inorg. Chem.* **2009**, *48*, 3639–3649.

[41] R. Pätow, D. Fenske, *Z. Anorg. Allg. Chem.* **2002**, *628*, 1279–1288.

[42] D. Fenske, A. Grissinger, M. Loos, J. Magull, *Z. Anorg. Allg. Chem.* **1991**, *598/599*, 121–128.

[43] S. Kamiguchi, H. Imoto, T. Saito, T. Chihara, *Inorg. Chem.* **1998**, *37*, 6852–6857.

[44] C. Magliocchi, X. Xie, T. Hughbanks, *Inorg. Chem.* **2016**, *39*, 5000–5001.

[45] X. Xie, R. E. McCarley, *Inorg. Chem.* **1997**, *36*, 4011–4016.

[46] T. Yoshimura, T. Ikai, T. Takayama, T. Sekine, Y. Kino, A. Shinohara, *Inorg. Chem.* **2010**, *49*, 5876–5882.

[47] Z. Zheng, J. R. Long, R. H. Holm, *J. Am. Chem. Soc.* **1997**, *119*, 2163–2171.

[48] F. Cecconi, C. A. Ghilardi, S. Midollini, A. Orlandini, *Inorganica Chim. Acta* **1997**, *254*, 387–389.

[49] M. Wunder, T. B. Rauchfuss, D. Fenske, *Z. Anorg. Allg. Chem.* **2004**, *630*, 1578–1580.

[50] G. Thiele, Z. You, S. Dehnen, *Inorg. Chem.* **2015**, *54*, 2491–2493.

[51] E. G. Tulsky, J. R. Long, *Inorg. Chem.* **2001**, *40*, 6990–7002.

[52] H. Stephan, G. Henkel, *Polyhedron* **1996**, *15*, 501–511.

[53] X. Jin, K. Tang, Y. Long, Y. Tang, *Acta Cryst. C* **1999**, *55*, 1799–1800.

[54] M. T. Aroz, M. C. Gimeno, M. Kulcsar, A. Laguna, V. Lippolis, *Chem. Eur. J.* **2011**, 2884–2894.

[55] A. Eichhöfer, D. Fenske, H. Pfistner, M. Wunder, *Z. Anorg. Allg. Chem.* **1998**, *624*, 1909–1914.

[56] P. A. W. Dean, J. J. Vittal, N. C. Payne, *Inorg. Chem.* **1987**, *26*, 1683–1689.

[57] R. Stieler, F. Bublitz, E. S. Lang, G. M. de Oliveira, *Polyhedron* **2012**, *31*, 596–600.

[58] B. M. Gimarc, J. J. Ott, *J. Am. Chem. Soc.* **1986**, *108*, 4298–4303.

[59] A. Haas, H. J. Kutsch, C. Krüger, *Chem. Ber.* **1987**, *120*, 1045–1048.

[60] A. Blecher, M. Dräger, B. Mathiasch, *Z. Naturforsch. B* **1981**, *36*, 1361–1367.

[61] A. Eichöfer, P. T. Wood, R. N. Viswanath, R. A. Mole, *Chem. Comm.* **2008**, 1596–1598.

[62] S. Behrens, D. Fenske, *Ber. Bunsenges. Phys. Chem.* **1997**, *101*, 1588–1592.

[63] A. Eichhöfer, *Eur. J. Inorg. Chem.* **2005**, 1245–1253.

[64] A. Eichhöfer, O. Hampe, S. Lebedkin, F. Weigend, *Inorg. Chem.* **2010**, *49*, 7331–7339.

[65] T. Wu, L. Wang, X. Bu, V. Chau, P. Feng, *J. Am. Chem. Soc.* **2010**, *132*, 10823–10831.

[66] S. Dehnen, M. K. Brandmayer, *J. Am. Chem. Soc.* **2003**, *125*, 6618–6619.

[67] C. Zimmermann, M. Melullis, S. Dehnen, *Angew. Chem. Int. Ed.* **2002**, *41*, 4269–4272.

[68] S. L. Chan, L. Shek, J. Huang, S. S. Chui, R. Wai-, Y. Sun, C. Che, *Angew. Chem. Int. Ed.* **2012**, *51*, 2614–2617.

[69] J.-F. You, R. H. Holm, *Inorg. Chem.* **1991**, *30*, 1431–1433.

[70] G. Jin, Y. Arikawa, K. Tatsumi, *J. Am. Chem. Soc.* **2001**, *123*, 735–736.

[71] D. Fenske, T. Langetepe, M. M. Kappes, O. Hampe, P. Weis, *Angew. Chem. Int. Ed.* **2000**, *39*, 1857–1860.

[72] C. E. Anson, A. Eichöfer, I. Issac, D. Fenske, O. Fuhr, P. Sevillano, C. Persau, D. Stalke, J. Zhang, *Angew. Chem. Int. Ed.* **2008**, *47*, 1326–1331.

[73] B. H. Krautscheid, D. Fenske, G. Baum, M. Semmelmann, *Angew. Chem. Int. Ed.* **1993**, *32*, 1303–1305.

[74] O. Fuhr, S. Dehnen, D. Fenske, *Chem. Soc. Rev.* **2013**, *42*, 1871–1906.

[75] H. Berwe, A. Haas, *Chem. Ber.* **1987**, *120*, 1175–1182.

[76] D. Kobelt, E. F. Paulus, H. Scherer, *Acta Cryst. B* **1972**, *28*, 2323–2326.

[77] Z. Hassanzadeh Fard, L. Xiong, C. Müller, M. Hołyńska, S. Dehnen, *Chem. Eur. J.* **2009**, *15*, 6595–6604.

[78] R. A. Varga, C. Silvestru, *Acta cryst. E* **2007**, *63*, 2789.

[79] J. P. Eußner, B. E. K. Barth, E. Leusmann, Z. You, N. Rinn, S. Dehnen, *Chem. Eur. J.* **2013**, *19*, 13792–13802.

[80] H. Kraus, K. Merzweiler, *Z. Naturforsch.* **1993**, *48 b*, 1009–1012.

[81] E. Dornsiepen, *Persönliche Mitteilung [{(PMe3Au)SnCl}3S4]* **2017**.

[82] Z. Hassanzadeh Fard, C. Müller, T. Harmening, R. Pöttgen, S. Dehnen, *Angew. Chem.* **2009**, *121*, 4507–4511.

[83] J. P. Eußner, B. E. K. Barth, U. Justus, N. W. Rosemann, S. Chatterjee, S. Dehnen, *Inorg. Chem.* **2015**, *54*, 22–24.

[84] B. E. K. Barth, E. Leusmann, K. Harms, S. Dehnen, *Chem. Comm.* **2013**, *49*, 6590–6592.

[85] B. E. K. Barth, B. A. Tkachenko, J. P. Eußner, P. R. Schreiner, S. Dehnen, *Organometallics* **2014**, *33*, 1678–1688.

[86] E. Leusmann, F. Schneck, S. Dehnen, *Organometallics* **2015**, *34*, 3264–3271.

[87] E. Leusmann, N. W. Rosemann, B. Weinert, S. Chatterjee, S. Dehnen, *Eur. J. Inorg. Chem.* **2016**, *2016*, 5300–5304.

[88] Z. You, K. Harms, S. Dehnen, *Eur. J. Inorg. Chem.* **2015**, *2015*, 5322–5328.

[89] Z. You, J. Bergunde, B. Gerke, R. Poettgen, S. Dehnen, *Inorg. Chem.* **2014**, *53*, 12512–12518.

[90] Z. You, S. Dehnen, *Inorg. Chem.* **2013**, *52*, 12332–12334.

[91] Z. You, D. Fenske, S. Dehnen, *Dalt. Trans.* **2013**, *42*, 8179–8182.

[92] Z. Hassanzadeh Fard, M. R. Halvagar, S. Dehnen, *J. Am. Chem. Soc.* **2010**, *132*, 2848–2849.

[93] M. R. Halvagar, Z. Hassanzadeh Fard, S. Dehnen, *Chem. Eur. J.* **2011**, *17*, 4371–4374.

[94] K. Merzweiler, R. Hauser, *Z. Anorg. Allg. Chem.* **2002**, *628*, 905–906.

[95] I. Schellenberg, C. Pöhlker, R. Pöttgen, S. Dehnen, *Chem. Comm.* **2010**, *46*, 2605–2607.

[96] J. P. Eußner, S. Dehnen, *Chem. Comm.* **2014**, *50*, 11385–11388.

[97] M. R. Halvagar, Z. Hassanzadeh Fard, S. Dehnen, *Chem. Comm.* **2010**, *46*, 4716–4718.

[98] J. J. Schneider, J. Hagen, D. Spickermann, D. Bläser, R. Boese, F. F. De Biani, F. Laschi, P. Zanello, *Chem. Eur. J.* **2000**, *6*, 237–246.

[99] J. S. L. Yeo, J. J. Vittal, T. S. A. Hor, W. Henderson, *Dalt. Trans.* **2001**, 315–321.

[100] Y. Matsuhashi, N. Tokitoh, R. Okazaki, *Organometallics* **1994**, *13*, 4387–4397.

[101] N. Rinn, J. P. Eußner, W. Kaschuba, X. Xie, S. Dehnen, *Chem. Eur. J.* **2016**, *22*, 3094–3104.

[102] N. Rinn, L. Guggolz, Y. Lange, S. Chatterjee, T. Block, R. Pöttgen, S. Dehnen, *Chem. Sci.* **2017**, eingereichtes Manuskript.

8. Wissenschaftlicher Lebenslauf

07/2007 Abitur an der Herderschule Gießen.

10/2007-10/2013 Studium der Chemie an der Philipps-Universität Marburg.

05/2010 Abschluss zum B. Sc. in Chemie unter Prof. Dr. Seema Agarwal.
Titel der Bachelorarbeit: „Synthesis of adamantane methacrylate/2-methylene-1,3-dioxepane copolymers“.

09/2011-03/2012 Forschungsaufenthalt an der Universität Hiroshima in der Arbeitsgruppe von Prof. Dr. Masahiro Sadakane.

11/2013 Abschluss zum M. Sc. in Chemie unter Prof. Dr. Stefanie Dehnen.
Titel der Masterarbeit: „Untersuchungen zur Bildung und gezielten Derivatisierung von organisch funktionalisierten Zinnselenid-Clustern“.

11/2013-08/2017 Doktorand und wissenschaftlicher Mitarbeiter an der Philipps-Universität Marburg in der Arbeitsgruppe von Prof. Dr. Stefanie Dehnen.

„Und was kommt danach?“

fragen sie jetzt.

„Gibt es ein Leben nach der Promotion?“

Und hier ist die Antwort:

Nein!

Man ist promoviert und das wars dann.

Tut mir leid, so ist es nun mal, beachten sie bitte meine Danksagung.

-Frei nach Walter Moers

Was noch zu sagen wäre

Meine Zeit in Marburg, besonders während meiner Promotion, war mir ein Fest! Nicht nur, aber vor allem an Weihnachten. Dafür danke ich den Leuten, die sich für meine persönliche Belustigung lächerlich gemacht haben und vor allen meiner Doktormutter, die ja spätestens seit der Erstversion meiner Promotionsschrift weiß, warum ich die letzten Jahre geforscht habe. Im Arbeitsalltag, auf Tagungen und zu ungezwungenen Anlässen hat sie den Mut und den Humor gehabt, mir viel freie Hand zu lassen. Sehr mutig.

Zugang zu diesem Arbeitskreis wurde mir von ein paar besonderen Personen gewährt. Wichtig ist Jens Eußner, der mir in Sachen Wissenschaft und unscheinbarem Humor ein Vorbild war. Er ist ein weiser Mann! Ebenso Herr Dr. Dr. Weinert und Frau Dr. Dr. Leusmann, die ihren intuitiv richtigen Ersteindruck von mir fallen gelassen haben. Mitschuld hieran trägt das gesungene Wort und Dr. Beatrix Barth.

Zahlreiche Leute wären im Arbeitskreis weiterhin positiv zu erwähnen. Hervorheben möchte ich Dr. Dejan Premužić, warmherziger Komplize bei so manchen Unternehmungen. Iss mehr Gemüse! Im Gegensatz dazu möchte Eugenie Geringer ausdrücklich nicht für einen Gemüseabend danken, für die Geschichten hingegen schon. Für das Anhören von Geschichten in der Mensa danke ich Dr. Robert „deutsch Robert“ James Wilson Junior, für das zusätzliche Erzählen dieser Frau Ursula Siepe. Zudem war sie helfende Hand bei Musikfindung und dem Ausfüllen von Formularen wie Dienstreiseanträgen. Eine Besondere dieser Reisen durfte ich gemeinsam mit Niels Lichtenberger, Stefan Mitzinger und Dr. Johanna Heine begehen. Ich danke besonders dafür, dass sie sich immer nach Ankunft in Manhattan zu einer halbstündigen Pause überreden ließen. Abseits von Pausen und Reisen muss ich auf die fruchtvolle Zusammenarbeit mit meinen Laborkollegen hinweisen, noch nicht genannt wären Annikka Kreher und Eike Dornsiepen. Der Arbeitsalltag fällt und steht mit den Leuten, mit denen man arbeitet und bei diesen Mitarbeitern ist er besonders standfest.

Für seinen unermüdlichen Einsatz um meine Veröffentlichungen in den letzten zwei Monaten möchte ich zudem Lukas Guggolz den Preis für den Mitarbeiter des Monats Juni und Juli 2017 verleihen. Herzlichen Glückwunsch! Zudem vergebe ich meine Jungautoren-Auszeichnung an Katharina Hanau im Bereich Arbeiten unter Zeitdruck. Ihr habt maßgeblich dazu beigetragen, dass ich die Arbeit fristgerecht einreichen konnte.

Es gab auch Studenten.
Wer davon trotz Vertragsbruch mehr war, wird es wissen.

In Marburg danke ich folgenden Wegbegleitern. Michael Müller, als mein letzter verbliebener Freund aus dem Ersten Semester. Frohes Backen bis zu deiner Promotion! Kayoko Lang für das Einführen in fernöstliche Sprache und Kilian Scherer für das Einführen in fernöstliche Kampfkunst. Den Aikidoka in Marburg danke ich dafür, sich von mir umschubsen zu lassen und fürs Zurückschubsen. Am Spieltisch habe ich manch kurzweilige Stunde mit meinem Bruder Andre und Daniel Hussain verbracht. Zudem ist die langjährige Freundschaft und Freizeitgestaltung mit dem GCS im In- und Ausland ein wichtiger Bestandteil meines Lebens gewesen.

Ich möchte an dieser Stelle Valerie Colling erwähnen, damit ihr Name wenigstens einmal in einer Promotionsschrift zu lesen ist.

Meinen Eltern wird fürs ewige Kümmern und Treusorgen sowie schon viel zu wenig gedankt. Ohne euch wäre ich nicht hier (das wollte ich schon immer mal schreiben). Sei es Geschwister, Großeltern, Tante, Onkel, Cousin und Cousinen der Rinn Clan stand mir immer zur Seite, auch wenn leider nicht mehr alle zugegen sind, die mich zum Start meiner Promotion begleitet haben.